SLAC-PUB-1972
July 1977
(T/E)

RECENT RESULTS IN ELECTRON-POSITRON ANNIHILATION ABOVE 2 GeV*

Gary J. Feldman and Martin L. Perl

Stanford Linear Accelerator Center
Stanford University, Stanford, California 94305

(Submitted to Physics Reports)

*Work supported by the Energy Research and Development Administration.

Table of Contents

Abstract

We review recent results in electron-positron annihilation above a center-of-mass energy of 2 GeV with particular emphasis on the production and properties of new particles. Topics include the total e^+e^- cross section, the properties of jet-like structure in high energy multi-particle events, the properties of the ψ family of charmonium states, the production and properties of the charmed D mesons, and evidence for and the properties of the τ, a new charged lepton.

1. INTRODUCTION

New results and important discoveries in electron-positron annihilation have been appearing with astonishing rapidity. This paper reviews the results and discoveries of the past two years, and it brings up to date our earlier review [1.1] of this subject, called ref. [I]. Again, as in that review, we restrict our discussion to total energies above 2 GeV. This is a review from the experimental viewpoint; the required theoretical background is provided as the paper progresses and a general review of the theory has been given in I and in a review [1.2] by Schwitters and Strauch called ref. [II]. Another general review by Wiik and Wolf [1.3] is called ref. [III].

In this article we do not review purely quantum electrodynamic processes [II,1.4] or particle production through two-virtual-photon processes [1.5]. The next two sections present new results on the production of hadrons thru one-photon exchange: section 2 discusses the total hadronic cross section and section 3 describes the jet structure in hadron production.

Sections 4 thru 6 review the new particles produced in e^+e^- annihilation. The extensive ψ/J family of particles is discussed in section 4. The discovery and properties of the charmed D mesons is described in section 5. Section 6 reviews anomalous lepton production in e^+e^- annihilation and its sources. There is now very good evidence that one source is a new charged lepton with a mass of 1.9 GeV/c^2 formerly called the U particle, and now called the τ. Properties of the τ are reviewed in section 6. Another source is the semi-leptonic decays of the charmed mesons such as the D's, also discussed in section 6.

This paper concludes with a discussion of the physics which may be studied at the e^+e^- colliding beams facilities now under construction: PEP and PETRA.

Descriptions of e^+e^- colliding beam facilities and their basic parameters are given in I, II, and III. We remind the reader that in these facilities the e^+ and e^- beams have equal energies E_{beam}. Their momenta are equal in magnitude

and opposite in direction. Hence the total momentum is zero and the total energy is

$$E_{cm} = 2E_{beam} \tag{1.1}$$

We also use

$$s = E_{cm}^2 \tag{1.2}$$

2. THE TOTAL HADRONIC CROSS SECTION IN e^+e^- ANNIHILATION

2.1. The Total Hadronic Cross Section and the Quark Model

Figure 2.1 shows somewhat schematically the total cross section, σ_{had}, for hadron production

$$e^+ + e^- \to \text{hadrons} \tag{2.1}$$

in e^+e^- annihilation. Purely quantum electrodynamics reactions such as

$$\begin{aligned} &e^+ + e^- \to e^+ + e^- \\ &e^+ + e^- \to \mu^+ + \mu^- \\ &e^+ + e^- \to e^+ + e^- + \mu^+ + \mu^- \end{aligned} \tag{2.2}$$

are excluded. The experimenter also attempts to exclude, or correct for, the two-virtual-photon processes [1.5]

$$e^+ + e^- \to e^+ + e^- + \text{hadrons} ; \tag{2.3}$$

so that the data can be compared with the theory of the dominant one-virtual-photon process of fig. 2.2a. However for the present, σ_{tot} <u>does include</u> the production and decay of a charged heavy lepton for which we now have evidence, section 6.

There are two simple ways at present to understand the photon-hadron vertex in fig. 2.2a. If the energy is such that the final hadronic state is dominated by a vector meson such as the ρ, ϕ, ψ/J, or ψ', then the vector meson dominance model can be used, fig. 2.2d. Discussion of this model and references are given in refs. [I,II,III].

In this section we concentrate on the model in fig. 2.2c; the quark model for production of hadrons <u>away</u> from a resonance. We call this the <u>continuum</u> region. In this model we decompose the photon-hadron vertex, fig. 2.2a, into the two step process shown in fig. 2.2c. First the virtual photon materializes

into a quark-antiquark pair, $q\bar{q}$. Then the $q\bar{q}$ pairs annihilates into hadrons. If we assume

a. the quarks are Dirac point particles with charge $\pm Qe$ (e being the electron charge),

b. the production of the $q\bar{q}$ pair is independent of their annihilation into hadrons;

then we can calculate the total cross section for this process. The $q\bar{q}$ pair production process is given by quantum electrodynamics; and assuming quarks cannot be free [2.1], the probability of the $q\bar{q}$ pair annihilating into hadrons is 1. Indeed neglecting the quark mass we obtain the formula

$$\sigma_{had}(E_{cm}) = \frac{4\pi\alpha^2 Q^2}{3E_{cm}^2} \tag{2.4}$$

Furthermore if there are N different kinds of quarks, each with charge $Q_n e$ and mass m_n, there are N processes of the type in fig. 2.2c. Then

$$\sigma_{had}(E_{cm}) = \frac{4\pi\alpha^2 \sum_{n=1}^{N} Q_n^2}{3E_{cm}^2} \quad ; \tag{2.4a}$$

for

$$E_{cm} >> 2m_n, \; n=1,2...N \tag{2.4b}$$

Here >> means at least 0.5 GeV or so greater.

The production of $q\bar{q}$ pairs involves the same diagram as the production of a $\mu^+\mu^-$ pair (fig. 2.2b)

$$e^+ + e^- \rightarrow \mu^+ + \mu^- \quad ; \tag{2.5}$$

The total μ-pair production cross section is [I]

$$\sigma_{\mu^+\mu^-}(E_{cm}) = \frac{4\pi\alpha^2}{3E_{cm}^2} \tag{2.6}$$

This is such a simple and powerful analogy that it has been conventional in

e^+e^- annihilation physics to define

$$R(E_{cm}) = \sigma_{had}(E_{cm})/\sigma_{\mu^+\mu^-}(E_{cm}) \tag{2.7}$$

Then this theory predicts for the continumm

$$R(E_{cm}) = \sum_{n=1}^{N} Q_n^2 \quad ; \quad \text{all } m_n << E_{cm}/2 \tag{2.8}$$

Figure 2.3 shows the experimental values of R. Ignoring the resonances and peaks, we see that R varies between 1 and 6. Most of the $E_{cm} \gtrsim 2$ GeV data comes from the SLAC-LBL Magnetic Detector Collaboration [2.2]. Their detector is shown in fig. 2.4. To test how well eq. (2.8) explains the data in fig. 2.3 we use the conventional fractionally charged quark model [2.3]. The charge and quantum numbers of these quarks are given in table 2.1, and a crude estimate of the effective mass of these quarks is given in table 5.3 Using the tables, assuming that each quark has an additional three-valued quantum number such as color [2.3] associated with it, eq. (2.8) yields

$$R(E_{cm} \gtrsim 4.5 \text{ GeV}) = 3\left[(\tfrac{2}{3})^2 + (\tfrac{1}{3})^2 + (\tfrac{1}{3})^2 + (\tfrac{2}{3})^2\right] = 3\tfrac{1}{3} \tag{2.9}$$

Hence the quark model certainly gives an order of magnitude explanation of the $E_{cm} \gtrsim 4.5$ GeV behavior of R (fig. 2.3). The model also expains the increase in R in the $E_{cm} \sim 4$ GeV region. Below $E_{cm} \sim 4$ GeV the charmed quark cannot participate in the process in fig. 2.3c; therefore we expect

$$R(2 \lesssim E_{cm} \lesssim 3.5 \text{ GeV}) = 3\left[(\tfrac{2}{3})^2 + (\tfrac{1}{3})^2 + (\tfrac{1}{3})^2\right] = 2 \tag{2.10}$$

This is in good agreement with the data.

But when we become more critical we see that there is a discrepancy in the $E_{cm} \gtrsim 4.5$ GeV region. Figure 2.3 gives an R of 5.0 to 5.5 in this region; eq. (2.9) gives 3.33! This discrepancy is reduced by the probable

existence of a new charged lepton, the τ, with a mass of 1.9 GeV/c^2 (see section 6). The τ is produced through the reaction

$$e^+ + e^- \rightarrow \tau^+ + \tau^- \tag{2.11}$$

the process being the same as that in fig. 2.2b. Indeed once E_{cm} is somewhat larger than $2m_\tau$, the production cross section is

$$\sigma_{\tau^+\tau^-} = \frac{4\pi\alpha^2}{3E_{cm}^2} \tag{2.12}$$

the same as eq. (2.6). The dominant decay modes would be

$$\tau^- \rightarrow \nu_\tau + e^- + \bar{\nu}_e$$

$$\tau^- \rightarrow \nu_\tau + \mu^- + \bar{\nu}_\mu$$

$$\tau^- \rightarrow \nu_\tau + \text{hadrons} \tag{2.13}$$

Here ν_τ is a neutrino associated with the τ. If we accept the existence of this heavy lepton than experimentally all the decay modes of the $\tau^+\tau^-$ pair produced in eq. (2.11) are <u>counted</u> in σ_{had}. Even the purely leptonic decay modes are counted in at present. Then eq. (2.11) contributes one unit of R at high E_{cm} and

$$R(E_{cm} \gtrsim 4.5 \text{ GeV}) = 3\tfrac{1}{3} + 1 = 4.33 \tag{2.14}$$

2.2. σ_{had} in the $3.8 \lesssim E_{cm} \lesssim 4.6$ GeV Region

The 3.8 to 4.6 GeV E_{cm} region has a rich structure in σ_{had}. The SLAC-LBL Magnetic Detector Collaboration data [2.4] in terms of R is shown in fig. 2.5. And recent R data from the PLUTO group at DORIS (J. Burmester et al., [2.5]) is shown in fig. 2.6. Figure 2.7 shows their detector. The two sets of data agree as to the main features of the energy dependence in R:

a. There is a complex enhancement in the E_{cm} = 4.0 to 4.1 GeV region. This enhancement has a steep rise which begins at $\sim$ 4.00 GeV and reaches a peak in the 4.03 to 4.05 GeV region. The 4.1 GeV enhancement then has a broad shoulder or second peak extending out to $\sim$4.20 GeV. The SLAC-LBL data shows a peak in this shoulder region at 4.11 GeV while the PLUTO data is more rounded and the shoulder has a maximum at $\sim$ 4.15 GeV. But these differences may be due to statistical fluctuations, and given the statistics, the overall 4.1 enhancement data is in good agreement.

b. There is a resonance-like structure at 4.4 GeV in both sets of data. The SLAC-LBL data [2.4] gives the following parameters for the resonance

$$\begin{array}{ll} \text{Mass} & 4414 \pm 7 \text{ MeV} \\ \Gamma & 33 \pm 10 \text{ MeV} \end{array} \qquad (2.15)$$

As pointed out by Burmester et al. [2.5] their average R values in the 4. to 5. GeV region are lower than those of the SLAC-LBL group. The difference in the R values is due to systematic errors in one or both experiments, and these differences are now being studied by both groups.

The obviously complicated 4.1 GeV enhancement may be caused by one or more phenomena:

a. This region is the threshold for charmed D meson pair production, section 5. In particular D mesons production is enhanced in the 4.03 - 4.05

region. If charmed F mesons exist, they could also contribute to the structure.

b. As σ_{had} passes thru the charmed quark threshold, about 3.8 GeV, there may be overshoots and oscillations in σ_{had} [2.6].

c. There may be one or more higher mass members of the ψ, ψ' family in this region, section 4, and these could lead to resonance peaks.

d. Collective "molecular" states of charmed particles have also been proposed [2.7] and might contribute to the structure of the 4.1 GeV enhancement. Clearly a great deal of work has to be done to fully understand the 4.1 GeV enhancement.

We know very little about the nature of the 4.4 GeV peak. It could be a higher mass member of the ψ, ψ' family, section 4. It could be related to an enhancement in charmed particle production, although preliminary data is inconclusive as to the extent of charmed particle production enhancement in the 4.4 GeV region. As with the 4.1 GeV region there is a great deal of work to be done here.

3. JET STRUCTURE

3.1. Introduction

One of the most beautiful and definitive predictions of the quark-parton constituent models of elementary particles is that a two-jet structure should characterize high energy e^+e^- annihilations [3.1 - 3.4]. These models postulate that the e^+e^- annihilate to form a virtual photon which produces a quark-antiquark pair, each of which fragments to hadrons, as shown in fig. 3.1. At sufficiently high energy, a two-jet structure arises due to the limited transverse momentum of the hadrons with respect to the quark-parton direction. In principle, the spin of the quark-parton can be determined from the angular distribution of the jets.

A special problem in studying jets in high energy e^+e^- annihilations is that about half the cross section comes from charm particle and heavy lepton (τ) production (see sections 5 and 6). Charm particle decays will tend to produce jets with slightly larger transverse momenta than jets from lighter quarks. Production of τ pairs will automatically produce jet-like structures and will tend to contaminate our study of hadronic jets. Fortunately, about 70% of all τ pairs result in only two charged particles. Since we shall restrict the study of jets to events with three or more observed prongs, τ decays will not appreciably affect the results.

The following sections will discuss the jet formalism, sphericity distributions, possible alternate explanations, angular distributions, and inclusive momentum distributions [3.5].

3.2. Formalism

The key to searching for jets lies in the definition of jet structure. One can characterize jet structure as the tendency for the transverse momentum to be limited with respect to some axis. This definition

allows us to quantify the amount of jet-like behavior by a single parameter: the average transverse momentum to the jet axis. (A second parameter will be needed to specify the angular distribution of the jet axis.)

The procedure for finding jets is based on a suggestion by Bjorken and Brodsky [3.3]. In words, the procedure is

(a) Find for each event the axis which minimizes the sum of the squares of transverse momenta to it. This axis will be defined as the reconstructed jet axis.

(b) Construct a quantitative measure of the amount of jet-like structure by comparing the relative amount of transverse momenta to orthogonal axes.

(c) Perform Monte Carlo simulations to evaluate the significance of the results.

The jet axis is found mathematically for each event by constructing the tensor

$$T_{\alpha\beta} = \sum_i \left(\delta_{\alpha\beta}\, p_i^2 - p_\alpha^i\, p_\beta^i\right) \tag{3.1}$$

where the summation is over all detected charged particles and α and β are Cartesian coordinates. This tensor is analogous to a moment of inertia tensor.

The tensor is diagonalized to yield three eigenvectors and three eigenvalues, λ_1,λ_2, and λ_3. The eigenvalues are the sum of the squares of the transverse momenta to the eigenvector directions. The smallest eigenvalue, λ_3, is the minimum sum of transverse momenta to any axis, and thus its associated eigenvector is the reconstructed jet axis.

To measure how jet-like an event is, we define the sphericity, S,

$$S \equiv \frac{3\,\lambda_3}{\lambda_1+\lambda_2+\lambda_3} = \frac{3\left(\sum p_{\perp i}^2\right)_{min}}{2\sum p_i^2} \quad . \tag{3.2}$$

For each event the sphericity is between 0 and 1.

Finally, to interpret the results, two types of Monte Carlo simulations were performed. In the first, the phase space model, events were simulated with the particles' momentum distributions given by invariant phase space. The mean multiplicity of produced particles and the ratio of charged to neutral particles were set in the Monte Carlo to match the observed mean charged multiplicity and average momentum. The second model, the jet model, differed only in that a matrix element squared,

$$|M|^2 = e^{-\left(\sum p_{\perp i}^2\right)/2r^2} \tag{3.3}$$

was inserted. The summation is taken over all of the produced particles, $p_\perp$ is the momentum transverse to the produced jet axis, and r is a free parameter which can be adjusted to give a desired mean transverse momentum.

In both models all particles were assumed to be pions. Calculations done with the addition of kaons, η's, and nucleons give substantially the same results.

3.3. Sphericity Distributions

The mean observed sphericity as a function of energy is shown in fig. 3.2. It is fairly constant between 3.0 and 4.8 GeV, but is significantly lower at 6.2 and 7.4 GeV. The expected mean observed sphericity based on the phase space model is given by the dashed line. It rises as

a function of energy in sharp contrast to the data. The rise predicted by this model is due to the increase in multiplicity with energy and will occur in any uncorrelated model. The solid curve shows the results of the jet model. The parameter r is fit to agree with the mean observed $p_\perp$ with respect to the jet axis. The mean $p_\perp$, corrected for acceptance, was found to be in the range 325 to 360 MeV/c with no particular energy dependence. A plot of the observed $p_\perp$ with respect to the jet axis at 7.4 GeV is shown in fig. 3.3. The jet model reproduces the data well, while the phase space model predicts too many particles at high $p_\perp$.

Figure 3.4 shows observed sphericity distributions at three energies. At 3.0 GeV, the phase space and jet models are essentially identical and both describe the distribution well. However, at 6.2 and 7.4 GeV, only the jet model provides a reasonable description of the data.

3.4. Alternate Explanations

These distributions provide the basic evidence for jet-like structure in e^+e^- annihilations. They show that at high energy the data are not described well by invariant phase space but can be described by a model in which the transverse momentum is limited. We will now consider some alternative explanations for this behavior.

The inclusive x distribution at 7.4 GeV does not agree with the predictions of the phase space model. This can be seen in fig. 3.5 where the 7.4 GeV inclusive momentum spectrum is plotted along with the Monte Carlo distributions. This disagreement is to be expected given the existence of jets, but a legitimate question can be asked: Is the existence of extra high momentum tracks sufficient to give jet-like sphericity distributions? The answer is no, as illustrated by fig. 3.6. Here the data at 7.4 GeV have been divided into two sets, one in which there is an observed particle

with $x > 0.4$, and one in which there is not. The latter set is in good agreement with the phase space momentum distribution, while the former set has an enriched sample of high momentum tracks and is thus closer to the (renormalized) phase space momentum distribution. In both cases the phase space sphericity distributions fail to describe the data, while the jet model distributions are reasonably close.

Another alternative explanation is that the jet structure is caused by the production of two meson resonances which decay. This process might dominate at present energies, but slowly die out at higher energies. We have not found any data to support this explanation. Figure 3.7 shows the distribution of observed jet masses, where the jet mass is defined by constructing a plane perpendicular to the reconstructed jet axis and calculating the invariant mass of the observed particles on either side of the plane. There are two discrete bins in fig. 3.7a, which correspond to the detection of zero and one charged particle. When two or more charged particles are detected in the jet, there is a smooth continuum of masses which is flat from threshold to about 750 MeV and then decreases. In fig. 3.7b and 3.7c, where two and three prong jets have been isolated, there is evidence for K_S^o's and ρ's but f and A mesons are not evident. In all there does not seem to be any evidence for copious resonance production.

3.5. Angular Distributions

Under the assumption of one photon exchange all angular distributions, whether they be of inclusive hadrons or of the jet axis, must be of the form

$$\frac{d\sigma}{d\theta} \propto 1 + \alpha \cos^2 \theta + P^2 \alpha \sin \theta \cos^2 2\phi \qquad (3.4)$$

where

$$\alpha = \frac{\sigma_T - \sigma_L}{\sigma_T + \sigma_L} \quad , \qquad (3.5)$$

σ_T and σ_L are transverse and longitudinal cross sections, θ is the polar angle to the beam, P is the transverse beam polarization, and ϕ is the azimuthal angle measured from the plane of the ring [3.6]. The only parameter in eq. (3.4), α, can be measured even if P is zero, so the transverse polarization gives no new theoretical information. However, since the SPEAR magnetic detector measures only a portion of the θ region, but is almost unbiased in ϕ, the polarization is extremely important experimentally.

Figure 3.8 shows the observed azimuthal angle of the jet axis at 7.4 GeV, where polarization has been observed, and at 6.2 GeV where polarization is absent due to a depolarizing resonance at that energy [3.7, 3.8]. The data at 7.4 GeV show a clear azimuthal dependence from which an α for the jet axis can be deduced with the aid of the jet model simulation,

$$\alpha_{jet} = 0.97 \pm 0.14 \ , \tag{3.6}$$

where the error reflects only the statistical uncertainty. This value is close to what one expects for jets originating from spin 1/2 partons, $\alpha = 1$, and is completely incompatible with the prediction of spin 0 partons, $\alpha = -1$.

The jet model also produces a good description of the inclusive hadron angular distribution [3.9]. Figure 3.9 shows α versus x for inclusive hadrons and the prediction of the jet model with $\alpha_{jet} = 0.97 \pm 0.14$. The change from isotropic particle production at low x to muon-like distributions at high x is reproduced.

3.6 Inclusive Momentum Distributions

In electroproduction of hadrons, it is customary to plot momentum spectra with respect to the direction of the virtual photon, which in

quark-parton models is approximately the direction of the struck parton. Similarly, in e^+e^- annihilation, the reconstructed jet axis approximates the direction of the original parton pair, and thus is the direction with respect to which momentum distributions should be plotted.

Figures 3.10 and 3.11 show the inclusive momentum spectra and the inclusive momentum spectra parallel to the jet axis at four center-of-mass energies. These spectra are presented as x vs s $d\sigma/dx$ and $x_{\parallel}$ vs s $d\sigma/dx_{\parallel}$ since the latter of these quantities is expected to scale in quark-parton models. Figure 3.11 shows that data at center-of-mass energies above 4.8 GeV appear to scale in s $d\sigma/dx_{\parallel}$ for all $x_{\parallel}$. The 3.0 GeV data cannot scale everywhere since the total cross section does not scale for these data, i.e., R is lower at 3.0 GeV than at 4.8 GeV and above. Nevertheless, for $x_{\parallel} > 0.6$, s $d\sigma/dx_{\parallel}$ appears to be the same for all four energies. For $x_{\parallel} < 0.6$, the slope of the 3.0 GeV data is similar to that of the higher energy data, but the magnitude of s $d\sigma/dx_{\parallel}$ is smaller.

To study $p_{\perp}$ and rapidity distributions, it is necessary to restrict the data sample to events with at least one particle with $x > 0.5$. If the entire data sample is used, the jet axis is often poorly defined and the corrections for using the wrong jet axis become enormous. Figure 3.12 shows $(1/\sigma) \cdot d\sigma/dp_{\perp}$ vs $p_{\perp}$ where $p_{\perp}$ is the transverse momentum relative to the jet axis and the distributions are normalized to the cross section for events with $x_{max} > 0.5$. The particle with the highest x is not plotted. The shape of the $p_{\perp}$ distribution is approximately the same at all energies. The area under the curve increases with energy because the multiplicity increases.

Figure 3.13 shows distributions in rapidity with respect to the jet axis normalized in the same way the $p_\perp$ distributions were. The rapidity is defined by

$$y = \frac{1}{2} \ln \left(\frac{E + p_\parallel}{E - p_\parallel} \right) , \qquad (3.7)$$

where E is the energy of the particle with a pion mass assumed and $p_\parallel$ is the component of particle momentum parallel to the jet axis. The widths of the distributions increase logarithmically with energy and at 7.4 GeV the rapidity distribution appears to develop a plateau. The rapidity distributions are similar in shape to those observed in proton-proton collisions [3.10].

3.7. Summary

We have seen a beautiful confirmation of the basic predictions of the quark-parton constituent models:

(1) Two-jet structure appears in high energy e^+e^- annihilations characterized by a transverse momentum which is roughly constant as a function of energy and which is similar to transverse momenta observed in hadron-hadron collisions.

(2) The jets have angular distribution which is consistent with the expected distribution for spin 1/2 partons.

(3) The quantity $s\, d\sigma/dx_\parallel$ approximately scales at energies of 4.8 GeV and above.

4. THE ψ FAMILY

4.1. Introduction

This section will cover the properties of the various members of the ψ family, the bound states of a charmed quark and a charmed anti-quark. The recent identification of charmed mesons in e^+e^- annihilation, which we shall discuss in section 5, has effectively removed other explanations of the origin of the ψ particles as viable alternatives. Accordingly, whenever it is convenient to do so, we shall assume that members of the ψ family are states of charmonium.

The known members of the ψ family fall into two classes, the ψ's, s-channel resonances which have $J^{PC} = 1^{--}$ and are produced at rest in e^+e^- annihilations, and the χ's, C-even states which are observed in the radiative decays of the ψ and ψ' [4.1]. The ψ's consist of two extremely narrow resonances, the ψ [$=\psi(3095)$ or J] and the ψ' [$=\psi(3684)$], and probably several broader resonances at higher mass. The mass region between 3.9 and 4.3 GeV/c^2 is quite complicated and not well understood. In addition to resonances, there are many thresholds for charmed meson production conspiring to create the complex structure seen in fig. 2.5. An isolated resonance, the $\psi(4414)$, appears above this region [4.2] and it is shown in more detail in fig. 4.1.

The most remarkable property of the ψ family is the narrowness of the states which lie below the threshold for charmed meson pair production. The strong decays of these particles are not inhibited by any conservation law, yet their rates are three to four orders of magnitude smaller than those for ordinary strong decays. This behavior is explained phenomenologically by the Okubo-Zweig-Iizuka (OZI) rule [4.3] which was formulated a decade ago to account

for the suppression of $\phi \to 3\pi$. The OZI rule as it applies to ϕ decays is illustrated in fig. 4.2. Quark diagrams which are disconnected are suppressed relative to diagrams which are not. A disconnected diagram is one in which one or more particles can be isolated by drawing a line which does not cross any quark lines. The ψ is the first known particle all of whose strong decays are OZI suppressed. We shall return to a discussion of this rule as it manifests itself in ψ decays in section 4.4.4.

4.2. Decay Widths

Figures 4.3 and 4.4 show the measured cross sections for hadron production, μ pair production, and e pair production (or scattering) in the vicinity of the ψ and ψ' [4.4,4.5]. These are only apparent cross sections because in both cases the true widths of the resonances are considerably smaller than the experimental resolution.

In cases such as this the true widths must be determined by a "trick". Here the trick is that we measure the ψe^+e^- coupling two different ways. As can be seen from fig. 4.5, $e^+e^- \to \psi \to$ anything is proportional to this coupling, while $e^+e^- \to \psi \to e^+e^-$ is proportional to the square.

The formalism is fairly simple. For any final state f, the resonant cross section will be given by

$$\sigma_{\psi,f} = \frac{\pi(2J+1)}{m^2} \frac{\Gamma_{ee}\Gamma_f}{(E-m)^2 + \Gamma^2/4} \tag{4.1}$$

where m is the mass of the ψ, J is its spin, Γ_f is the partial decay width to the state f, and Γ is the total decay width.

Integrating eq. (4.1) and using J = 1 we obtain

$$\Sigma_{\psi,f} \equiv \int \sigma_{\psi,f}\, dE = \frac{6\pi^2 \Gamma_{ee}\Gamma_f}{m^2\Gamma} \tag{4.2}$$

We can now use eq. (4.2) to obtain all the widths. In particular,

$$\Gamma_{ee} = \frac{m^2}{6\pi^2} \Sigma_{\psi,all} \tag{4.3}$$

and

$$\Gamma = \frac{\Sigma_{\psi,all}}{\Sigma_{\psi,ee}} \Gamma_{ee} \tag{4.4}$$

For simplicity we have ignored radiative effects and interference between ψ decays and the direct channel $e^+e^- \to f$. These effects can be included in a straightforward way.

The widths determined by the SLAC-LBL collaboration for the ψ,ψ', and higher resonances are given in table 4.1 [4.2,4.4,4.5]. (The world averages for the ψ and ψ', which are only slightly different, will be given later in a complete list of decay modes.) Note that although we don't know how many resonances are in the 4.1 GeV region or their locations and widths, we can still determine that the branching fractions to electron pairs are of order 10^{-5} since they are only proportional to the peak cross sections.

4.3. Spin, Parity, and Charge Conjugation

If the ψ particles are states of charmonium, they should be produced in e^+e^- annihilations by coupling to the photon, in which case they would have the same quantum numbers, $J^{PC} = 1^{--}$. This would not have to be the case, however, if they coupled directly to leptons, so an experimental check is clearly important.

We can determine the quantum numbers directly by observing the interference between the leptonic decays of the ψ particles and the direct production of lepton pairs. The formalism can be found in I.6.3.

The ratio of muon pairs to electron pairs as a function of energy

is shown for the ψ and the ψ' in fig. 4.6. This ratio is used because it is least sensitive to normalization effects and because the electron pairs are expected to have a small constructive interference below the resonance (due to interference with the spacelike diagram). The data are inconsistent with no interference by 2.7 standard deviations in the ψ region [4.4] and by 4.9 standard deviations in the ψ' region [4.5]. This is sufficient to confirm that the quantum numbers of both the ψ and ψ' are those of the photon, $J^{pc} = 1^{--}$.

4.4. Decays of the ψ

4.4.1. Table of Results

Table 4.2 contains a compendium of the world measurements of ψ decays. The cutoff date for inclusion of data in this table (and other tables in section 4) was March 15, 1977. In the following subsections we shall examine the consequences of these measurements.

4.4.2. Isospin and G Parity

We can determine the G parity of the ψ by observing whether it decays into even or odd numbers of pions. It turns out that the ψ decays into both even and odd numbers of pions -- a violation of I spin. However, this violation occurs in precisely the way we expect it to occur, and in the way it is required to occur, if the ψ couples to a photon.

Consider the three diagrams in fig. 4.7. Figure 4.7a shows the direct decay of the ψ into hadrons, (b) shows the decay of the ψ into hadrons via an intermediate photons, and (c) show the decay into μ pairs. In (b), the nature of the final state, except for a phase factor, must be the same as the non-resonant final state produced in e^+e^- annihilation at the same energy. This state need not conserve isospin and may be quite different from the state produced by (a). Furthermore, we know what contribution (b)

must make because the ratio between (b) and (c) must be the same as it would be if the ψ were not in the diagram, about 2.5. Thus, from the data in table 4.2, we deduce that if the ψ couples to a photon (a) contributes 67% to the width of the ψ, (b) contributes 18%, and the leptonic modes contribute 15%, neglecting possible interference terms between (a) and (b).

To test this hypothesis we want to compare the ratio of all pion final state cross sections to μ pair cross sections on- and off-resonance we compute the ratio α, defined by

$$\alpha = \frac{\sigma^{\psi}_{n\pi}}{\sigma^{\psi}_{\mu\mu}} \Bigg/ \frac{\sigma^{3.0}_{n\pi}}{\sigma^{3.0}_{\mu\mu}} , \tag{4.5}$$

where data at 3.0 GeV are used as the off-resonance sample. Values of α for three to seven pion production are shown in fig. 4.8 [4.16]. The results are consistent with all of the even number of pion production (G even, I odd) coming from the intermediate photon decay, fig. 4.7. Most of the odd pion production comes from the direct ψ decay, fig. 4.7 and the ψ appears to decay directly into a pure $I^G = (\text{even})^-$ state.

It is relatively easy to show that I=0 using the data in table 4.2. One way is to compare $\psi \to \rho^o \pi^o$ and $\psi \to \rho^{\pm} \pi^{\mp}$. For this decay either I=0 of I=2. If I=0, then $\Gamma_{\rho^o \pi^o} = \Gamma_{\rho^+ \pi^-}$, whereas for I=2, $\Gamma_{\rho^o \pi^o} = 4\Gamma_{\rho^+ \pi^-}$. The data indicate that $\Gamma_{\rho^o \pi^o} = (1.20 \pm 0.26)\Gamma_{\rho^+ \pi^-}$, strongly favoring I=0. These properties, the coupling to photon pairs via a photon, the conservation of isospin in direct decays, and I=0, are just the properties we expect of a state of charmonium.

4.4.3. SU(3)

If the ψ is a state of charmonium, then we expect it to behave as a singlet with respect to the approximate SU(3) symmetry of the three

lighter quarks. For each SU(3) multiplet there is a generalized charge conjugation, $\mathscr{C}$, which is equal to C of the I=0 part of the multiplet. If the ψ is an SU(3) singlet, then it cannot decay into two mesons with the same $\mathscr{C}$ [4.27].

If we consider the well established pseudoscalar (P), vector (V), and tensor (T) meson multiplets, then decays to PP, PT, VV, and TT meson pairs are forbidden, while decays to PV and VT pairs are allowed. Examining table 4.2 for decays involving K, $K^*(890)$, and $K^{**}(1420)$, we find that in each case the allowed modes are observed and the forbidden modes are not. In particular note that

$$\frac{\Gamma(K\bar{K}^*)}{\Gamma(K\bar{K})} > 30 \tag{4.6}$$

and

$$\frac{\Gamma(p\bar{p})}{\Gamma(K\bar{K})} > 25 \quad . \tag{4.7}$$

It is not true in general that heavy particles do not decay into two pseudoscalars. The $\chi(3415)$ decays into both $\pi^+\pi^-$ and K^+K^- with branching fractions of about 1%.

For the two allowed modes, PV and VT, we can proceed one step further and ask whether the branching fractions to individual channels are in accord with SU(3) symmetry. In the PV case, per channel,

$$\Gamma(\pi\rho) \quad : \quad \Gamma(KK^*) \quad : \quad \Gamma(\eta\phi) \tag{4.8}$$

should be

$$1.0 \quad : \quad 1.0 \quad : \quad 0.48 \quad . \tag{4.9}$$

Correcting for phase space (4.9) becomes

$$1.0 \quad : \quad 0.84 \quad : \quad 0.36 \quad . \tag{4.10}$$

Normalizing $\rho\pi$ to unity the data from table 4.2 are

$$1.00 \pm 0.14 \quad : \quad 0.41 \pm 0.05 \quad : \quad 0.27 \pm 0.16 \tag{4.11}$$

Dividing by the predicted ratios (4.10), we obtain

$$1.00 \pm 0.14 \quad : \quad 0.49 \pm 0.06 \quad : \quad 0.75 \pm 0.44 \tag{4.12}$$

Thus $\Gamma(\rho\pi)$ is about a factor of two larger than expected from $\Gamma(KK^*)$.

For the VT decays, we expect, per channel

$$\Gamma(\rho A_2) \quad : \quad \Gamma(K^*K^{**}) \quad : \quad \Gamma(\phi f') \quad : \quad \Gamma(\omega f) \tag{4.13}$$

to be

$$1.0 \quad : \quad 1.0 \quad : \quad 1.0 \quad : \quad 1.0 \tag{4.14}$$

Correcting for s-wave phase space (4.14) becomes

$$1.0 \quad : \quad 0.90 \quad : \quad 0.78 \quad : \quad 1.01 \tag{4.15}$$

Normalizing ρA_2 to unity, the data are

$$1.00 \pm 0.54 \quad : \quad 1.20 \pm 0.46 \quad : \quad 0.29 \pm 0.18 \quad : \quad 1.00 \pm 0.36 \tag{4.16}$$

Dividing by the predictions, (4.15), we obtain

$$1.00 \pm 0.54 \quad : \quad 1.33 \pm 0.51 \quad : \quad 0.37 \pm 0.23 \quad : \quad 0.99 \pm 0.36 \tag{4.17}$$

In this case there is good agreement between ρA_2, K^*K^{**} and ωf. $\phi f'$ is low, but its predicted rate is sensitive to the assumption of s-wave phase space.

Thus, in general, the ψ does appear to behave as an SU(3) singlet. Allowed decays are observed and forbidden ones are not. Decay rates are roughly correct, but the discrepancy between $\pi\rho$ and KK^* indicates some SU(3) breaking.

Although we have not yet discussed their decays, this is probably the best place to make a few remarks on the SU(3) properties of other

members of the ψ family. The only evidence we have for the ψ' is that the decay to $p\bar{p}$ has been observed and is at least four times larger than the decay to $K\bar{K}$, which has not been seen. This indicates some inhibition of the $K\bar{K}$ mode.

There are several predictions for the χ states under the assumption that they are SU(3) singlets. These are listed in table 4.3. Although the errors are large, there is no apparent deviation from the SU(3) predictions.

4.4.4. Tests of the OZI Rule

As we noted previously, the ψ is narrow because all of its decays are suppressed by the OZI rule. The decays $\psi \to \omega\pi\pi$ and $\psi \to \phi\pi\pi$ allow the examination of this phenomenological rule further since the $\phi\pi\pi$ decay corresponds to a doubly disconnected diagram as illustrated in fig. 4.9a and 4.9b.

From table 4.2

$$\frac{\Gamma(\phi\pi\pi)}{\Gamma(\omega\pi\pi)} = 0.26 \pm 0.12 \qquad (4.18)$$

which gives an overall suppression factor of about four. However, this overall factor is quite misleading. To understand the dynamics better, we want to study the ratio in eq. 4.18 as a function of $\pi\pi$ mass, which is plotted in fig. 4.10. Above 1100 MeV/c^2, there is only one observed $\phi\pi\pi$ event and the suppression factor is of order 70. But below 1100 MeV/c^2, there does not appear to be any suppression.

One way this could occur is shown in fig. 4.9c [4.15]. Two pair of $s\bar{s}$ quarks could be formed with only single OZI suppression. One pair forms a ϕ, the other a $s\bar{s}$ state near or below

threshold for K pairs, for example the $S^*(993)$. Because of either phase space, this state will be forced to decay into pions rather than kaons.

Additional striking evdience for the OZI rule in ψ decays comes from the decays into ωf, $\phi f'$, ωf and $\phi f'$. The decays ωf and $\phi f'$ are observed, while the similar decays $\omega f'$ and ϕf are not. From table 4.2,

$$\frac{\Gamma(\psi \to \omega f)}{\Gamma(\psi \to \omega f')} \gtrsim 17, \tag{4.19}$$

and

$$\frac{\Gamma(\psi \to \phi f')}{\Gamma(\psi \to \phi f)} \gtrsim 2 \tag{4.20}$$

Assuming ideal mixing, the ω and f are made up of non-strange quarks and the ϕ and f' are made up of strange quarks. Thus the decays $\psi \to \omega f'$ and $\psi \to \phi f$ are doubly disconnected while the decays $\psi \to \omega f$ and $\psi \to \phi f'$ are only singly disconnected.

4.4.5. Radiative Decays

Recent data from DORIS [4.23,4.24] allow us to draw some interesting conclusions from ψ radiative decays to ordinary psuedoscalar mesons. The decay $\psi \to \gamma\pi^0$ has a very small branching fraction, $(7.3 \pm 4.7) \times 10^{-5}$. The decays $\psi \to \gamma\eta$ and $\psi \to \gamma\eta'$ have branching fractions which are around an order of magnitude larger, $(8.8 \pm 1.9) \times 10^{-4}$ and $(2.4 \pm 0.6) \times 10^{-3}$ respectively.

Three processes which could account for these decays are shown in fig. 4.11. In fig. 4.11a the photon is emitted from the light quarks. The SU(3) coupling here is a singlet going to a pair of octets. From SU(3) we would expect $\gamma\pi^0$ to be three times $\gamma\eta$. This clearly cannot be an important mechanism since the $\gamma\pi^0$ branching fraction is very small.

The second mechanism (fig. 4.11b) is for the photon to be emitted from

the charmed quark pair. This SU(3) coupling must be a singlet going to a pair of singlets. This diagram should be completely dominated by $\gamma\eta'$ since η' is almost a pure SU(3) singlet, while the η is almost pure octet. If this diagram is to account for all of the radiative decays, it is hard to understand why the η to η' ratio is so large.

This brings us to an interesting suggestion [4.28,4.29]. If there is a small amount of $c\bar{c}$ mixing in the η and η' (there can be no mixing in the π^o by isospin conservation), then the radiative decays can occur without OZI suppression, as shown in fig. 4.10c. The data on radiative decays give support to this suggestion. Additional support will be presented in the next subsection and in section 4.5.2. where we discuss the $\psi' \to \psi\eta$ decay.

An interesting sidelight is that part of figs. 4.11b and 4.11c can be calculated by applying vector dominance to the decay $\psi' \to \psi\eta$, as shown in fig. 4.12. This calculation gives a value which is an order of magnitude too large [4.27,4.30]. This should at least caution us that the use of vector dominance to extrapolate in q^2 from zero to m_ψ^2 dangerous.

4.4.6. Is Anything Missing?

With all of the data that have now been collected on ψ decays, it is interesting to determine to what extent we can account for all of the ψ decays. To do this we employ a statistical model to uniquely predict branching fractions for all charge states of a channel, given the observation of one charge state of that channel [4.15,4.31]. We assume that isospin is conserved in ψ decays so that the final state has I=0. The only exceptions are states consisting solely of even numbers of pions. As discussed in section 4.4.2., these decays proceed via a second-order electromagnetic interaction and we assume that I=1 for these states.

The results are given in table 4.4. By using present measurements and the statistical model, we can account for 53.2 $\pm$ 3.4% of ψ decays. Three

types of decays have not been included in table 4.4 because there are no measurements of them: (a) decays with higher multiplicities, (b) decays involving photons (other than $\gamma\pi^0$, $\gamma\eta$, and $\gamma\eta'$), and (c) decays involving η's and η''s (other than $\phi\eta$ and $p\bar{p}\eta$). By using smooth multiplicity curves we can estimate the first class to contribute about 6%. The decay $\psi \to \gamma X(2830)$, which we will discuss in section 4.7, contributes less than 1.7% and radiative decays to ordinary hadrons should not contribute more than an additional 2%. Adding all these contributions together, we can account for no more than 63% of the ψ decays. This leaves 37% of all decays (or 43% of hadronic decays) which can be accounted for only if they contain an η or η'.

Additional evidence for a substantial fraction of ψ decays containing η's comes from the $\gamma\gamma$ group at Adone [4.7]. They have determined the average number of charged particles in ψ decays to be 3.8 ± 0.3 and the average number of photons to be 6.2 ± 1.6. Since the ψ has I=0, there should only be 3.8 photons per decay from direct π^0's. If we assign the excess 2.4 ± 1.6 photons per event to η production, there are an average of 0.9 ± 0.6 η's per decay.

Detectors with high resolution photon detection will be operational soon and be able to measure η production directly. A large fraction of decays with η's would support the hypothesis of $c\bar{c}$ mixing in pseudoscalar mesons [4.29].

4.5. Decays of the ψ'

4.5.1. Table of Results

There are four classes of ψ' decays which we will discuss: (a) $\psi' \to \psi$ decays, (b) second-order electromagnetic decays, (c) direct decays to ordinary hadrons and (d) radiative decays to intermediate

states (χ states). Table 4.5 contains a compendium of world measurements of these decays.

4.5.2. $\psi' \to \psi$ Decays

The ψ' decays over half the time into the ψ. These decays have now been measured at both SPEAR [4.32,4.34-4.37] and DORIS [4.38,4.39] with consistent results from both laboratories. Some of the experimental techniques were discussed in I.6.8.

There are three important conclusions to be drawn from the measurements of $\psi' \to \psi$ decays. First, the ψ' and ψ are closely related. There is much more phase space for $\psi' \to \omega\pi\pi$ than for $\psi' \to \psi\pi\pi$, yet the branching fraction for the latter decay is more than two orders of magnitude larger than that for the former.

Second, as expected for a state of charmonium, isospin is conserved in the decay and is equal to zero. This can be seen from the ratio of the $\psi\pi^0\pi^0$ mode to the $\psi\pi^+\pi^-$ mode which is equal to 0.48 ± 0.09. Correcting for phase space, we expect this ratio to be 0.52 for I=0, 0 for I=1, and 2.1 for I=2. Additional evidence for isospin conservation comes from the observation of $\psi' \to \psi\eta$ but not $\psi' \to \psi\pi^0$. The latter decay is not observed at the level of 3% of the former and it is inhibited only by isospin.

The third conclusion has to do with the only real surprise in the $\psi' \to \psi$ decays, the size of $\psi' \to \psi\eta$. This decay is quite large -- it is about a 4% branching fraction -- even though it has everything working against it:

1) There is little phase space; the Q value is only 40 MeV.
2) This is a P-wave decay, so there is an angular momentum barrier.
3) The decay is SU(3) forbidden in the limit that the η is pure octet.

We have already discussed a way out of these difficulties. If there is some $c\bar{c}$ mixing in the η, $\psi' \to \psi\eta$ is no longer OZI suppressed and its large branching fraction can easily be understood.

4.5.3. Second Order Electromagnetic Decays

The arguments of section 4.4.2. which were applied to the ψ apply equally well to the ψ'. The branching fractions to e^+e^- and to $\mu^+\mu^-$ are each about 1%. Therefore the branching fraction for hadrons produced via an intermediate photon (fig. 4.7b) should be about 3% since the non-resonant value of R in the vicinity of the ψ' is about 3.

4.5.4. Direct Decays to Hadrons

Few direct decays of the ψ' to ordinary hadrons have been observed and only two modes, $p\bar{p}$ and $K^+K^-\pi^+\pi^-$, have been measured well. This is partially because the direct decays are usually masked by a large background of $\psi' \to \psi\pi\pi$ decays and partially because not enough effort has been expended on finding these decays. Both the $p\bar{p}$ and $K^+K^-\pi^+\pi^-$ modes were measured in the process of working on χ decays.

Nevertheless, these two modes given us a considerable amount of information on direct ψ' decays. Table 4.6 shows a comparison of ψ and ψ' decays to these two modes and to lepton pairs. For all three decays the ratio of the ψ' to ψ partial widths is equal within errors. This can be understood if

$$\Gamma(\text{hadrons}) \propto |\Psi(0)|^2 \tag{4.21}$$

where $\Psi(0)$ is the wave function at the origin [4.45]. A heuristic argument for eq. (4.21) is that the annihilating charmed quarks are heavy and so the interaction is fairly local.

If we assume the validity of eq. (4.21), then the branching fraction for ψ' direct decay to ordinary hadrons is about 9%.

4.5.5. $\psi' \to \gamma\chi$ Decays

If we consider the ψ as the triplet S ground state of charmonium and the ψ' a radially excited state of the ψ, other states should exist which could be reached by radiative transitions from the ψ' [4.46-4.49]. The expected scheme is shown in fig. 4.13. There are three triplet P states and two singlet S states. The states above the ψ could decay radiatively to the ψ or could decay directly to ordinary hadrons. As will be discussed below, the P states are now well established. There are also candidates for the two pseudoscalar S states, but they are in need of further experimental confirmation.

The $\psi' \to \gamma\chi$ decays have been detected by three techniques: 1) by detecting the hadronic decay of the χ's, 2) by detecting the ψ and one or both of the cascade photons in $\psi' \to \gamma\chi \to \gamma\gamma\psi$, and 3) by detecting monochromatic photons. We shall now discuss each of these techniques in turn.

<u>χ Decays to Hadrons</u>

These decays are detected by finding events in which the missing mass recoiling against all of the observed charged particles is consistent with that of a photon [4.50]. In general there is insufficient resolution to distinguish between a photon and a π^0, but fortunately ψ' decays involving a single π^0 occur infrequently enough that they are not a severe background.

Figure 4.14 shows χ mass spectra obtained by this technique after a one constraint fit has been performed [4.44]. Figure 4.14a shows the data for $\chi \to 4\pi^{\pm}$. Here events with masses above 3.60 GeV/c^2 are consistent with the second order electromagnetic decay $\psi' \to 4\pi$. There are three other clear peaks at masses of about 3415, 3500, and 3550 MeV/c^2 each of which we identify with a χ state.

Figures 4.14b, 4.14c, 4.14d show the mass plots for χ decays to $K^+K^-\pi^+\pi^-$, $3\pi^+3\pi^-$, and $\pi^+\pi^-$ or K^+K^-. The same three states are found in these plots, but not as clearly in all cases. In the $K^+K^-\pi^+\pi^-$ mode the $\chi(3510)$ is weak. In the $3\pi^+3\pi^-$ mode the $\chi(3510)$ and $\chi(3550)$ are not resolved. In the $\pi^+\pi^-$ or K^+K^- mode, the $\chi(3415)$ is quite clear and there are eleven events in the vicinity of the $\chi(3550)$ with an estimated background of only two or three events. There are only two events in the vicinity of the $\chi(3510)$ and these are consistent with backgrounds. These decays into two pseudoscalars will be important when we consider the spin assignments of the χ states in section 4.6.2.

<u>χ Decays to $\gamma\psi$</u>

Two methods have been used to detect the $\psi' \to \gamma\chi \to \gamma\gamma\psi$ cascade. In both methods the ψ is observed in its muon pair decay, so that the final state corresponds to $\psi' \to \gamma\gamma\mu^+\mu^-$.

In the first method, which has been used in the SPEAR magnetic detector, one detects $\mu^+\mu^-$ and observes a conversion of one of the photons in the 0.052 radiation lengths of material surrounding the beam pipe [4.35]. A one constraint fit is then performed to the event. A computer reconstruction of this type of event is shown in fig. 4.15.

In the second method, which has been used both at SPEAR [4.35] and at DORIS [4.38], both photons are detected in shower counters and the angle measurements are used to give a two constraint fit. This method provides worse resolution, but much higher statistics than the first method. It will prove useful in section 4.6.2. where we discuss the angular distributions.

Whichever method is used, there are two solutions for each event since one does not know <u>a priori</u> which photon was emitted first. This two-fold

ambiguity can be resolved by observing the widths of the reconstructed χ masses since the first photon will be monochromatic, while the second is Doppler shifted by the motion of the χ.

Figure 4.16 shows the $\gamma\psi$ masses obtained by the first method at SPEAR [4.37]. There are four clusters of events. The $\chi(3510)$ and $\chi(3550)$ are clearly visible and the two-fold ambiguity is resolved in favor of the higher mass states in agreement with the observation of χ's from their hadronic decays. There is a single event consistent with coming from the $\chi(3415)$.

The new element in fig. 4.16 is the cluster of four events at 3454 MeV/c^2. Since the expected background in all of fig. 4.16 is only one event, it seems unlikely that this cluster is due to background. Nevertheless, these four events are the only evidence for this possible state; it clearly is on shaky experimental ground and badly needs confirmation. We shall tentatively dub it the $\chi(3455)$ and discuss it, but the reader is forewarned of its weak status.

The latest data from DORIS [4.39] show the same pattern as fig. 4.16, but with fewer events and worse resolution. There are five events at the $\chi(3510)$, one event each consistent with coming from the $\chi(3415)$ and $\chi(3550)$, and one event ambiguous between the $\chi(3510)$ and the $\chi(3455)$

Monochromatic Photons

In order to measure the branching ratio for $\psi' \to \gamma\chi$, it is necessary to detect the monochromatic photons. Two measurements of this type have now been performed. The first comes from the magnetic detector at SPEAR [4.37]. Photons were detected by observing conversions in the material around the beam pipe. For low energy photons, the rms energy resolution is about 2%

for this technique. Photon energy spectra from ψ and ψ' decays are shown in fig. 4.17. A peak is seen in the ψ' spectrum at 261 MeV, corresponding to the $\chi(3415)$. The branching fraction for $\psi' \to \gamma\chi(3415)$ from these data is 0.075 ± 0.026. The other χ states correspond to lower photon energies and are not visible because of rapidly falling acceptance in this region.

A special experiment was conducted at SPEAR to search for monochromatic photons by a collaboration from Maryland, Pavia, Princeton, San Diego, SLAC, and Stanford (MPPSDSS) [4.25]. Arrays of large NaI crystals were used to detect the photons with about 5% rms energy resolution. The data from ψ and ψ' decays are shown in fig. 4.18. There are no significant peaks in the ψ spectrum, but four clear peaks are apparent in the ψ' spectrum. The first three correspond to the $\chi(3550)$, $\chi(3510)$ and $\chi(3415)$, and the last is from the Doppler broadened photon in $\chi(3510) \to \gamma\psi$ decay. The branching ratios for $\psi' \to \gamma\chi$ are 0.072 ± 0.023, 0.071 ± 0.019, and 0.070 ± 0.020 for the $\chi(3415)$, $\chi(3510)$, and $\chi(3550)$, respectively. The branching fractions for $\psi' \to \gamma\chi(3415)$ determined by these two experiments are in excellent agreement.

4.5.6. Is Anything Missing?

Two years ago, before the χ states and direct ψ' decays were found, there was a large fraction of ψ' decays that could not be accounted for [4.33]. It is now interesting to ask whether the situation has been rectified. The accounting is given in table 4.7. We can account for $(89 \pm 9)\%$ of the ψ' decays. There is still room for new decay modes but they are no longer mandated by the data.

4.6. χ States

4.6.1. Masses and Branching Ratios

Table 4.8 lists the mass determinations of the χ states. The average values are 3413 ± 5, 3454 ± 7, 3508 ± 4, and 3552 ± 6 MeV/c^2.

Tables 4.9, 4.10, and 4.11 give a compendium of χ branching ratios.

4.6.2. Spins and Parities

Although we have not explicitly determined the spin of any of the χ states, we now have enough information to give an experimentally preferred assignment under the mild, but powerful, assumption that we are dealing with the low lying states of a fermion-antifermion system.

We will assume that the possible spin-parity states are those shown in fig. 4.13, 0^-, 0^+, 1^+, and 2^+. We shall then go through a series of arguments which will exclude certain spin-parity assignments for certain states. At the end, if we make the additional assumption that each of the four spin states should be assigned to one of the four χ states, we obtain a unique solution.

The first piece of evidence for spin assignments comes from χ decays to two pseudoscalars, $\pi^+\pi^-$ or K^+K^-. The possible J^{PC} states for two pseudoscalars are 0^{++}, 1^{--}, 2^{++}, etc. The χ states have even C since they are reached by radiative transitions from the ψ'. Therefore any χ state which decays to $\pi^+\pi^-$ or K^+K^- must have $J^P = 0^+$, 2^+, etc. In fig. 4.14 there is overwhelming evidence that the $\chi(3415)$ decays to $\pi^+\pi^-$ or K^+K^- and there is strong evidence for the $\chi(3550)$ decay to $\pi^+\pi^-$ or K^+K^-.

The other technique which can be used to determine χ spins is a study of angular distributions of the photons. The most information comes from the $\psi' \to \gamma\chi \to \gamma\gamma\psi \to \gamma\gamma\mu\mu$ cascade [4.51-4.53]. There are five independent angles as illustrated in fig. 4.19. For spin 0, the distribution is unique,

$$W(\theta, \phi, \Theta, \theta', \phi') = (1 + \cos^2\theta)(1 + \cos^2\theta') \quad . \qquad (4.22)$$

For other spins, the distirbutions are quite complex and depend on which multipoles are excited. A study has been made at SPEAR of these distribu-

tions for the $\chi(3510)$ using the second method of detecting cascade events discussed in section 4.5.5. [4.21]. Preliminary results indicate that the observed distributions completely exclude spin 0. Work is now in progress to determine whether spin 1 or 2 is favored and which multipoles are involved in the decay.

The DESY-Heidelberg collaboration has also concluded that the $\chi(3510)$ spin is not zero by just studying the θ distribution [4.54].

The angular distribution of the photon in the production of the $\chi(3415)$ and the $\chi(3550)$ has been studied in $\chi \to 4\pi$ and $\chi \to K^+K^-\pi^+\pi^-$ decays [4.44]. Figure 4.20 shows the θ distributions when χ's are detected in these modes. The angular distribution must be of the form

$$W(\theta) \propto 1 + \alpha \cos^2\theta, \tag{4.23}$$

and from eq. (4.22), $\alpha = 1$ for spin 0. Fits for α to all of the data for all hadronic modes give [4.44].

$$\alpha = 0.3 \pm 0.4 \text{ for } \chi(3550), \tag{4.24}$$

$$\alpha = 0.1 \pm 0.4 \text{ for } \chi(3510), \tag{4.25}$$

and

$$\alpha = 1.4 \pm 0.4 \text{ for } \chi(3425). \tag{4.26}$$

Thus, the $\chi(3415)$ is consistent with spin 0, but the $\chi(3550)$ is inconsistent with spin 0 to about two standard deviations.

All of these arguments are summarized in table 4.12. A number of conclusions can be drawn: Without any assumptions, none of the three well established states, $\chi(3415)$, $\chi(3510)$, or $\chi(3550)$, can be pseudoscalar. Also if the $\chi(3550)$ has a spin below 4, its spin-parity must be 2^+. If we assume that the four candidate spin states each correspond to one of the

four χ states, there is a unique assignment:

State	
$\chi(3550)$	2^+
$\chi(3510)$	1^+
$\chi(3445)$	0^-
$\chi(3415)$	0^+ .

Note that the $\chi(3455)$ has been assigned to be a pseudoscalar, not because we know anything about it, but because that was the only slot left. There are other possibilities. Jaffe suggested that this state could be an exotic [4.55] and Harari suggested that it could be a singlet D state, $J^{PC} = 2^{-+}$ [4.56].

4.6.3. Comparisons to Theoretical Models

The data on P states appear to be in reasonable agreement with most charmonium models. First, the order of the states is correct. In all models the 2^+ state should be heaviest and the 0^+ state should be lightest. Second, the ratio of $\psi' \to \gamma\chi$ partial widths is in agreement with the simplest assumption: that they should be proportional to the phase space factor for dipole transitions. We expect:

$$\begin{array}{ccccc} & (\psi' \to \chi(3550)) & : & (\psi' \to \chi(3510) & : & \chi(\psi' \to \chi(3415) \\ = & 5k^3 & : & 3k^3 & : & k^3 \\ = & 1.0 & : & 1.4 & : & 1.6 \ , \end{array} \qquad (4.27)$$

where k is the available momentum and the coefficients are spin factors. With large errors the observed values are:

$$1.0 \quad : \quad 1.01 \quad : \quad 1.04 \ . \qquad (4.28)$$

The $\chi(3510)$ has a larger branching fraction to $\gamma\psi$ than either the $\chi(3415)$ or $\chi(3550)$, presumably due to a suppression of $\chi(3510) \to$ hadrons. This behavior was expected for the 1^+ P state in models in which C-even states decay to hadrons via two massless vector gluons [4.57]. Since a spin 1 particle cannot decay into two massless vector particles, these decays are suppressed.

The assignment of the $\chi(3455)$ as the η_c' appears to be in strong disagreemnt with models where it decays via two vector gluons. Chanowitz and Gilman [4.58] point out that the matrix element for $\psi' \to \gamma\eta_c$ is related to that for $\eta_c' \to \gamma\psi$. From this they conservatively deduce that the total decay width of the $\chi(3455)$ is at most a few tens of keV whereas one expects a width of several MeV in these models.

4.7. The X(2830)

Two experiments at DORIS have reported evidence for a state at about 2830 MeV/c^2 which is detected in the sequence $\psi \to \gamma X \to \gamma\gamma\gamma$ [4.24,4.59]. Only the photon angles are measured and a one-constraint fit is performed. Backgrounds are $\psi \to \gamma\eta$, $\psi \to \gamma\eta'$, and radiative (non-resonant) two photon production.

The highest $\gamma\gamma$ invariant mass for each event is plotted in fig. 4.21, along with a curve showing the expected events from radiative two photon production and reflections from $\gamma\eta$ and $\gamma\eta'$ decays. The peak around 2.83 GeV/c^2 contains 30 events with 14 expected from backgrounds. This corresponds to about a four standard deviation effect.

No experiment at SPEAR has been sensitive to the three photon mode. Originally, it was reported from DORIS that $\psi \to \gamma X \to \gamma p\bar{p}$ with a branching fraction of

about 2×10^{-4}, based on the observation of two events [4.38]. This result was later withdrawn [4.39], but in the meantime a search was made for the $p\bar{p}$ decay mode in the SPEAR magnetic detector [4.20]. The background is $\psi \to p\bar{p}\pi^0$ since a π^0 and photon will not be completely separable by missing mass. The data are shown in fig. 4.22. There is no sign of the X(2830) and an upper limit on the branching fraction for $\psi \to \gamma X \to \gamma p\bar{p}$ can be set at 4×10^{-5}. Searches for X(2830) decays into other hadronic modes have all been unsuccessful, but none of the limits are small enough to cast doubt on the existence of the X(2830).

The status of the X(2830) and the $\chi(3455)$ are quite similar. We have enough evidence to take these state seriously, but not enough to conclusively establish them. Confirmation of both is badly needed.

4.8. Summary

In the two and one half years after the discovery of the ψ, we have learned a great deal about it and its relatives. In some cases we understand a state of charmonium better than its analogue in light quarks. An attempt to summarize as much of this information as possible on one page is made in fig. 4.23.

As we look to future work in this field it is clear that a great deal of it should and will go into understanding the structure of the charmonium states in the 4 GeV region and into studying the spectroscopy of charmed particles. There is, however, more work that should be done on ψ and ψ' decays. Below is a list in no particular order. Some of these items can be worked on now, others will have to await better detectors.

1) The status of the 0^- states is clearly the outstanding question. The masses and transition widths to these states are crucial parameters for charmonium calculations.

2) Although we now have a preferred set of χ spin assignments, it is important to determine the spins directly without imposing assumptions on the possible values.

3) There is still a missing P state, the singlet 1^{+-} state. The best way of finding it may be in the $\chi(3550) \rightarrow \gamma 1^{+-}$ decay.

4) The direct ψ' decays to ordinary hadrons needs much more study.

5) The suggestions that there is $c\bar{c}$ mixing with the lighter quarks in the pseudoscalar states should be followed up. We have seen evidence for it in radiative ψ decays and in the rate of $\psi' \rightarrow \psi n$. Inclusive and exclusive state studies of η and η' production in ψ decays would be useful for the further study of this possible mixing.

6) Finally there is a great deal of bread and butter physics to be done. We can image mega- and multimega-event runs with powerful second generation detectors. Systematic measurements of all ψ and ψ' decay modes from these data could have three separate objectives:

a) To study the dynamics of charmonium annihilation.

b) To study ordinary hadron spectroscopy from a new perspective. In section 4.4.3, we saw that ψ decays to PV and VT mesons were allowed and that all channels were populated approximately equally. The scalar (S) and axial vector vector (A^+, A^-) multiplets of ordinary mesons are not well understood yet. By studying the allowed VS, VA^+, and PA^- ψ decays we may gain new insight into them. Note that the possible ϕS^* decay discussed in section 4.4.4. is a VS type decay; by SU(3) all the others should be present too.

c) And finally, to look for surprises which may provide the germ of the next level of understanding.

5. CHARMED MESONS PRODUCED IN e^+e^- ANNIHILATION

The theory of the quark structure and the decay properties of charmed mesons is discussed in sections 5.1 - 5.3. Section 5.4 gives a general description of the experimental detection of the D mesons in e^+e^- annihilation. Present measurements of all the masses, decay modes, spins, and production cross sections of the D mesons are given in sections 5.5 and 5.6. This chapter concludes with a discussion of the inclusive K spectrum above and below the charmed meson production threshold, section 5.7, and with a brief description of searches for F mesons and charmed baryons, section 5.8.

5.1. The Quark Structure and Masses of Singly Charmed Hadrons

The discovery of the charmed D mesons, which is recounted in this chapter, is a beautiful confirmation of another prediction of the charmed quark theory [5.1, 5.2], a theory which originally seemed tentative and abstract. In this section we describe the quark structure of the singly charmed mesons and baryons.

In quark theory, mesons consist of a quark-antiquark pair, the ordinary mesons being made up of a quark-antiquark pair selected from the non-charmed quarks u, d, s (table 2.1); and the ψ family consisting of a $c\bar{c}$ pair. The extension of this concept to a pair consisting of one u, d or s quark and one $\bar{c}$ (or the charge conjugate) leads to the prediction of charmed mesons. Table 5.1 presents the structure and internal quantum number of the pseudoscalar (D and F) and vector (D^* and F^*) families of charmed mesons [5.1]. It is interesting to look at the SU_4 pseudoscalar multiplets, fig. 5.1, which contains the D, F, and η_c as well as the ordinary pseudoscalar mesons. We

note that the D and D* mesons have been found and studied in e^+-e^- annihilation events, but as this review is being written no evidence for the existence of F mesons has been found in any experiment.

Turning to the baryons, we can construct them with a total of one, two or three charmed quarks, but we shall consider here only the singly charmed baryons. Table 5.2 gives some of the properties of the spin 1/2 singly charmed baryons. which are predicted [5.1, 5.2, 5.5]. Evidence for the existence of a charmed baryon has been found by B. Knapp et al.[5.3] and by E. G. Cazzoli et al [5.4] at proton accelerators. But as of this writing, no direct evidence has been found in e^+e^- annihilation events.

The mass of a charmed hadron, $M(h_c)$, is given by

$$M(h_c) = \sum_q m_q + \Delta m_{split} \tag{5.1}$$

where $\sum_q m_q$ is the sum of the effective quark masses and very crudely gives the mass scale of the charmed hadrons. Δm_{split} is the correction to $\sum m_q$ which depends on the angular momentum and spin configuration.

We can obtain a crude set of quark masses by using the approximate relationships

$$m_u = m_d = 1/2\ \rho \text{ mass} \tag{5.2a}$$

$$m_s = 1/2\ \phi \text{ mass} \tag{5.2b}$$

$$m_c = 1/2\ \psi \text{ mass} \tag{5.2c}$$

to construct table 5.3.

From table 5.1 and table 5.3, this crude theory predicts $m_D \approx 1.94$ GeV/c^2, which is close to the experimental values for the D and D^* mesons. It predicts the F and F^* mesons should be heavier, $m_F \approx 2.06$ GeV/c^2. The lowest lying charm baryons, the Λ_c and Σ_c should have masses near 2.33 GeV/c^2 Thorough discussions of the theory of charmed hadron masses occur in the classic paper of De Rújula et al., [5.5], and in the review paper of Jackson [5.2].

We have discussed here only the lower mass states of the singly charmed hadrons. Clearly, as with ordinary hadrons, higher and higher mass states can also exist. Indeed, now that we know that the D mesons exist, we are confident that higher mass states must exist. Hence, while the data which are discussed in this section cover only the lower mass states, we should remember that we are probably looking at only a small part of an elaborate and extensive family of particles—a family as rich in structure as that of the ordinary hadrons.

Having discussed the nature of the charmed mesons, we discuss next their decay properties. We discuss first the decay of the lowest mass states, that is, those charmed mesons which energetically can only decay to ordinary mesons.

5.2. Weak Decay of Charmed Mesons to Ordinary Mesons

The basic postulate of charm theory is that charm, like strangeness, is conserved in strong and electromagnetic interactions. Hence the decays of the charmed mesons to ordinary mesons are expected to occur only through weak interactions. A simple way to understand the decay of these mesons is to consider the decay properties of the constituent quarks.

The conventional Weinberg-Salam weak interaction theory applied to the quarks [5.1, 5.2] divides them into two doublets

$$\begin{pmatrix} u \\ d' \end{pmatrix}, \begin{pmatrix} c \\ s' \end{pmatrix} \tag{5.3a}$$

where

$$d' = d \cos \theta_c - s \sin \theta_c \quad , \tag{5.4a}$$

$$s' = d \sin \theta_c + s \cos \theta_c \; ; \tag{5.4b}$$

and θ_c is the Cabibbo angle [5.6]

$$\sin \theta_c \approx .23 \tag{5.5}$$

The two doublets, eq.(5.3a), combined with the two conventional lepton doublets

$$\begin{pmatrix} \nu_\mu \\ \mu^- \end{pmatrix} \begin{pmatrix} \nu_e \\ e^- \end{pmatrix} \tag{5.3b}$$

have a 4-fermion interaction given by

$$H_W = \frac{G}{\sqrt{2}} (J_\ell + J_h)(J_\ell + J_h)^+ \tag{5.6}$$

Here J_ℓ and J_h are the leptonic and hadronic weak currents. Following Jackson [5.2], it is useful to sort out the particle content of H_W. We obtain [5.6] :

charged leptonic current

$$J_\ell^c = \bar{\nu}_e e + \bar{\nu}_\mu \mu \tag{5.7a}$$

neutral leptonic current

$$J_\ell^N = \bar{\nu}_e \nu_e + \bar{\nu}_\mu \nu_\mu - \bar{e} e - \bar{\mu} \mu \tag{5.7b}$$

charged hadronic current

$$J_h^C = \cos\theta \, (\bar{u} d + \bar{c} s) + \sin \theta \, (\bar{u} s - \bar{c} d) \tag{5.7c}$$

neutral hadronic current

$$J_h^N = \bar{u} u + \bar{c} c - \bar{d} d - \bar{s} s \tag{5.7d}$$

We note that the strangeness changing charged hadronic current ($\bar{u}s$) is suppressed relative to the non-strangeness changing term ($\bar{u}d$) by the factor $\sin\theta_c/\cos\theta_c$; and this is the basic reason for the introduction of θ_c. We also note that there is no strangeness changing neutral hadronic current; and this is one of the basic reasons for introducing the charmed quark.

Concentrating our attention on the charm terms in eq. (5.7c), we observe that the weak interaction decay amplitude for the c quark going to the s quark is proportional to $\cos\theta_c$, whereas the amplitude for c going to d is proportional to $\sin\theta_c$. Since the ratio $\cos^2\theta_c/\sin^2\theta_c \approx .05$, almost all decays of D or D^* mesons will contain an s quark and hence a K meson.

There is a nice way, fig. 5.2, to represent these considerations pictorially using the hypothetical intermediate boson $W^{\pm}$, fig. 5.2. Figures 5.3a, b, and c show Cabibbo allowed weak decays of the D^0 to $K^-\pi^+$, K^- + hadrons, and the semi-leptonic final state $K^- + e^+ + \nu_e$. From fig. 5.3, we expect that some of the prominent decays of the D^0 will be

$$\text{hadronic final states } K^-\pi^+,\ K^{*-}\pi^+,\ K^-\pi^+\pi^-\pi^+,\ \bar{K}^0\pi^0,\ \bar{K}^0\pi^+\pi^- \tag{5.8a}$$

$$\text{semi-leptonic final states } K^-e^+\nu_e,\ K^{*-}e^+\nu_e,\ K^-\mu^+\nu_\mu,\ K^{*-}\mu^+\nu_\mu \tag{5.8b}$$

Indeed we expect that the semi-leptonic branching ratios should be similar in size to the branching ratios to individual hadronic final states. Hence the semi-leptonic decays of lowest state singly charmed mesons are an important signature for the charmed origin of the leptons, section 5.7 and chapter 6.

The decay of the D^+ meson will also be dominated by the production of a K^- or $\bar{K}^0$; hence some prominent decay modes are $\bar{K}^0\pi^+$ and $K^-\pi^+\pi^+$. The $D^+ \longrightarrow$

$K^-\pi^+\pi^+$ is an important signature for charm because such a decay is forbidden if the D^+ consists of ordinary quarks, namely $\bar{s}u$. However, for ordinary mesons, the decay $M^+ \longrightarrow K^-\pi^+\pi^+$ is exotic but the decay $M^+ \longrightarrow K^+\pi^-\pi^+$ is allowed. Therefore, if the $K^-\pi^+\pi^+$ mode is detected and the $K^+\pi^-\pi^+$ is not detected, this is strong evidence for charm.

The decays of the F meson to ordinary mesons can be understood in a similar way. The decay of the F mesons' c quark to an s quark leaves an s and $\bar{s}$ in the final state. Therefore, prominent decay modes should be

$$F^+ \longrightarrow K^+\bar{K}^o,\ K^+K^-\pi^+ \ldots\ldots \tag{5.9a}$$

Another decay mode

$$F^+ \longrightarrow \eta\pi^+ \tag{5.9b}$$

may also be prominent if the s and $\bar{s}$ form η.

The total hadronic decay width of the D can be estimated using figures 5.3a and 5.3b; and taking the probability of the $(u + \bar{d})$ system to decay to hadrons to be about 1. Then the rate is given simply by the weak decay of the c quark.

$$c \longrightarrow s + u + \bar{d} \tag{5.10a}$$

analogous to muon decay

$$\mu^- \longrightarrow \nu_\mu + e^- + \bar{\nu}_e \tag{5.10b}$$

Putting in a factor of 3 for color,

$$\Gamma_{total}(D \to \text{hadrons}) = 3\left(\frac{m_c}{m_\mu}\right)^5 \cos^4\theta_c\, \Gamma(\mu \to \bar{\nu}_\mu e \nu_e) \sim 9\times 10^{11}\,\text{sec}^{-1} \tag{5.11}$$

Gaillard et al. [5.1] multiply by an enhancement factor which increases Γ_{total} $(D \to \text{hadrons})$ to 10^{13} sec^{-1}. Calculations [5.1, 5.2] of partial decay rates for

the states discussed above have varied from a few percent to tens of percent. Table 5.4 gives some recent calculations [5.7].

We turn next to the decay of the higher mass singly charged mesons which are not limited to weak interaction transitions.

5.3. Strong and Electromagnetic Decays between Charmed Mesons

Strong and electromagnetic decays of singly charmed mesons to lower mass singly charmed mesons can obviously occur if charm and strangeness are conserved in the decay. Consider the D^o and D^{*o}, taking the mass of the D^{*o} to be greater than that of the D^o, as has been found by experiment, section 5.5. Then we expect the electromagnetic decay

$$D^{*o} \longrightarrow D^o + \gamma \quad ; \tag{5.11a}$$

and since the mass difference is sufficiently large, section 5.5, also the strong decay

$$D^{*o} \longrightarrow D^o + \pi^o \tag{5.11b}$$

Both decays have been detected, section 5.5. The strong decay

$$D^{*+} \longrightarrow \pi^+ + D^o \tag{5.11c}$$

has also been found, section 5.5.

Our present picture of the charmed mesons is thus analogous to that of the ordinary mesons. The higher mass states decay by strong and electromagnetic interactions and will increase in width as their mass increases. The lowest lying states must decay by weak interactions and will have narrow widths characteristic of weak interactions.

5.4. Production and Detection of D Mesons in e^+e^- Annihilation

The search for D meson production in e^+e^- annihilation was based on three predicted characteristics of the D's. First, since they must be produced in pairs to conserve charm, the energy range for the search should begin at the ψ' and extend into the $4 \lesssim E_{cm} \lesssim 5$ GeV region. Second, narrow resonances in $K\pi$, $K\pi\pi$, $K\pi\pi\pi$ will be the signature. Third, the branching ratio into a particular mode may be less than 5 or 10%, hence large statistics are needed. Indeed, an earlier search [5.8] using 10,000 hadronic events at $E_{cm} = 4.8$ GeV did not find the D's. Finally, in a sample of 29,000 hadronic events of the SLAC-LBL Magnetic Detection Collaboration in the energy range $3.9 \leq E_{cm} \leq 4.60$ GeV, narrow invariant mass peaks with an average mass of 1.865 GeV/c^2 were found by G. Goldhaber and F. Pierre in the neutral states [5.9] $K^{\pm}\pi^{\mp}$ and $K^{\pm}\pi^{\mp}\pi^{+}\pi^{-}$, fig. 5.4. We show next that it is very reasonable to interpret these sytems as decay modes of the D^o.

The narrow widths and presence of K's are two arguments for believing that these are the decay modes of the charmed D^o meson. A further argument [5.9] comes from fig. 5.5, the spectra of the masses recoiling against the $K\pi$ and $K\pi\pi\pi$ systems. The lower limit on the observed masses of the recoil systems is about 1.87 GeV/c^2. Hence the D^o production is consistent with

$$e^+ + e^- \longrightarrow D^o + X^o \tag{5.12a}$$

where

$$m_{X^o} \gtrsim m_{D^o} \quad , \tag{5.12b}$$

so that the recoil X^o system can always contain a D^o mass particle. A final argument [5.9] is that the threshold for production of the $K\pi$ and $K\pi\pi\pi$ systems is above 3.7 GeV/c^2 since no $K\pi$ or $K\pi\pi\pi$ signals were found in very large ψ and ψ' samples.

Similar evidence [5.10] has been found for the $K^{\mp}\pi^{\pm}\pi^{\pm}$ decay mode of the $D^{\pm}$ at a mass of 1.876 GeV/c^2 in a sample of 19,000 hadronic events produced at E_{cm} = 4.03 GeV, fig. 5.6. A strong argument for the charm explanation of this decay mode is that there is no signal in the non-exotic $K^{\mp}\pi^{\pm}\pi^{\mp}$ system. And again the masses of the recoil system are above 1.87 GeV/c^2, as is required by the charm explanation. The assignment of the $K\pi$, $K\pi\pi\pi$ systems and the $K\pi\pi$ system to the same D isospin doublet is reasonable for five reasons: The masses are similar, all the widths are narrow, all the decays contain K mesons, the recoil mass spectra are similar, and the charm theory predicts such a doublet.

An important step in confirming the existence of the D and perhaps other charmed mesons was the discovery of electrons which must come from the semi-leptonic decay modes of these mesons (see eq. (5.8b)). This subject is discussed and the references given in section 6.6 because it must be considered in conjunction with a discussion of heavy lepton sources of electrons.

Another test of the charm explanation of the D mesons is to see if the decay of the D^o is indeed weak and hence violates parity conservation. First we note that the final state in the decay $D^o \longrightarrow K^{\pm}\pi^{\mp}$ consists of two pseudoscalar mesons and hence has a natural spin-parity, $J^P = 0^+, 1^-, 2^+, \ldots$ but the spin-parity of the final state in $D^{\pm} \longrightarrow K^{\mp}\pi^{\pm}\pi^{\pm}$ can be studied via a Dalitz plot. It is found [5.11] that for this state J^P is <u>not</u> compatible with 1^- or 2^+. We also note that a three pseudoscalar final state cannot have $J^P = 0^+$. Hence assuming that

the $D^o, D^{\pm}$ are an isospin doublet, we find parity conservation is violated in the decay of the D.

In order to learn more about the D meson family, we turn to a detailed study of the D^* to D decay and the recoil spectra against D mesons.

5.5. Masses, Spins, and Decay Modes of the D Meson Family

The only D^* decay which has been directly observed is $D^{*+} \rightarrow D^o\pi^+$. The SLAC-LBL collaboration has observed this decay at an average E_{cm} of 6.8 GeV, where the π^+ has enough momentum to be visible in the detector [5.17]. Figure 5.7 shows the $D^{*+} - D^o$ mass difference.

There are four important features of this decay:

1. The restrictive kinematics of the decay caused by the very small Q value leads to an extremely accurate measurement of the $D^{*+} - D^o$ mass difference, which is found to be 145.3 ± 0.5 MeV/c^2. This measurement becomes an important constraint in fitting the D recoil spectra, which we discuss below.

2. The kinematics also allow unusually good mass resolution, as can be seen from fig. 5.7. We can determine that, at the 90% confidence level, the full width of the D^{*+} must be less than 2.0 MeV/c^2.

3. Finally the kinematics leads to an extremely background-free signal as can also be seen from fig. 5.7. The improvement in signal to background in detecting $D^{*+} \rightarrow D^o\pi^+ \rightarrow K^-\pi^+\pi^+$ rather than just $D^o \rightarrow K^-\pi^+$ is about two orders of magnitude and the event rate, for full acceptance is lower by only a factor of four. Thus, this decay mode may prove important in studying charm particle production from reactions on fixed targets, where background suppression is crucial

4. An added bonus in detecting this decay is that it provides clear evidence against any large $D^o - \overline{D^o}$ mixing. In fig. 5.7 there is a clear signal

in $(K^-\pi^+)\pi^+$ (fig. 5.7a) but at most a small signal consistent with background in $(K^+\pi^-)\pi^+$. At the 90% confidence level, the D^o decays as if it were a $\overline{D^o}$ (i.e. to $K^+\pi^-$ rather than $K^-\pi^+$) less than 16% of the time. It is likely that any first order charm-changing neutral currents would produce D^o to $\overline{D^o}$ transitions on a time scale considerably shorter than the D^o lifetime. Thus the absence of large $D^o - \overline{D^o}$ mixing indicates the absence of first order charm changing neutral currents.

The SLAC-LBL Collaboration has obtained the charmed meson production data near threshold shown in table 5.5. The 4.028 and 4.415 energy points were chosen because they are the peaks in the total hadronic cross section, fig. 2.5, where charmed meson production may be largest. The 4.028 point is also close enough to the threshold of D production to apply the theoretical analyses of De Rújula et al., [5.12] and of Lane and Eichten [5.13]. For simplicity we base the following discussion on the former paper [5.12].

Figure 5.8 shows the expected level structure of the D and D* mesons and the possible decays of the D* to the D. Therefore near threshold the simplest sources of D^o are:

$$e^+ + e^- \longrightarrow D^o + \overline{D}^o \tag{5.13a}$$

$$e^+ + e^- \longrightarrow D^o + \overline{D}^{*o} \tag{5.13b}$$

$$e^+ + e^- \longrightarrow D^{*o} + \overline{D}^o,\ D^{*o} \longrightarrow D^o + \pi^o \tag{5.13c}$$

$$e^+ + e^- \longrightarrow D^{*o} + \overline{D}^o,\ D^{*o} \longrightarrow D^o + \gamma \tag{5.13d}$$

$$e^+ + e^- \longrightarrow D^{*o} + \overline{D}^{*o},\ D^{*o} \longrightarrow D^o + \pi^o \tag{5.13e}$$

$$e^+ + e^- \longrightarrow D^{*o} + \overline{D}^{*o},\ D^{*o} \longrightarrow D^o + \gamma \tag{5.13f}$$

$$e^+ + e^- \longrightarrow D^{*+} + D^-,\ D^{*+} \longrightarrow D^o + \pi^+ \tag{5.13g}$$

$$e^+ + e^- \longrightarrow D^{*+} + D^{*-},\ D^{*+} \longrightarrow D^o + \pi^+ \tag{5.13h}$$

It is obvious that reactions 5.13a and 5.13b will give recoil mass spectra which peak at the $\overline{D}^o$ and $\overline{D}^{*o}$ masses, respectively. It may not be so obvious that near threshold the other reactions also produce peaks in the recoil mass spectra. That

this is so can be seen by considering reactions 5.13c and supposing that the energy is exactly at threshold for this reaction. Then the D^{*o} and $\bar{D}^{o}$ are produced at rest, and the recoil mass is simply

$$m(\bar{D}^{o} + \pi^{o}) = \left(m^{2}_{\bar{D}^{o}} + 2E_{\pi^{o}} m_{\bar{D}^{o}} + m^{2}_{\pi^{o}}\right)^{1/2} \; ; \; E_{\pi^{o}} \approx m_{\pi^{o}} \qquad (5.14)$$

Indeed, given sufficient statistics, we might expect a recoil mass spectrum with many peaks.

However, as shown in fig. 5.9, there are just two strong peaks at about 2.01 GeV/c^2 and about 2.15 GeV/c^2, and a possible very weak peak at about 1.87 GeV/c^2. A very reasonable explanation of these peaks is shown schematically in fig.5.10. The 2.01 peak corresponds to the $\bar{D}^{*o}$ mass peak in reaction 5.13b superimposed on the $\bar{D}^{o} + \pi^{o}$, $\bar{D}^{o} + \gamma$, and $D^{-} + \pi^{+}$ reflection masses from reactions 5.13c, 5.13d, 5.13e, and 5.13g. This superposition occurs because of the confluence of two effects:

1. At $E_m = 4.028$ GeV, the reaction $e^{+} + e^{-} \longrightarrow D^{*o} + \bar{D}^{o}$ is close to threshold so that eq. 5.14 is approximately correct.
2. As shown below, the Q of the decay $D^{*o} \longrightarrow D^{o} + \pi^{o}$ is only a few MeV. Hence

$$m(D^{o} + \pi^{o}) \approx m_{D^{o}} + m_{\pi^{o}} \approx m_{D^{*o}} \qquad (5.15)$$

Similarly the 2.15 peak is a superposition of the reflection masses $\bar{D}^{*o} + \pi^{o}$ and $\bar{D}^{*o} + \gamma$ from reactions 5.13e and 5.13f, respectively.

Quantitative fits to the recoil mass spectra have been made using the momentum of the D^{o} [5.14] and using the kinetic energy [5.15, 5.16]. This fitting procedure is difficult and only preliminary results are available [5.14, 5.15]. These preliminary results are given in table 5.6. We make some comments on these results:

(a) $D^{*o} \to D^o$ has just enough energy to produce the π^o. This suppresses the strong decay of the D^{*o} so that the electromagnetic decay is equally strong.

(b) The $D^o\bar{D}^o$ pair production is barely observed, and the $D^o\bar{D}^{*o}$ and $D^{*o}\bar{D}^{*o}$ production are much larger. These results are not in quantitative agreement with the predictions of De Rújula et al. [5.12] based on spin arguments.

(c) At this energy all D^o production can be explained by the reactions in eq. (5.13); there is no need for "inelastic" production reactions such as

$$e^+ + e^- \longrightarrow D^o + \bar{D}^{*o} + \text{additional hadrons} \qquad (5.16)$$

This is surely because the energy is close to threshold. At higher energy, we certainly expect the "pair" production reactions in eq. (5.13) to have small cross sections compared to either "inelastic" reactions such as eq. (5.16) or to the production of higher mass charmed mesons.

To summarize our knowledge of the D and D^* masses: the electromagnetic mass splitting of the D or D^* is only a few MeV, the separation between the D and D^* is about a pion mass, the reactions

$$D^{*o} \longrightarrow D^o + \pi^o, \gamma \qquad (5.17a)$$

$$D^{*+} \longrightarrow D^o + \pi^+ \qquad (5.17b)$$

$$D^{*+} \longrightarrow D^+ + \gamma \qquad (5.17c)$$

are energetically allowed, the reaction

$$D^{*+} \longrightarrow D^+ + \pi^o \qquad (5.17d)$$

may be energetically allowed, but the reaction

$$D^* \longrightarrow D^+ + \pi^- \qquad (5.17e)$$

is energetically forbidden.

The angular distributions of D's produced near threshold gives information on the D and D^* spins. First we note that since charm is conserved in all interactions that conserve parity, the parity of the D is arbitrary and we can define it to be negative following the usual convention. The existence of the decay $D^* \to D\pi$ then determines that the D^* parity is given by

$$P_{D^*} = (-1)^{(J_D - J_{D^*})} \tag{5.18a}$$

if either J_D or J_{D^*} is zero. The existence of the decay $D^* \to D\gamma$ trivially determines that the spins of the D and the D^* cannot both be zero. Thus using eq. (5.18a), if $(J_D + J_{D^*}) < 2$, the only possibilities are

$$J_D^P = 0^-, \quad J_{D^*}^P = 1^- \tag{5.18b}$$

or

$$J_D^P = 1^-, \quad J_{D^*}^P = 0^- \tag{5.18c}$$

The latter possibility is ruled out by two separate distributions, the distribution of the K^- from $D^o \to K^-\pi^+$ decays relative to the D^o direction in reaction (5.13b) and the distribution of D^o polar angles from reaction (5.13e) [5.15,5.23] . Thus, we conclude that either $(J_D + J_{D^*}) \geq 2$ or the spin and parities are given by eq. (5.18b). The latter possibility is what we expect for the bound states of a quark-antiquark pair.

5.6. D Production Cross Sections and Branching Ratios

In Table 5.7, we give $\sigma \cdot B$, the product of the D production cross sections σ and the decay branching ratio B. To make a rough calculation of B we assume that at $E_{cm} = 4.028$ GeV, half of the total hadronic cross section, σ_h is due to charm production, and that 3/4 of the charm cross section leads to D^o or $\overline{D^o}$ as opposed to $D^{\pm}$ production. Then, using $\sigma_h = 33$ nb and table 5.7

$$B(D^o \to K^-\pi^+) \sim .57/(2\cdot\tfrac{1}{2}\cdot\tfrac{3}{4}\cdot 33) \sim 2\% \tag{5.19a}$$

The factor 2 in eq. (5.19a) occurs because both the D^o and $\overline{D^o}$ are counted in

the .57 value. Similarly

$$B(D^0 \to K^0\pi^+\pi^- \text{ or } \overline{K^0}\pi^+\pi^-) \sim 4\% \tag{5.19b}$$

$$B(D^0 \to K^-\pi^+\pi^-\pi^+) \sim 3\% \tag{5.19c}$$

$$B(D^+ \to K^-\pi^+\pi^+) \sim 5\% \tag{5.19d}$$

These ratios are smaller than originally predicted [5.1].

5.7. Inclusive K Meson Cross Sections

As discussed in section 5.2, we expect that almost all the decay modes of the D meson and many of the decay modes of the F meson will contain a K meson, either charged or neutral. Therefore an important test for the existence of charmed mesons is that the production of K mesons increase when the beam energy is above the charmed meson production threshold.

Clear evidence for such an increase has been seen in charged K production by the DASP Group [5.18]; in K_S^0 production by the PLUTO Group [5.19], and in K_S^0 production by the SLAC-LBL Magnetic Detector Collaboration [5.20]. We discuss these results in that order.

The DASP Group's cross section [5.18] for

$$e^+ + e^- \longrightarrow K^\pm + X \tag{5.20}$$

is shown in fig. 5.11. We note the dramatic increase in the cross section for $E_{cm} \gtrsim 4.0$ GeV and the peak at 4.03 GeV. A quantitative test of the prediction that almost all D meson decays contain a K meson is provided by defining

$$R_K(E_{cm}) = \sigma_K(E_{cm}) / \sigma_{\mu\mu}(E_{cm}) \tag{5.21a}$$

in analogy to

$$R(E_{cm}) = \sigma_{had}(E_{cm}) / \sigma_{\mu\mu}(E_{cm}) \tag{5.21b}$$

(See eq. 2.7.) Here σ_K is the total cross section for <u>events containing a charged or neutral kaon.</u>

Next we choose an E_{cm} below the charmed meson production threshold. Following ref. 5.18, we use 3.6 GeV. Then we define

$$\begin{aligned} R_K^{new}(E_{cm}) &= R_K(E_{cm}) - R_K(3.6) \\ R^{new}(E_{cm}) &= R(E_{cm}) - R(3.6) \\ &= R(E_{cm}) - 2.5 \end{aligned} \tag{5.21c}$$

Here 2.5 is taken as the average value of R in the $E_{cm} = 3.6$ region. If the increase in σ_{had} above 4 GeV is due completely to D meson production, we expect

$$R_K^{new}(E_{cm}) = R^{new}(E_{cm}) \qquad E_{cm} \gtrsim 4 \text{ GeV} \tag{5.22}$$

To test this experimentally, one uses [5.18] the expected relationship

$$\sigma_K = \sigma_{K^\pm} + \sigma_{K^o, \bar{K}^o} = 2\sigma_{K^\pm} \tag{5.23}$$

Figure 5.13 shows the comparison of R_K^{new} with R^{new}. In Fig. 5.12a R_K^{new} is seen on the average to be lower than R^{new}. However, if the contribution to R by a heavy lepton is subtracted from R^{new}, Fig. 5.12b, good agreement is obtained.

The inclusive cross sections for

$$e^+ + e^- \longrightarrow K_s^o + X \tag{5.24}$$

corrected for the unobserved $K_s^o \longrightarrow 2\pi^o$ decay mode, is shown in fig. 5.13 for the PLUTO Group data [5.19]. Figure 5.14 shows the data of the SLAC-LBL Magnetic Detector Collaboration [5.20]. The latter is in terms of an R'_K defined by

$$R'_K = 2\sigma_{K_s^o}/\sigma_{\mu\mu} \quad , \tag{5.25}$$

the $\sigma_{K_s^o}$ having been corrected for the unobserved $K_s^o \longrightarrow 2\pi^o$ decay mode and the detection efficiency. We note that, as we expect, the $\sigma_{K_s^o}$ has the same behavior as $\sigma_{K^\pm}$: a dramatic rise at $E_{cm} \sim 4.0$ GeV and a strong peak at $E_{cm} = 4.03$ GeV. Thus there is general agreement between all three experiments. The only difference is that the SLAC-LBL data shows an enhanced kaon yield at the 4.41 GeV peak in the total cross section, fig. 2.5; however, the DASP Group and PLUTO Group do not see the same enhancement.

5.8. Searches for F Mesons and Charmed Baryons

As this review is being written, no evidence for the existence of F mesons has been found in e^+e^- annihilation experiments or in any other experiments. Thus, while the great successes of the charm give us strong motivation for looking for the F mesons, as scientists who ultimately must base our knowledge on experiment, we must keep the F meson in the category of unconfirmed particles.

The situation with respect to charmed baryons is somewhat better. Cazzoli et al. [5.4] have found an event

$$\nu_\mu + p \longrightarrow \mu^- + \Lambda + \pi^+ + \pi^+ + \pi^+ + \pi^- \tag{5.26}$$

in a muon neutrino bubble chamber experiment which violates the $\Delta S = \Delta Q$ rule if it involves only non-charmed particles. An alternative explanation is that

the $\Lambda\pi^+\pi^+\pi^+\pi^-$ is the decay of a charmed baryon with mass 2426 ± 12 MeV/c^2. Such a mass is in reasonable agreement with the predicted [5.5] Σ_c^* mass of 2420 MeV/c^2 or the Σ_c mass of 2360 MeV/c^2, (see table 5.2).

More evidence for the existence of charmed baryons has been found by Knapp et al. [5.3] in a photoproduction experiment. They find a $\bar{\Lambda}\pi^-\pi^-\pi^+$ invariant mass peak at 2260 ± 10 MeV/c^2 with a width less than 75 MeV/c^2; and a higher mass state $\bar{\Lambda}(4\pi)^0$ at $\sim$ 2500 MeV/c^2. The latter decays into the former. The authors state that the 2260 MeV/c^2 state could be the charmed baryon Λ_c (table 5.2), and the $\sim$ 2500 MeV/c^2 state could be the Σ_c^* mentioned above.

No direct evidence for charmed baryons has been found in e^+e^- annihilation experiments as this review is being written. That is, no statistically significant invariant mass peaks have been found in states such as $\Lambda\pi$, $\Lambda 3\pi$ or $\Lambda 5\pi$. However, the SLAC-LBL Magnetic Detector Collaboration has some preliminary indirect evidence [5.21] that charmed baryons may begin to be produced in e^+e^- annihilations as E_{cm} increases from 4 to 5 GeV. As E_{cm} increases from 4 to 5 GeV, the production of Λ or $\bar{\Lambda}$'s and of antiprotons increases relative to the increase in the production of all particles in multiparticle events. Now, as indicated above, we expect charmed baryon masses to be in the range of 2.2 - 2.5 GeV/c^2. Hence the onset of charmed baryon production in the E_{cm} = 4 to 5 GeV region would simply explain the observed effect.

Clearly a great deal of fascinating work lies ahead of us in the search for the F meson and charmed baryons in e^+e^- annihilation physics. And the experimenters in the field, which include the authors, must keep an open mind as to what they will find.

6. ANOMALOUS LEPTON PRODUCTION IN e^+e^- ANNIHILATION

By anomalous lepton production we mean the production of electrons or muons by processes which are not contained in ordinary quantum electrodynamics and are not simply the decay of ordinary hadrons such as $\pi^- \to \mu^- + \bar{\nu}_\mu$ or $K^- \to e^- + \bar{\nu}_e + \pi^0$. Two anomalous sources have been found. One source is the leptonic decays of a particle of mass $1.90 \pm .10$ GeV/c^2 which seems to be a new, charged heavy lepton [6.1]. This particle called the U during the initial studies [6.1-6.4] will be called the τ in this paper because it appears to be the third charged lepton to be found. Theoretical properties of charged heavy leptons based on conventional weak interaction theory are discussed in section 6.1. The $e\mu$ events from the reaction

$$e^+ + e^- \to e^\pm + \mu^\mp + \text{no other detected particles}, \qquad (6.1)$$

which provided the first evidence for the existence of the τ are described in section 6.4; and the measured properties of the τ based on the $e\mu$ events are also given . More evidence for the existence of the τ and additional measured properties are given in section 6.5 where 2-prong, single lepton, inclusive events are discussed.

The second anomalous source of leptons to be found in e^+e^- annihilation is the semi-leptonic decays of charmed hadrons [6.4-6.8]; with the best studied component being the semi-leptonic decay of the D mesons just above their $E_{cm} \sim 4$ GeV production threshold. The theory of semi-leptonic decays of charmed mesons is outlined in section 6.2. In section 6.6 the experimental evidence for the decays is presented.

To complete the theoretical presentation, we discuss in section 6.3 the purely leptonic decays of integral spin particles; an anomalous source which has <u>not</u> been found in e^+e^- annihilation.

6.1. The Conventional Theory of Charged Heavy Leptons

6.1.1. Decays of a Sequential Heavy Lepton

It is an old idea [6.9] that the e and μ could be the first members of a sequence of leptons with charged and neutral members:

$$\begin{array}{ll} e^{\pm} & \nu_e, \bar{\nu}_e \\ \mu^{\pm} & \nu_\mu, \bar{\nu}_\mu \\ \ell_1^{\pm} & \nu_{\ell_1}, \bar{\nu}_\ell \\ \ell_2^{\pm} & \nu_{\ell_2}, \bar{\nu}_{\ell_2} \\ \cdot & \cdot \\ \cdot & \cdot \\ \cdot & \cdot \end{array} \tag{6.2}$$

Here each charged pair would have a unique lepton number which is carried only by the charged pair and their associated neutrinos, and all lepton numbers would be separately conserved. As is discussed in sections 6.4 and 6.5 there is now good evidence for the existence of the third charged lepton in the series. Using $\tau^{\pm}$ (from the Greek τριτον) to designate that member, and ν_τ for its associated neutrino, there are some simple predictions on its properties which can be made from conventional weak interaction theory.

Assuming that the τ lepton number is conserved, the electromagnetic decays

$$\tau^- \not\to e^- + \gamma \quad , \quad \tau^- \to \mu^- + \gamma \tag{6.3}$$

are forbidden. Unconventional theories [6.10] would allow a small relative decay rate to these modes. Then the τ is stable unless the mass, m_{ν_τ}, is less than the τ mass, m_τ. Assuming

$$m_\tau > m_{\nu_\tau} \; ; \tag{6.4}$$

the τ has the purely leptonic decays:

$$\tau^- \rightarrow \nu_\tau + e^- + \bar{\nu}_e \tag{6.5a}$$

and

$$\tau^- \rightarrow \nu_\tau + \mu^- + \bar{\nu}_\mu \tag{6.5b}$$

Following the e,μ conventions, the τ^- and ν_τ are called particles, the τ^+ and $\bar{\nu}_\tau$ are called anti-particles. Depending on the m_τ, m_{ν_τ} difference hadronic decays are also allowed:

$$\tau^- \rightarrow \nu_\tau + \pi^- \tag{6.6a}$$

$$\tau^- \rightarrow \nu_\tau + \rho^- \tag{6.6b}$$

$$\tau^- \rightarrow \nu_\tau + K^- \tag{6.6c}$$

$$\tau^- \rightarrow \nu_\tau + A_1^- \tag{6.6d}$$

$$\tau^- \rightarrow \nu_\tau + \text{2-or-more-hadrons} \tag{6.6e}$$

. .
. .
. .

Conventional weak interaction theory as first carried out by Thacker and Sakurai [6.11] and by Tsai [6.12] predicts the decay ratios for the purely leptonic modes. The addition of some theoretical concepts and data [6.11,6.12, 6.19] allows the calculation of decay rates to single hadron final states such as π,ρ,K,K^* and A_1. The calculation for final states in which there are 2-or-more-hadrons, usually called the continuum, requires additional knowledge as to how the hypothetical intermediate boson W decays into many hadrons. Fortunately this knowledge can be obtained in part from e^+e^- annihilation data itself by using the analogy between the diagram in fig. 6.1a and the quark model for hadron production in e^+e^- annihilation, fig. 6.1b. Relative decay rates as a function of m_τ are shown in fig. 6.2a assuming that the τ-ν_τ coupling is V-A and $m_{\nu_\tau} = 0.0$. Assuming the τ-ν_τ-W coupling constant

is the universal $G = 1.02 \times 10^{-5}/M^2_{proton}$, the corresponding τ lifetime is given in fig. 6.2b. An important experimental consequence follows from column 3 of table 6.1; 85% of the decay modes of this mass and type of heavy lepton contain only 1 charged particle.

Relaxing some of our assumptions, such as changing to V+A coupling or giving the ν_τ a several hundred MeV/c^2 mass, will not change the relative decay rates. On the other hand, setting m_{ν_τ} to 1. or 1.5 GeV/c^2 will severely affect the relative decay rates.

After the publication of the data on anomalous $e\mu$ events by the SLAC-LBL Magnetic Detector Collaboration [6.1,6.2] a number of theoretical papers appeared which discussed the production of charged heavy lepton pairs in e^+e^- annihilation and the behavior of their decay products, momentum distributions, angular distributions, tests of the nature of the coupling, alternative explanations, and so forth. Reference [6.13] contains a partial list along with some earlier references which applies to our case of unpolarized e^+e^- beams and moderate statistics.

6.1.2. Paraleptons

Llewellyn Smith [6.9] defines <u>paraleptons</u> as charged heavy leptons with the same lepton number as the <u>oppositely</u> charged e or μ; hence such leptons cannot decay electromagnetically. Thus Bjorken and Llewllyn Smith [6.13b] define the E^- and M^- to have the lepton numbers of the e^+ and μ^+ respectively. The lower bounds on the M^- mass set by Barish <u>et al</u>. [6.14] means that the M cannot be produced by currently operating e^+e^- colliding beam machines. The E^- with decay modes

$$E^- \rightarrow \bar{\nu}_e + e^- + \bar{\nu}_e \qquad (6.7a)$$

$$E^- \rightarrow \bar{\nu}_e + \mu^- + \bar{\nu}_\mu \qquad (6.7b)$$

$$E^- \rightarrow \bar{\nu}_e + \text{hadrons} \qquad (6.7c)$$

is not excluded by existing neutrino production data.

6.1.3. Ortholeptons

Ortholeptons [6.9] are charged heavy leptons with the same lepton number as the same charge e or μ. Ordinarily the e^* with the same lepton number as the e^- would decay electromagnetically

$$e^{*-} \rightarrow e^- + \gamma \qquad (6.8a)$$

However, the coupling constant at the $e^*e\gamma$ vertex is arbitrary as pointed out by Low [6.13c]; and we may make it so small that the weak decays

$$e^{*-} \rightarrow \nu_e e^- \bar{\nu}_e \quad , \quad \nu_e \mu^- \bar{\nu}_\mu , \quad \nu_e \text{hadrons} \qquad (6.8b)$$

are stronger than the decay in eq. (6.8a). A similar remark holds for the μ^{*-} with the lepton number of the μ^-. We also call such leptons excited electrons or excited muons.

6.1.4. Production of Heavy Leptons in e^+e^- Annihilation

The simplest assumption is that a heavy lepton is a spin ½ point particle obeying the Dirac equation. The lepton is pair produced through the one-photon exchange diagram of fig. 6.3, the same diagram which leads to μ pair production. Indeed once $E_{cm} >> 2m_{lepton}$ the heavy lepton is produced as copiously as the μ meson; and this is the reason why e^+e^- annihilation has been such a fertile field for heavy lepton searches. Using the spin ½, Dirac point particle, assumptions; the total production cross section is

$$\sigma_{e^+e^- \rightarrow \tau^+\tau^-} = \frac{2\pi\ \alpha^2\ \beta(3-\beta^2)}{3s} = \frac{43.4\ \beta(3-\beta^2)}{E_{cm}^2}\ \text{nb} \qquad (6.9)$$

where E_{cm} is in GeV and β is the velocity of the τ in units of c. As an aside, we note that in the $E_{cm} \lesssim 8$ GeV energy range of this paper we ignore the two-virtual-photon process [6.15].

$$e^+ + e^- \rightarrow \tau^+ + \tau^- + e^+ + e^- \quad ; \qquad (6.10)$$

a process which will become important at higher energies.

6.2. Semi-Leptonic Decays of Charmed Hadrons as Anomalous Lepton Sources

We began the discussion of the semi-leptonic decays of charmed hadrons in section 5. The important quark diagram is the decay of the c quark to an s quark and an $e^+\nu_e$ or $\mu^+\nu_\mu$ pair, fig. 6.4a. Taking color into account, this quark decay amplitude should be one third as large as the decay of a c to an s and a $u\bar{d}$ pair, fig. 6.4b. Thus ignoring possible hadronic enchancements the the semi-leptonic decays of charmed hadrons should be comparable to the hadronic decays. This has important consequences:

1. The existence of a relatively large semi-leptonic decay rate in a large mass hadron (mass $\gtrsim$ 1.5 GeV/c^2 say) is an indication that the hadron may be charmed.

2. The relatively large semi-leptonic decay rates in large mass charmed hadrons make it possible to study weak interaction decay dynamics where four-momentum transfers are large, and hence where form-factor effects will be large.

The charmed D^o mesons provide the simplest examples of what sort of semi-leptonic decays we expect in charmed hadrons. Remembering that the c decays to an s we expect

$$\begin{aligned} D^o &\to K^- + e^+ + \nu_e \\ D^o &\to K^{*-} + e^+ + \nu_e \\ D^o &\to K^- + \pi^o + e^+ + \nu_e \\ D^o &\to \bar{K}^o + \pi^- + e^+ + \nu_e \end{aligned} \qquad (6.11)$$

Various calculations of charmed hadron semi-leptonic decay rates have been carried out [6.16,1.17]; and some examples are given in table 5.4

The production processes for charmed hadrons are of course very much more complicated than for heavy leptons. The latter is given simply by fig. 6.3

and eq. (6.9). Near threshold the former (using the D^o as an example) is given by

$$
\begin{aligned}
&e^+ + e^- \to D^o + \bar{D}^o \\
&e^+ + e^- \to D^o + \underset{\hookrightarrow\ \bar{D}^o}{\bar{D}^{*o}} \qquad\qquad (6.12)\\
&e^+ + e^- \to \underset{\hookrightarrow\ D^o}{D^{*o}} + \underset{\hookrightarrow\ \bar{D}^o}{\bar{D}^{*o}}
\end{aligned}
$$

At energies above the threshold region we expect

$$e^+ + e^- \to D^o + \bar{D}^o + \text{additional hadrons} \qquad (6.13a)$$

and

$$e^+ + e^- \to \underset{\hookrightarrow\ D^o}{H_c} + \underset{\hookrightarrow\ \bar{D}^o}{\bar{H}_c} + \text{additional hadrons} \qquad (6.13b)$$

where H_c represents a higher mass charmed hadron which can decay to a D^o.

Combining the production processes in eqs. (6.12 and 6.13) with the decay process in eq. (6.11) we come to a very important point emphasized by Wiik [6.5] and by Feldman et al. [6.4]. The total final state of a process involving the e^+e^- production of a charmed hadron and its semi-leptonic decay will on the average have much higher charged particle and photon multiplicity than the total final state of a process involving the e^+e^- production of a heavy lepton and its leptonic decay.

6.3. Purely Leptonic Decays of Integral Spin Particles

An integral spin particle whether an hadronic boson or a point particle can clearly have the 2-body, purely leptonic decay modes [6.18]

$$M^- \to e^- + \bar{\nu}_e \quad , \quad M^- \to \mu^- + \bar{\nu}_\mu \qquad (6.14)$$

In any study of anomalous lepton production in e^+e^- annihilation such sources must clearly be considered, and we will do so. For example, if the F^* has spin 1 and has lower mass than the F, then $F^{*-} \to e^-\bar{\nu}_e$ or $\mu^-\bar{\nu}_\mu$ might compete with semi-leptonic decays of the F^*. A point particle example is the intermediate boson with decay $W^- \to e^-\bar{\nu}_e$ or $\mu^-\bar{\nu}_\mu$; although we must remember that present lower limits on the W mass preclude its production at existing e^+e^- colliding beam facilities.

For a spin zero particle the $e^-\bar{\nu}_e$ decay mode will be strongly suppressed relative to the $\mu^-\bar{\nu}_\mu$ decay mode by helicity conservation and the left-handedness of the V-A coupling; just as it is in π^- and K^- decay. Therefore we restrict our considerations in this section to spins of 1 or larger.

The production cross section for

$$e^+ + e^- \to M^+ + M^- \qquad (6.15)$$

can be quite complicated even when the spin is 1. We shall use the simple form:

$$\sigma_{e^+e^- \to M^+M^-} = \frac{A\beta^3}{s} \left|F_M(s)\right|^2 \qquad (6.16)$$

Here β^3 is a threshold factor, A is a constant, and $F_M(s)$ is a form factor which is less than 1 when M is hadronic and s is far above threshold.

6.4. The eμ Events Produced in e^+e^- Annihilation

6.4.1. Discovery of the eμ Events

The cleanest signature for the existence of charged heavy leptons in the production and decay process:

$$e^+ + e^- \to \tau^+ + \tau^- \qquad \tau^+ \hookrightarrow e^+\nu_e\bar{\nu}_\tau, \quad \tau^- \hookrightarrow \mu^-\bar{\nu}_\mu\nu_\tau \tag{6.17}$$

or its charge conjugate. Experimentally one would see

$$e^+ + e^- \to e^{\pm} + \mu^{\mp} + \text{no other detected particles} \tag{6.18}$$

We call these events signature eμ events. The first evidence for such events was presented by Perl [6.1] in the summer of 1975 using the data of the SLAC-LBL Magnetic Detector Collaboration obtained at SPEAR. The collaboration has published two papers [6.2,6.3] on these events, the second based on a total of 105 events after background subtraction. The discussion in this section is based on that set of events augmented with more recent SLAC-LBL Magnetic Detector Collaboration data. These total data contain 190 eμ events with a background of 46 events giving 144 signature eμ events after background subtraction. These events occur in the energy range $3.8 \lesssim E_{cm} \leq 7.8$ GeV.

The signature eμ events were selected using the following criteria:

1. One particle identified as an e, the other identified as a μ.
2. The e and μ have opposite sign electric charge.
3. $p_e \gtrsim 0.65$ GeV/c and $p_\mu \gtrsim 0.65$ GeV/c. These lower limits are necessary to insure that e's and μ's can be separated from hadrons.
4. The e and μ are acoplanar with $\theta_{copl} \gtrsim 20^\circ$ where

$$\cos\theta_{copl} = -|(\underset{\sim}{n}_e \times \underset{\sim}{n}_+) \cdot (\underset{\sim}{n}_\mu \times \underset{\sim}{n}_+)|/(|\underset{\sim}{n}_e \times \underset{\sim}{n}_+||\underset{\sim}{n}_\mu \times n_+|) \tag{6.19}$$

$\underset{\sim}{n}_e$, $\underset{\sim}{n}_\mu$ and $\underset{\sim}{n}_+$ are unit vectors in the direction of motion of the e, μ and incident positron beam respectively. This cut removes contamination

from coplanar ee and $\mu\mu$ pairs.

5. No other charged particles are detected.

6. No photons are detected.

To show that the signature $e\mu$ events so selected might come from heavy leptons via reaction (6.17) it was necessary to prove that they met two general conditions:

A. It was necessary to prove that the e and μ were neither misidentified hadrons nor the decay products of π, K's or other hadrons. This has been fully discussed in a series of papers [6.1-6.4,6.19]. We only note here that due to misidentification or decay a hadron is called an e 10 to 20% of the time, and a hadron is called a μ 10 to 20% of the time in the SLAC-LBL Magnetic Detector. On the average 20% of the $e\mu$ events are misidentified hadronic events. In addition 2% of the signature $e\mu$ events are from misidentified ee pairs.

B. With the majority of the signature $e\mu$ events shown to be genuine, it was necessary to show [6.4,6.19] that they did not come from

$$e^+ + e^- \rightarrow e^{\pm} + \mu^{\mp} + \text{charged hadrons and/or } \pi^0\text{'s}, \qquad (6.20a)$$

where the charged hadrons or π^0's were <u>not</u> detected.

Furthermore they must not come from

$$e^+ + e^- \rightarrow e^{\pm} + \mu^{\mp} + K_L^0\text{'s} \qquad (6.20b)$$

This is because reactions such as in eqs. (6.20) would indicate a semi-leptonic decay source of the $e\mu$ events; for example the semi-leptonic decays of a $D^0\overline{D^0}$ pair, eqs. (6.11), could produce the reaction in eq. (6.20a). Reaction (6.20a) was eliminated as a major source of the signature $e\mu$ events by showing that there were much too few $e\mu$ events <u>with</u> additional charged particles or π^0's detected. Reaction (6.20b) was eliminated as a

major source by showing that there were very few eμ events of the form

$$e^+ + e^- \rightarrow e^{\pm} + \mu^{\mp} + K_S^o\text{'s} \qquad (6.20c)$$

the K_S^o's being detected through their $\pi^+\pi^-$ decay mode. To summarize, it was shown [6.4,6.19] that the 90% confidence upper limit on the fraction of signature eμ events coming from the reactions in eq. (6.20) was 0.39 (table 6.2).

Since the signature eμ events met these two conditions they were candidates for heavy lepton related events. It was next necessary to see if the signature eμ events had the expected behavior of heavy lepton related events, and to see if these were alternative explanations of these events. Later in this section we describe how these studies are done. But first we summarize the data on the signature eμ events found by the PLUTO group at DORIS.

6.4.2. The eμ Events of the PLUTO Group

In the summer of 1976, H. Meyer [6.20] described the findings of signature eμ events eq. (6.18) in the PLUTO detector at DORIS. Further information on those events was presented at the 1977 Coral Gables Conference [6.21], and that information is summarized here. Twelve eμ events, that is signature eμ events, were found in the energy range $4.0 < E_{cm} < 4.8$ GeV; and the calculated background was less than 1.5 events. In the same data sample, 7 eμ events were found with additional charged particles but the calculated background was 6 events. Hence the 12 signature eμ events could not come from the reactions in eqs. (6.20); and therefore condition B, discussed before, is met by these PLUTO events. This is particularly important because the PLUTO detector has larger solid angle coverage than the SLAC-LBL Magnetic Detector, .85 of 4π compared to .70 of 4π.

6.4.3. The Observed Production Cross Sections for the Signature eμ Events

Figure 6.5 shows $\sigma_{e\mu}$, the observed production cross section for the sample of signature eμ events of the SLAC-LBL Magnetic Detector Collaboration. The background has been subtracted. The solid curves show the theoretical $\sigma_{e\mu}$, eq. (6.9), for a sequential heavy lepton with V-A coupling, $m_{\nu_\tau} = 0.0$ and $m_\tau = 1.8$ or 2.0 GeV/c^2. These theoretical curves have been corrected for the momentum and angle cuts and for the geometric acceptance of the detector. They are fit to the observed $\sigma_{e\mu}$ by adjusting the leptonic branching ratios of the τ. We note that the goodness of fit is not sensitive to m_τ, except that as m_τ increases above 1.9 GeV/c^2 the signature eμ events at $E_{cm} = 3.8$ GeV must be attributed to background. This latter observation will be used later as one way of fixing limits on m_τ. The quality of fit is also not sensitive to the nature of the coupling.

However the introduction of a form factor does decrease the quality of the fit. The dashed curve in fig. 6.5 is for a mass 1.8 GeV/c^2, heavy lepton with the production cross section of eq. (6.9), but with the form factor $F_M = C/s$ where C is a constant. We note that even such a monopole form factor gives a poor fit to the data. Hence the observed $\sigma_{e\mu}$ favors a point production cross section. This is an additional argument against any hadronic semi-leptonic decay source of the signature eμ events. Such a source is restricted to pure hadron pair production and its form factor dependence on s would be strong.

6.4.4. Observed Kinematics Distributions of the Signature eμ Events

In figs. 6.6 and 6.7 we show the missing mass squared (m_m^2) and invariant mass squared (m_i^2) distributions for the signature eμ events for $4.8 < E_{cm} < 7.8$ GeV. Here

$$m_m^2 = (E_{cm} - E_e - E_\mu)^2 - (\underset{\sim}{p}_e + \underset{\sim}{p}_\mu)^2 \qquad (6.21a)$$

$$m_i^2 = (E_e + E_\mu)^2 - (p_e + p_\mu)^2 \qquad (6.21b)$$

where E_e, $\underset{\sim}{p}_e$ and E_μ, $\underset{\sim}{p}_\mu$ are the energy and three-momentum of the e and μ respectively. There is no sharp peak in either distribution, as there should <u>not</u> be if the source is reaction (6.17). Other E_{cm} ranges have similar distributions.

Of much more value are the momentum distributions of the e and μ. To combine data from various E_{cm} ranges we define

$$r = \frac{p - 0.65}{p_{max} - 0.65} \qquad (6.22a)$$

Here p is the momentum of the e or μ in GeV/c and p_{max} is its maximum value in reaction 6.17. The e and μ masses are set to zero. Since 0.65 GeV/c is the lower limit in p, r has the range

$$0 \lesssim r \lesssim 1 \qquad (6.22b)$$

Figures 6.8 show the background subtracted r distributions for the signature eμ events for four energy ranges. A V-A heavy lepton with $m_\tau = 1.90\ \mathrm{GeV/c^2}$ and $m_{\nu_\tau} = 0.0$ is a good fit, table 6.3, except in the $E_{cm} = 4.8$ GeV data.

These same curves can be used to eliminate an alternative hypothesis, that the signature eμ events came from the 2-body decays of an integral spin particle called M, section 6.3. Two cases are considered, fig. 6.8a and table 6.3. In one case the M is taken to be unpolarized. This gives a flat r spectrum which disagrees with data. In the other case the M is taken to have spin 1 and to be polarized so that it is only produced in the helicity = 0 state. This also disagrees with the data. Hence the r spectrum shows that the e and μ do not come from 2-body decays. The possibility that the e and μ come from 4-or-more-body decays is also eliminated because the observed r spectrum is too "hard" for that hypothesis.

From these conclusions and from the fact that the signature eμ events meet conditions A and B in sections 6.4.1. and 6.4.2.; we are led to the τ charged heavy lepton as the simplest explanation of the signature eμ events. Our next task is to determine the properties of the τ and to see if all these properties are consistent with those expected of a heavy lepton. For example, fig. 6.9 shows that the $\cos\theta_{coll}$ distributions are consistent with those expected for a heavy lepton. Here

$$\cos\theta_{coll} = -\underset{\sim}{p}_e \cdot \underset{\sim}{p}_\mu / (|\underset{\sim}{p}_e||\underset{\sim}{p}_\mu|); \qquad (6.23)$$

and the distribution is strongly affected by the θ_{copl} and momentum cuts in section 6.4.1.

6.4.5. Properties of the τ Charged Lepton Using the eμ Events.

<u>τ Mass</u>: In the first method of studying m_τ we vary m_τ and study the quality of the fit to $\sigma_{e\mu}$ in fig. 6.5. This method is particularly effective in setting an upper limit on m_τ because all eμ events with $E_{cm} < 2m_\tau$ must be attributed to background. Table 6.4 gives the results.

The second method uses the kinematic distributions. A particularly effective distribution is a pseudo-transverse momentum, $p_\perp$, pictured in the inset in fig. 6.10 and defined by

$$p_\perp = (\underset{\sim}{p}_e \times \underset{\sim}{p}_\mu)/|\underset{\sim}{p}_e - \underset{\sim}{p}_\mu| \qquad (6.24)$$

Table 6.5 gives the values of m_τ for different hypotheses as to the coupling and m_{ν_τ}. A related method uses the average value of $\cos\theta_{coll}$, fig. 6.9, for $\theta_{coll} \lesssim 90^\circ$. Another method uses the r distributions [6.22]. There are a number of conclusions we can draw from table 6.5.

1. The $p_\perp$, $\cos\theta_{coll}$, and r methods are in good agreement although we believe the $p_\perp$ method is more reliable because it is less dependent on how the background is subtracted.

2. V-A coupling and m_{ν_τ} in the range of 0.0 to 0.5 GeV/c^2 (see below also) is consistent with the m_τ limits in table 6.4 Using V-A coupling and $m_{\nu_\tau} = 0.0$, as does our standard model, we note

$$m_\tau = 1.91 \pm .05 \text{ GeV}/c^2 \qquad (6.25)$$

based on the $p_\perp$ method where the error is statistical. However due to the differences in the $p_\perp$ and cos θ methods and some systematic uncertainties we use

$$m_\tau = 1.90 \pm .10 \text{ GeV}/c^2 \qquad (6.26)$$

for our standard model.

3. We note, table 6.5a, that m_τ is the same in the high and low E_{cm} ranges. This shows that our τ lepton interpretation of the data is consistent over the entire E_{cm} range, and it argues against the existence of a second charged heavy lepton with a mass greater than the τ but less than 3 or so GeV/c^2.

Coupling: Figure 6.11 compares the experimental r distribution with V+A coupling and $m_{\nu_\tau} = 0.0$. From fig. 6.11 and the comparison of table 6.5a and 6.5b we note that pure V+A coupling is less favored than pure V-A coupling [6.22].

Mass of the τ neutrino: Figure 6.11 shows that as m_{ν_τ} increases the goodness of fit to the r distributions decreases. For V-A coupling

and $m_\tau = 1.9$ GeV/c^2 the 95% confidence level upper limit on m_{ν_τ} is

$$m_{\nu_\tau} \lesssim 0.60 \text{ GeV}/c^2$$

<u>Leptonic branching ratio</u>: Using the $\sigma_{e\mu}$ data in fig. 6.5, $m_\tau = 1.9$ GeV/c^2, $m_{\nu_\tau} = 0.0$, V-A coupling, the point particle production cross section (eq. (6.9)), and <u>assuming</u> the equality of the τ decay rates to e and μ

$$\frac{\Gamma(\tau^- \to \nu_\tau e^- \bar{\nu}_e)}{\Gamma(\tau^- \to \text{all})} = \frac{\Gamma(\tau^- \to \nu_\tau \mu^- \bar{\nu}_\mu)}{\Gamma(\tau^- \to \text{all})} = 0.186 \pm .030 \qquad (6.27)$$

in agreement with the theoretical prediction, table 6.1. Some tests of this equality assumption are given in the next section.

6.5. Consistency Checks on the τ being a Heavy Lepton

6.5.1. Point-like Energy Dependence.

We have shown in section 6.4.3. that the energy dependence of the production is consistent with being point like.

6.5.2. Total e^+e^- Annihilation Cross Section

R, the ratio between the total e^+e^- annihlation cross section and the μ pair production cross section, measures the sum of squares of charges of the fundamental fermions in the conventional models. Thus if we have a new lepton, we must have room for it in the total cross section. This point was discussed in detail in section 2. We not only have room for it, but measurements of R seem to require a new fermion.

A more direct demonstration is contained in the work of the PLUTO group [2.5]. They show, fig. 6.12, that the directly measured total cross section for 2-prong events is large enough to easily contain the 2-prong events from $\tau^+\tau^-$ production assuming relative decay rates similar to those in table 6.1.

6.5.3. Anomalous ee and $\mu\mu$ events.

Since we interpret the anomalous $e\mu$ events to be the result of independent decays, one containing an e and one containing a μ, we expect half as many anomalous ee and $\mu\mu$ events if the τ decay rates to the e and μ are equal. These events are harder to measure because there are backgrounds from leptonic processes which are comparable to the anomalous signal. Using the SLAC-LBL

Magnetic Detector Collaboration data we have subtracted backgrounds from

$$\begin{aligned} e^+ + e^- &\to \ell^+ + \ell^- + \gamma \\ e^+ + e^- &\to \ell^+ + \ell^- + \gamma + \gamma \\ e^+ + e^- &\to e^+ + e^- + \ell^+ + \ell^- \end{aligned} \tag{6.28}$$

where ℓ stands for either e or μ. The results [6.23] are given in table 6.6 which is consistent with equal decay rates to e and μ. This measurement eliminates the possibility that the τ is an electron-related paralepton of the type discussed in section 6.1.2.

6.5.4. SLAC-LBL Collaboration Anomalous, 2-prong, Muon Inclusive Events

In the reaction

$$e^+ + e^- \to \underset{\hookrightarrow\ \mu^+\nu_\mu\bar{\nu}_\tau}{\tau^+} + \underset{\hookrightarrow\ \text{anything}}{\tau^-} , \tag{6.29}$$

or its charge conjugate, the "anything" ought to contain a <u>single</u> charged particle 85% of the time according to table 6.1. Therefore we should be able to find events of the form

$$e^+ + e^- \to \mu^{\pm} + x^{\mp} + \geq 0 \text{ photons} \tag{6.30}$$

where x is an e, μ, or hadron. Such events have been found by the SLAC-LBL Magnetic Detector Collaboration [6.4,6.19] using an extended muon detector (called the muon tower) on top of the main detector, fig. 2.4. We will refer to muons being identified at three levels (see fig. 2.4). Level 1 corresponds to particles which penetrate the shower counters, the coil, and the flux return. The original data were analyzed exclusively at this level. Level 2 or 3 correspond to particles which penetrate level 1 and one or two concrete slabs; the total amount of material before levels 2 and 3 is equivalent to 65 and 92 cm of iron, respectively. The solid angle of level 2 is 1.1 sr and the minimum average muon momentum required to reach level 2 is 910 MeV/c.

We took as the initial sample of events all two-prong events, with or without photons, in which one prong is a muon candidate at level two or three of the muon tower. A muon candidate is defined as a particle which has sufficient momentum and is heading in the right direction to fire a muon spark chamber if it were a muon. To simplify the background calculations, events in which both prongs are identified as electrons are eliminated. We then required the two prongs to be acoplanar with the incident beams by at least 20° and for the square of the missing mass recoiling against the two observed prongs to be greater than 1.5 $(GeV/c^2)^2$. Backgrounds from hadron penetration and decay and leptonic backgrounds were then subtracted to obtain the number of anomalous two-prong μ events.

A very clear signal exists in the $5.8 \lesssim E_{cm} \lesssim 7.8$ energy range, fig. 6.13 and table 6.7. A statistically weaker signal appears at lower energies, table 6.7. The anomalous, 2-prong, muon cross section in all three energy ranges is compatible with that expected from the decays of pairs of τ heavy leptons. Figure 6.14a shows that the μ momentum spectrum is also consistent with that expected from the τ.

Finally we note that since the comparison in the bottom two lines in table 6.7 is based on table 6.1 and the equality of the τ decay rate to e and μ; the success of this comparison is a consistency check on that equality.

6.5.5. Other results on Anomalous, 2-prong, Muon Inclusive Events

Two other experiments have made measurements of inclusive anomalous muon production to two-prong events. The Maryland-Princeton-Pavia group reported 13 events with 4 background at 4.8 GeV, corresponding to a cross section of $285 \begin{smallmatrix} +151pb \\ -113pb \end{smallmatrix}$ [6.24]. These were the <u>first</u> such events reported. As analyzed by Snow [6.25], these data are compatible with the heavy lepton hypothesis.

Preliminary, high statistics measurements of anomalous, 2-prong, muon inclusive spectra in the energy range $4.0 \lesssim E_{cm} \lesssim 4.8$ GeV were reported [6.21]

by the PLUTO group at the 1977 Coral Gables Conference. These spectra were also consistent with coming from the production of a pair of heavy leptons of mass about 1.95 GeV/c^2

6.5.6. Anomalous, 2-prong, Electron Inclusive Events.

At the 1977 Chicago Meeting of the American Physical Society, R. Felst of the DASP Group from DORIS reported [6.26] preliminary data on anomalous, 2-prong, electron inclusive events analogous to the muon events in eq. (6.30) He reported that the energy dependence of the observed production cross section in the energy range $4. \lesssim E_{cm} \lesssim 5$ GeV, and the momentum spectrum of the electron, were consistent with that expected from a heavy lepton of mass $\sim$1.9 GeV/c^2.

6.5.7. Anomalous, 2-prong, Muon-Hadron Events

If we identify the x particle in reaction (6.30) we ought to be able to find hadrons as well as e's and μ's. In 59 of the two-prong events with $5.8 < E_{cm} < 7.8$ GeV in table 6.7, the second prong can be identified as a μ, e, or hadron. After correcting for all backgrounds and misidentifications there are 6.8 ± 6.3 $\mu\mu$ events, 14.2 ± 4.8 μe events, and 19.5 ± 6.5 μ hadron events. These statistics are too poor to check the predicted hadronic decay rates in table 6.1; but at least an overall hadronic decay mode has been seen.

6.5.8. Consistency Conclusions

All published and conference-reported data relevent to the heavy lepton are in agreement with the existence of a charged lepton with mass $m_\tau = 1.90 \pm .10$ GeV/c^2. While it is not required, all this data is also consistent with our standard model: V-A coupling and $m_{\nu_\tau} = 0.0$.

6.6. Observation of the Semi-Leptonic Decays of New Hadrons

6.6.1. Anomalous, Multiprong, Electron Inclusive Events

The first observations of the semi-leptonic decays of new hadrons, undoubtedly charmed hadrons, were made by the DASP [6.27,6.5] and PLUTO [6.28,6.21,6.5] groups from DORIS. The DASP group's discovery [6.27] of anomalous, multiprong, electron inclusive events is described in this section; and the PLUTO group's discovery [6.28] of K_S^o e correlations is described in section 6.6.3.

The DASP detector, fig. 6.15, was modified for this work by the installation of electron-sensitive, threshold Cerenkov counters at the entrance to each of the magnetic spectrometer arms. Additional hadron rejection was obtained by shower counters at the rear of each arm. In addition most of the remaining solid angle was covered by a non-magnetic detector capable of identifying electron, photons and hadrons. The events considered here met the following criteria:

1. a total of at least 4 or more charged particles plus photons in the event;
2. an electron identified by the Cerenkov counter and shower counter magnetic spectrometer system; and
3. at least one "non-showering" particle, that is hadron or muon, in the event.

The importance of criteria 1) is that high multiplicity events should come from semi-leptonic decays of hadrons; but low multiplicity events should come from heavy lepton decays as discussed in section 6.2. These events then have the form

$$e^+ + e^- \rightarrow e^{\pm} + n_c \text{ charged particles} + n_\gamma \text{ photons} \qquad (6.31)$$

where

$$n_c + n_\gamma \geq 3$$

Some early data on the electron momentum spectrum of such events is shown in fig. 6.16; and the energy dependence of the observed cross section is shown in fig. 6.17. The momentum spectrum in fig. 6.16 is too soft to

be from a heavy lepton.

The connection of these e-associated, multi-prong events with the production of singly charmed mesons is made by studying their threshold behavior. See fig. 6.17 and ref. 6.27. They are not observed below the charmed meson threshold at $E_{cm} \sim 4.0$ GeV; and their production cross section is maximum in the 4.0 to 4.1 GeV region where D^0 and $D^{\pm}$ production is maximum (section 5). Therefore it is very reasonable to associate these observed events with the charmed mesons and in particular with the D mesons. In the 4.0 - 4.2 GeV region, the DASP group finds [6.5]

$$\sigma(e^+ + e^- \to e^{\pm} + \text{hadrons})_{\text{multiprong}} = 2 \cdot \sigma(e^+e^- \to M_c\bar{M}_c) \cdot B(M_c \to e^{\pm} + \nu_e(\bar{\nu}_e) + \text{hadrons}) > 1 \text{ nb} \tag{6.32}$$

where $\sigma(e^+e^- \to M_c\bar{M}_c)$ is the inclusive cross section for $M_c\bar{M}_c$ pairs, M_c is a charmed meson, and B is its branching ratio to semi-leptonic decay modes. Taking $\sigma(e^+e^- \to M_c\bar{M}_c)$ as about 10 nb, we find

$$B(M_c \to e^{\pm} + \nu_e(\nu_e) + \text{hadrons}) \gtrsim .05 \tag{6.33}$$

which is compatible with the discussion in section 6.2.

6.6.2. Anomalous, Multiprong, Muon Inclusive Events.

Feldman et al. [6.4] have observed events of the form

$$e^+ + e^- \to \mu^{\pm} + \geq 2 \text{ charged particles} \pm \geq 0 \text{ photons} \tag{6.34}$$

in the energy range $5.8 \lesssim E_{cm} \lesssim 7.8$ GeV. Figures 6.13b and 6.14b give the multiplicity distribution and the μ momentum spectrum. Neither observation is compatible with that expected from a heavy lepton. Therefore it is natural to associate these events with the semi-leptonic decays of hadrons. The energy, E_{cm}, is too high to associate these events directly with D charmed meson production as was done in the previous section. Undoubtedly some of these events are from D decays. Others may be from singly charmed baryon

decays, from other charmed hadrons, or from yet unknown massive hadrons which only decay weakly.

6.6.3. K-e Correlated Events.

The PLUTO group [6.28] has observed correlations between K_S^o mesons and electrons, thus providing a more immediate way to study the semi-leptonic decays of the charmed mesons. As discussed in section 5, K mesons are expected to occur in almost all D meson decays and in many F meson decays. In this work the K_S^o is detected through its $K_S^o \rightarrow \pi^+\pi^-$ decay mode, the K_S^o appearing as an invariant mass peak in the mass spectrum of pairs of oppositely charged hadrons. Below the expected charmed meson threshold there is no correlation of the e's with the K_S^o, but such a correlation is observed at $E_{cm} = 4.1$ GeV. This result is of course just what we expect for the behavior of the D meson. Figure 6.18 is an early presentation of this data.

A similar observation of $K^{\pm}$ - e correlations has been made by the DASP group [6.27,6.5]. At $E_{cm} = 4.0$ to 4.2 GeV they see a $K^{\pm}$ - e correlation but not a $\pi^{\pm}$ - e correlation.

6.6.4 Conclusion on Semi-Leptonic Decays

The semi-leptonic decays of massive hadrons which only decay weakly have been observed in $e^+ - e^-$ annihilation in the energy range $4. \lesssim E_{cm} \lesssim 7.8$ GeV. Near 4 GeV the decays are compatible with coming from D mesons.

The thorough experimental study of the semi-leptonic decays of charmed hadrons will be a much more complex undertaking than the study of the leptonic or hadronic decays of the τ heavy lepton, because the production

and decay processes of the former are so complex. Nevertheless substantial progress in finding the semi-leptonic decays of the singly charmed mesons has already been made.

7. e^+e^- ANNIHILATIONS AT HIGHER ENERGIES

7.1. Introduction

Now that the first round of experiments at SPEAR and DORIS have been concluded and higher energy storage rings are being built, it is appropriate to ask what we can expect at higher energies based on what we have learned. There are two areas in which data at present energies indicate the possibilities of spectacular results at higher energies: jet structure and possible new quarks and leptons.

7.2. Jet Structure

Using a typical transverse momentum of 310 MeV/c, the jet model which gives a good description of SPEAR data at 7.4 GeV can be used to generate a description of e^+e^- annihilations at 30 GeV [7.1]. Figure 7.1 shows the mean sphericity as predicted by the phase space and jet models. The distributions are almost completely disjoint. Jet structure will be completely obvious and no fancy sphericity analysis will be necessary to establish it. This is further illustrated by fig. 7.2 where the cosine of the angle between any pair of particles is plotted.

After the basic properties of jets have been measured, interest will quickly shift to studying deviations from two jet behavior. Non-jetlike events may signal thresholds for new heavy particles. The possibility of multi-jet events has also been discussed [7.2,7.3].

7.3. New Quarks and Leptons

The existence of the τ upsets the lepton-quark symmetry that the charmed quark was designed to restore [7.4]. This coupled with indications of new particles in neutrino interactions [7.5] makes it likely that new quarks

and/or leptons may be produced in higher energy e^+e^- annihilations. If new quarks exist then we should also expect new narrow ψ-like states to be present. Eichten and Gottfried [7.6] point out that for each quark mass greater than 3.5 GeV/c^2, three narrow ^3S, bound $q\bar{q}$ states should exist below the threshold for OZI allowed decays. This will lead to an incredibly rich and complex array of photon and hadron transitions. Figures 7.3 and 7.4, taken from the work of ref. 7.6, illustrate some of the leading photon and hadron transitions expected from a series of ψ-like states, β, β', and β'', corresponding to a quark of mass 5 GeV/c^2.

Acknowledgements

We are indebted to our colleagues with whom we have worked on the magnetic detector at SPEAR for many insights into the marvels of e^+e^- annihilation. We would also like to thank Paul Tsai for discussions on heavy leptons, and we would particularly like to thank Fred Gilman for almost daily discussions on the physics of e^+e^- annihilation.

REFERENCES SECTION 1

1.1 G.J. Feldman and M.L. Perl, Physics Reports 19C, 234(1975); called I.

1.2 R.F. Schwitters and K. Strauch, Ann. Rev. Nucl. Sci. 26, 89(1976); called II.

1.3 B.H. Wiik and G. Wolf, Lectures given at the Les Houches Summer School, 1976; DESY Report DESY 77/01 (1977); called III.

1.4 R.F. Schwitters in Proceedings of the XVIII International Conference on High Energy Physics (Tbilisi, 1976); also issued as SLAC-PUB-1832 (1976).

1.5 For a general review see the Proceedings of the Colloque International sur les Collisions Photon-Photon dans les Anneaux de Stockage Electron-Positron, Supplément au Joural de Physique Tome 35, Fast. 3, C-2 (1974).

REFERENCES SECTION 2

2.1 An alternative theory which holds that integrally charged free quarks can exist leads to the same result. If these quarks were produced occasionally they would have short lifetimes, decaying primarily into hadrons before they can be detected.

2.2 See ref. [1.4] and references contained therein.

2.3 For a recent review see J.D. Jackson in Proceedings of the Summer Institute on Particle Physics - 1976 (SLAC, 1976); SLAC Report No. 198.

2.4 J. Siegrist et al., Phys. Rev. Lett. 36, 700(1976).

2.5 H. Meyer in Proceedings of the Orbis Scientiae - 1977 (Coral Gables, 1977); J. Burmester et al., Phys. Lett. 66B, 395(1977).

2.6 F.J. Gilman in Proceedings of the 1975 International Symposium on Lepton and Photon Interactions at High Energy (SLAC, 1975).

2.7 A. De Rújula et al., Phys. Rev. Lett. 38, 317(1977) and references contained therein.

References for Section 3

1. S. D. Drell, D. J. Levy, and T. M. Yan, Phys. Rev. 187, 2159 (1969), and Phys. Rev. D1, 1617 (1970).

2. N. Cabibbo, G. Parisi, and M. Testa, Lett. Nuovo Cimento 4, 35 (1970).

3. J. D. Bjorken and S. J. Brodsky, Phys. Rev. D1, 1416 (1970).

4. R. P. Feynman, Photon-Hadron Interactions, W. A. Benjamin, Inc., Reading, Mass. (1972).

5. All of the results in this section are based on the work of Gail Hanson, whom we wish to thank for many useful discussions. We follow closely her talks at the VIIth International Colloquium on Multiparticle Reactions, Tutzing/Munich, Germany, 21-25 June 1976, and the XVIIIth International Conference on High Energy Physics, Tbilisi, USSR, 15-21 July 1976, which are available as SLAC report number SLAC-PUB-1814 (1976). Earlier work can be found in G. Hanson et al., Phys. Rev. Letters 35, 1609 (1975).

6. V. N. Baier, in Physics with Intersecting Storage Rings, Proceedings of the International School of Physics "Enrico Fermi," Course XLVI, edited by B. Touschek (Academic, New York, 1971), pp. 1-49; and F. J. Gilman, private communication.

7. J. G. Learned, L. K. Resvanis, and C. M. Spencer, Phys. Rev. Letters 35, 1688 (1975).

8. A. W. Chao and R. F. Schwitters, SLAC report number SPEAR-194, and PEP-217 (1976).

9. R. F. Schwitters et al., Phys. Rev. Letters 35, 1320 (1975).

10. P. Capiluppi et al., Nucl. Phys. B79, 189 (1974).

REFERENCES SECTION 4

4.1 The use of the name X for states of charmonium was suggested over a decade ago by J.D. Bjorken and S.L. Glashow, Phys. Lett. 11, 255(1964).

4.2 J. Siegrist et al., Phys. Rev. Lett. 36, 700(1976).

4.3 S. Okubo, Phys. Lett. 5, 165(1963); G. Zweig, unpublished work (1964); and J. Iizuka, Suppl. Prog. Theor. Phys. 37-38, 21(1966).

4.4 A.M. Boyarski et al., Phys. Rev. Lett. 34, 1357(1975).

4.5 V. Lüth et al., Phys. Rev. Lett. 35, 1124(1975).

4.6 W. Braunschweig et al., Phys. Lett. 56B, 491(1975).

4.7 R. Baldini-Celio et al., Phys. Lett. 58B, 471(1975).

4.8 B. Esposito et al., Lett. Nuovo Cimento 14, 73(1975).

4.9 C. Bemporad in Proceedings of the 1975 International Symposium on Lepton and Photon Inteactions at High Energies (Stanford University, 1975), p. 113.

4.10 R.L. Ford et al., Phys. Rev. Lett. 34, 604(1975).

4.11 L. Criegee et al., DESY report 75/32(1975).

4.12 A.D. Lieberman in Proceedings of the 1975 International Symposium on Lepton and Photon Interactions at High Energies (Stanford University, 1975), p. 55.

4.13 J. Burmester et al., DESY report number 76/53(1976).

4.14 W. Brauschweig et al., Phys. Lett. 63B, 487(1976).

4.15 F. Vannucci et al., Phys. Rev. D15, 1814(1977).

4.16 B. Jean-Marie et al., Phys. Rev. Lett. 36, 291(1976).

4.17 J. Burmester et al., contribution to the 18th International Conference on High Energy Physics, Tbilisi, USSR, July 15-21, 1976.

4.18 W. Bartel et al., Phys. Lett. 64B, 483(1976).

4.19 L. Criegee, Invited talk at the Winter Meeting of the American Physical Society, Stanford, California, December 20-22, 1976.

4.20 G. Goldhaber in Proceedings of the International Conference on the Production of Particles with New Quantum Numbers (University of Wisconsin, 1976), p. 40.

4.21 G.J. Feldman in Proceedings of the SLAC Summer Institute on Particle Physics, August 2-13, 1976 (SLAC report number 198).

4.22 G. Goldhaber in Proceedings of the IVth International Symposium on Nucleon-Antinucleon Interactions (Syracusce University, 1976).

4.23 W. Bartel et al., DESY report number 76/65(1976).

4.24 W. Braunschweig et al., DESY report number 77/2(1977).

4.25 C.J. Biddick et al., University of California at San Diego report (1977).

4.26. W. Bartel et al., Contribution to the 18th International Conference on High Energy Physics, Tbilisi, USSR, July 15-21, 1976.

4.27 F.J. Gilman in Proceedings of the 6th International Conference on High Energy Physics and Nuclear Structure, Sante Fe, New Mexico, June 9-13, 1975, (A.I.P. Conference Proceedings number 26), p. 331.

4.28 R.N. Cahn and M.S. Chanowitz, Phys. Lett. 59B, 277(1976).

4.29 H. Harari, Phys. Lett. 60B, 172(1976).

4.30 T.F. Walsh, Nuovo Cimento Lett. 14, 290(1975).

4.31 A. Pais, Phys. Rev. Lett. 32, 1081(1974). We are indebted to F.J. Gilman and W. Tanenbaum for detailed discussions on the model.

4.32 E. Hilger et al., Phys. Rev. Lett. 35, 625(1975).

4.33 V. Lüth in Proceedings of the EPS International Conference, Palermo, Italy, June 23-28, 1975 (Editrice Compositori, Bologna, 1976), p. 54.

4.34 G.S. Abrams, et al., Phys. Rev. Lett. 34, 1181(1975).

4.35 W. Tanenbaum et al., Phys. Rev. Lett. 35, 1323(1975).

4.36 W. Tanenbaum et al., Phys. Rev. Lett. 36, 402(1976).

4.37 J.S. Whitaker et al., Phys. Rev. Lett. 37, 1596(1976).

4.38 B. Wiik in Proceedings of the 1975 International Sympoisum of Lepton and Photon Interactions at High Energies (Stanford University, 1975), p. 69.

4.39 B. Wiik in Proceedings of the XVII International Conference on High Energy Physics, Tbilisi, USSR, July 15-21, 1976.

4.40 F.M. Pierre, LBL report number LBL-5324(1976).

4.41 G.S. Abrams in Proceedings of the 1975 International Symposium on Lepton and Photon Interactions at High Energies (Stanford University, 1975), p. 25.

4.42 E.B. Hughes et al., Phys. Rev. Lett. 36, 76(1976).

4.43 W. Braunschweig et al., DESY report number 77/3(1977).

4.44 G.H. Trilling in Proceedings of the SLAC Summer Institute on Particle Physics, August 2-13, 1976 (SLAC report number 198).

4.45 T. Appelquist and H.D. Politzer, Phys. Rev. Lett. 34, 43(1975).

4.46 C.G. Callan et al., Phys. Rev. Lett. 34, 52(1975).

4.47 T. Appelquist et al., Phys. Rev. Lett. 34, 365(1975).

4.48 E. Eichten et al., Phys. Rev. Lett. 34, 369(1975).

4.49 B.J. Harrington et al., Phys. Rev. Lett. 34, 706(1975).

4.50 G.J. Feldman et al., Phys. Rev. Lett. 35, 821(1975).

4.51 G. Karl, S. Meshkov, J.L. Rosner, Phys. Rev. D13, 1203(1976).

4.52 L.S. Brown and R.N. Cahn, Phys. Rev. D13, 1195(1976).

4.53 P.K. Kabir and A.J.G. Hey, Phys. Rev. D13, 3161(1976).

4.54 H. Rieseberg, Invited talk at the 2nd International Conference at Vanderbilt University on New Results in High Energy Physics, Nashville, Tennessee, March 1-3, 1976.

4.55 R.L. Jaffe, (unpublished).

4.56 H. Harari, Phys. Lett. 64B, 469(1976).

4.57 R. Barbieri, R. Gatto, and E. Remiddi, Phys. Lett. 61B, 465(1976).

4.58 M.S. Chanowitz and F.J. Gilman, Phys. Lett. 63B, 178(1976).

4.59 J. Heintze in Proceedings of the 1975 International Symposium on Lepton and Photon Interactions at High Energies (Stanford University, 1975), p. 97.

REFERENCES

5.1. For an early review of charm theory, see M.K. Gaillard, B.W. Lee and J.L. Rosner, Rev. Mod. Phys. 47, 277(1975).

5.2. For a recent review of charm theory, see J.D. Jackson in Proceedings of the SLAC Summer Institute on Particle Physics (SLAC, Stanford University, 1976).

5.3. B. Knapp et al., Phys. Rev. Letters 37, 882(1976).

5.4. E.G. Cazzoli et al., Phys. Rev. Letters 34, 1125(1975).

5.5. A. De Rújula, H. Georgi and S.L. Glasgow, Phys. Rev. 12D, 147(1975).

5.6. For a simple discussion on the subject see L.H. Ryder, Elementary Particles and Symmetries (Gordan and Breach, New York, 1975), Chapters 12 and 13.

5.7. J. Ellis et al., Nucl. Phys. B100, 313(1975).

5.8. A.M. Boyarski et al., Phys. Rev. Letters 34, 1357(1975).

5.9. G. Goldhaber et al., Phys. Rev. Letters 37, 255(1976).

5.10. I. Peruzzi et al., Phys. Rev. Letters 37, 569(1976).

5.11. J.E. Wiss et al., Phys. Rev. Letters 37, 1531(1976).

5.12. A. De Rújula, H. Georgi and S.L. Glashow, Phys. Rev. Letters 37, 398(1976).

5.13. K. Lane and E. Eichten, Phys. Rev. Letters 37, 498(1976).

5.14. G. Goldhaber in Proceedings of the 1976 Summer Institute on Particle Physics (SLAC, Stanford University, 1976); also issued as LBL preprint LBL-5534.

5.15. J.E. Wiss, Invited talk at the Fifth International Conference on Experimental Meson Spectroscopy, Boston, Mass., April 29-30, 1977.

5.16. R. Schindler and R. Schwitters, private communication.

5.17. G.J. Feldman, et al., Phys. Rev. Letters (to be published).

5.18. R. Brandelik et al., Phys. Letters (to be published); also issued as DESY Preprint DESY 77/12 (1977).

5.19. J. Burmester et al., Phys. Letters (to be published); also issues as DESY Preprint, DESY 77/14 (1977).

5.20. V. Lüth in Proceedings of the XII Rencontre de Moriond, Flaine (1977, edited by Tran Thanh Van, R.M.I.E.M., Orsay.

5.21. D. Lüke et al., Bull. Am. Phys. Soc. 22, 544(1977).

5.22. M. Piccolo et al., (to be published).

5.23. H.K. Nguyen et al., (to be published).

REFERENCES SECTION 6

6.1 M.L. Perl in Proceedings of the Summer Institute on Particle Physics (SLAC, Stanford, Calif. 1975), p. 333; also issued as SLAC-PUB-1664. M.L. Perl in Proceedings of the Canadian Institute of Particle Physics Summer School (McGill University, Montreal, 1975); also issued as SLAC-PUB-1592.

6.2 M.L. Perl et al., Phys. Rev. Lett. 35, 1489(1975).

6.3 M.L. Perl et al., Phys. Lett. 63B, 466(1976).

6.4 G.J. Feldman et al., Phys. Rev. Lett. 38, 117(1976).

6.5 B.H. Wiik, Proceedings of the XVIII International Conference on High Energy Physics - Tbilisi, 1976 (Dubna, 1977) also issued as DESY Report 76/52 (1976).

6.6 J. Burmester et al., paper presented to the XVIII International Conference on High Energy Physics (Tbilisi, 1976).

6.7 W. Braunchweig et al., Phys. Lett. 63B, 466(1976).

6.8 J. Burmester et al., Phys. Lett. 64B, 369(1976).

6.9 Some recent general reviews on leptons are C.H. Llewellyn Smith, Oxford Univ. Preprint 33/76 (1976), submitted to Proc. Royal Soc. ; H. Fritzsch in Proceedings of the XII Rencontre de Moriond, Flaine, 1977, edited by Tran Thanh Van, R.M.I.E.M. Orsay; Ya. I. Azimov et al., in Proceedings of the XVIII International Conference on High Energy Physics - Tbilisi, 1976 (Dubna, 1977); also Leningrad Nuclear Physics Institute Preprint 275 (1976). An earlier general review is M.L. Perl and P. Rapidis, SLAC-PUB-1496 (1974) (unpublished). For theories in which the heavy lepton has some strong interaction properties see J.C. Pati and A. Salam, Proceedings of the Neutrino Conference 1976 (Aachen, 1976, to be published), also issued as International Center for Theoretical Physics Report IC/76/76, and the re-

ferences contained therein. See also G. Feinberg and T.D. Lee, Phys. Rev. 13D, 307(1976); T. Hagiwaru and A.I. Sanda, Phys. Rev. 13D, 3067(1976).

6.10 For recent general discussion and references see A. Pais, "Current Problems in the Weak Interactions," Rockefeller Univ. Report COO-2232B-118 (1977). See also H. Fritzsch and P. Minkowski, Calif. Inst. Tech. Preprint CALT-68-538(1976).

6.11 H.B. Thacker and J.J. Sakurai, Phys. Lett. 36B, 103(1971).

6.12 Y.S. Tsai, Phys. Rev. D4, 2821(1971). Another useful reference on heavy lepton decays is K.J.F. Gaemers and R. Raitio, Phys. Rev. D14, 1262(1976).

6.13a Some references on properties of sequential heavy leptons are:

A. Ali and Z.Z. Aydin, DESY Report 77/04(1977);

W. Alles and V. Alles Borelli, Nuovo Cimento 35a, 125(1976);

G.J. Aubrecht et al., Phys. Rev. 14D, 2955(1976);

Ya. I. Azimov et al., Leningrad Nuclear Physics Inst. Preprint 76-245(1976) and Preprint 286(1976);

R. Budny and A. McDonald, Phys. Rev. D15, 81(1977);

K. Fujikawa and N. Kawamoto, Phys. Rev. 13D, 2534(1976);

K. Fujikawa and N. Kawamoto, Phys. Rev. 14D, 59(1976);

T. Hagiwara et al., Rockefeller Univ. Preprint COO-2232B-105 (to be published in Ann. Phys. (N.Y.));

S. Kawasaki et al. Prog. Theor. Phys. 49, 1656(1973);

O. Nachtmann and A. Pais, Phys. Lett. 65B, 59(1976);

A. Pais and S.B. Breiman, Phys. Rev. 14D, 293(1976).

S.Y. Park and A. Yildiz, Phys. Rev. 14D, 2941(1976);

S. Pi and A.I. Sanda, Rockefeller Univ. Preprint COO-2232B-109 (to be published in Ann. Phys. (N.Y.)).

6.13b Some references on paraleptons are:

E. Lipmanov Zh, Eksp. Teor. Fiz. 43, 893(1962) (Sov. Phys. JETP 16, 634(1963);

Ya. B. Zel'Dovich, Usp. Fiz. Nauk 78, 549(1962) (Sov. Phys. Usp. 5, 931 (1963);

S.S. Gerstein and V.N. Folomeshkin, Yad. Fiz. 8, 768(1968) (Sov. J. Nucl. Phys. 8, 447(1969);

J.D. Bjorken and C.H. Llwellyn Smith, Phys. Rev. D7, 88(1973);

A. Ali and T.C. Yang, Phys. Rev. D14, 3052(1976).

6.13c F.E. Low, Phys. Rev. Lett. 14, 238(1965).

6.14 B.C. Barish et al., quoted by D.C. Cundy in Proceedings of the XVII International Conference on High Energy Physics (London, 1974), p. IV-147.

6.15 J. Smith et al., Inst. for Theoretical Physics Preprint (ITP-SB-77-5 (1977); the importance of this process at high energies was first pointed out to us by K.J.F. Gaemers.

6.16 Some references on semi-leptonic branching ratios are:

J. Ellis et al., Nucl. Phys. B100, 313(1975);

J.L. Rosner in Proceedings of Orbis Scientiae-1977 (Coral Gables, 1977, to be published), also issued as Preprint COO-2220-102.

6.17 Some references on the lepton momentum spectrum in the semi-leptonic decay of charmed mesons are:

A. Ali and T.C. Yang, Phys. Lett. 65B, 275(1976),

F. Bletzacker et al., Institute for Theoretical Physics Preprint IPP-SB-76-62 (1976);

D. Hitlin in Proceedings of the 1976 Summer Institute on Particle Physics (SLAC, Stanford, 1976).

6.18 A. Gavrielidis and T.K. Kuo, Phys. Lett. 64B, 196(1976), Phys. Rev. D15, 75(1977); F. Bletzacker and H.T. Nieh, Inst. for Theor. Phys. Preprint ITP-SB-76-32(1976).

6.19 G.J. Feldman, Proceedings of the 1976 Summer Institute on Particle Physics (SLAC, Stanford, 1976); also issued as SLAC-PUB-1852 (1976).

6.20 H. Meyer, paper presented to the 1976 Summer Institute on Particle Physics (SLAC, Stanford, 1976).

6.21 H. Meyer in Proceedings of the Orbis Scientiae-1977 (Coral Gables, 1977); see also V. Blobel in Proceedings of the XII Rencontre de Moriond (Flaine, 1977) edited by Tran Thanh Van, R.M.I.E.M. Orsay.

6.22 M.L. Perl in Proceedings of the XII Rencontre de Moriond (Flaine, 1977) edited by Tran Thanh Van, R.M.I.E.M. Orsay.

6.23 F.B. Heile et al., Bull. Am. Phys. Soc. 21, 568(1976), (to be published).

6.24 M. Cavalli-Sforza et al., Phys. Rev. Lett. 36, 588(1976). See ref. 6.19 for a discussion of this result.

6.25 G. Snow, Phys. Rev. Lett. 36, 766(1976).

6.26 R. Felst, paper presented at the Chicago Meeting of the American Physical Society (Feb. 1977); see also W. Wallraft in Proceedings of the XII Rencontre de Moriond (Flaine, 1977), edited by Tran Thanh Van, R.M.I.E.M. Orsay.

6.27 W. Braunschweig et al., Phys. Lett. 63B, 471(1976).

6.28 J.L. Burmester et al., Phys. Lett 64B, 369(1976).

6.29 D. Hitlin, Proceedings of the 1976 Summer Institute on Particle Physics (SLAC, Stanford, 1976).

REFERENCES SECTION 7

7.1 G. Hanson and P. Oddone, Proceedings of the 1975 PEP Summer Study, Stanford Linear Accelerator Center report number SLAC-190, p. 8.

7.2 J.Ellis, M.K. Gaillard, and G.G. Ross, Nucl. Phys. B111, 253(1976).

7.3 A.M. Polyakov, Sov. Phys.-JETP 33, 850(1971).

7.4 S.L. Glashow, J. Iliopoulos, and L. Maiani, Phys. Rev. D2, 1285(1970).

7.5 See for example R.M. Barnett, invited talk at Orbis Scientiae, University of Miami, Coral Gables, Florida, January 17-21, 1977 (SLAC report number SLAC-PUB-1891) and references therein.

7.6 E. Eichten and K. Gottfried, Phys. Lett. 66B, 286(1977).

TABLE 2.1

Properties of the previously accepted u,d,s quarks and the recently accepted c quark. I, I_z, Q, B, S and C are the isotopic spin, z component of the isotopic spin, charge, baryon number, strangeness and charm.

Name	u	d	s	c
Other Name	p	n	λ	p'
I	1/2	1/2	0	0
I_z	+1/2	-1/2	0	0
Q	+2/3	-1/3	-1/3	+2/3
B	1/3	1/3	1/3	1/3
S	0	0	-1	0
C	0	0	0	1

Table 4.1

Widths of the ψ particles. SLAC-LBL values [4.2, 4.4, 4.5].

	$\psi(3095)$	$\psi(3684)$	"4.1 region"	$\psi(4414)$
Γ(MeV)	0.069 ± 0.015	0.228 ± 0.056	~ 200	33 ± 10
Γ_{ee}(KeV)	4.8 ± 0.6	2.1 ± 0.3	~ 2	0.44 ± 0.14
$B_{ee} = \frac{\Gamma_{ee}}{\Gamma}$	0.069 ± 0.009	0.0093 ± 0.0016	$\sim 10^{-5}$	$(1.3 \pm 0.3) \times 10^{-5}$

Table 4.2

Decay modes of $\psi(3095)$

General modes include resonant contributions, e.g. $K^+K^-\pi^+\pi^-$ includes a contribution from $\phi\pi^+\pi^-$. The branching fraction always refers to the mode plus its charge conjugate state and unless qualified to the sum of all possible charge states, e.g. $\rho\pi = \Sigma(\rho^+\pi^- + \rho^o\pi^o + \rho^-\pi^+)$. Upper limits are at the 90% confidence level.

MODE	FRACTION (%)	REF.	FOOTNOTES
$e^+ e^-$	7.3 ± 0.5	4.4,4.6-4.13	a
$\mu^+ \mu^-$	7.5 ± 0.5		
$\pi^+ \pi^-$	0.011 ± 0.006	4.14,4.15	b
$\pi^+ \pi^- \pi^o$	1.6 ± 0.6	4.16	c
$2\pi^+ 2\pi^-$	0.4 ± 0.1	4.16	d
$2\pi^+ 2\pi^- \pi^o$	4.3 ± 0.5	4.16,4.17	
$3\pi^+ 3\pi^-$	0.4 ± 0.2	4.16	d
$3\pi^+ 3\pi^- \pi^o$	2.9 ± 0.7	4.16	
$4\pi^+ 4\pi^- \pi^o$	0.9 ± 0.3	4.16	
$\rho\ \pi$	1.12 ± 0.15	4.14,4.16,4.18	e
$A_2^+ \pi^-$	<0.43	4.14	f
$\omega\ \pi\ \pi$	0.82 ± 0.10	4.15,4.19	g
$\omega\ f$	0.28 ± 0.11	4.15,4.19	h
$B\ \pi$	0.38 ± 0.09	4.19	
$\rho\ \pi\ \pi\ \pi$	1.8 ± 0.45	4.16	g
$\rho\ A_2$	0.84 ± 0.45	4.15	g
$\omega\ 2\pi^+ 2\pi^-$	0.85 ± 0.34	4.15	

Table 4.2 continued

MODE	FRACTION (%)	REF.	FOOTNOTES
$K^+ K^-$	0.017 ± 0.011	4.14,4.15	i
$K_S K_L$	<0.0089	4.15	h,j
$K_S K^- \pi^+$	0.26 ± 0.07	4.15	
$K^+ K^- \pi^+ \pi^-$	0.72 ± 0.23	4.15	
$K^+ K^- \pi^+ \pi^- \pi^o$	1.2 ± 0.3	4.15	
$K^+ K^- 2\pi^+ 2\pi^-$	0.31 ± 0.13	4.15	
$2K^+ 2K^-$	0.07 ± 0.03	4.15	
$K^+ K^{-*}$	0.34 ± 0.05	4.14,4.15	k
$K^o \bar{K}^{o*}$	0.27 ± 0.06	4.15	k
$K^+ K^{-**}$	<0.15	4.15	h,k
$K^o \bar{K}^{o**}$	<0.20	4.15	h,k
$K^{o*} \bar{K}^{o*}$	<0.05	4.15	h,k
$K^{o*} \bar{K}^{o**}$	0.67 ± 0.26	4.15	k
$K^{o**} \bar{K}^{o**}$	<0.29	4.15	h,k
$\phi \pi \pi$	0.21 ± 0.09	4.15	g
ϕf	<0.037	4.15	
$\phi 2\pi^+ 2\pi^-$	<0.15	4.15	
$\omega K \bar{K}$	0.16 ± 0.10	4.15	g
$\omega f'$	<0.016	4.15	
$\phi K \bar{K}$	0.18 ± 0.80	4.15	g
$\phi f'$	0.08 ± 0.05	4.15	
$\phi \eta$	0.10 ± 0.06	4.15	
$\phi \eta'$	<0.13	4.15	

Table 4.2 continued

MODE	FRACTION (%)	REF.	FOOTNOTES
$p\,\bar{p}$	0.21 ± 0.02	4.11,4.14,4.20	ℓ
$p\,\bar{n}\,\pi^-$	0.38 ± 0.08	4.21	
$p\,\bar{p}\,\pi^o$	0.10 ± 0.02	4.21	
$p\,\bar{p}\,\eta$	0.19 ± 0.04	4.20	
$p\,\bar{p}\,\pi^+\,\pi^-$	0.41 ± 0.08	4.21	
$p\,\bar{p}\,\pi^+\,\pi^-\,\pi^o$	0.11 ± 0.04	4.21	
$p\,\bar{p}\,\omega$	0.05 ± 0.01	4.21	
$\Lambda\,\bar{\Lambda}$	0.16 ± 0.07	4.22	ℓ
$\Lambda\,\bar{\Sigma}$	<0.04	4.22	f
$\Xi^-\,\overline{\Xi^-}$	∿0.04	4.21	m
$\gamma\,\gamma$	< 0.05	4.23	
$\gamma\,\pi^o$	0.0073 ± 0.0047	4.24	
$\gamma\,\eta$	0.088 ± 0.019	4.23,4.24	
$\gamma\,\eta'$	0.24 ± 0.06	4.23,4.24	
γ X(2830)	<1.7	4.25	
γ X(2830) $\rightarrow 3\gamma$	0.013 ± 0.004	4.24,4.26	
γ X(2830) $\rightarrow \gamma\,p\,\bar{p}$	<0.004	4.20	
$\gamma\,\gamma\,\gamma$ (non-resonant)	<0.0078	4.24	

a. From a simultaneous fit to measurements on leptonic and total widths. The fit value for the total width is 67 ± 6 KeV.

b. This decay is isospin violating and thus presumably proceeds via a second-order electromagnetic interaction. With this assumption, $|F_\pi(q^2 - m_\psi^2)|^2 = (6.0 \pm 3.3) \times 10^{-3}$.

c. Mainly $\pi\rho$.

Table 4.2 footnotes continued

d. Proceeds via a second-order electromagnetic interaction. The total hadronic decay fraction via this type of interaction is (17 ± 3)% (Ref. 4.4).

e. $\Gamma(\rho^o\pi^o)/(\rho^+\pi^-) + \Gamma(\rho^+\pi^-) = 0.60 \pm 0.13$. (Ref. 4.16 and 4.18)

f. Forbidden by isospin.

g. Isospin invariance used to calculate modes with more than one neutral.

h. Error multiplied by 1.8 due to high χ^2.

i. This decay is SU(3) violating and probably proceeds via a second-order electromagnetic interaction. With this assumption, $|F_{K\pm}(q^2 = m^2)|^2 = (1.1 \pm 0.7) \times 10^{-2}$.

j. Implies $|F_{K^o}(q^2 = m_\psi^2)|^2 < 5.7 \times 10^{-3}$.

k. $K^* \equiv K^*(892)$ and $K^{**} \equiv K^*(1420)$.

l. Angular distribution of $1 + \cos^2\theta$ assumed. This is in agreement with measurements of the $\psi \to p\bar{p}$ mode.

m. Four events observed.

n. Forbidden for a spin 1 particle.

o. Error multiplied by 1.2 due to high χ^2.

Table 4.3

SU(3) tests for the χ states.

STATE	MODES	EXPECTED RATIO	OBSERVED RATIO
$\chi(3415)$	$\frac{\pi^+ \pi^-}{K^+ K^-}$	1	1.0 ± 0.4
$\chi(3415)$	$\frac{K^{*o} K^- \pi^+ + c.c.}{\rho^o \pi^+ \pi^-}$	$\frac{4}{3}$	1.4 ± 0.7
$\chi(3510)$	$\frac{K^{*o} K^- \pi^+ + c.c}{\rho^o \pi^+ \pi^-}$	$\frac{4}{3}$	1.2 ± 1.2
$\chi(3550)$	$\frac{K^{*o} K^- \pi^+ + c.c}{\rho^o \pi^+ \pi^-}$	$\frac{4}{3}$	1.0 ± 0.8

Table 4.4

ψ decay modes using the statistical model. All final states are assumed to have I=0 except $n\pi$ states with n even, for which I=1 is assumed.

Observed mode	General mode	$\frac{\Gamma(\text{observed})}{\Gamma(\text{general})}$	Branching fraction (general) %
$e^+ e^-$	$e^+ e^-$	1	7.3 ± 0.5
$\mu^+ \mu^-$	$\mu^+ \mu^-$	1	7.5 ± 0.5
$\pi^+ \pi^-$	2π	1	0.011 ± 0.006
$\pi^+ \pi^- \pi^o$	3π	1	1.6 ± 0.6
$2\pi^+ 2\pi^-$	4π	2/5	1.0 ± 0.25
$2\pi^+ 2\pi^- \pi^o$	5π	2/3	6.45 ± 0.75
$3\pi^+ 3\pi^-$	6π	5/28	2.2 ± 1.1
$3\pi^+ 3\pi^- \pi^o$	7π	5/12	7.0 ± 1.7
$4\pi^+ 4\pi^- \pi^o$	9π	7/29	3.7 ± 1.2
$K^+ K^- + K_S K_L$	$K \bar{K}$	1	0.017 ± 0.011
$K^o K^- \pi^+ + c.c$	$K \bar{K} \pi$	2/3	0.78 ± 0.21
$K^+ K^- \pi^+ \pi^-$	$K \bar{K} 2\pi$	1/4	2.9 ± 0.9
$K^+ K^- \pi^+ \pi^- \pi^o$	$K \bar{K} 3\pi$	9/40	5.3 ± 1.3
$K^+ K^- 2\pi^+ 2\pi^-$	$K \bar{K} 4\pi$	1/9	2.8 ± 1.2

Table 4.4 continued

$2K^+ 2K^-$	$2K\ 2\bar{K}$	1/6	0.42 ± 0.18
$\phi\eta$	$\phi\ \eta$	1	0.10 ± 0.06
$p\ \bar{p}$	$N\ \bar{N}$	1/2	0.42 ± 0.04
$p\ \bar{p}\ \pi^o$ $p\ \bar{n}\ \pi^-$ $\bar{p}\ n\ \pi^+$	$N\ \bar{N}\ \pi$	5/6	0.58 ± 0.10
$p\ \bar{p}\ \eta$	$N\ \bar{N}\ \eta$	1/2	0.38 ± 0.08
$p\ \bar{p}\ \pi^+\ \pi^-$	$N\ \bar{N}\ 2\pi$	1/4	1.64 ± 0.32
$p\ \bar{p}\ \pi^+\ \pi^-\ \pi^o$	$N\ \bar{N}\ 3\pi$	9/40	0.49 ± 0.18
$\Lambda\ \bar{\Lambda}$	$\Lambda\ \bar{\Lambda}$	1	0.16 ± 0.07
$\Xi^-\ \bar{\Xi}^-$	$\Xi\ \bar{\Xi}$	1/2	0.08 ± 0.08
$\gamma\ \pi^o$	$\gamma\ \pi^o$	1	0.007 ± 0.005
$\gamma\ \eta$	$\gamma\ \eta$	1	0.088 ± 0.019
$\gamma\ \eta'$	$\gamma\ \eta'$	1	0.24 ± 0.06
		TOTAL	53.2 ± 3.4

Table 4.5

Decay Modes of $\psi'(3684)$. (See heading for Table 4.2)

MODE	FRACTION (%)	REF.	FOOTNOTES
$e^+ e^-$	0.88 ± 0.13	4.5,4.13, 4.32	a
$\mu^+ \mu^-$	0.88 ± 0.13		
$\psi \pi^+ \pi^-$	33.1 ± 2.6	4.25,4.23, 4.34-4.39	b
$\psi \pi^o \pi^o$	15.9 ± 2.8		
$\psi \eta$	4.1 ± 0.7		
$\psi \gamma + \psi \pi^o$	<0.15	4.36	c
$\pi^+ \pi^-$	<0.005	4.21	d
$2\pi^+ 2\pi^-$	0.08 ± 0.02	4.40	e,m
$2\pi^+ 2\pi^- \pi^o$	0.35 ± 0.15	4.41	
$\rho \pi$	<0.1	4.18	
$K^+ K^-$	<0.005	4.21	f
$K^+ K^- \pi^+ \pi^-$	0.14 ± 0.04	4.40	m
$p \bar{p}$	0.023 ± 0.007	4.21	g,m
$\Lambda \bar{\Lambda}$	<0.04	4.21	
$\Xi^- \bar{\Xi}^-$	<0.02	4.21	h

Table 4.5 continued

$\gamma\ \gamma$	<0.5	4.42	i
$\gamma\ \pi^o$	<0.7	4.42	
$\gamma\ \eta$	<0.042	4.43	
$\gamma\ \eta'$	<0.11	4.18	
$\gamma\ \chi(2830)$	<1.0	4.25,4.37	
$\gamma\ \chi(2830) \rightarrow 3\gamma$	<0.034	4.43	
$\gamma\ \chi(3415)$	7.3 ± 1.7	4.25,4.37	j
$\gamma\ \chi(3510)$	7.1 ± 1.9	4.25	k
$\gamma\ \chi(3550)$	7.0 ± 2.0	4.25	k
$\gamma\ \chi(3455)$	<2.5	4.25	
$\gamma\ \chi(3455) \rightarrow \gamma\ \gamma\ \psi$	0.6 ± 0.4	4.37,4.39	l
$\gamma\ \chi(3455) \rightarrow 3\gamma$	<0.031	4.43	

a. From a simultaneous fit to measurements on leptonic and total widths with $\Gamma(ee) = \Gamma(\mu\mu)$ assumed. Without this assumption $\Gamma(\mu\mu)/\Gamma(ee) = 0.89 \pm 0.16$ (Ref. 4.33). The total decay width was determined to be 212 ± 34 KeV.

b. From a simultaneous fit to measurements of $\psi' \rightarrow \psi$ + anything, $\psi' \rightarrow \psi$ + neutrals, $\psi' \rightarrow \psi\pi^+\pi^-$, $\psi' \rightarrow \psi\pi^o\pi^o$, $\psi' \rightarrow \psi\eta$, and $\psi' \rightarrow \gamma\chi \rightarrow \gamma\gamma\psi$.

c. $\psi\gamma$ forbidden by C and $\psi\pi^o$ forbidden by isospin.

d. Forbidden by isospin.

e. Proceeds by second-order electromagnetic interaction. The total hadronic decay fraction via this type of interaction is $(2.9 \pm 0.4)\%$ (Ref. 4.5).

Table 4.5 footnotes continued

f. Forbidden by SU(3)

g. Angular distribution of $1 + \cos^2\theta$ assumed. This is in agreement with measurements of the $\psi \to p\bar{p}$ decay.

h. Two events observed.

i. Forbidden for a spin 1 particle.

j. Angular distribution of $1 + \cos^2\theta$ assumed in agreement with spin 0 assignment and experimental measurements (Ref. 4.44).

k. Angular distribution assumed to be isotropic.

l. The references listed are the primary measurements, but the value comes from the overall fit described in footnote b.

m. Non-resonant background has not been subtracted. It is about 50% of the signal for $2\pi^+2\pi^-$ and a smaller but undetermined amount for other decay modes.

Table 4.6

Comparison of direct ψ and ψ' decays.

MODE	Γ_ψ(KeV)	$\Gamma_{\psi'}$(KeV)	$\Gamma_{\psi'}/\Gamma_\psi$
$e^+ e^-$	4.9 ± 0.3	1.9 ± 0.3	0.39 ± 0.07
$p \bar{p}$	0.14 ± 0.01	0.05 ± 0.02	0.36 ± 0.11
$K^+ K^- \pi^+ \pi^-$	0.48 ± 0.16	0.30 ± 0.09 [a]	0.62 ± 0.28

[a]Non-resonant background has not been subtracted.

Table 4.7

Summary of ψ' decay modes.

MODE	BRANCHING FRACTION (%)
lepton pairs	1.8 ± 0.3
hadrons via second-order e.m. interaction	2.9 ± 0.4
direct decays to ordinary hadrons	9 ± 5
$\psi \pi \pi$, $\psi \eta$	53.3 ± 4.4
$\gamma \chi$	22 ± 6
TOTAL	89 ± 9

Table 4.8

Mass Determinations of the χ States

Masses are referenced to $m_{\psi'} = 3684$ MeV/c^2. See footnote c.

State	Mass (MeV/c^2)	ψ' Decay Mode	Ref.	Footnotes
$\chi(3415)$	3415 ± 10	γ + hadrons	4.44	
	3413 ± 11	monochromatic γ	4.37	
	3413 ± 10	$\gamma\gamma\psi$	4.37	a
	3413 ± 9	monochromatic γ	4.25	
average	3413 ± 5			
$\chi(3455)$	3454 ± 7	$\gamma\gamma\psi$	4.37	b
$\chi(3510)$ or P_c	3500 ± 10	γ + hadrons	4.44	
	3504 ± 7	$\gamma\gamma\psi$	4.37	
	3511 ± 7	monochromatic γ	4.25	
	3512 ± 7	$\gamma\gamma\psi$	4.38	c
average	3508 ± 4			
$\chi(3550)$	3550 ± 10	γ + hadrons	4.44	
	3543 ± 7	$\gamma\gamma\psi$	4.37	
	3561 ± 7	monochromatic γ	4.25	
average	3552 ± 6			d

a. A single event.

b. The existence of this state needs confirmation

c. DORIS mass assignments have been increased by 4 MeV/c^2 to correct for the difference in ψ' mass measurements between SPEAR and DORIS.

d. Error increased by 30% due to high χ^2.

Table 4.9

Decay Modes of the $\chi(3415)$

The branching fraction for $\psi' \to \gamma\chi(3415)$ is assumed to be 0.073 (Refs. 4.25 and 4.37) in calculating the χ branching fractions. See heading for Table 4.2.

Mode	$B(\psi' \to \gamma\chi)\cdot B_\chi(\%)$	$B_\chi(\%)$	Ref.	Footnote
$\gamma\ \psi$	0.2 ± 0.2	$3. \pm 3.$	4.25,4.37 4.39	a
$\pi^+\ \pi^-$	0.07 ± 0.02	1.0 ± 0.3	4.44	
$K^+\ K^-$	0.07 ± 0.02	1.0 ± 0.3	4.44	
$2\pi^+\ 2\pi^-$	0.32 ± 0.06	4.4 ± 0.8	4.44	
$K^+\ K^-\ \pi^+\ \pi^-$	0.27 ± 0.07	3.7 ± 1.0	4.44	
$p\ \bar{p}\ \pi^+\ \pi^-$	0.04 ± 0.013	0.5 ± 0.2	4.44	
$3\pi^+\ 3\pi^-$	0.14 ± 0.05	1.9 ± 0.7	4.44	
$\rho^o\ \pi^+\ \pi^-$	0.12 ± 0.04	1.7 ± 0.6	4.44	
$K^{o*}\ K^+\ \pi^-$	0.17 ± 0.06	2.3 ± 0.8	4.44	
$\gamma\ \gamma$	< 0.04	< 0.55	4.43	

a. The references listed are the primary references, but the value comes from the overall fit described in Table 4.5, footnote b.

Table 4.10

Decay Modes of the $\chi(3510)$ or P_c

The branching fraction for $\psi' \to \gamma\chi(3510)$ is assumed to be 0.071 (Ref. 4.25) in calculating the χ branching fractions. See heading for Table 4.2.

Mode	$B(\psi' \to \gamma\chi)\cdot B_\chi(\%)$	$B_\chi(\%)$	Ref.	Footnote
$\gamma\ \psi$	2.5 ± 0.5	$35. \pm 7.$	4.25,4.37 4.39	a
$\pi^+\ \pi^-$ and $K^+\ K^-$	<0.015	<0.21	4.44	b
$2\pi^+\ 2\pi^-$	0.11 ± 0.04	1.5 ± 0.6	4.44	
$K^+\ K^-\ \pi^+\ \pi^-$	0.06 ± 0.03	0.85 ± 0.42	4.44	
$p\ \bar{p}\ \pi^+\ \pi^-$	0.01 ± 0.008	0.14 ± 0.11	4.44	
$3\pi^+\ 3\pi^-$	0.17 ± 0.06	2.4 ± 0.8	4.44	
$\rho^o\ \pi^+\ \pi^-$	0.026 ± 0.022	0.37 ± 0.31	4.44	
$K^{o*}\ K^+\ \pi^-$	0.031 ± 0.022	0.44 ± 0.31	4.44	
$\gamma\ \gamma$	<0.026	<0.37	4.43	c

a. The references listed are the primary references, but the value comes from the overall fit described in Table 4.5, footnote b.

b. Forbidden for a $J^P = 1^+$ state.

c. Forbidden for a spin 1 particle.

Table 4.11

Decay Modes of the $\chi(3550)$

The branching fraction for $\psi' \to \gamma\chi(3550)$ is assumed to be 0.070 (Ref. 4.25) in calculating the χ branching fractions. See heading for Table 4.2

Mode	$B(\psi' \to \gamma\chi)\cdot B_\chi(\%)$	$B_\chi(\%)$	Ref.	Footnote
$\gamma\ \psi$	1.0 ± 0.4	$14. \pm 6.$	4.25,4.37, 4.39	a
$\pi^+\ \pi^-$ and $K^+\ K^-$	0.02 ± 0.01	0.29 ± 0.14	4.44	
$2\pi^+\ 2\pi^-$	0.16 ± 0.04	2.3 ± 0.6	4.44	
$K^+\ K^-\ \pi^+\ \pi^-$	0.14 ± 0.04	2.0 ± 0.6	4.44	
$p\ \bar{p}\ \pi^+\ \pi^-$	0.02 ± 0.01	0.29 ± 0.14	4.44	
$3\pi^+\ 3\pi^-$	0.08 ± 0.05	1.1 ± 0.7	4.44	
$\rho^o\ \pi^+\ \pi^-$	0.05 ± 0.030	0.71 ± 0.43	4.44	
$K^{o*}\ K^+\ -$	0.052 ± 0.031	0.74 ± 0.44	4.44	
$\gamma\ \gamma$	< 0.02	< 0.29	4.43	

a. The references listed are the primary references, but the value comes from the overall fit described in Table 4.5, footnote b.

Table 4.12

Spin assignments of the χ states. The preferred assignments depend on assumptions discussed in the text.

State/J^P	0^-	0^+	1^+	2^+
$\chi(3550)$	excluded by $\chi \to \pi^+\pi^-$ or K^+K^- and by angular distribution in $\psi' \to \gamma\chi \to \gamma$ hadrons	excluded by angular distribution in $\psi' \to \gamma\chi \to \gamma$ hadrons	excluded by $\chi \to \pi^+\pi^-$ or K^+K^-	preferred
$\chi(3510)$	excluded by angular distribution in $\psi' \to \gamma\chi \to \gamma\gamma\psi$	excluded by angular distribution in $\psi' \to \gamma\chi \to \gamma\gamma\psi$	preferred	
$\chi(3455)$	preferred			
$\chi(3415)$	excluded by $\chi \to \pi^+\pi^-$ or K^+K^-	preferred	excluded by $\chi \to \pi^+\pi^-$ or K^+K^-	

Table 5.1

Quark content and internal quantum numbers of the D and F type single charmed mesons. Only the particles are shown.

Type	D		F
Charm	+1		+1
I	1/2		0
Strangeness	0		+1
Quark Content	$c\bar{d}$	$c\bar{u}$	$c\bar{s}$
Pseudoscalar Name	D^+	D^0	F^+
Vector Name	D^{*+}	D^{*0}	F^{*+}

Table 5.2

Quark content and internal quantum numbers of spin 1/2, singly charmed baryons. The pairs of ordinary quarks are classified into symmetric and anti-symmetric states

Type	Isospin	Strangeness	Name		Quark Content
C_1	1	0	C_1^{++}	Σ_c^{++}	c u u
			C_1^{+}	Σ_c^{+}	$c\,(ud)_{sym}$
			C_1^{o}	Σ_c^{o}	c d d
C_o	0	0	C_o^{+}	Λ_c^{+}	$c\,(ud)_{anti}$
S	$\frac{1}{2}$	-1	S^{+}		$c\,(su)_{sym}$
			S^{o}		$c\,(sd)_{sym}$
A	$\frac{1}{2}$	-1	A^{+}		$c\,(su)_{anti}$
			A^{o}		$c\,(sd)_{anti}$
T	0	-2	T^{o}		c s s

Table 5.3

Effective quark masses from eq. (5.2).

Quark	Effective Mass (GeV/c^2)
u	0.39
d	0.39
s	0.51
c	1.55

Table 5.4

Some predicted branching ratios for singly charmed mesons from ref.[5.7]. M_c means D^0, $D^\pm$, or $F^\pm$. ℓ, ν_e means e or u and the corresponding neutrino or antineutrino.

Decay Mode	Branching Ratio
$M_c \longrightarrow \ell + \nu_e +$ hadrons	.1 - .25
$D \longrightarrow \ell + \nu_e + K$	.03 - .08
$F \longrightarrow \ell + \nu_e + K$	.02 - .05
$D^0 \longrightarrow K\pi$	.03 - .18
$D^+ \longrightarrow K\pi$	.02 - .10
$F^+ \longrightarrow \eta\pi^+$ or $F^+ \longrightarrow \bar{K}K$	.02 - .12

Table 5.5

Summary of charmed meson data of SLAC-LBL Magnetic Detector Collaboration

E_{cm} (GeV)	When obtained	Hadronic Events	Integrated Luminosity (nb^{-1})
3.9 - 4.6	before May, 1976	29,000	~ 1830
4.028	May-July, 1976	25,000	~ 1280
4.415	May-July, 1976	26,000	~ 1630

Table 5.6a

Preliminary values of some properites of the D^*-D system obtained the recoil mass spectra against the D^o and D^+ at E_{cm} = 4.028 GeV, ref.[5.14-5.17] .

Parameter	Value
M_{D^o}(MeV/c^2)	1865 ± 3
M_{D^+}(MeV/c^2)	1875 ± 5
$M_{D^{*o}}$(MeV/c^2)	2006 ± 1.5
$M_{D^{*+}}$(MeV/c^2)	2010 ± 3
$\Gamma(D^{*o} \to D^o\gamma)/\Gamma(D^{*o} \to \text{all})$	0.55 ± 0.15

Table 5.6b

Preliminary values of relative cross sections for D^o and D^{*o} production at E_{cm} = 4.028 GeV, ref.[5.14-5.15].

Reaction	Relative Cross Section (Arbitrary Units)
$e^+ + e^- \to D^o + \overline{D^o}$	1.0 ± 0.6
$e^+ + e^- \to D^o + \bar{D}^{*o}$ and $D^o + D^{*o}$	9.4 ± 1.6
$e^+ + e^- \to D^{*o} + \bar{D}^{*o}$	9.6 ± 1.6

Table 5.7

Preliminary values for cross sections times branching ratios ($\sigma \cdot B$) for D^o and D^+ production [5.15,5.22].

Meson	Decay Mode	$\sigma \cdot B$(nb) $E_{cm} = 4.028$
$D^o, \overline{D^o}$	$K^{\pm}\pi^{\mp}$	0.57 ± 0.11
	$K^o\pi^+\pi^- + \overline{K^o}\pi^+\pi^-$	1.09 ± 0.30
	$K^{\pm}\pi^{\mp}\pi^+\pi^-$	0.83 ± 0.27
	$\pi^+\pi^-$	0.04
	K^+K^-	0.04
$D^{\pm}$	$K^{\pm}\pi^{\mp}\pi^{\mp}$	0.40 ± 0.10
	$K^{\pm}\pi^+\pi^-$	0.02
	$\pi^{\pm}\pi^+\pi^-$	0.03
	$K^+K^-\pi^{\pm}$	0.06
	$K^o\pi^{\pm} + \overline{K^o}\pi^{\pm}$	0.18

Table 6.1

Predicted branching ratios for a τ^- sequential charged heavy lepton with a mass 1.9 GeV/c^2, an associated neutrino mass of 0.0, and V-A coupling. The predictions are based on Refs. 6.11 and 6.12 as discussed in Ref. 6.19. The hadron continuum branching ratio assumes a threshold at 1.2 GeV for production of $\bar{u}d$ quark pairs whose final state interaction leads to the hadron continuum

decay mode	branching ratio	number of charged particles in final state
$\nu_\tau e^- \bar{\nu}_e$	.20	1
$\nu_\tau \mu^- \bar{\nu}_\mu$	.20	1
$\nu_\tau \pi^-$	.11	1
$\nu_\tau K^-$	.01	1
$\nu_\tau \rho^-$	.22	1
$\nu_\tau K^{*-}$	.01	1
$\nu_\tau A_1^-$	.07	1, 3
ν_τ (hadron continuum)$^-$	.18	1, 3, 5

Table 6.2

90% confidence level upper limits on the fraction of decays in reaction(6.18) which can contain an undetected particle or combination of particles.

undetected particle(s)	90% confidence upper limit
K^o	0.09
π^o or γ	0.18
Charged particle	0.09
Charged particle + π^o or γ	0.11
TOTAL	0.39

Table 6.3

χ^2 probabilities for the fits in Fig. 6.8

Theory	E_{cm} range (GeV)	χ^2 probability
Heavy Lepton: m_τ=1.90 GeV/c^2, m_{ν_τ} = 0.0,	$3.8 < E_{cm} < 4.8$	.92
	$E_{cm} = 4.8$	.01
V-A, 3-body lepton, decay.	$4.8 < E_{cm} < 7.8$	.46
	$3.8 < E_{cm} < 7.8$	.50
Boson: m_τ=1.90 GeV/c^2, 2-body decay, unpolarized.	$3.8 < E_{cm} < 7.8$	$<10^{-4}$
Boson: m_τ=1.90 GeV/c^2, 2-body decay , helicity=0 state only .	$3.8 < E_{cm} < 7.8$	$<10^{-4}$

Table 6.4

Probabilities that the mass m_τ can yield the observed $\sigma_{e\mu}$ cross section in Fig. 6.5. $P_T(m_\tau)$ is the probability that all $e\mu$ events produced at $E_{cm} < 2\ m_\tau$ comes from background.

m_τ (GeV/c^2)	$P_T(m_\tau)$
1.7	no $e\mu$ events with $E_{cm} < 3.8$ GeV
1.8	
1.9	0.10
1.95	0.06
2.00	0.06
2.05	0.06
2.10	0.008
2.15	0.002

Table 6.5a

Mass measurements of the τ in GeV/c^2, assuming V-A coupling for the τ-ν_τ, and $m_{\nu_\tau} = 0.0$. The three methods are based on: $p_\perp$, the pseudo-transverse momentum; $\cos\theta_{coll}$, the cosine of the collinearity angle; and r, the scaled momentum distribution. They are explained in the text. The errors are statistical.

E_{cm} range (GeV)	Method $p_\perp$	$\cos\theta_{coll}$	r
$3.8 < E_{cm} < 4.8$	1.88 ± .08	1.91 ± .25	1.83 ± .06
$E_{cm} = 4.8$	2.11 ± .13	1.82 ± .22	1.83 ± .08
$4.8 < E_{cm} < 7.8$	1.86 ± .08	1.85 ± .12	2.27 ± .31
$3.8 < E_{cm} < 7.8$	1.91 ± .05	1.85 ± .10	1.88 ± .06

Table 6.5b

Mass measurements of the τ in GeV/c^2 for two models: V-A coupling for the τ-ν_τ and $m_{\nu_\tau} = 0.5$ GeV/c^2; and V+A coupling for the τ-ν_τ and $m_{\nu_\tau} = 0.0$. The three methods: $p_\perp$, $\cos\theta_{coll}$, and r are explained in the text. The entire $3.8 < E_{cm} < 7.8$ range is used and the errors are statistical.

Model	Method $p_\perp$	$\cos\theta_{coll}$	r
V-A $m_{\nu_\tau} = 0.5$ GeV/c^2	2.01 ± .05	1.90 ± .09	1.70 ± .12
V+A $m_{\nu_\tau} = 0.0$	2.12 ± .05	1.95 ± .10	upper limit is 1.76 with 95% confidence.

Table 6.6

Ratios of the observed cross sections σ_{ee}, $\sigma_{e\mu}$ and $\sigma_{\mu\mu}$ for anomalous pair production. The errors are statistical. See Ref. 6.23 for a discussion of the systematic errors and the data sets.

Data Set	E_{cm} Range (GeV)	$\sigma_{ee}/\sigma_{e\mu}$	$\sigma_{\mu\mu}/\sigma_{e\mu}$
2	3.9 - 4.3	.30 ± .24	.75 ± .26
	4.3 - 4.8	.86 ± .38	1.46 ± .49
	4.8 - 6.8	.45 ± .16	.52 ± .14
	6.8 - 7.4	.56 ± .26	.51 ± .20
1	3.9 - 4.8	.37 ± .33	.63 ± .35
	4.8	.68 ± .30	.27 ± .20
1 and 2	all events	.52 ± .10	.63 ± .10

Table 6.7

Anomalous 2-prong muon production results. A candidate is a particle which has sufficient momentum and the proper direction to be detected by the muon spark chambers at level 2 or 3 if it were a muon, but events in which both prongs are electrons are excluded. The backgrounds which are listed and subtracted are from radiative μ pairs, from $ee\mu\mu$ events, and from hadron penetration and decay. The expected heavy lepton contribution is for $m_\tau = 1.90$ GeV/c^2, $m_{\nu_\tau} = 0.0$, V-A coupling, and the relative decay rates in Table 6.1. From Refs. 6.4 and 6.19 .

E_{cm} range (GeV)	3.9 to 4.3	4.3 to 4.8	5.8 to 7.8
Average E_{cm} (GeV)	4.05	4.4	6.9
Candidates	181	224	902
Muons	24	29	177
Radiative μ pairs	2.3	2.2	17
$ee\mu\mu$ events	1.4	1.8	29
Hadron penetration or decay	5.0	6.4	28
Anomalous muons	15.3 ± 5.1	18.6 ± 5.7	103 ± 18
Anomalous cross section (pb)	194 ± 71	253 ± 71	212 ± 49
Expected heavy lepton lepton contribution (pb)	252 to 57	290 to 197	218 to 191

FIGURE CAPTIONS

Fig. 2.1. Simplified presentation of σ_{had} versus E_{cm}. The shaded areas indicate large uncertainties in the value of σ_{had}. See fig. 2.3 for a detailed presentation of the experimental errors and uncertainties.

Fig. 2.2. Feynman diagrams for (a) the one-photon exchange process for hadron production, (b) muon pair production, (c) the quark model for hadron production, and (d) the resonance model for hadron production.

Fig. 2.3. $R = \sigma_{had}/\sigma_{\mu^+\mu^-}$. The references for this data are given in I, II, and ref. [1.4]. The $E_{cm} > 2$ GeV data is from the SLAC-LBL Magnetic Detector Collaboration. See ref. [2] for very recent data from the PLUTO group in the $4 < E_{cm} < 5$ GeV region.

Fig. 2.4. The SLAC-LBL Magnetic Detector, ref. [I].

Fig. 2.5. R in the $E_{cm} = 3.8$ to 4.6 GeV region from the SLAC-LBL Magnetic Detector Collaboration, ref. [2.4].

Fig. 2.6. R in the $E_{cm} = 3.5$ to 5.0 GeV region from the PLUTO Group, ref. [2.5]. The dotted line is used to guide the eye. The full line is the cross section for a pointlike heavy lepton of mass 1.95 GeV, (section 6).

Fig. 2.7. The PLUTO Group's detector, ref.[2.5].

Figure Captions for Section 3

1. Hadron production in e^+e^- annihilations in quark-parton models.
2. Observed mean sphericity vs E_{cm} for data, jet model (solid curve), and phase-space model (dashed curve).
3. Observed $p_\perp$ with respect to jet axis for 7.4 GeV data. The predicted distributions for the jet model (solid curve) and the phase-space model (dashed curve) are also shown.
4. Observed sphericity distributions for data, jet model (solid curves) and phase-space model (dashed curves) for (a) E_{cm} = 3.0 GeV, (b) E_{cm} = 6.2 GeV, and (c) E_{cm} = 7.4 GeV.
5. Observed x distributions at E_{cm} = 7.4 GeV for data, jet model (solid curve), and phase-space model (dashed curve).
6. Observed sphericity distributions at E_{cm} = 7.4 GeV for data, jet model (solid curves), and phase-space model (dashed curves) for (a) events with largest $x \leq 0.4$ and (b) events with largest $x > 0.4$.
7. Observed jet mass distributions at E_{cm} = 7.4 GeV for (a) all jets, (b) 2-prong, charge = 0 jets, and (c) 3-prong, charge = $\pm$ 1 jets. Pion masses were used for all particles. The arrows indicate the masses of particles or resonances having the indicated decay modes.
8. Observed distributions of jet axis azimuthal angles from the plane of the storage ring for jet axes with $|\cos\theta| \leq 0.6$ for (a) E_{cm} = 6.2 GeV and (b) E_{cm} = 7.4 GeV.
9. Observed inclusive α vs x for particles with $|\cos\theta| \leq 0.6$ in hadronic events at E_{cm} = 7.4 GeV. The prediction of the jet model Monte Carlo simulation for a jet axis angular distribution with $\alpha = 0.97 \pm 0.14$ is represented by the shaded band.

10. $s\, d\sigma/dx$ vs x for E_{cm} = 3.0, 4.8, 6.2, and 7.4 GeV.

11. $s\, d\sigma/dx_{\parallel}$ vs $x_{\parallel}$ for E_{cm} = 3.0, 4.8, 6.2, and 7.4 GeV. $x_{\parallel} = 2p_{\parallel}/E_{cm}$ where $p_{\parallel}$ is the component of particle momentum parallel to the jet axis.

12. $(1/\sigma)\, d\sigma/dp_{\perp}$ vs $p_{\perp}$ for events with $x_{max} > 0.5$ for E_{cm} = 3.0, 4.8, 6.2, and 7.4 GeV. x_{max} is not plotted. The distributions are normalized to the cross sections for events with $x_{max} > 0.5$. $p_{\perp}$ is the component of particle momentum perpendicular to the jet axis.

13. $(1/\sigma)\, d\sigma/dy$ vs y for events with $x_{max} > 0.5$ for E_{cm} = 3.0, 4.8, and 7.4 GeV. x_{max} is not plotted. The distributions are normalized to the cross sections for events with $x_{max} > 0.5$. y is the rapidity of the particle with respect to the jet axis. Pion masses were assumed.

FIGURE CAPTIONS

Fig. 4.1. R, the ratio of the cross section for the production of hadrons to the cross section for the production of μ pairs, as a function of center-of-mass energy in the vicinity of the $\psi(4414)$. The curve is the fit to the $\psi(4414)$ line shape. The data are from ref. [4.2].

Fig. 4.2. Quark diagrams illustrating the OZI rule in ϕ decays.

Fig. 4.3. Cross sections for (a) hadron production, (b) μ pair production, and, (c) e pair production and scattering in the vicinity of the ψ. Data are from ref. [4.4].

Fig. 4.4. Cross sections for (a) hadron production, (b) μ pair production, and (c) e pair production and scattering in the vicinity of the ψ'. Data are from ref. [4.5].

Fig. 4.5. Diagrams for (a) $e^+e^- \to \psi \to$ anything, and (b) $e^+e^- \to \psi \to e^+e^-$.

Fig. 4.6. The ratio of μ pair yield to e pair yield in the vicinity of (a) the ψ and (b) the ψ' for $|\cos\theta| \lesssim 0.6$. Data are from ref. [4.4] and [4.5].

Fig. 4.7. Diagrams for (a) direct ψ decays to hadrons, (b) ψ decays to hadrons via an intermediate photon, and (c) ψ decay to μ pairs.

Fig. 4.8. α(defined in eq. 4.5) versus number of pions in ψ decays. Data are from ref. [4.16].

Fig. 4.9. Quark diagrams illustrating (a) $\psi \to \omega\pi^+\pi^-$, (b) $\psi \to \phi\pi^+\pi^-$, (c) $\psi \to \phi S^* \to \phi\pi^+\pi^-$.

Fig. 4.10. Invariant mass of $\pi^+\pi^-$ in (a) $\psi \to \phi\pi^+\pi^-$, and (b) $\psi \to \omega\pi^+\pi^-$. Data are from ref. [4.15].

Fig. 4.11. Quark diagrams illustrating three mechanisms for $\psi \to \gamma\pi^0$, $\psi \to \gamma\eta$, and $\psi \to \gamma\eta'$ decays.

Fig. 4.12. Diagram for calculating $\psi \to \gamma\eta$ from $\psi' \to \chi\eta$ using vector meson dominance.

Fig. 4.13. States and radiative transitions expected from bound fermion-anti-fermion system.

Fig. 4.14. Invariant χ mass distributions for $\psi' \to \gamma\chi$ for (a) $2\pi^+2\pi^-$ (b) $\pi^+\pi^-K^+K^-$ (c) $3\pi^+3\pi^-$, and (d) the sum of $\pi^+\pi^-$ and K^+K^-. Data are from ref. [4.44].

Fig. 4.15. Computer reconstruction of a $\psi' \to \gamma\chi \to \gamma\gamma\psi \to \gamma\gamma\mu\mu \to \gamma e^+e^-\mu^+\mu^-$ cascade in the SLAC-LBL Magnetic Detector at SPEAR. The short boxes represent trigger counters and the long boxes represent shower counters. The uncoverted γ is detected by the isolated shower counter on the left.

Fig. 4.16. Scatter plot of the two solutions for the mass of χ states in $\psi' \to \gamma\chi \to \gamma\gamma\psi$ events. Data are from ref. [4.37].

Fig. 4.17. Inclusive photon energy distributions for (a) ψ decays and (b) ψ' decays (ref. [4.37]) observed with converted photons in the SLAC-LBL Magnetic Detector at SPEAR.

Fig. 4.18. Inclusive photon energy distributions for (a) ψ decays and (b) ψ' decays measured by the MPPSDSS experiment at SPEAR (ref. [4.25]). Part (c) shows the ψ distributions with backgrounds subtracted. The dotted curves represent Monte Carlo calculations and fits.

Fig. 4.19. Definition of angles for the cascade decay $\psi' \to \gamma\chi \to \gamma\gamma\chi \to \gamma\gamma\mu^+\mu^-$.

Fig. 4.20. Distribution of cos θ for $\psi' \to \gamma\chi$, $\chi \to 2\pi^+2\pi^-$ or $K^+K^-\pi^+\pi^-$. Data are from ref. [4.40].

Fig. 4.21. The highest $\gamma\gamma$ mass combination for each event in $\psi \to 3\gamma$. The dashed curve is the expected contribution from radiative two photon production and reflections from $\gamma\eta$ and $\gamma\eta'$ decays. Data are from ref. [4.24].

Fig. 4.22. Invariant mass of $p\bar{p}$ in $\psi \to pp\pi^0$ and $pp\gamma$ decays. Data are from ref. [4.20].

Fig. 4.23. Summary of observed charmonium states and transitions. Uncertain states and transitions are indicated by dashed lines. Numbers indicate branching fractions in per cent. The symbol "γ^*" stands for second-order electromagnetic decays including decays to lepton pairs.

FIGURE CAPTIONS

Fig. 5.1. The SU_4 multiplet for the pseudoscalar mesons.

Fig. 5.2. Decays of the c quark: (a) non-leptonic, and (b) leptonic. The associated term gives the effect of the Cabibo angle on the amplitude.

Fig. 5.3 Quark diagrams for decays of the D^o meson.

Fig. 5.4. The $K\pi$ and $K3\pi$ invariant mass spectra data in which the D^o was first found. Note that the mass enhancement at 1865 MeV/c^2 occurs only in the expected K and π combinations. ref. [5.9].

Fig. 5.5. Recoil-mass spectra for combinations in the $K\pi$ and $K3\pi$ peaks.

Fig. 5.6. The $K2\pi$ invariant mass spectra data in which the $D^{\pm}$ was first found, ref. [5.10].

Fig. 5.7. $D\pi$-D mass difference spectra for (a) $D^o\pi^+$ and $\overline{D^o}\pi^-$ (i.e. $K^{\mp}\pi^{\pm}\pi^{\pm}$) combinations, and (b) $\overline{D^o}\pi^+$ and $D^o\pi^-$ (i.e. $K^{\mp}\pi^{\pm}\pi^{\mp}$ combinations).

Fig. 5.8. Level structure and possible decays of the D^*-D system.

Fig. 5.9. The recoil mass spectra at E_{cm} = 4.028 GeV against (a) $K^{\pm}\pi^{\pm}$, (b) $(K3\pi)^o$, and (c) $K^{\mp}\pi^{\pm}\pi^{\pm}$ from ref. [5.14].

Fig. 5.10. Prediction for the shape of the recoil mass spectra against the D^o at E_{cm} = 4.05 GeV, from ref [5.12]. The contributions are: 1 from eq. (5.13a); 2 from eq. (5.13b); 3 from eqs. (5.13c) and (5.13d); 4 from eq. (5.13g); 5 from eqs. (5.13e) and (5.13f); and 6 from eq. (5.13h).

Fig. 5.11. The inclusive cross section for $e^+e^- \to K^{\pm}X$ from ref. [5.18].

Fig. 5.12. (a) Comparison of R_K^{new} and R^{new} from ref. [5.18]. See the text for an explanation of R_K^{new} and R^{new}. The R^{new} data is from ref. [2.5].
(b) The same data as (a) with heavy lepton contribution subtracted from R^{new}.

Fig. 5.13. The total inclusive K_s^o cross section for $p(K_s^o) > 0.2$ GeV/c as function of $\sqrt{s}$ (GeV), from ref. [5.19].

Fig. 5.14. $R_K' = 2\sigma_{K_s}/\sigma_{\mu\mu}$ as a function of E_{cm} from ref.[5.20].

FIGURE CAPTIONS

Fig. 6.1. Analogy between (a) the decay of a τ charged heavy lepton to hadrons, and (b) the production of hadrons in e^+e^- annihilation.

Fig. 6.2. (a) Relative decay rates for a sequential heavy lepton with V-A coupling, zero neutrino mass, and mass m, based on the input in table 6.1 and R = 10/3 for $E_{cm} > 2.0$ GeV, and (b) the corresponding lifetime.

Fig. 6.3. Feynman diagram for $e^+ + e^- \rightarrow \tau^+ + \tau^-$ via one-photon exchange.

Fig. 6.4. Quark diagram for (a) the semi-lepton decay of the charm quark, and (b) the hadronic decay of the charm quark.

Fig. 6.5. $\sigma_{e\mu}$, the observed production cross section for signature $e\mu$ events. The vertical bars are statistical errors. The horizontal bars indicate the E_{cm} range covered by each point. There were no events before background subtraction in the $3.0 < E_{cm} < 3.6$ GeV range. The solid curves are best fits to $\sigma_{e\mu}$ for point production of a V-A heavy lepton pair, eq. (6.9), for $m_{\nu_\tau} = 0.0$ and $m_\nu = 1.8$ or 2.0 GeV/c^2 as indicated. The dashed line is for a mass 1.8 GeV/c^2 heavy lepton pair production with a constant/s form factor. The curves are corrected for the angle and momentum cuts, and for E_{cm} dependent efficiencies.

Fig. 6.6. The missing mass squared, m_m^2, distribution for $4.8 < E_{cm} < 7.8$ GeV.

Fig. 6.7. Then invariant mass squared, m_i^2, distribution for $4.8 < E_{cm} < 7.8$ GeV.

Fig. 6.8. The scaled momentum distribution, $r = (p - 0.65)/(p_{max} - 0.65)$ where p is the momentum of the e or μ for (a) all events and (b) three E_{cm} ranges. The solid curve is the theoretical prediction for the 3-body leptonic decay (eq. (6.5)) of an $m_\tau = 1.90$ GeV/c^2, $m_{\nu_\tau} = 0.0$,

V-A, heavy lepton. The dashed and dot-dashed curves are for an m_τ = 1.90 GeV/c^2 boson with 2-body leptonic decay modes (eq. (6.14)); the former for an unpolarized boson and the latter for a spin 1 boson produced only in the helciity = 0 state. The curves are corrected for the angle and momentum cuts. The data is corrected for background. The bump at r = 0.9 in the m_τ = 1.9 GeV/c^2, 2-body decay model is caused by our having a few events at E_{cm} = 3.8 GeV.

Fig. 6.9. The cos θ_{coll} distribution for 3 energy ranges. The background is subtracted. A value of zero indicates no events in that bin. The theoretical curves are for an m_τ = 1.90 GeV/c^2, m_{ν_τ} = 0.0, V-A, heavy lepton; they are corrected for angle and momentum cuts.

Fig. 6.10. The pseudo-transverse momentum, $p_\perp$, distribution for $4.8 < E_{cm} \leq 7.8$ GeV eμ events. $p_\perp$ is defined by finding the axis AA' in the $\underset{\sim}{p}_e$, $\underset{\sim}{p}_\mu$ plane such that the perpendicular components of $\underset{\sim}{p}_e$ and $\underset{\sim}{p}_\mu$ with respect to that axis are equal and minimum.

Fig. 6.11. Comparison of the r distribution for all eμ events with various models for the τ heavy lepton. The solid curves are for V-A coupling, m_τ = 1.90 GeV/c^2 and m_{ν_τ} = 0.0, 0.5, and I.0 GeV/c^2 as indicated. The dashed curve is for V+A coupling, m_τ = 1.90 GeV/c^2 and m_{ν_τ} = 0.0. The curves have been corrected for the angle and momentum cuts. The background is subtracted.

Fig. 6.12. A comparison of the measured total cross section for two-prong events with that expected for the two prong events from a mass 1.95 GeV/c sequential heavy lepton. From ref. [2.5].

Fig. 6.13. (a) Anomalous muon production cross section, and (b) ratio of anomalous muons to candidates versus the number of observed charged prongs in the E_{cm} range 5.8 to 7.8 GeV. Note that the

two-prong cross section is not corrected for a coplanarity cut and is thus artificially suppressed relative to multiprong cross sections. In calculating the two-prong μ fraction, the number of candidates has been corrected to eliminate leptonic reactions. From ref. [6.4].

Fig. 6.14. Differential cross section for anomalous muon production versus momentum for (a) two-prong events, and (b) multiprong events in the E_{cm} range 5.8 to 7.8 GeV. The solid curve represents the expected cross section from the decays of heavy leptons with parameters as specified in the text. From ref. [6.4].

Fig. 6.15. The DASP detector, ref. [6.27].

Fig. 6.16. Early data on the electron momentum spectrum for large multiplicity events obeying eq. (6.31) from the DASP Group [6.27]. More recent data from that group [6.26] shows that the data reaches a peak above 0.2 GeV/c. The theoretical curves from ref. [6.29] are for a particle (D or heavy lepton) with $\beta = 0.3$.

Fig. 6.17. The observed cross sections for large multiplicity events obeying eq. (6.31) versus E_{cm} [6.27].

Fig. 6.18. The observed cross section for events containing a K_s^o and an e from the PLUTO Group [6.28].

FIGURE CAPTIONS

Fig. 7.1. Predicted sphericity distributions at 30 GeV by the phase space and jet model Monte Carlo calculations.

Fig. 7.2. Predicted distribution of the cosine of the angle between any two particles at 30 GeV by the phase space and jet model Monte Carlo calculations.

Fig. 7.3. The spectrum of electron dipole photon transitions expected from a series of ψ-like states β, β', and β'' for a quark mass of 5 GeV/c^2. For the sake of clarity mulitplet splittings are exaggerated and spin singlets are not shown.

Fig. 7.4. The spectrum of important hadronic transitions expected from a series of ψ-like states β, β', and β'' for a quark mass of 5 GeV/c^2. Two pion and η transitions are indicated by solid and dash-dotted lines. Other transitions are indicated explicitly. For the sake of clarity spin transitions between P states of different spin are not indicated. The electric dipole transition $1^1P_1 \rightarrow 1^1S_o$ is shown here since 1^1P_1 can be reached most easily via $3^3S_1 \rightarrow 1^1P_1 + 2\pi$.

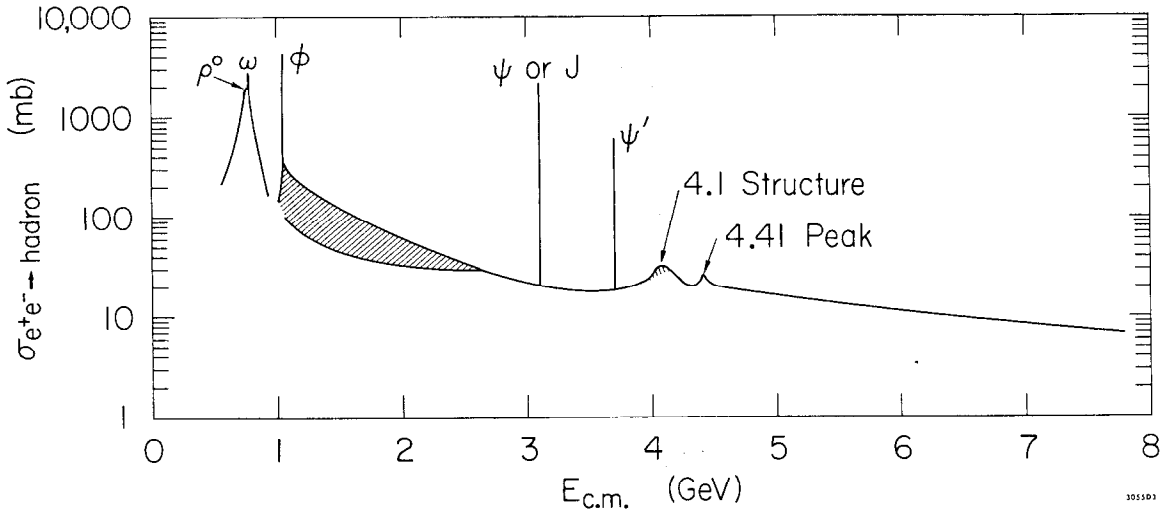
10,000
1000
100
10
1
$\sigma_{e^+e^- \to hadron}$ (mb)
ρ^o ω
ϕ
ψ or J
ψ'
4.1 Structure
4.41 Peak
0
1
2
3
4
5
6
7
8
$E_{c.m.}$ (GeV)
3055D3

FIG. 2.1

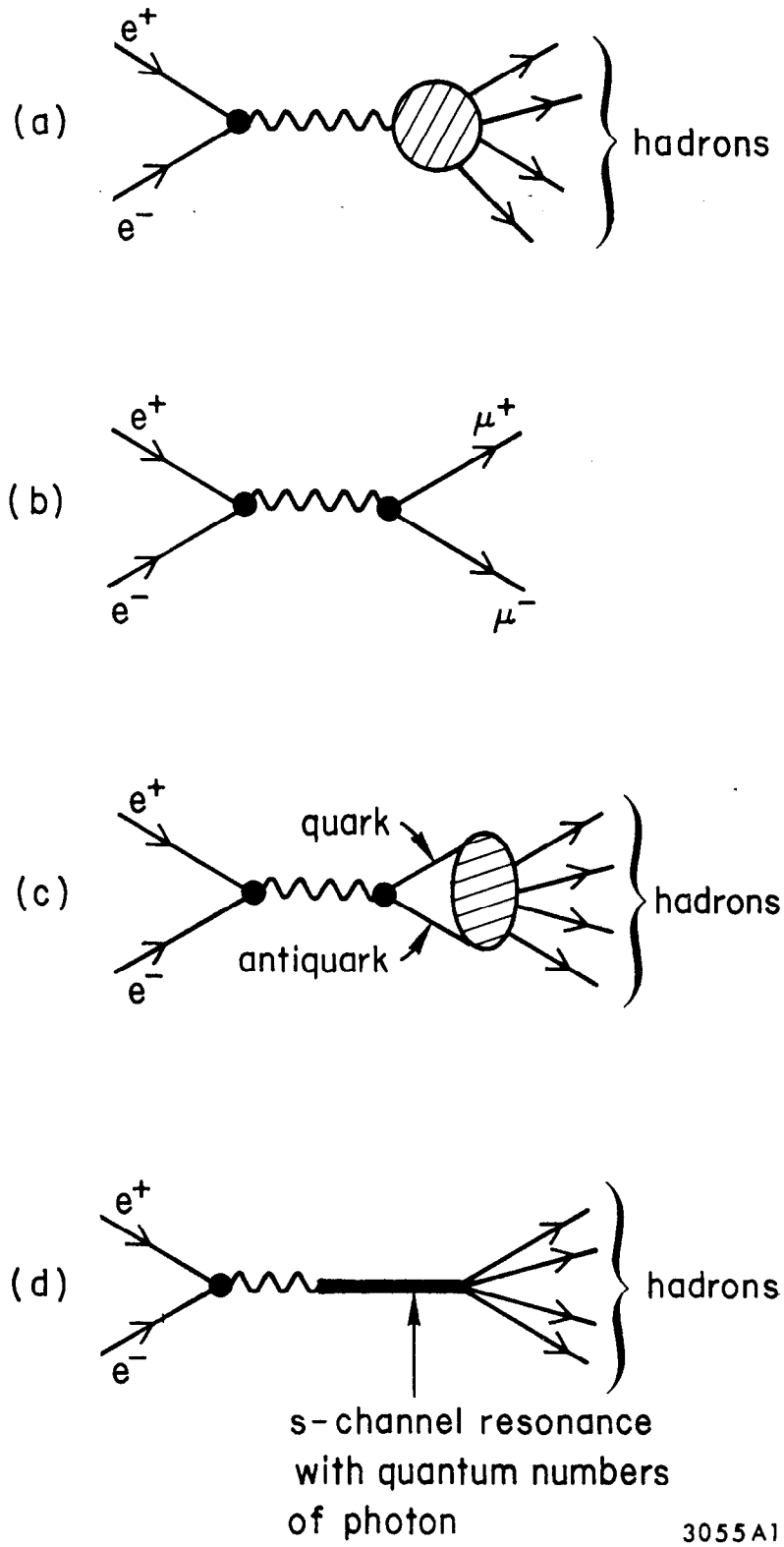
(a)
e+
e−
hadrons
(b)
e+
e−
μ+
μ−
(c)
e+
e−
quark
antiquark
hadrons
(d)
e+
e−
hadrons
s-channel resonance
with quantum numbers
of photon
3055A1

FIG. 2.3

FIG. 2.2

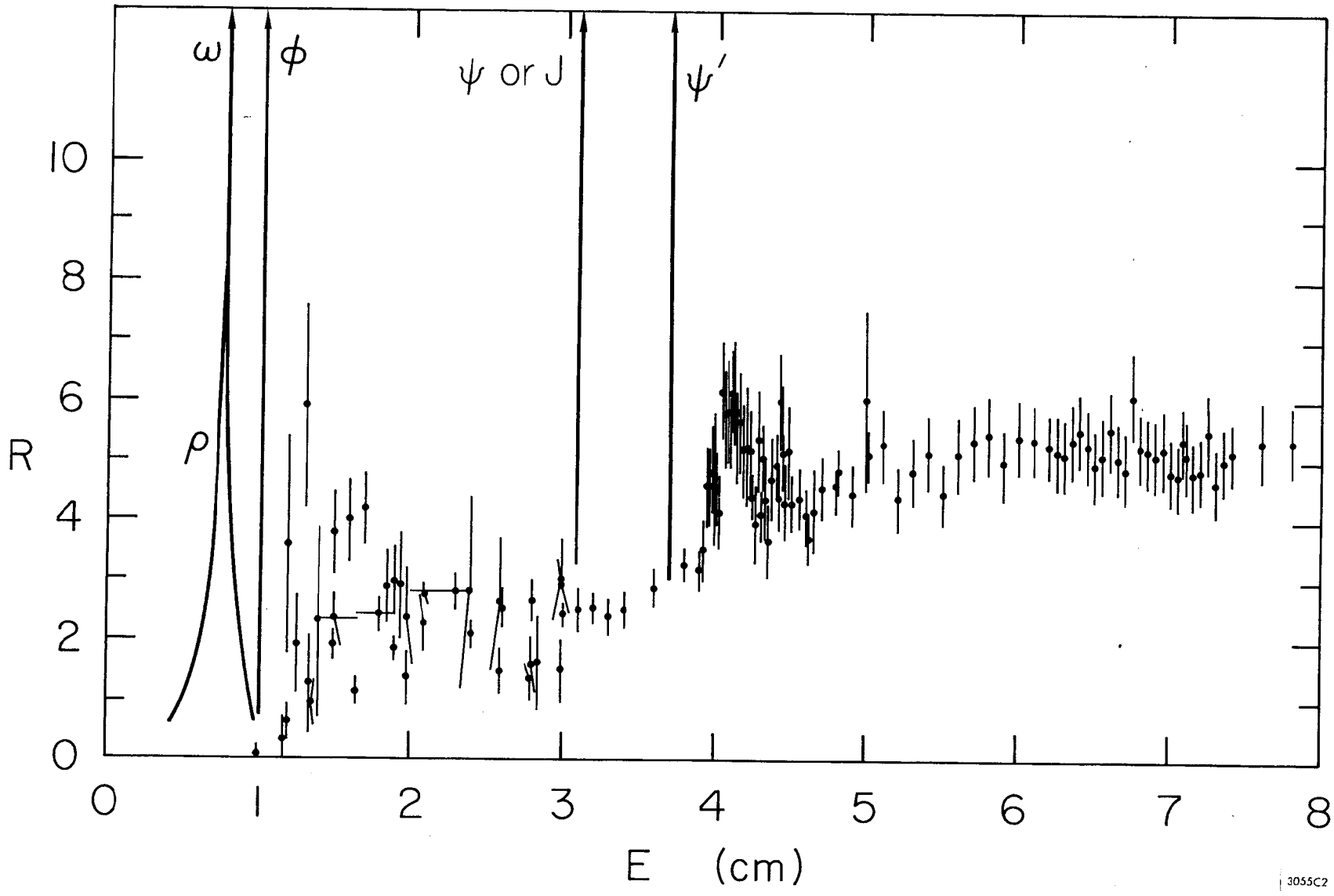
ω
φ
ψ or J
ψ′
ρ
R
0
2
4
6
8
10
0
1
2
3
4
5
6
7
8
E (cm)
3055C2

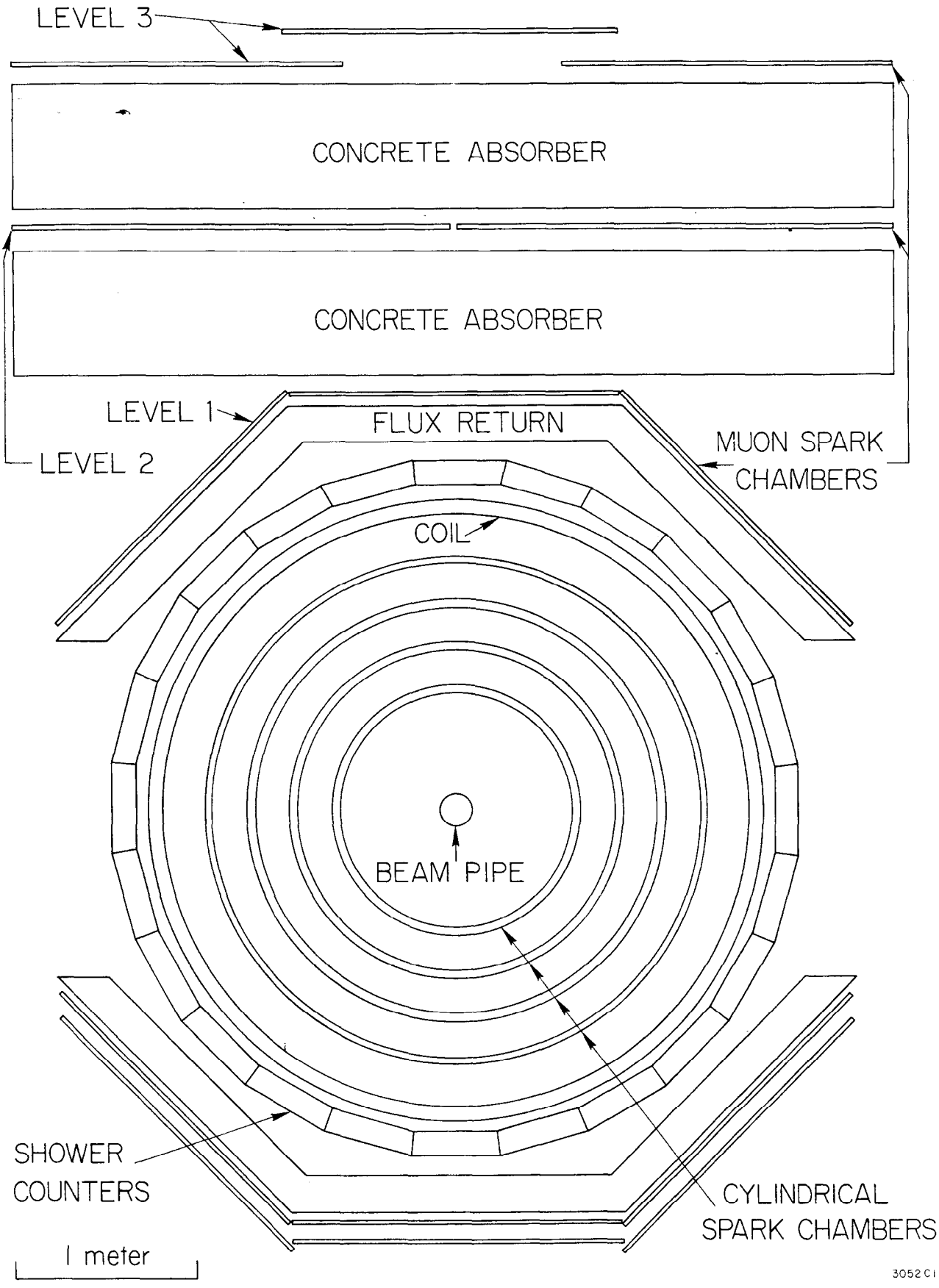
LEVEL 3
CONCRETE ABSORBER
CONCRETE ABSORBER
LEVEL 1
FLUX RETURN
LEVEL 2
MUON SPARK
CHAMBERS
COIL
BEAM PIPE
SHOWER
COUNTERS
CYLINDRICAL
SPARK CHAMBERS
1 meter
3052C1

FIG. 2.4

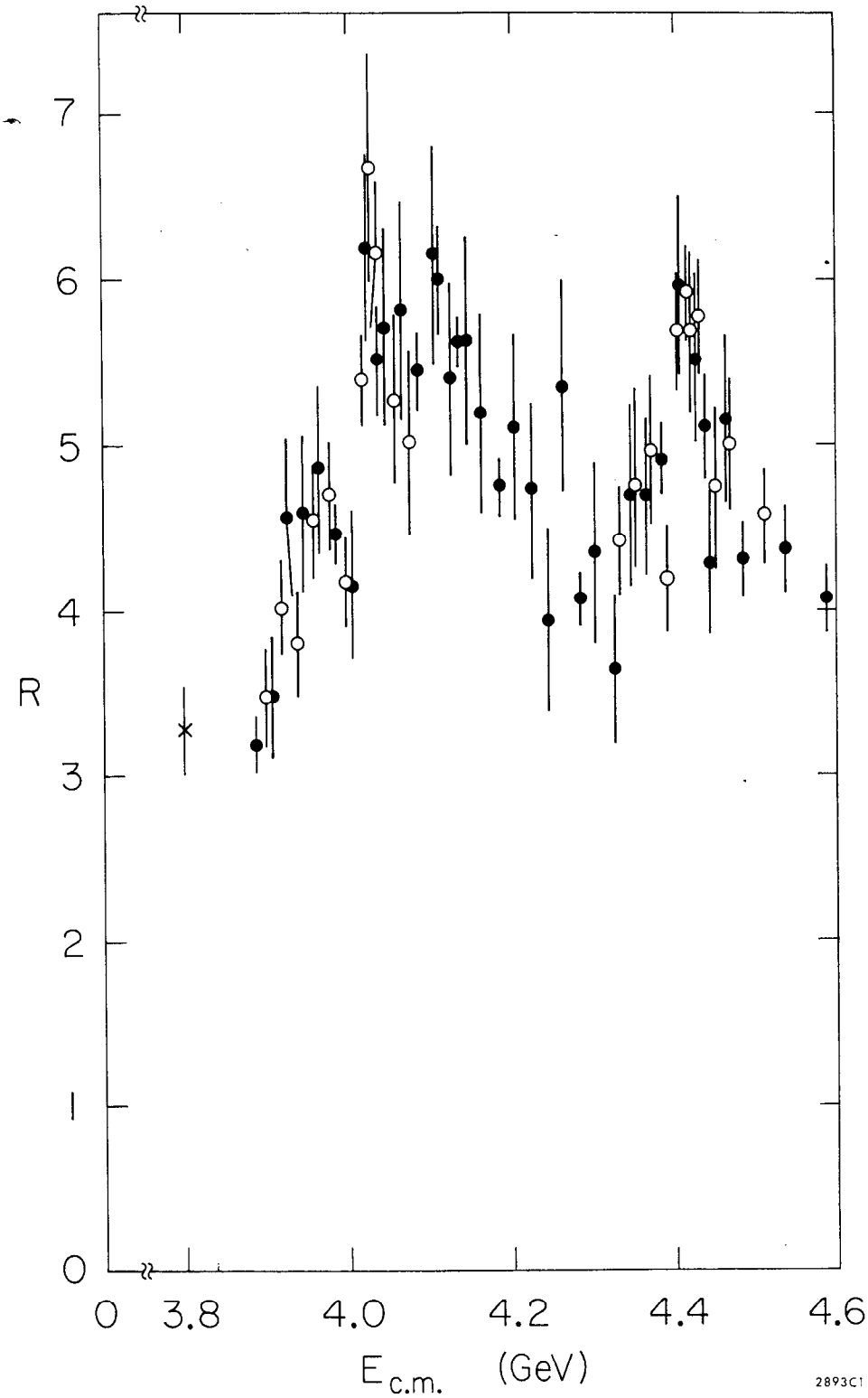

FIG. 2.5

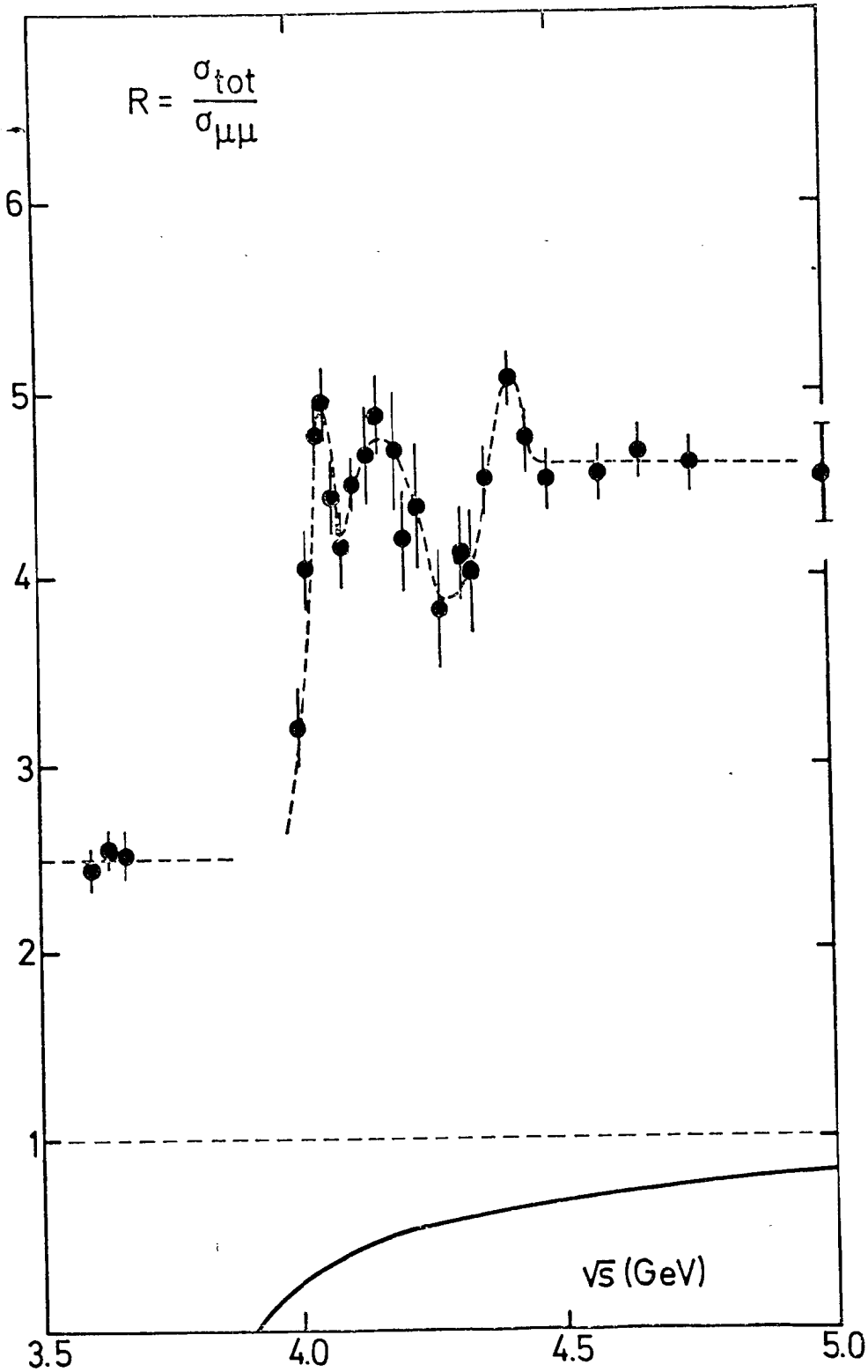

FIG. 2.6

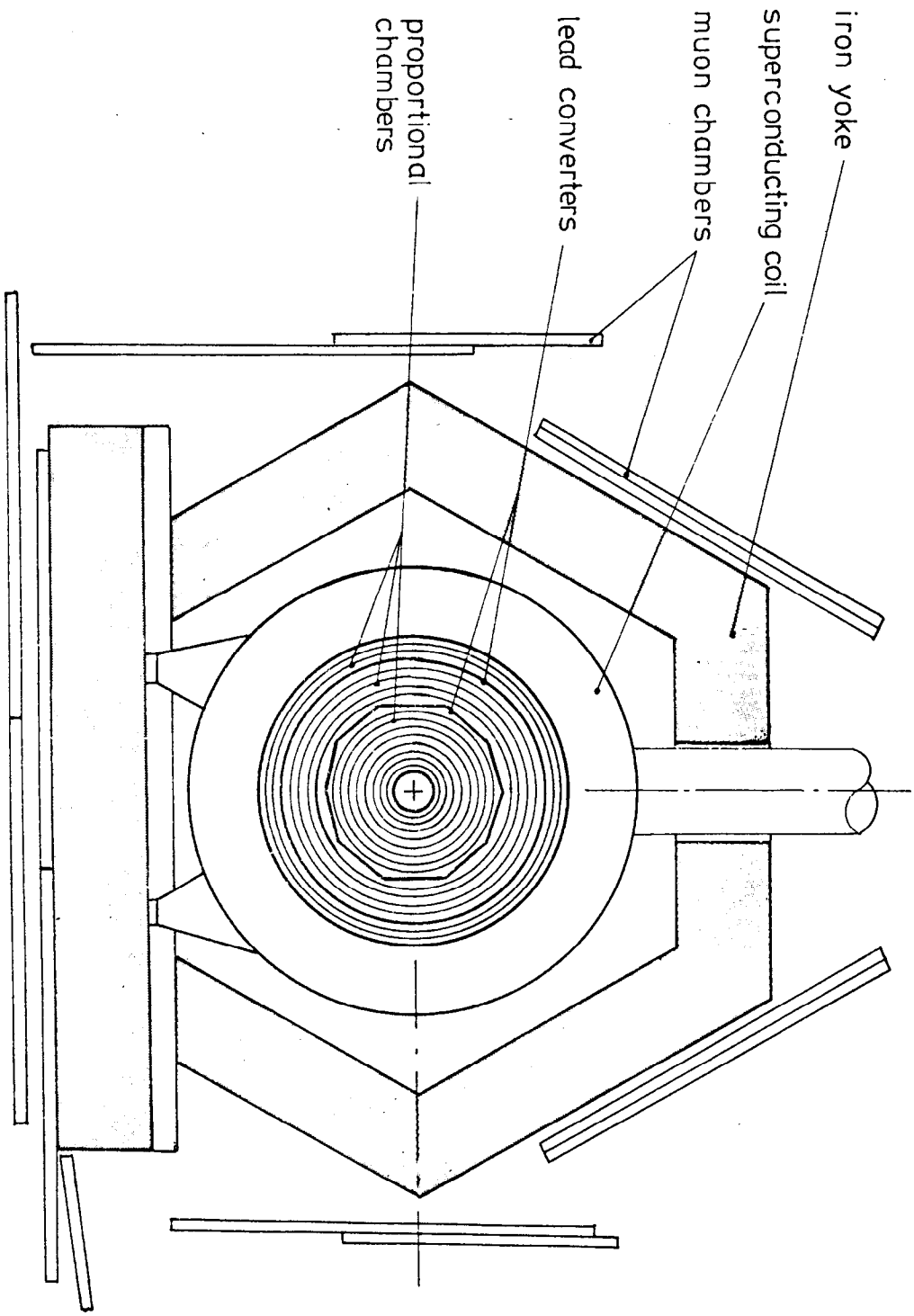
iron yoke
superconducting coil
muon chambers
lead converters
proportional chambers

FIG. 2.7

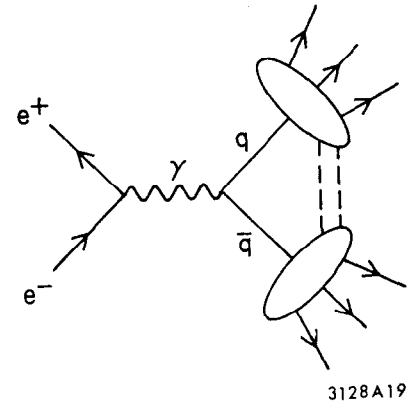

FIG. 3.1

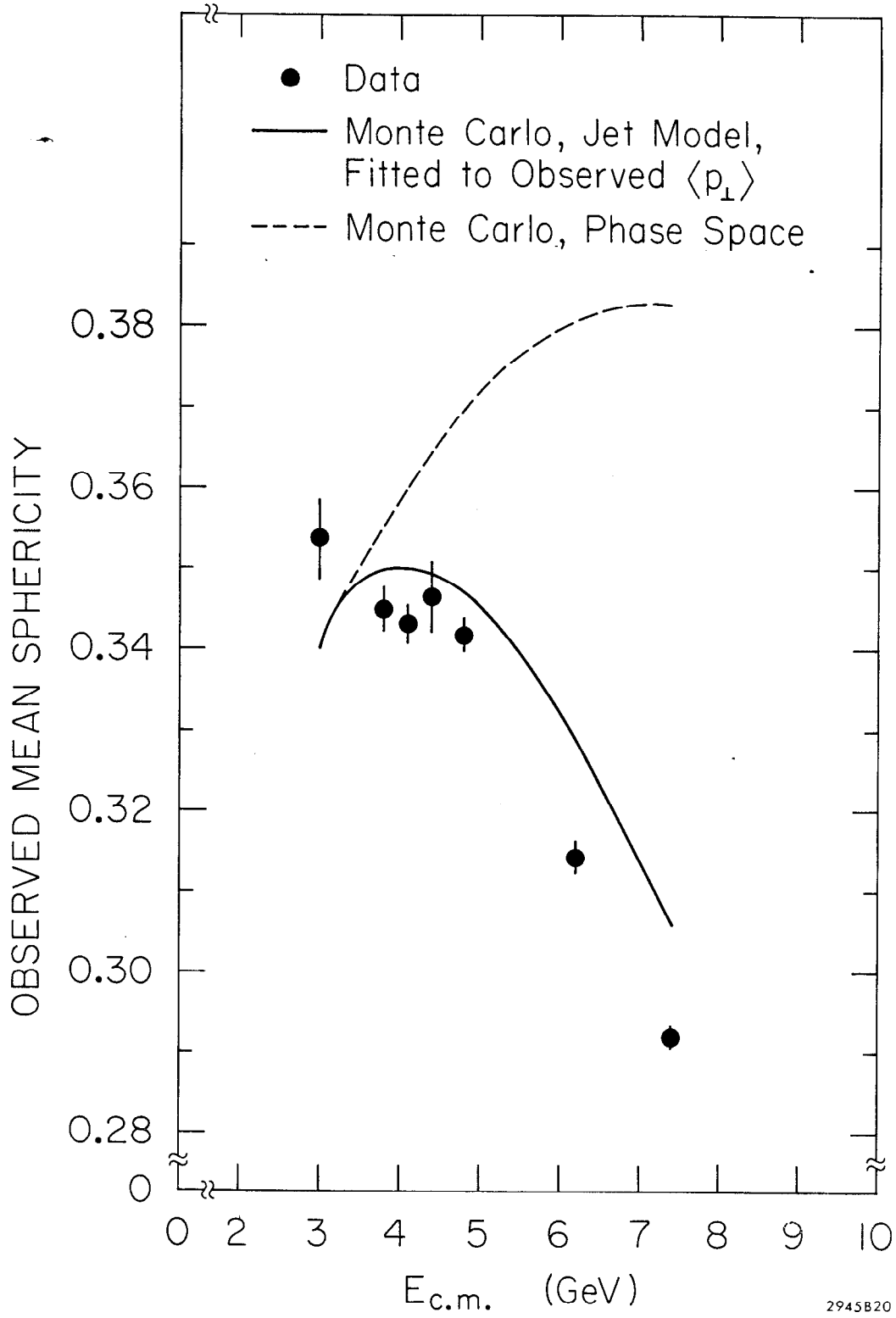
Data
Monte Carlo, Jet Model, Fitted to Observed ⟨p⊥⟩
Monte Carlo, Phase Space
OBSERVED MEAN SPHERICITY
0.38
0.36
0.34
0.32
0.30
0.28
0
0 2 3 4 5 6 7 8 9 10
Ec.m. (GeV)
2945B20

FIG. 3.2

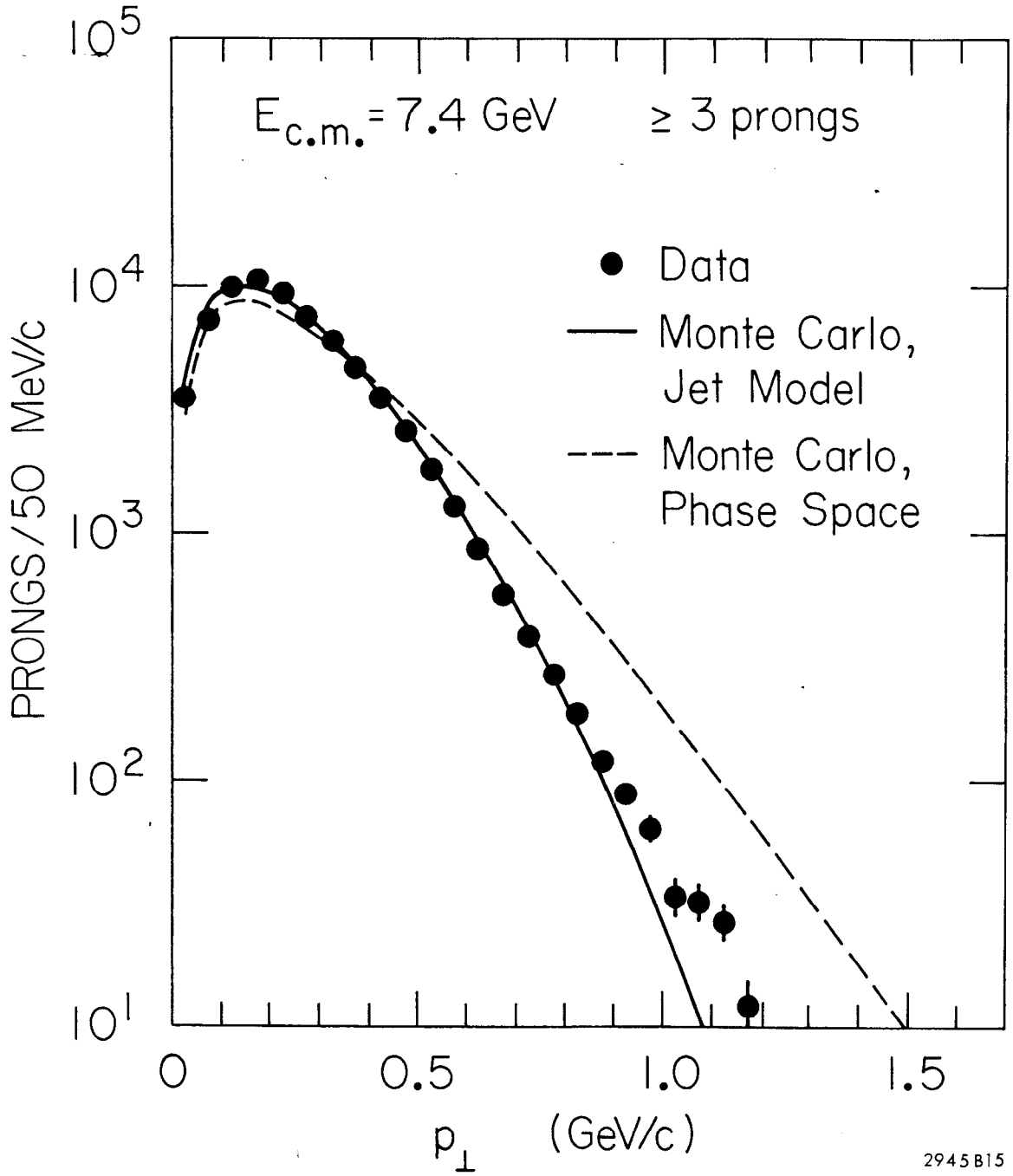
$E_{c.m.}$ = 7.4 GeV
≥ 3 prongs
Data
Monte Carlo, Jet Model
Monte Carlo, Phase Space
PRONGS/50 MeV/c
10^5
10^4
10^3
10^2
10^1
0
0.5
1.0
1.5
$p_\perp$ (GeV/c)
2945B15

FIG. 3.3

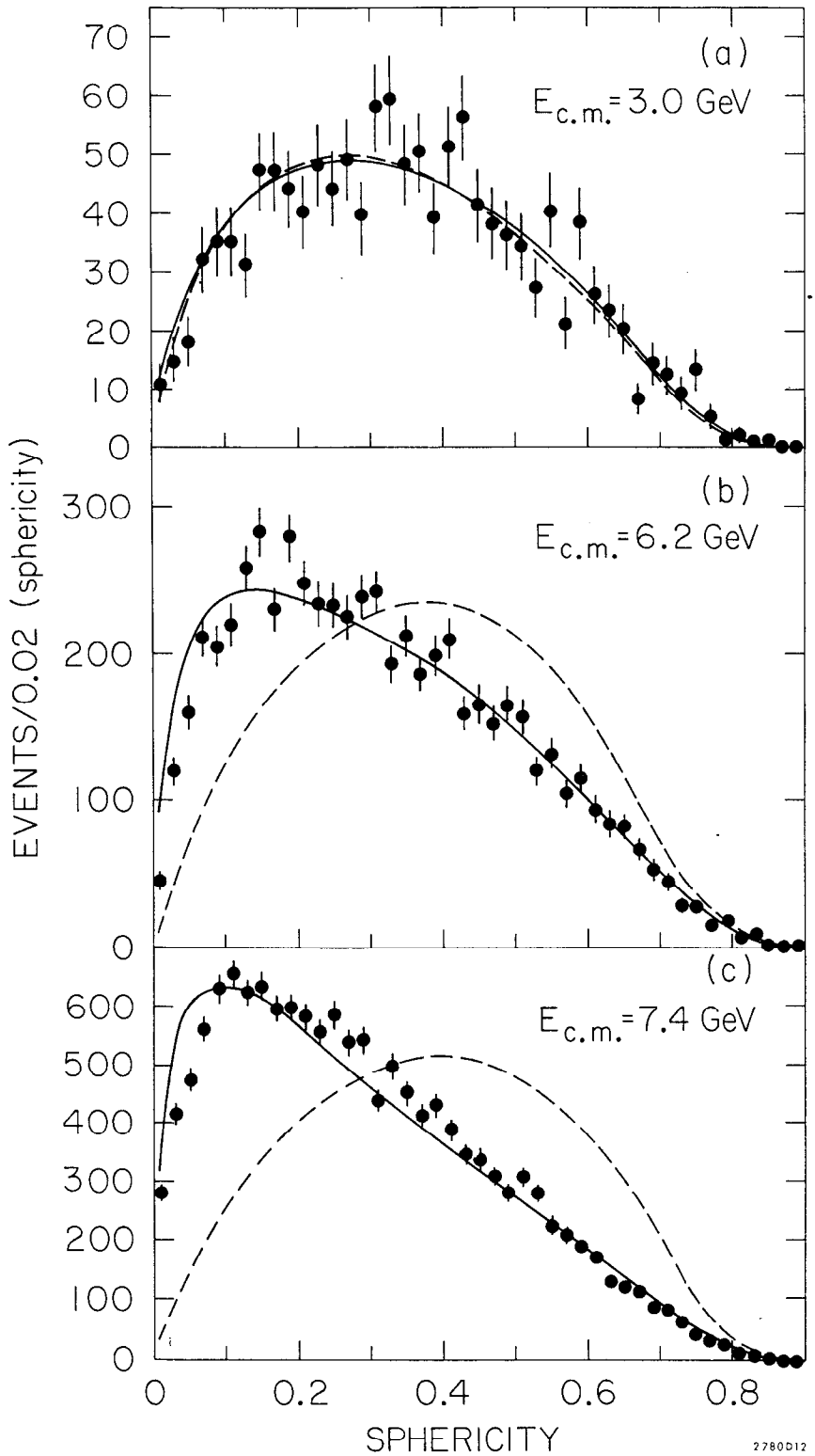
(a)
$E_{c.m.}$=3.0 GeV
(b)
$E_{c.m.}$=6.2 GeV
(c)
$E_{c.m.}$=7.4 GeV
EVENTS/0.02 (sphericity)
SPHERICITY
2780D12

FIG. 3.4

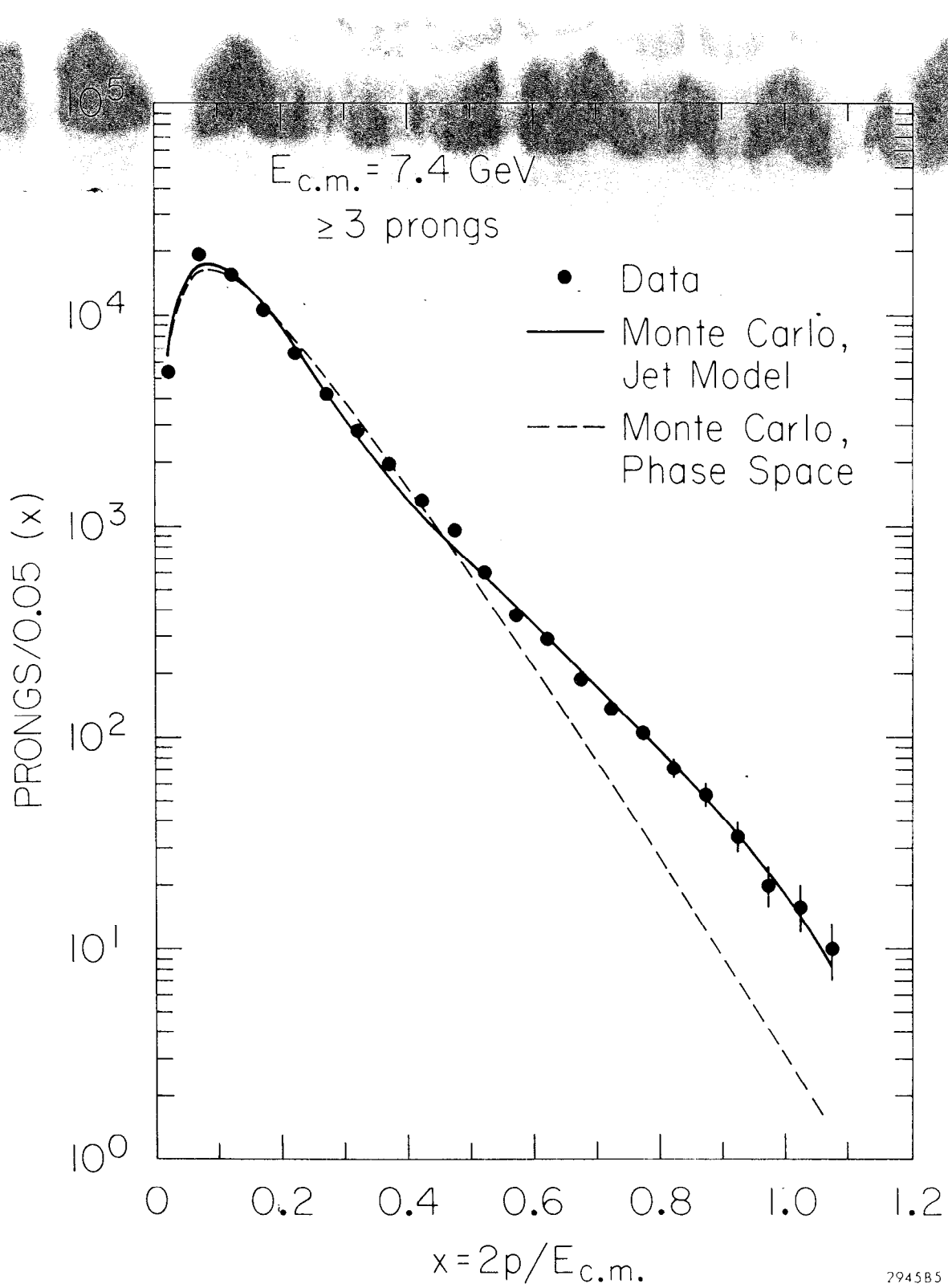
$E_{c.m.} = 7.4$ GeV
≥ 3 prongs
Data
Monte Carlo, Jet Model
Monte Carlo, Phase Space
PRONGS/0.05 (x)
10^5
10^4
10^3
10^2
10^1
10^0
0
0.2
0.4
0.6
0.8
1.0
1.2
$x = 2p/E_{c.m.}$
2945B5

FIG. 3.5

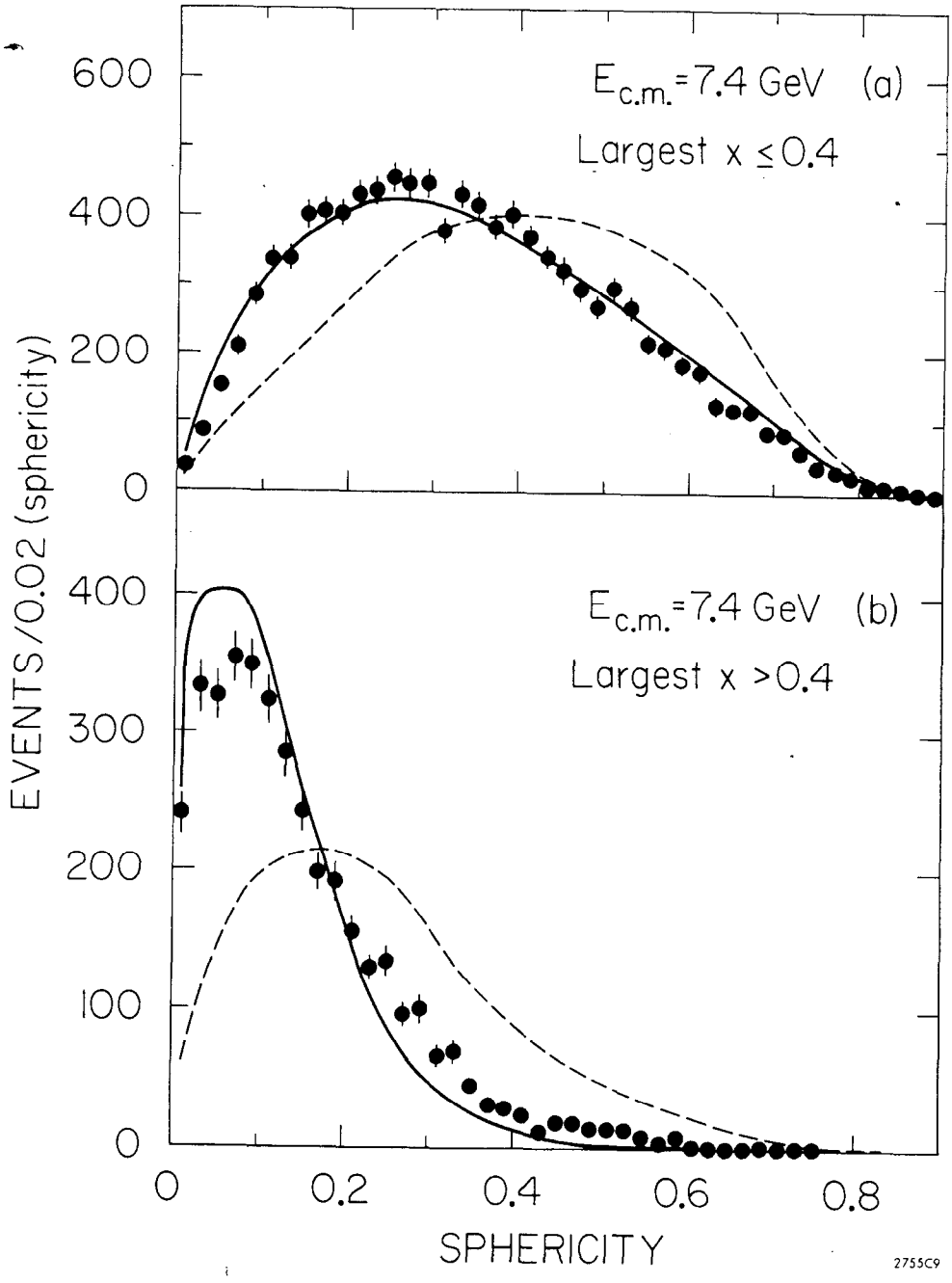
600
400
200
0
400
300
200
100
0
EVENTS/0.02 (sphericity)
$E_{c.m.}$=7.4 GeV (a)
Largest x ≤0.4
$E_{c.m.}$=7.4 GeV (b)
Largest x >0.4
0
0.2
0.4
0.6
0.8
SPHERICITY
2755C9

FIG. 3.6

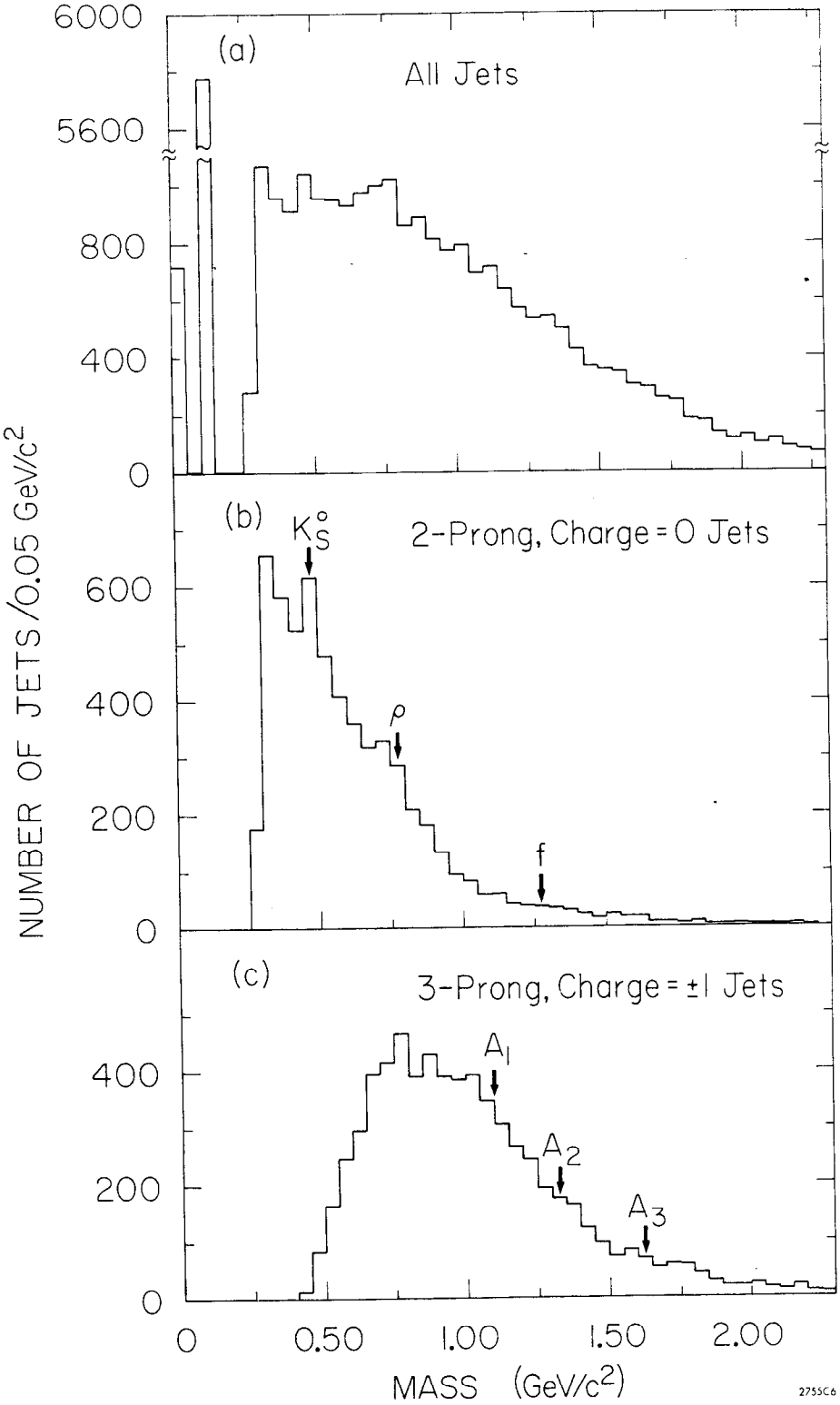
6000
5600
800
400
0
(a)
All Jets
NUMBER OF JETS/0.05 GeV/c²
(b)
K_S^o
2-Prong, Charge = 0 Jets
600
400
200
0
ρ
f
(c)
3-Prong, Charge = ±1 Jets
400
200
0
A_1
A_2
A_3
0
0.50
1.00
1.50
2.00
MASS (GeV/c²)
2755C6

FIG. 3.7

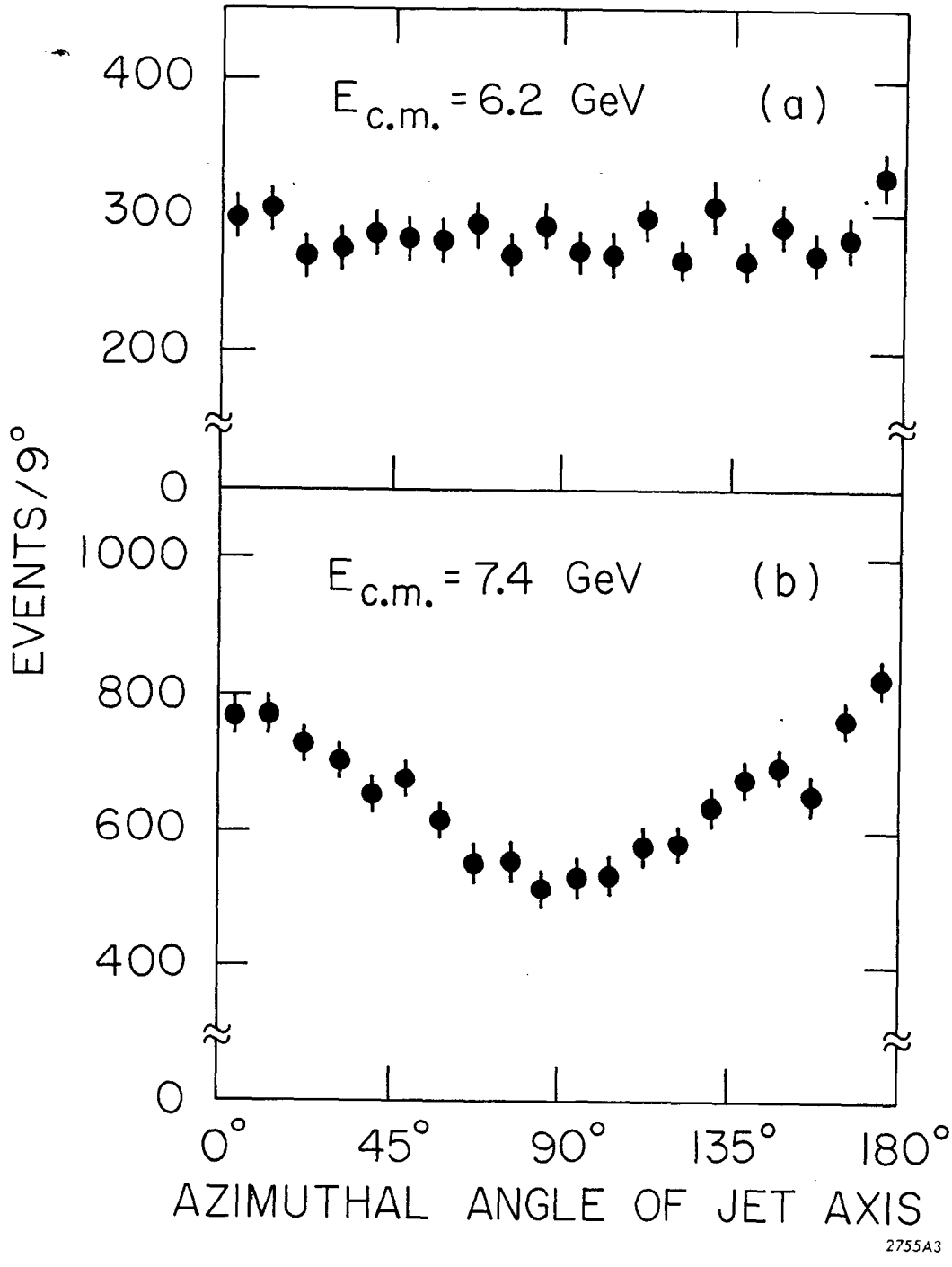
400
300
200
0
1000
800
600
400
0
EVENTS/9°
$E_{c.m.}$ = 6.2 GeV
(a)
$E_{c.m.}$ = 7.4 GeV
(b)
0°
45°
90°
135°
180°
AZIMUTHAL ANGLE OF JET AXIS
2755A3

FIG. 3.8

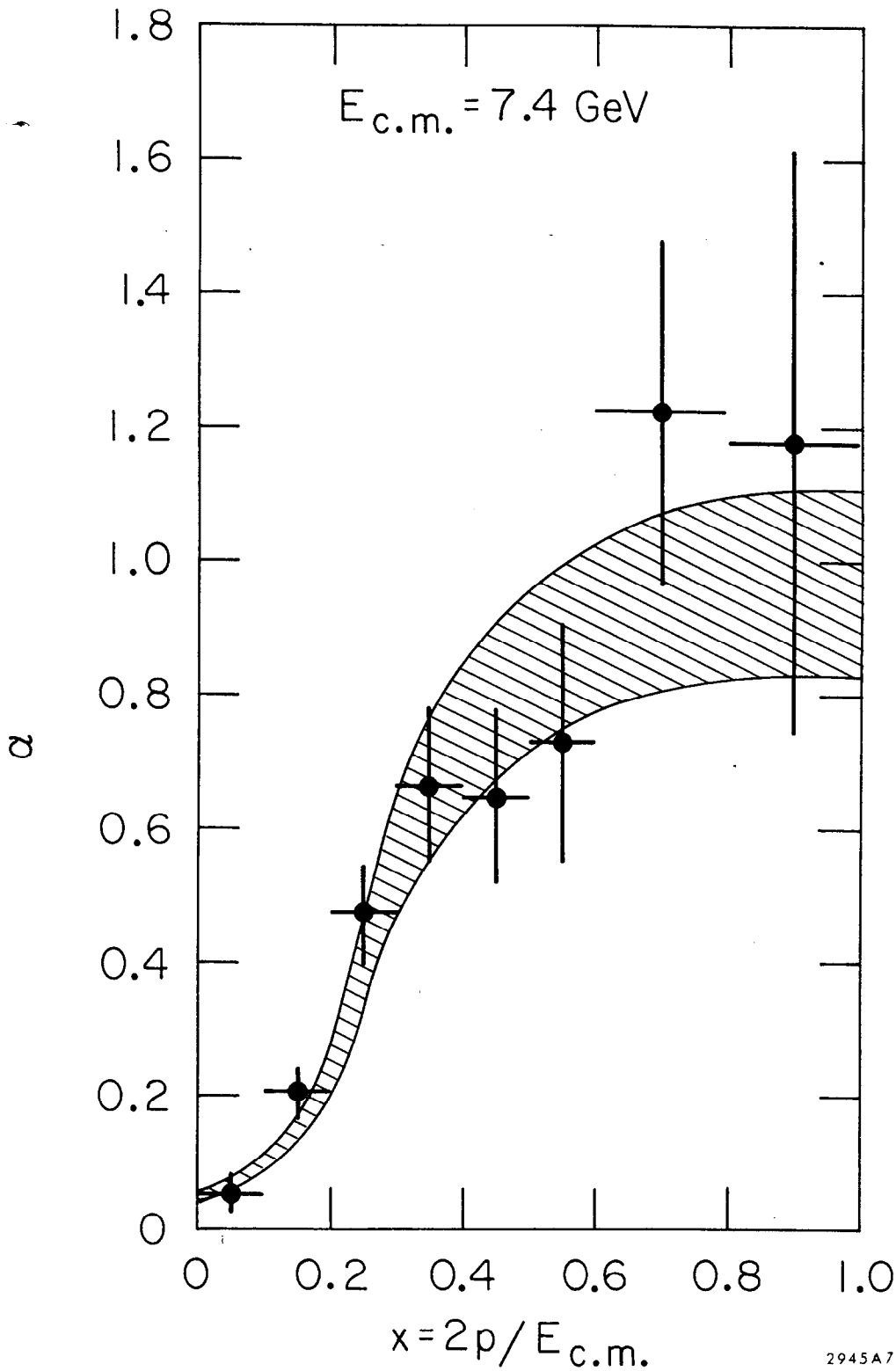
$E_{c.m.} = 7.4$ GeV
1.8
1.6
1.4
1.2
1.0
0.8
0.6
0.4
0.2
0
α
0
0.2
0.4
0.6
0.8
1.0
$x = 2p/E_{c.m.}$
2945A7

FIG. 3.9

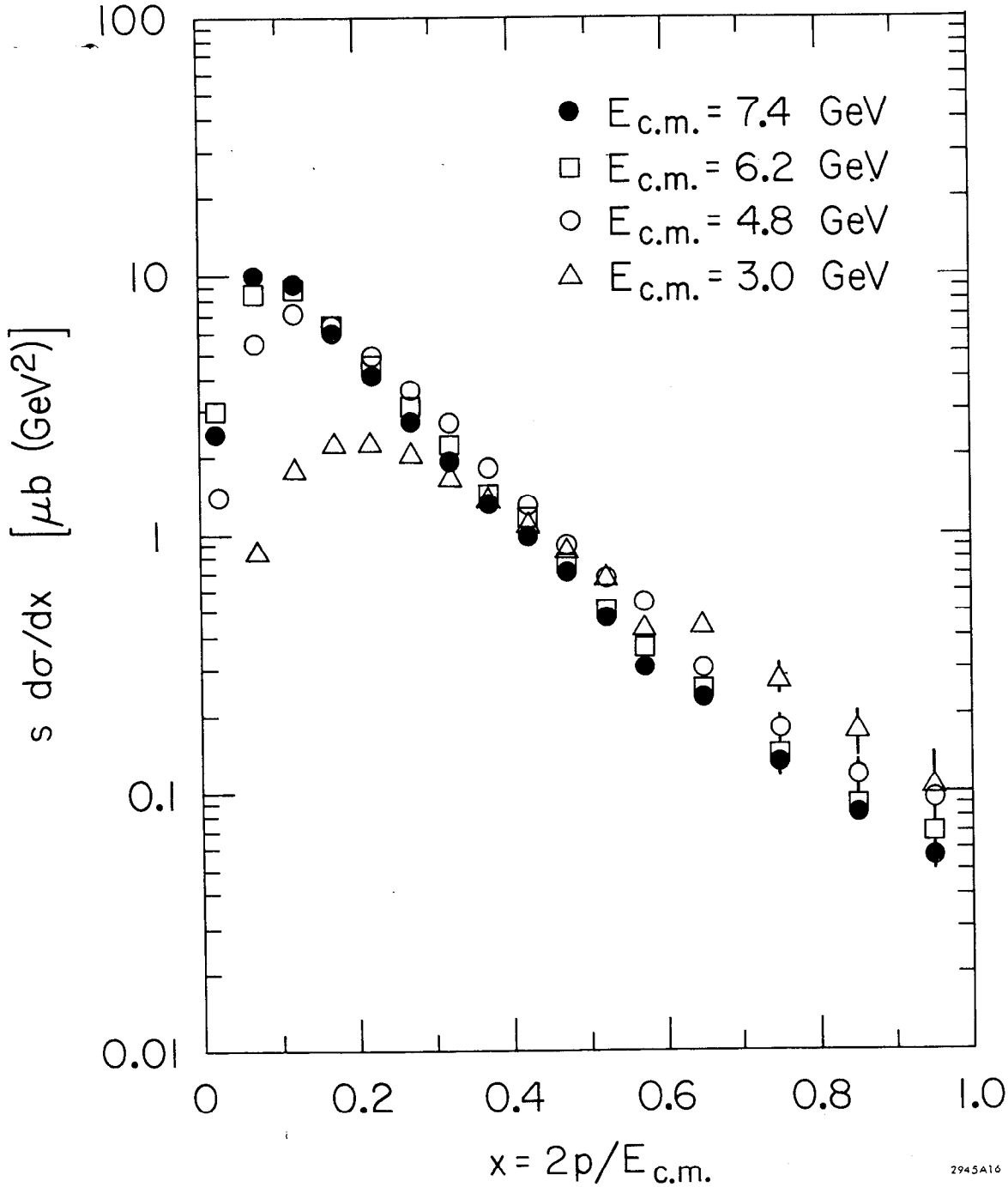
100
10
1
0.1
0.01
0
0.2
0.4
0.6
0.8
1.0
s dσ/dx [μb (GeV²)]
x = 2p/E c.m.
E c.m. = 7.4 GeV
E c.m. = 6.2 GeV
E c.m. = 4.8 GeV
E c.m. = 3.0 GeV
2945A16

FIG. 3.10

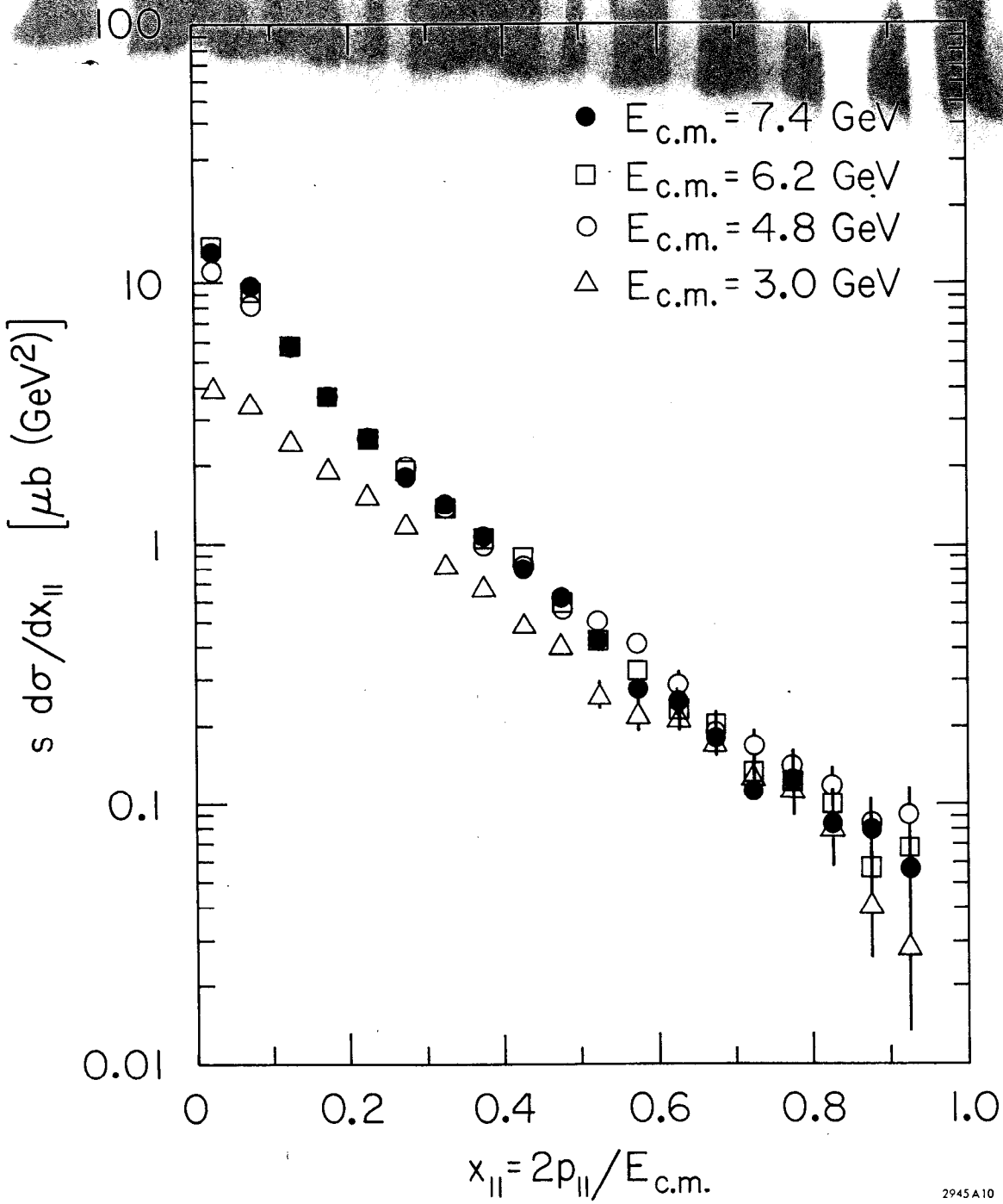
100
10
1
0.1
0.01
0
0.2
0.4
0.6
0.8
1.0
$E_{c.m.} = 7.4$ GeV
$E_{c.m.} = 6.2$ GeV
$E_{c.m.} = 4.8$ GeV
$E_{c.m.} = 3.0$ GeV
$s\, d\sigma/dx_{\parallel}$ [μb (GeV^2)]
$x_{\parallel} = 2p_{\parallel}/E_{c.m.}$
2945A10

FIG. 3.11

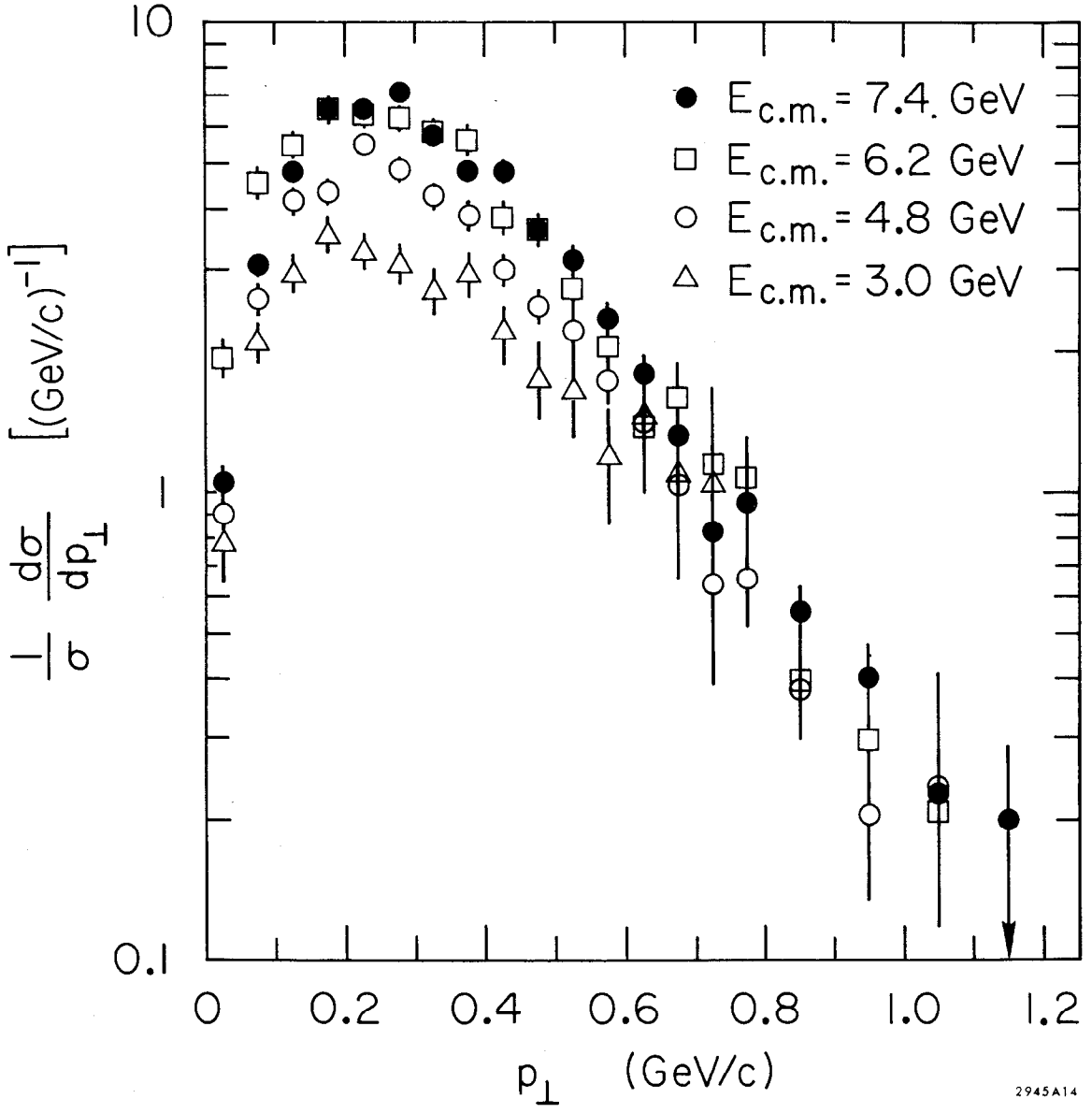
10
1
0.1
0
0.2
0.4
0.6
0.8
1.0
1.2
$\frac{1}{\sigma}\frac{d\sigma}{dp_\perp}$ [(GeV/c)$^{-1}$]
$p_\perp$ (GeV/c)
$E_{c.m.}$ = 7.4 GeV
$E_{c.m.}$ = 6.2 GeV
$E_{c.m.}$ = 4.8 GeV
$E_{c.m.}$ = 3.0 GeV
2945A14

FIG. 3.12

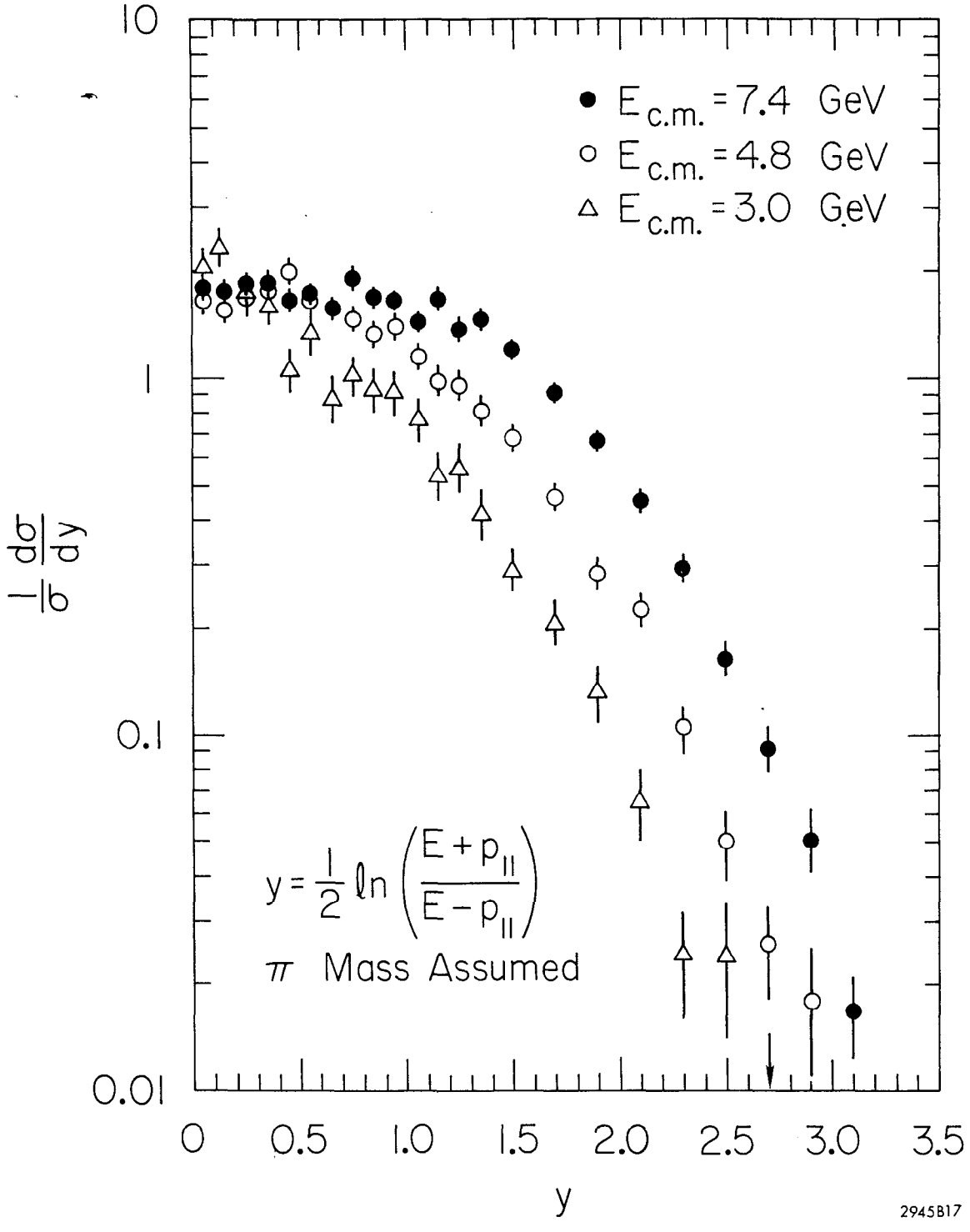
10
1
0.1
0.01
$\frac{1}{\sigma}\frac{d\sigma}{dy}$
$E_{c.m.} = 7.4$ GeV
$E_{c.m.} = 4.8$ GeV
$E_{c.m.} = 3.0$ GeV
$y = \frac{1}{2} \ln \left(\frac{E + p_{\parallel}}{E - p_{\parallel}} \right)$
π Mass Assumed
0
0.5
1.0
1.5
2.0
2.5
3.0
3.5
y
2945B17

FIG. 3.13

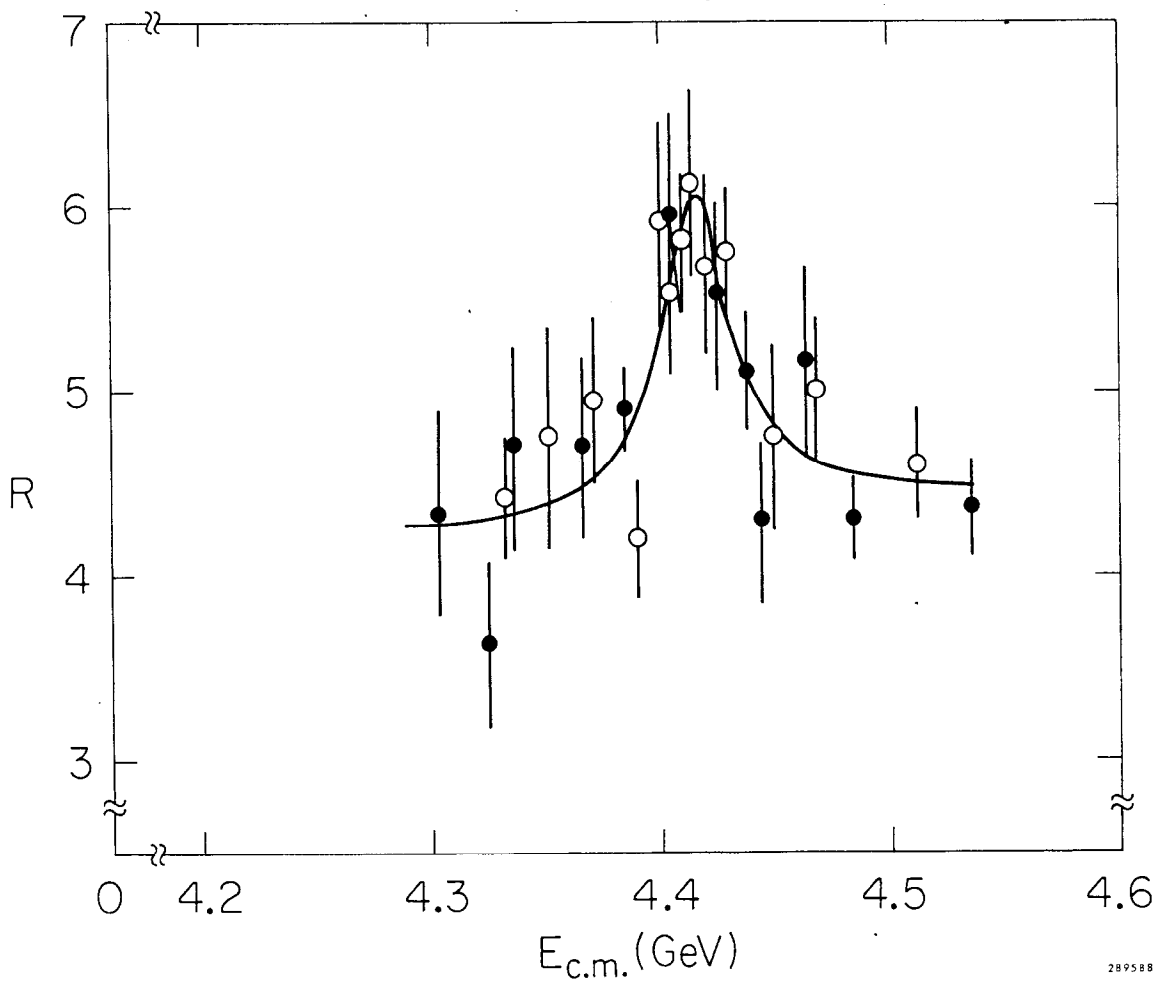

FIG. 4.1

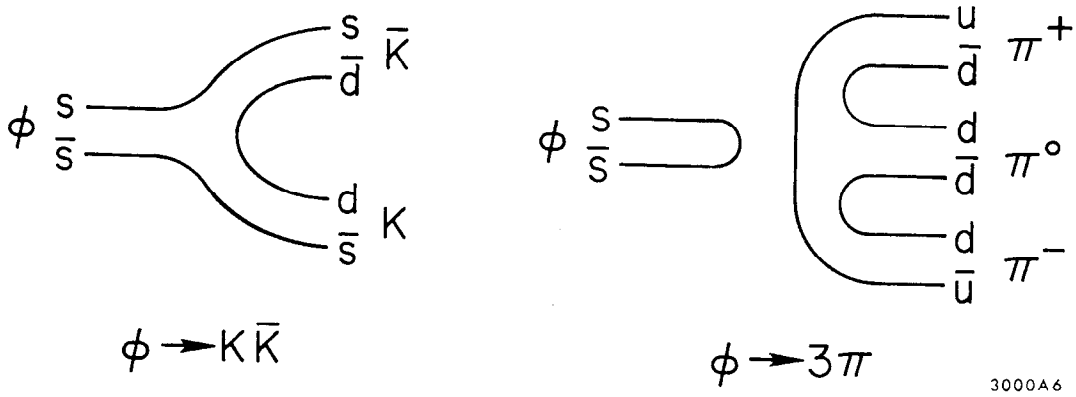

FIG. 4.2

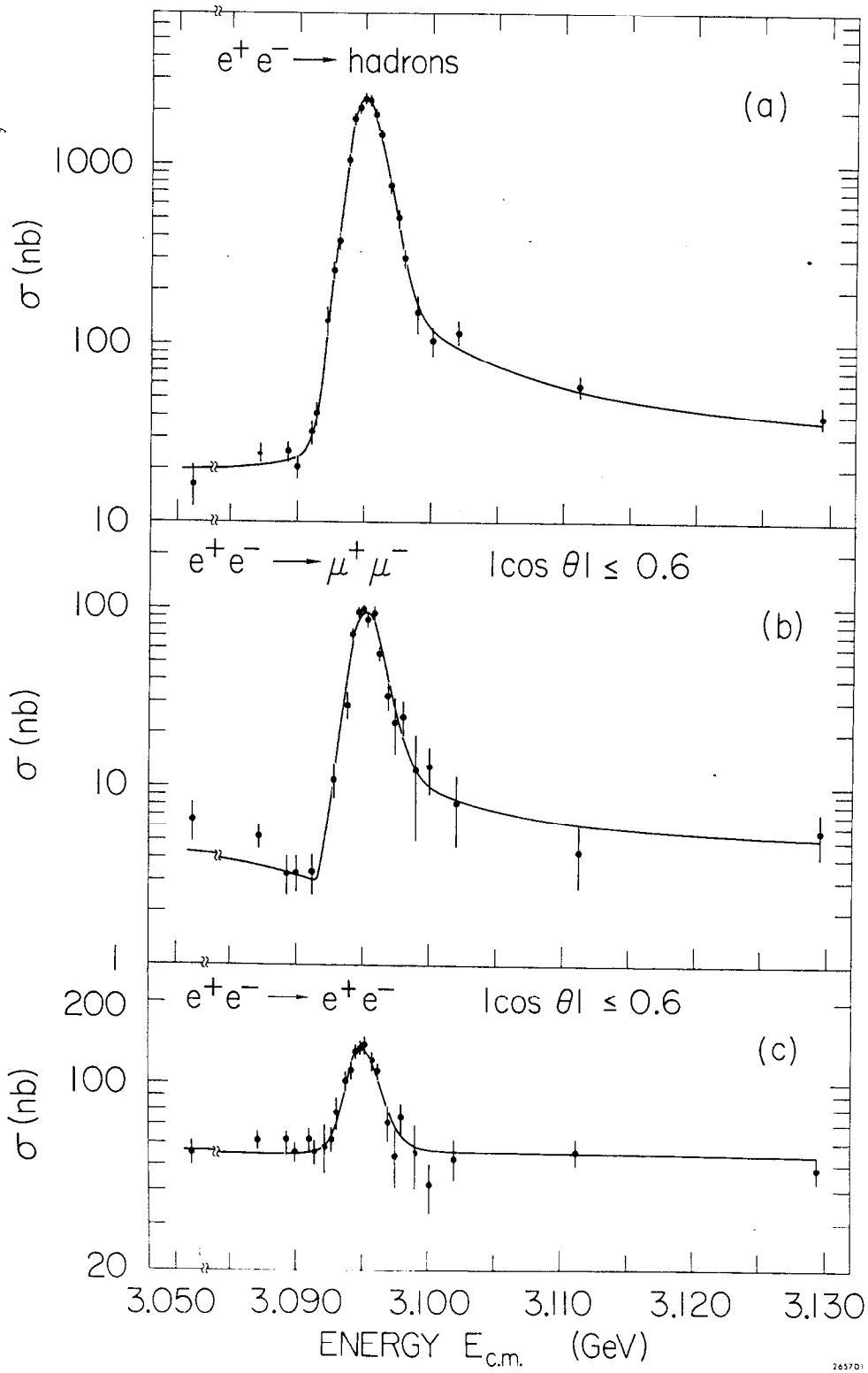
e+ e− → hadrons
(a)
1000
100
10
σ (nb)
e+e− → μ+μ−
|cos θ| ≤ 0.6
(b)
100
10
1
σ (nb)
e+e− → e+e−
|cos θ| ≤ 0.6
(c)
200
100
20
σ (nb)
3.050
3.090
3.100
3.110
3.120
3.130
ENERGY E c.m. (GeV)
2657D1

FIG. 4.3

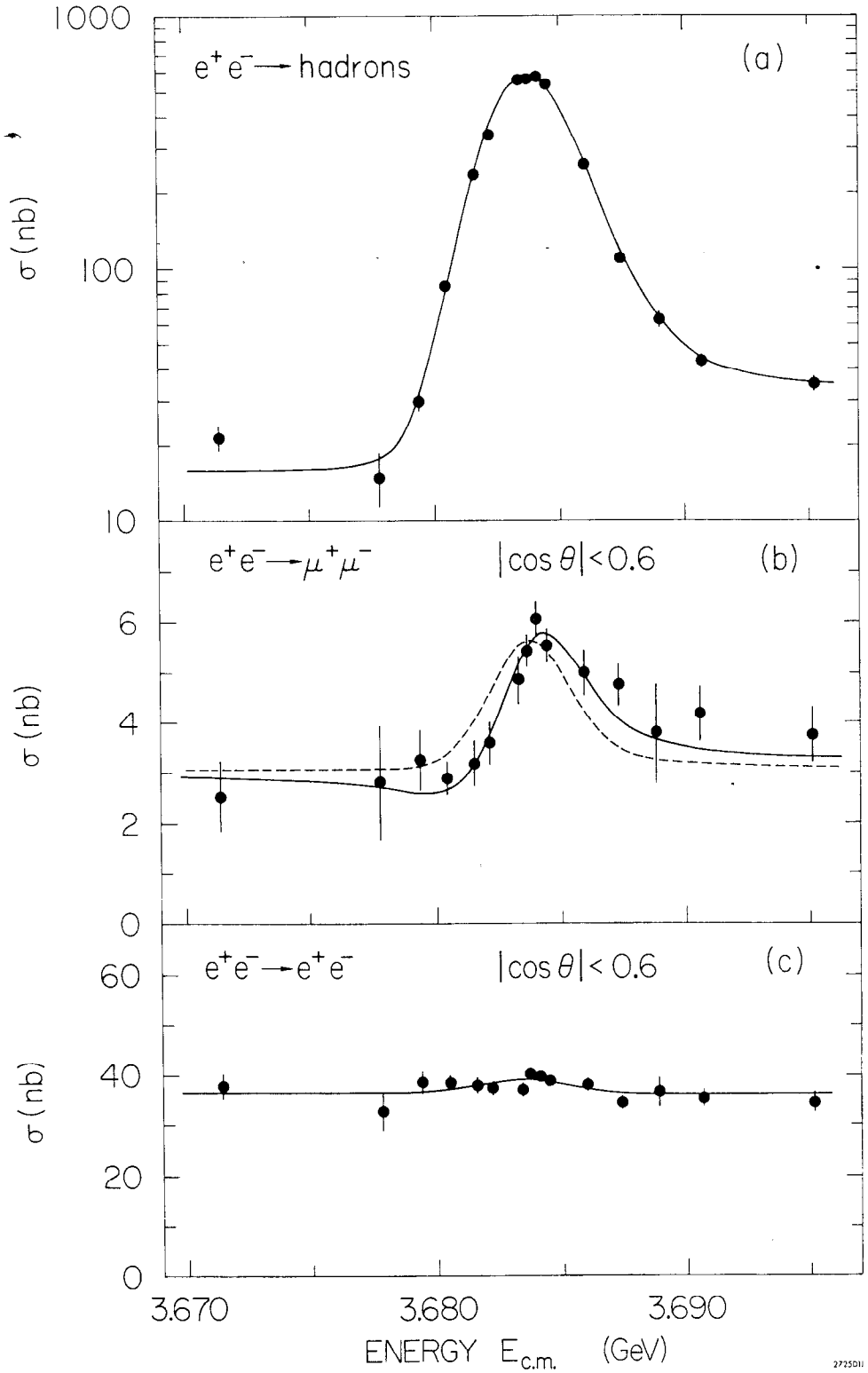
1000
100
10
σ (nb)
e⁺e⁻ → hadrons
(a)
e⁺e⁻ → μ⁺μ⁻
|cos θ| < 0.6
(b)
6
4
2
0
σ (nb)
e⁺e⁻ → e⁺e⁻
|cos θ| < 0.6
(c)
60
40
20
0
σ (nb)
3.670
3.680
3.690
ENERGY E c.m. (GeV)
2725D11

FIG. 4.4

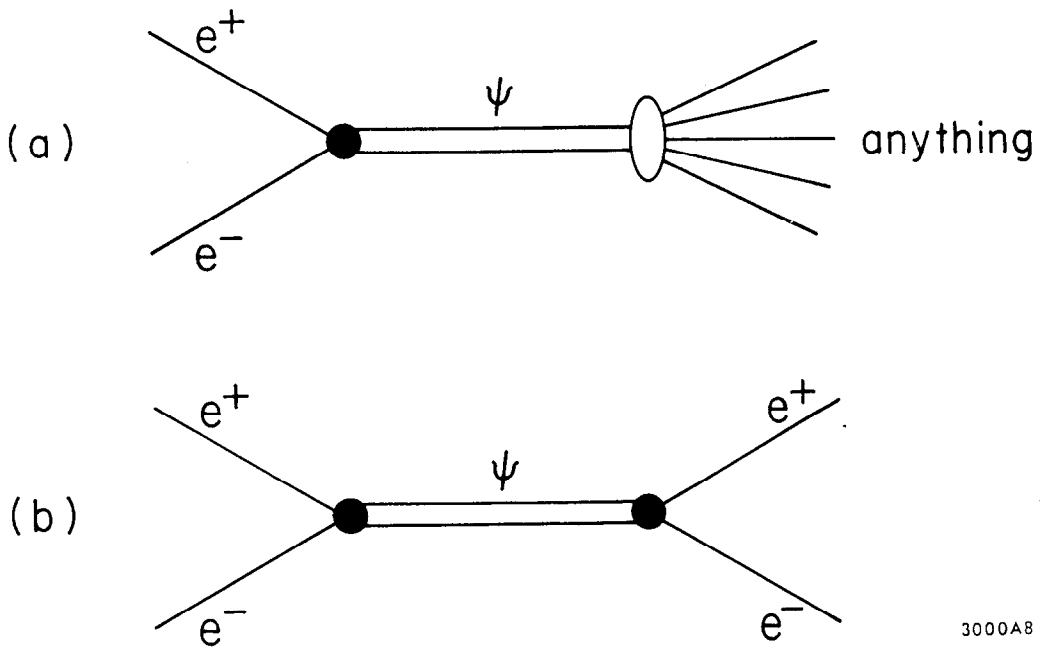

FIG. 4.5

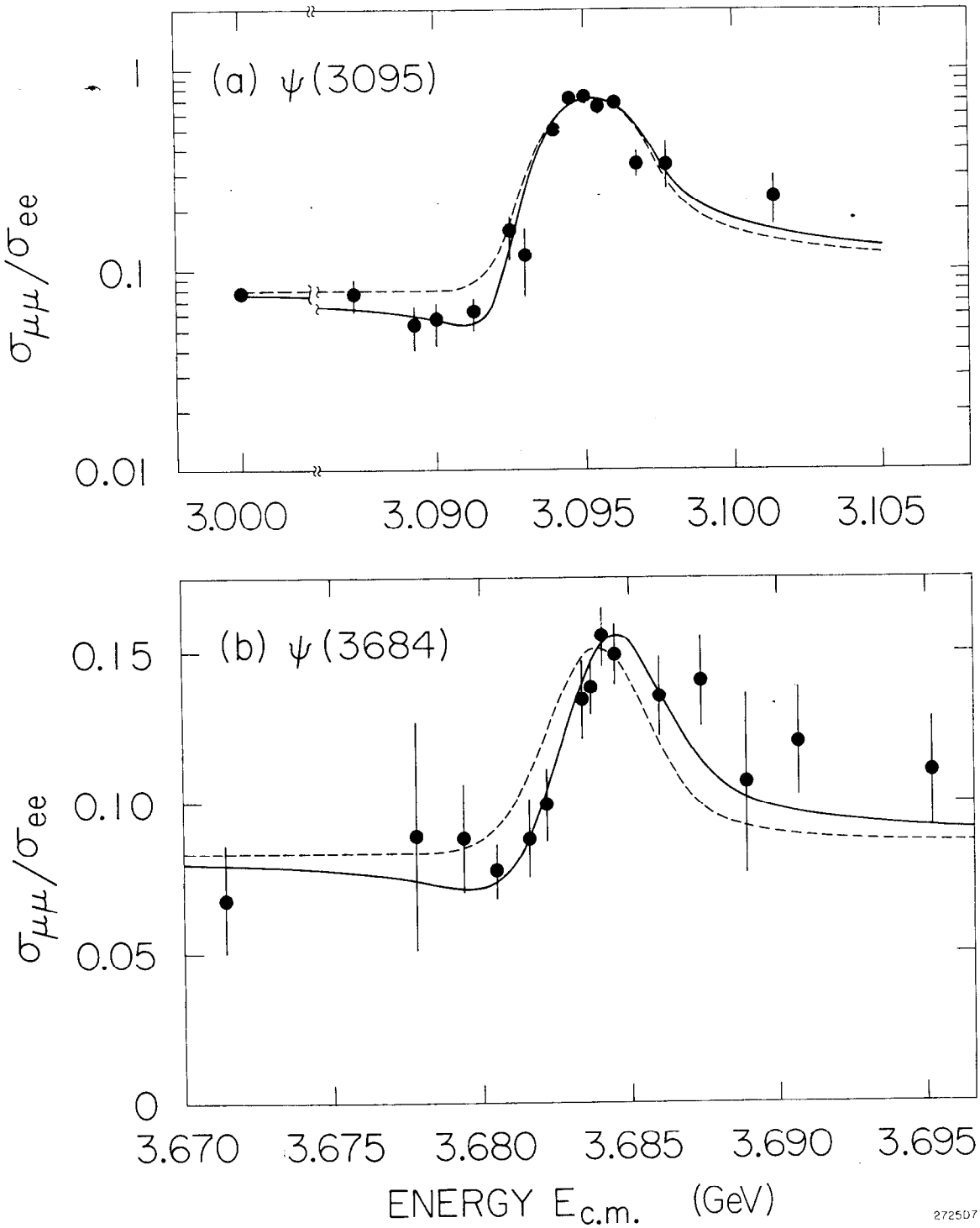
(a) ψ(3095)
1
0.1
0.01
$\sigma_{\mu\mu}/\sigma_{ee}$
3.000
3.090
3.095
3.100
3.105
(b) ψ(3684)
0.15
0.10
0.05
0
$\sigma_{\mu\mu}/\sigma_{ee}$
3.670
3.675
3.680
3.685
3.690
3.695
ENERGY $E_{c.m.}$ (GeV)
2725D7

FIG. 4.6

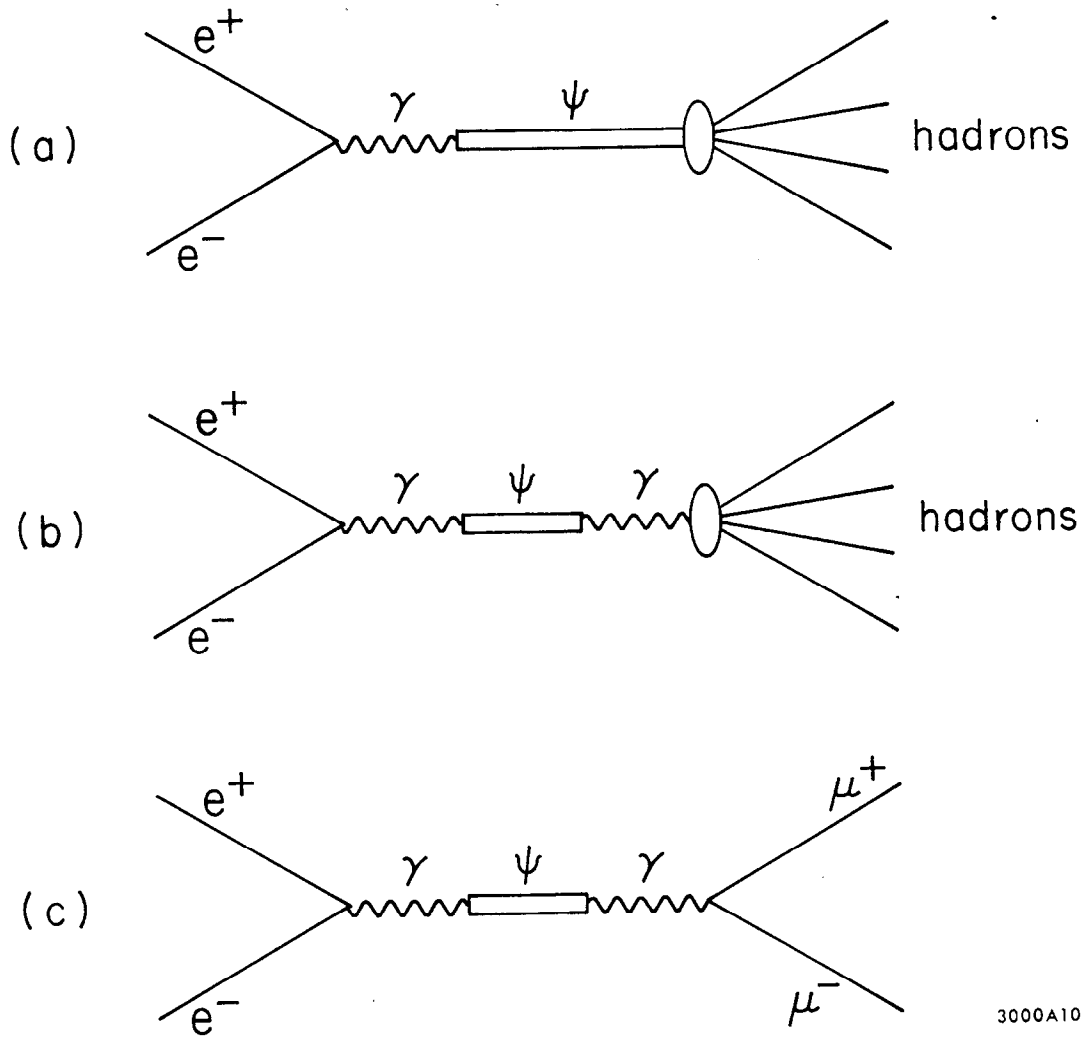

FIG. 4.7

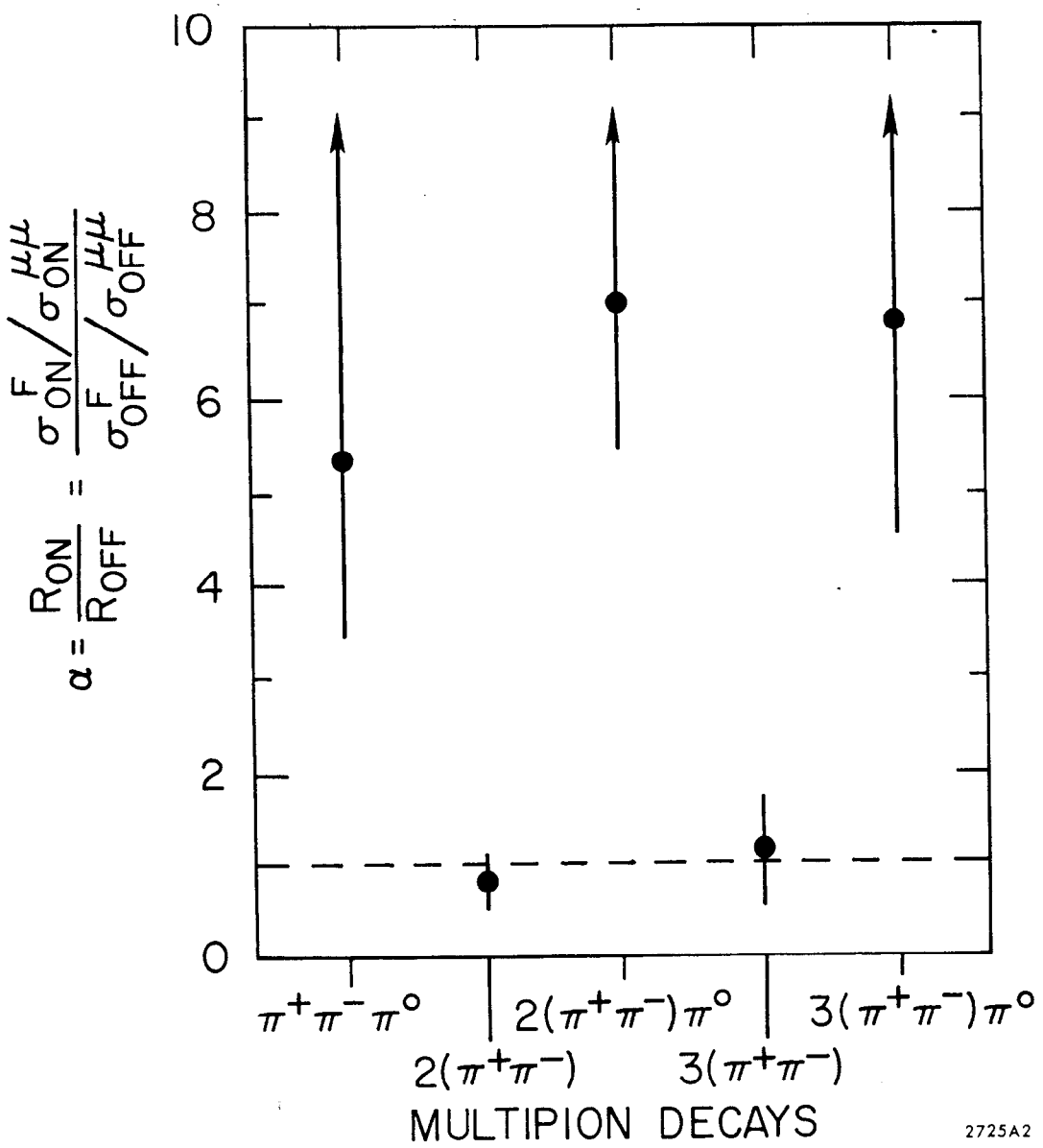
$\alpha = \frac{R_{ON}}{R_{OFF}} = \frac{\sigma^F_{ON}/\sigma^{\mu\mu}_{ON}}{\sigma^F_{OFF}/\sigma^{\mu\mu}_{OFF}}$
10
8
6
4
2
0
$\pi^+\pi^-\pi^0$
$2(\pi^+\pi^-)\pi^0$
$3(\pi^+\pi^-)\pi^0$
$2(\pi^+\pi^-)$
$3(\pi^+\pi^-)$
MULTIPION DECAYS
2725A2

FIG. 4.8

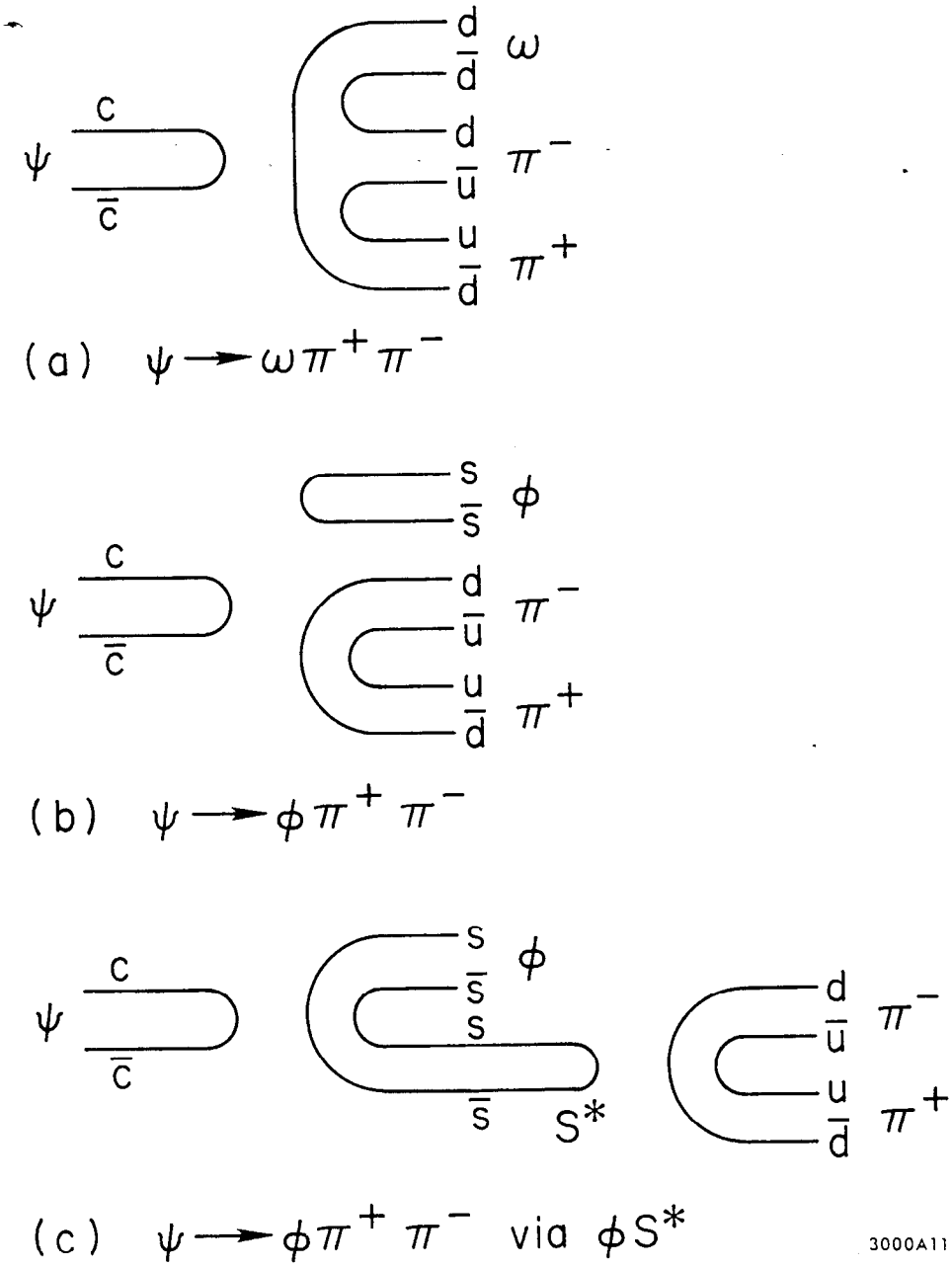
ψ
c
c̄
d
d̄
ω
d
ū
π⁻
u
d̄
π⁺
(a) ψ → ωπ⁺π⁻
s
s̄
φ
d
ū
π⁻
u
d̄
π⁺
(b) ψ → φπ⁺π⁻
s
s̄
s
φ
s̄
S*
d
ū
π⁻
u
d̄
π⁺
(c) ψ → φπ⁺π⁻ via φS*
3000A11

FIG. 4.9

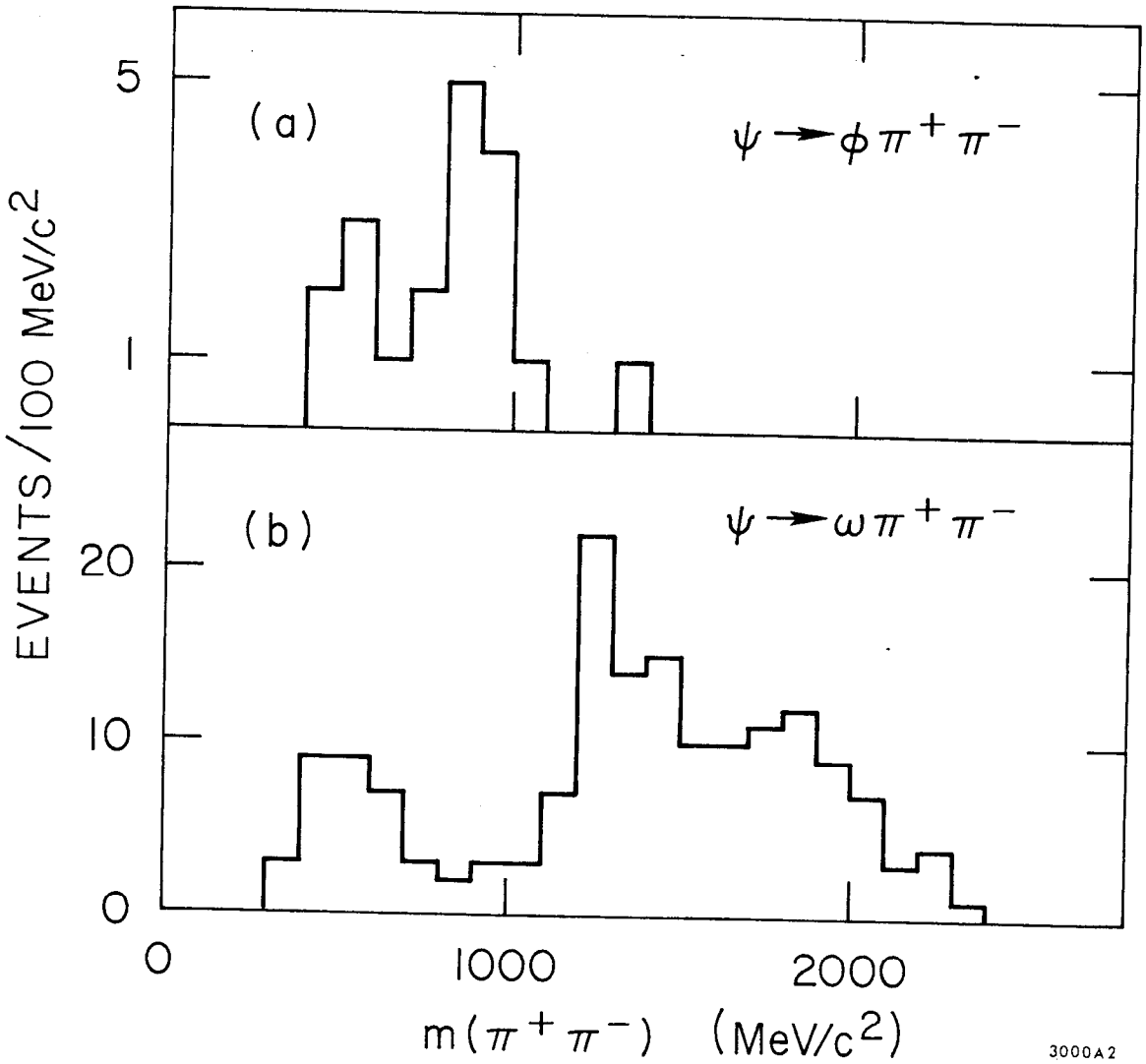
5
1
(a)
$\psi \rightarrow \phi \pi^+ \pi^-$
EVENTS/100 MeV/c^2
20
10
0
(b)
$\psi \rightarrow \omega \pi^+ \pi^-$
0
1000
2000
m($\pi^+ \pi^-$) (MeV/c^2)
3000A2

FIG. 4.10

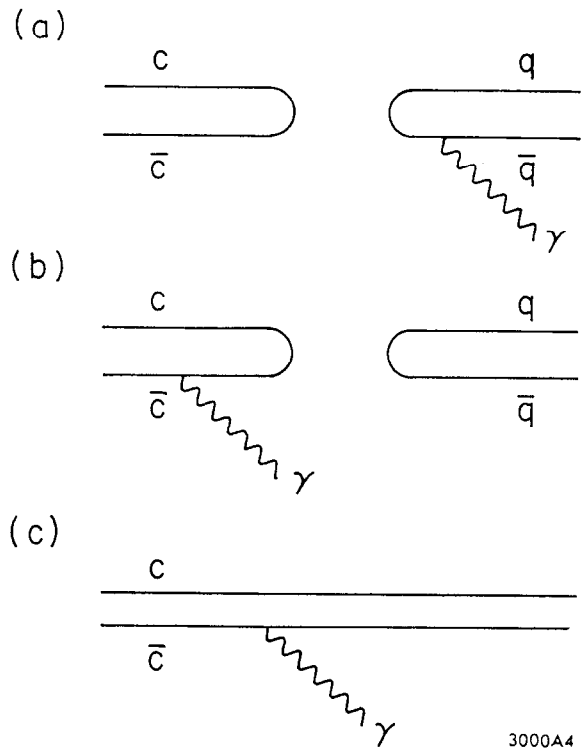

FIG. 4.11

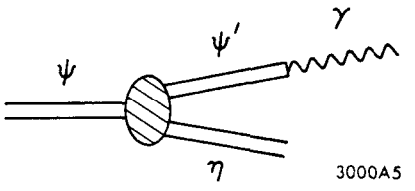

FIG. 4.12

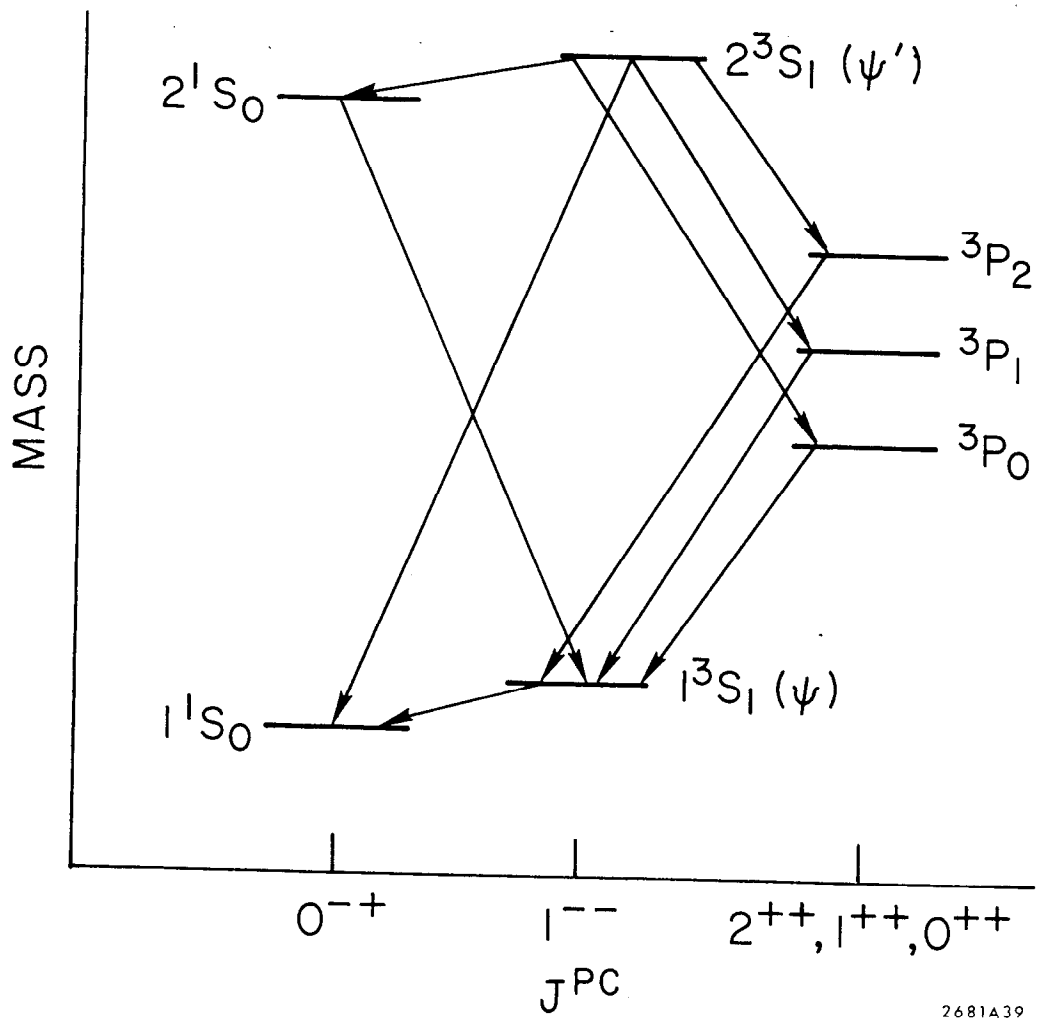
2^3S_1 (ψ')
2^1S_0
$^3P_2$
$^3P_1$
$^3P_0$
MASS
1^3S_1 (ψ)
1^1S_0
0^{-+}
1^{--}
$2^{++}, 1^{++}, 0^{++}$
J^{PC}
2681A39

FIG. 4.13

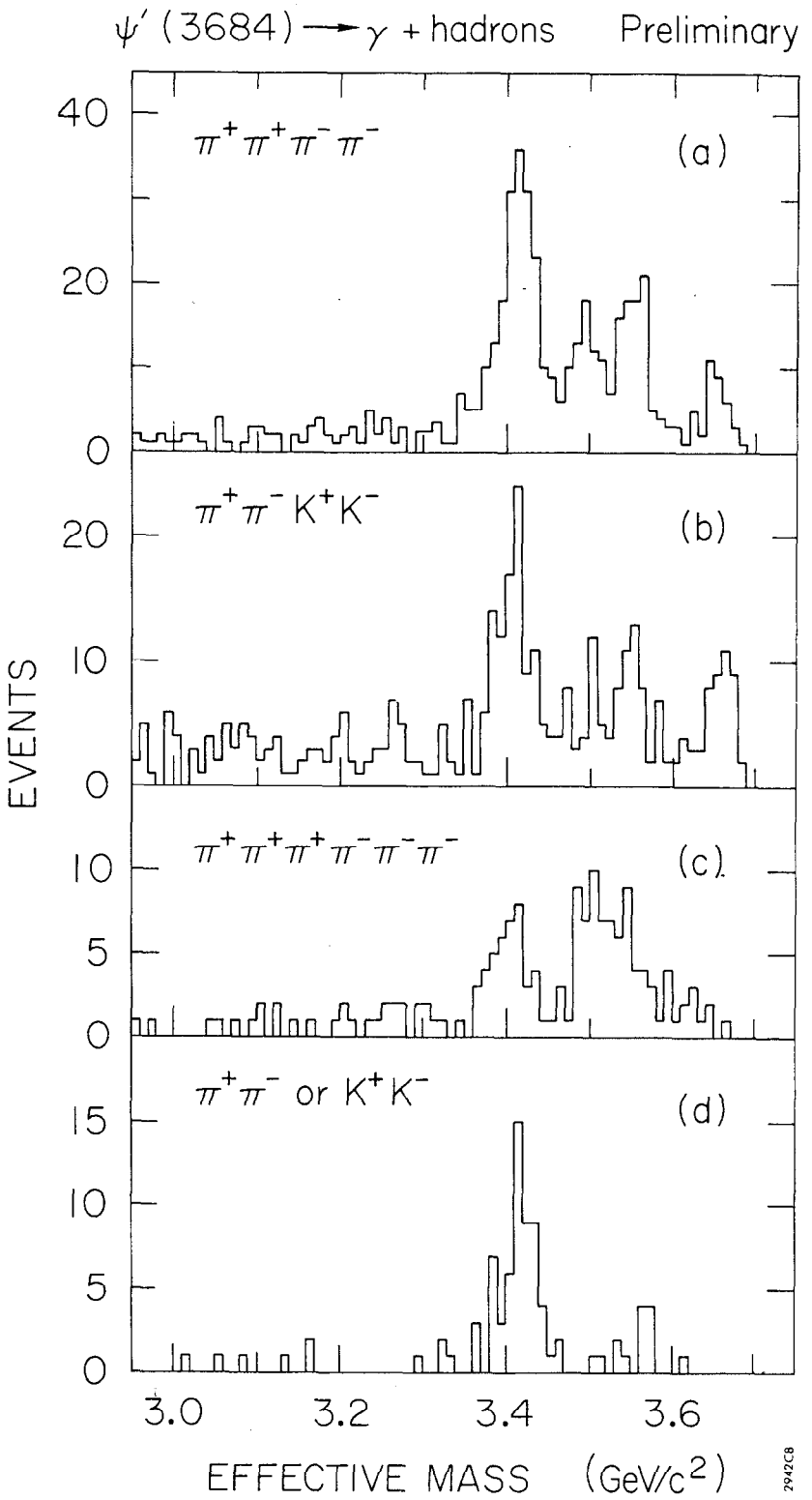
ψ′ (3684) → γ + hadrons
Preliminary
π⁺π⁺π⁻π⁻
(a)
π⁺π⁻K⁺K⁻
(b)
π⁺π⁺π⁺π⁻π⁻π⁻
(c)
π⁺π⁻ or K⁺K⁻
(d)
EVENTS
EFFECTIVE MASS (GeV/c²)
3.0
3.2
3.4
3.6
2942C8

FIG. 4.14

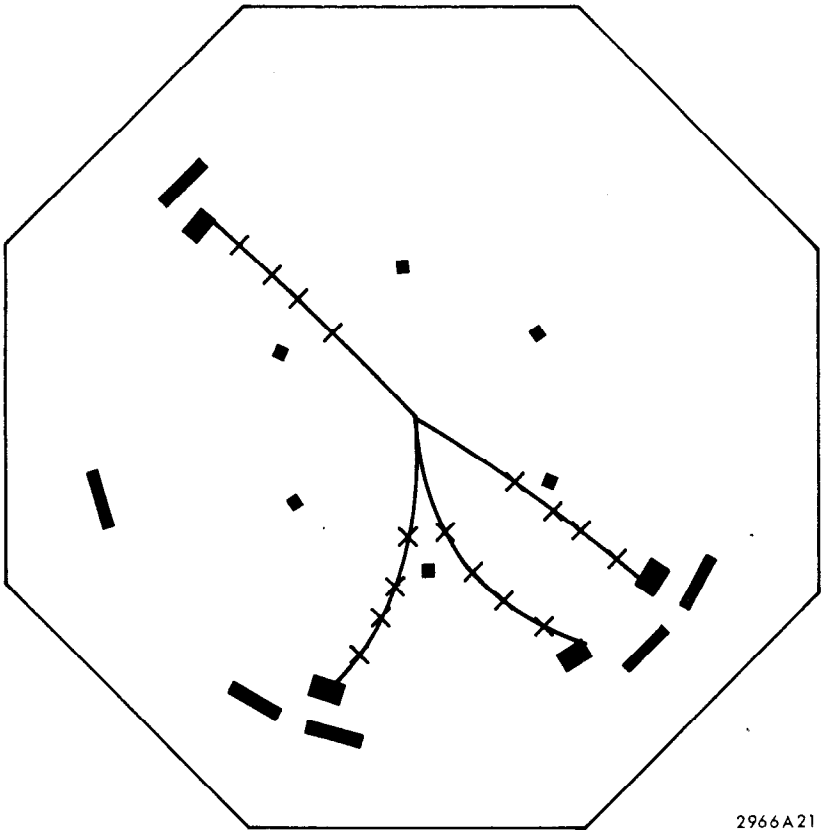

FIG. 4.15

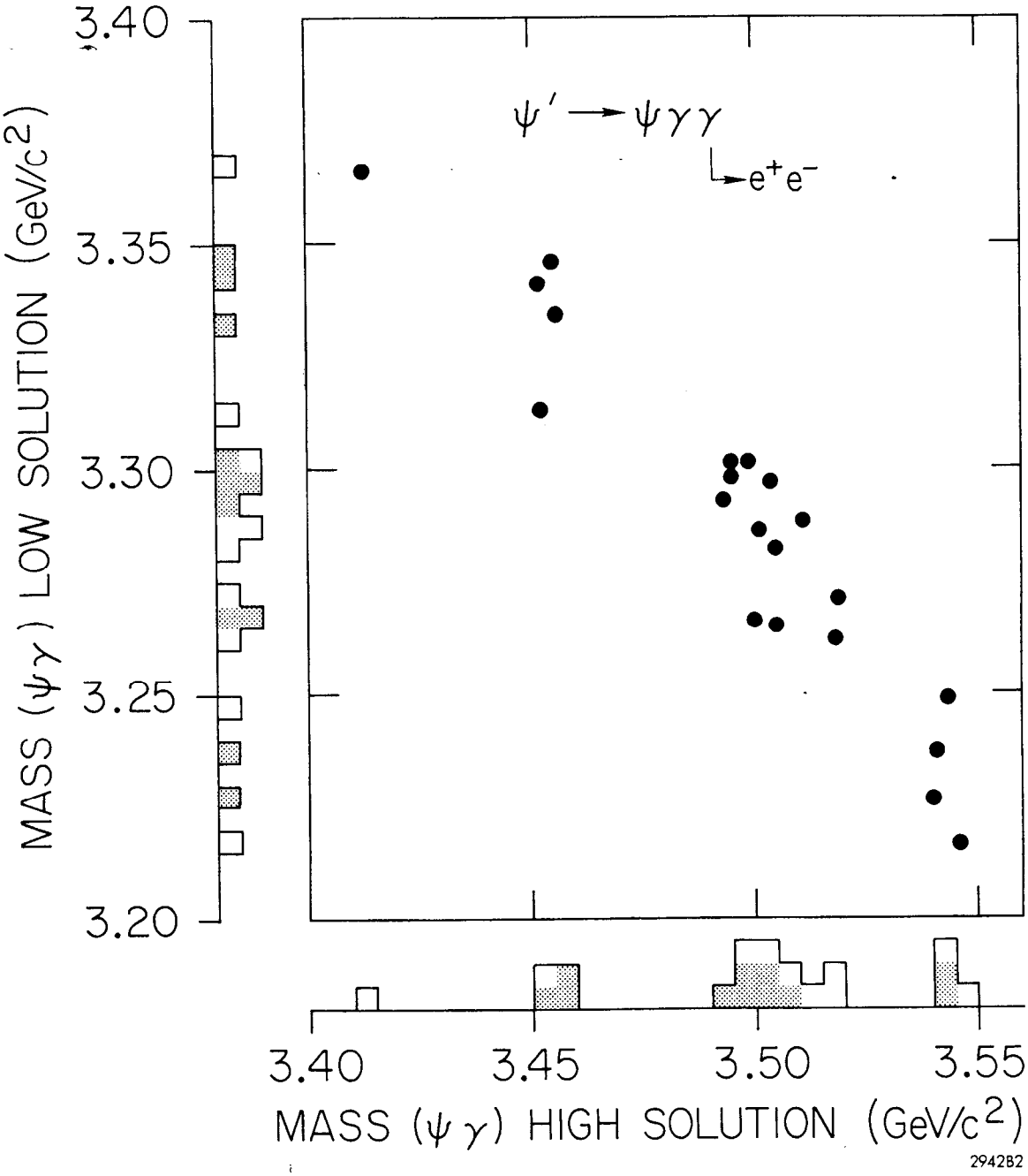
3.40
3.35
3.30
3.25
3.20
MASS ($\psi\gamma$) LOW SOLUTION (GeV/c^2)
$\psi' \rightarrow \psi\gamma\gamma$
$\hookrightarrow e^+e^-$
3.40
3.45
3.50
3.55
MASS ($\psi\gamma$) HIGH SOLUTION (GeV/c^2)
2942B2

FIG. 4.16

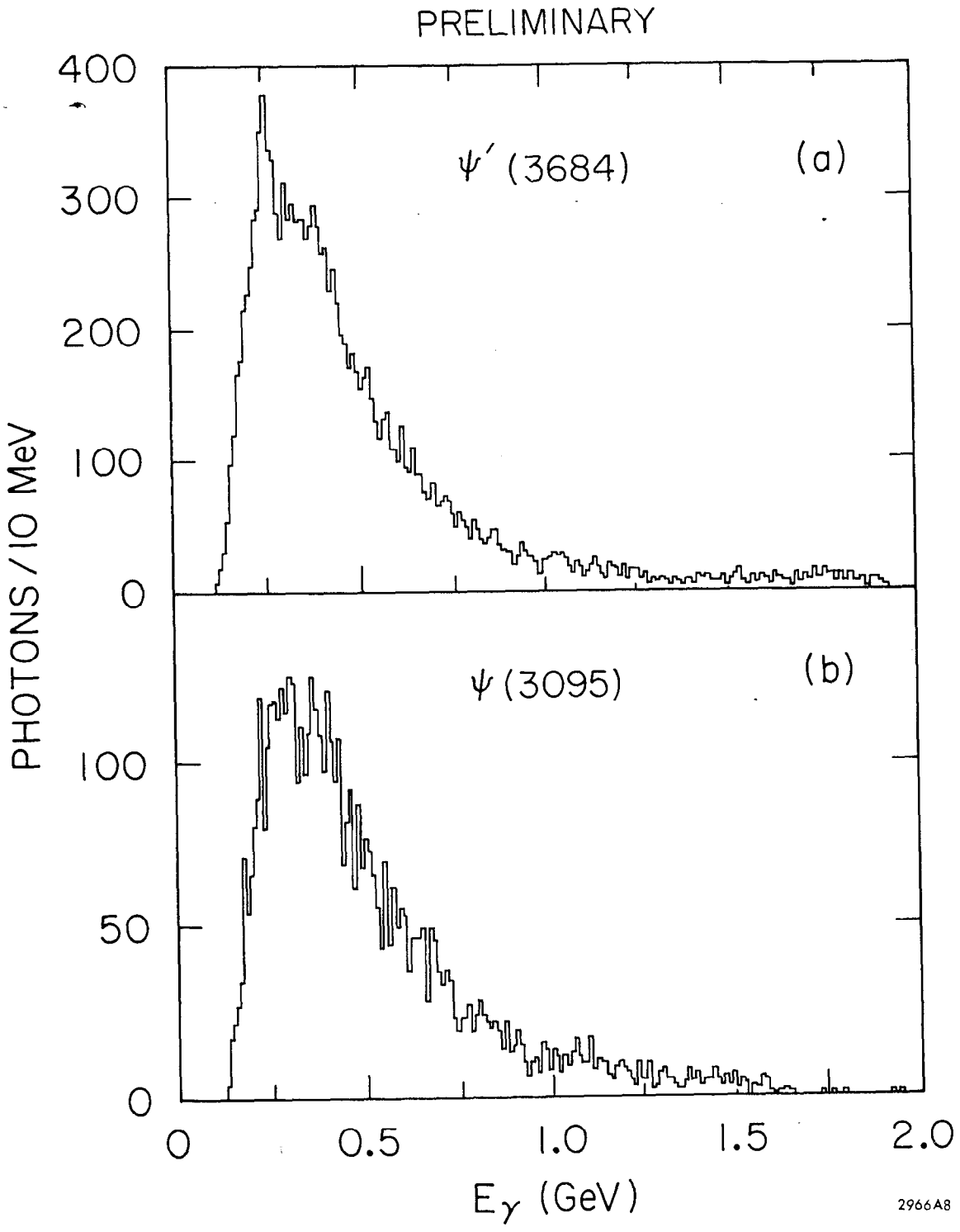
PRELIMINARY
400
300
200
100
0
ψ′ (3684)
(a)
PHOTONS / 10 MeV
100
50
0
ψ (3095)
(b)
0
0.5
1.0
1.5
2.0
Eγ (GeV)
2966A8

FIG. 4.17

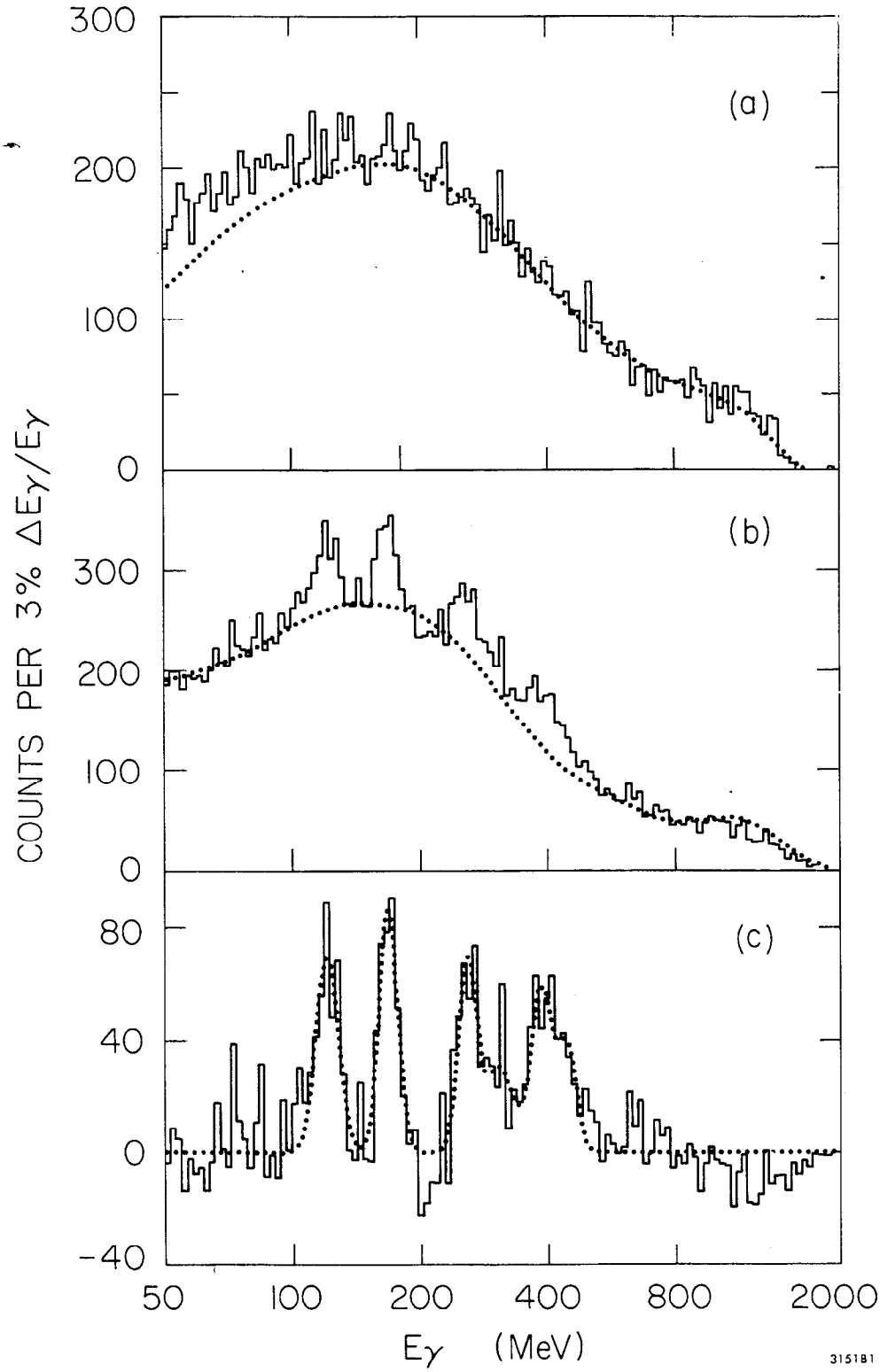
300
200
100
0
(a)
300
200
100
0
(b)
80
40
0
-40
(c)
COUNTS PER 3% ΔEγ/Eγ
50
100
200
400
800
2000
Eγ (MeV)
3151B1

FIG. 4.18

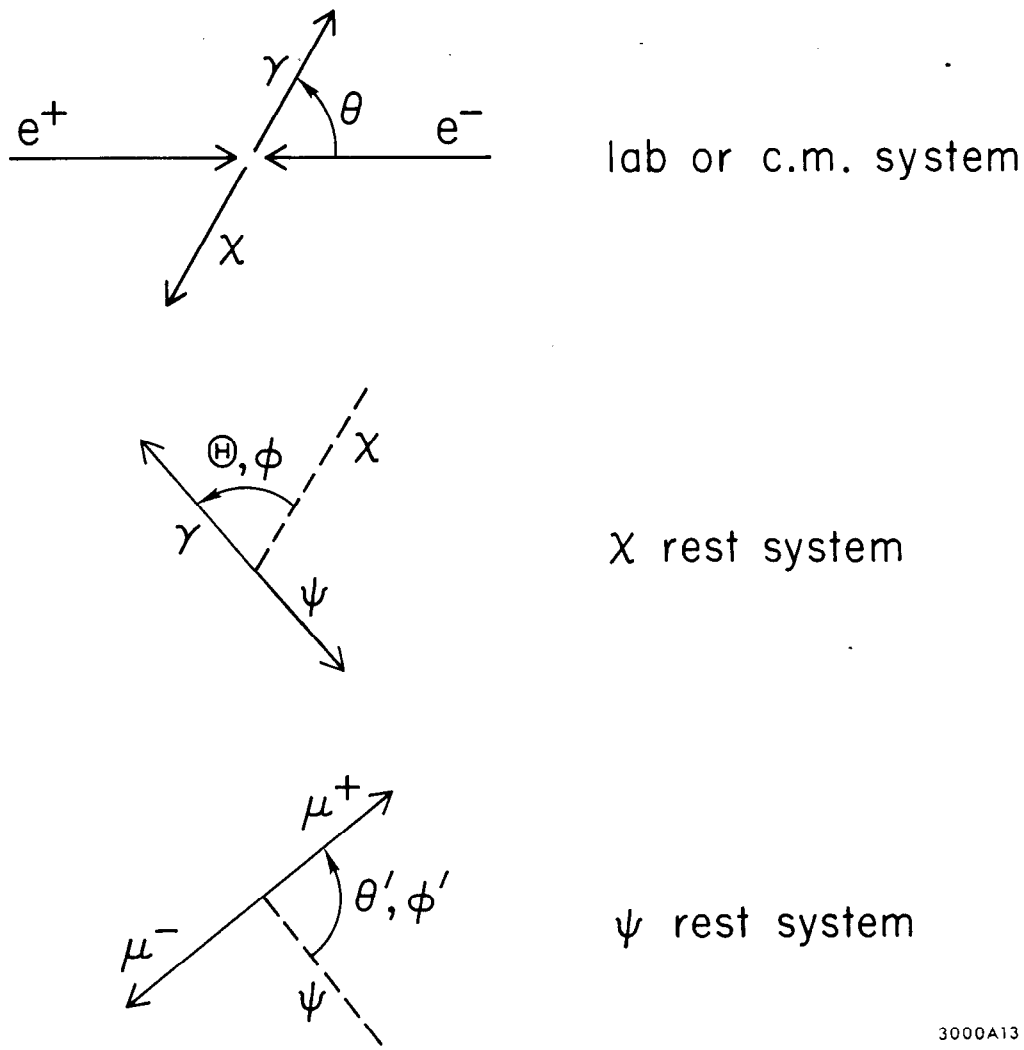
e^+
γ
θ
e^-
χ
lab or c.m. system
Θ, ϕ
χ
γ
ψ
χ rest system
μ^+
θ', ϕ'
μ^-
ψ
ψ rest system
3000A13

FIG. 4.19

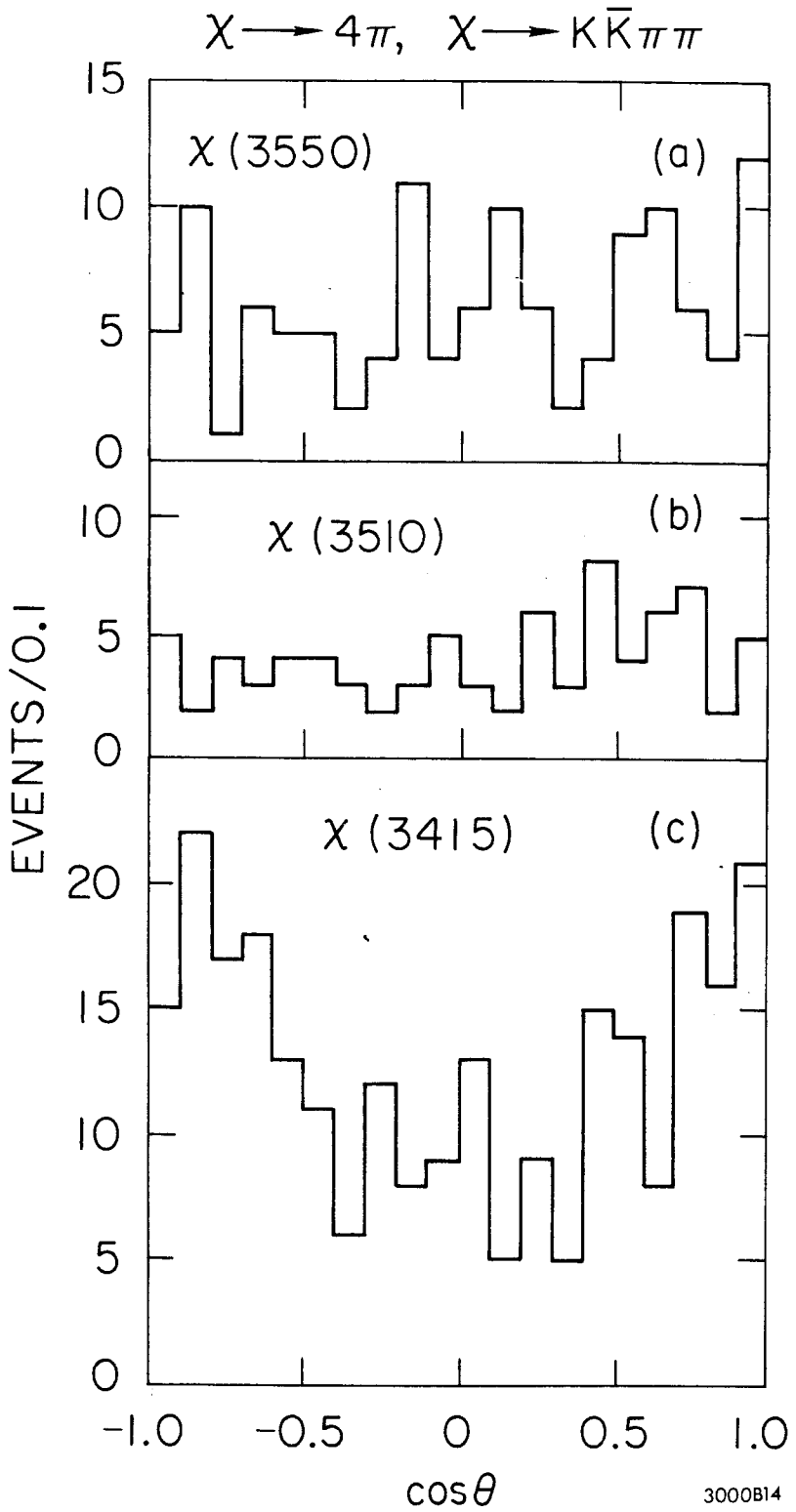
$\chi \longrightarrow 4\pi$, $\chi \longrightarrow K\bar{K}\pi\pi$
χ (3550)
(a)
χ (3510)
(b)
χ (3415)
(c)
EVENTS/0.1
15
10
5
0
10
5
0
20
15
10
5
0
-1.0
-0.5
0
0.5
1.0
$\cos\theta$
3000B14

FIG. 4.20

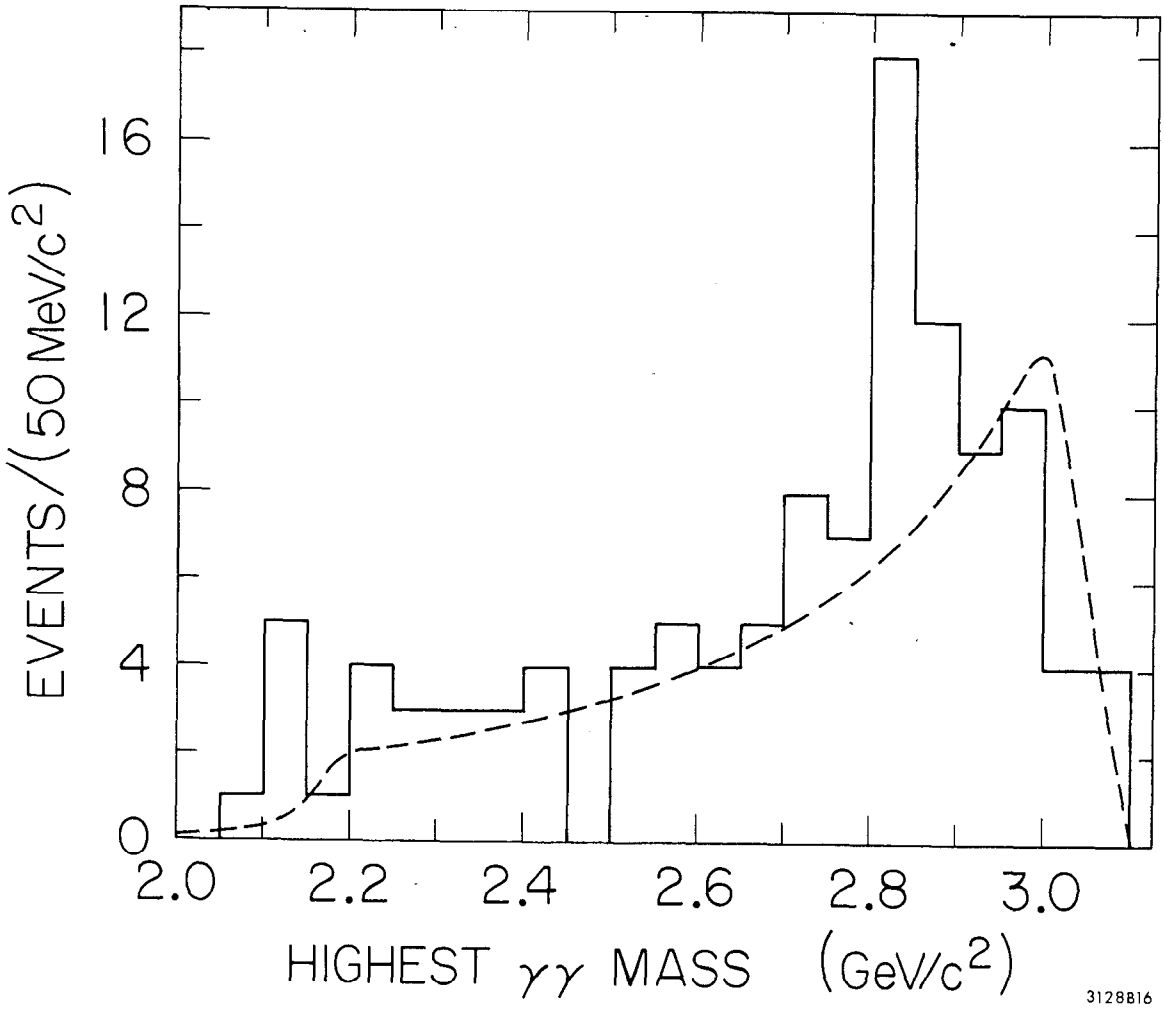
EVENTS/(50 MeV/c²)
0
4
8
12
16
2.0
2.2
2.4
2.6
2.8
3.0
HIGHEST γγ MASS (GeV/c²)
3128B16

FIG. 4.21

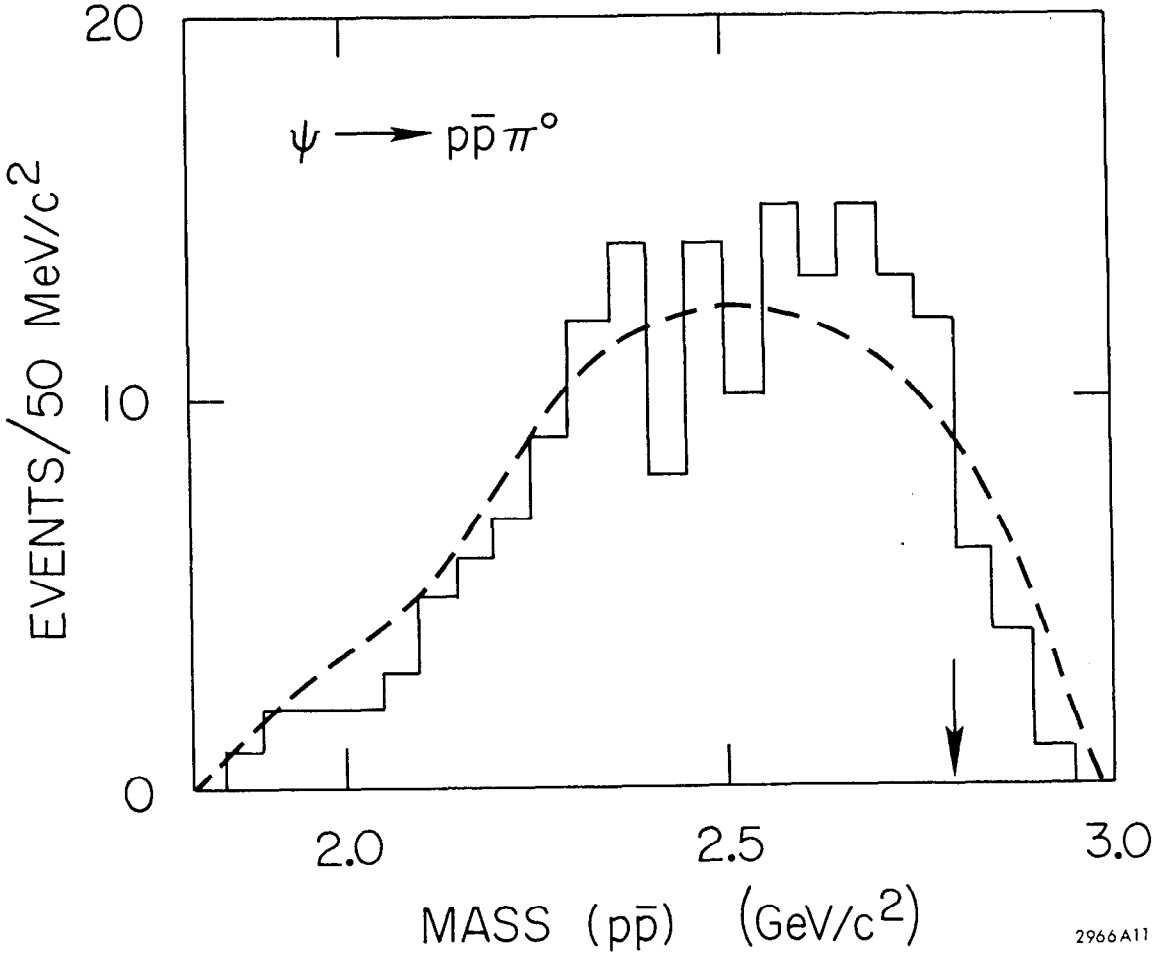
20
10
0
EVENTS/50 MeV/c^2
$\psi \longrightarrow p\bar{p}\pi^0$
2.0
2.5
3.0
MASS ($p\bar{p}$) (GeV/c^2)
2966A11

FIG. 4.22

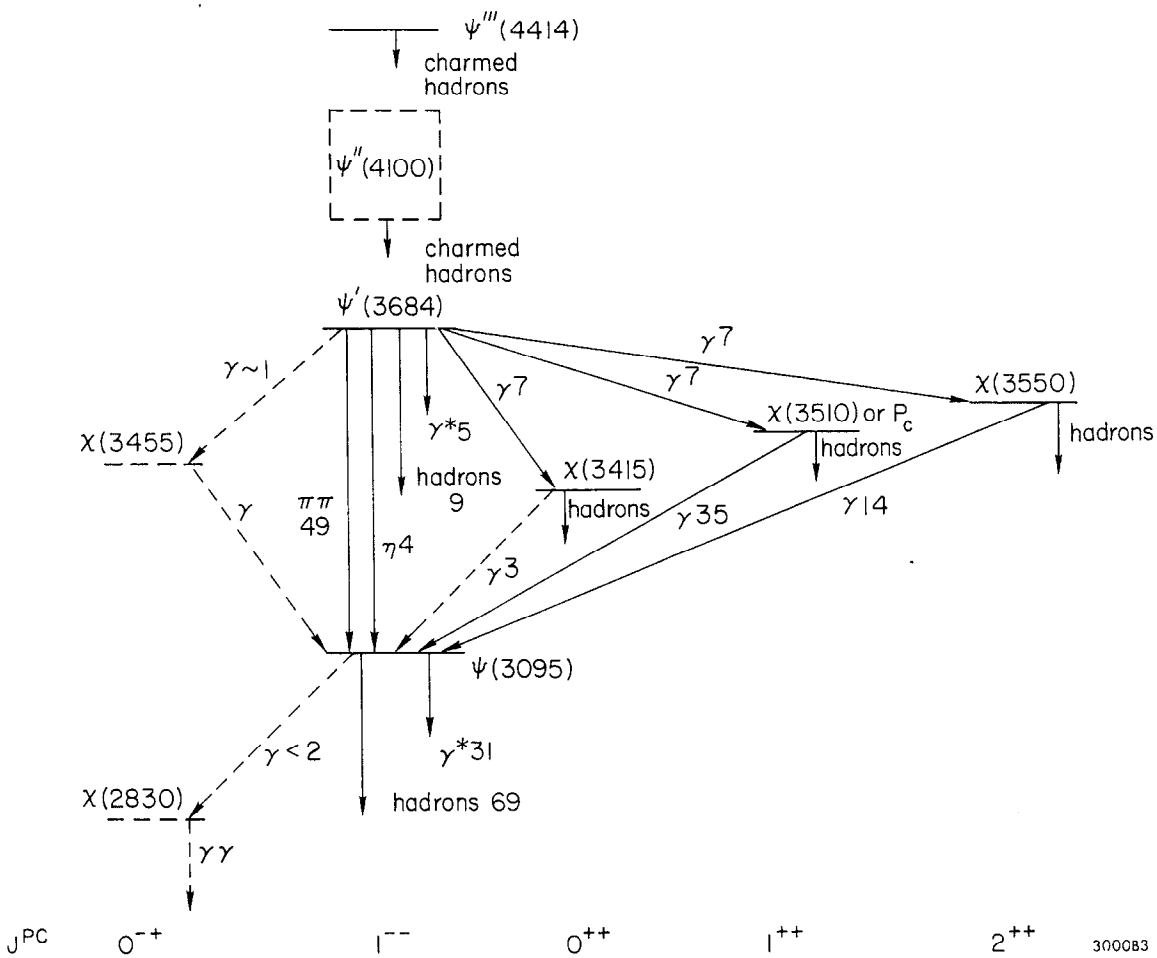
ψ'''(4414)
charmed hadrons
ψ''(4100)
charmed hadrons
ψ'(3684)
γ7
γ~1
γ7
γ7
χ(3550)
χ(3510) or P_c
hadrons
χ(3455)
γ*5
hadrons 9
χ(3415)
hadrons
hadrons
γ
ππ 49
η4
γ35
γ14
γ3
ψ(3095)
γ<2
γ*31
χ(2830)
hadrons 69
γγ
J^PC
0^-+
1^--
0^++
1^++
2^++
3000B3

FIG. 4.23

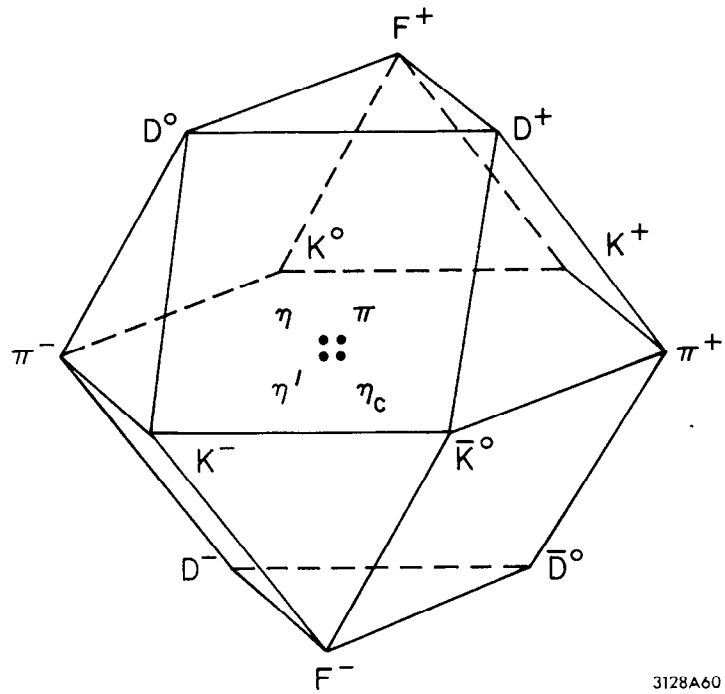

FIG. 5.1

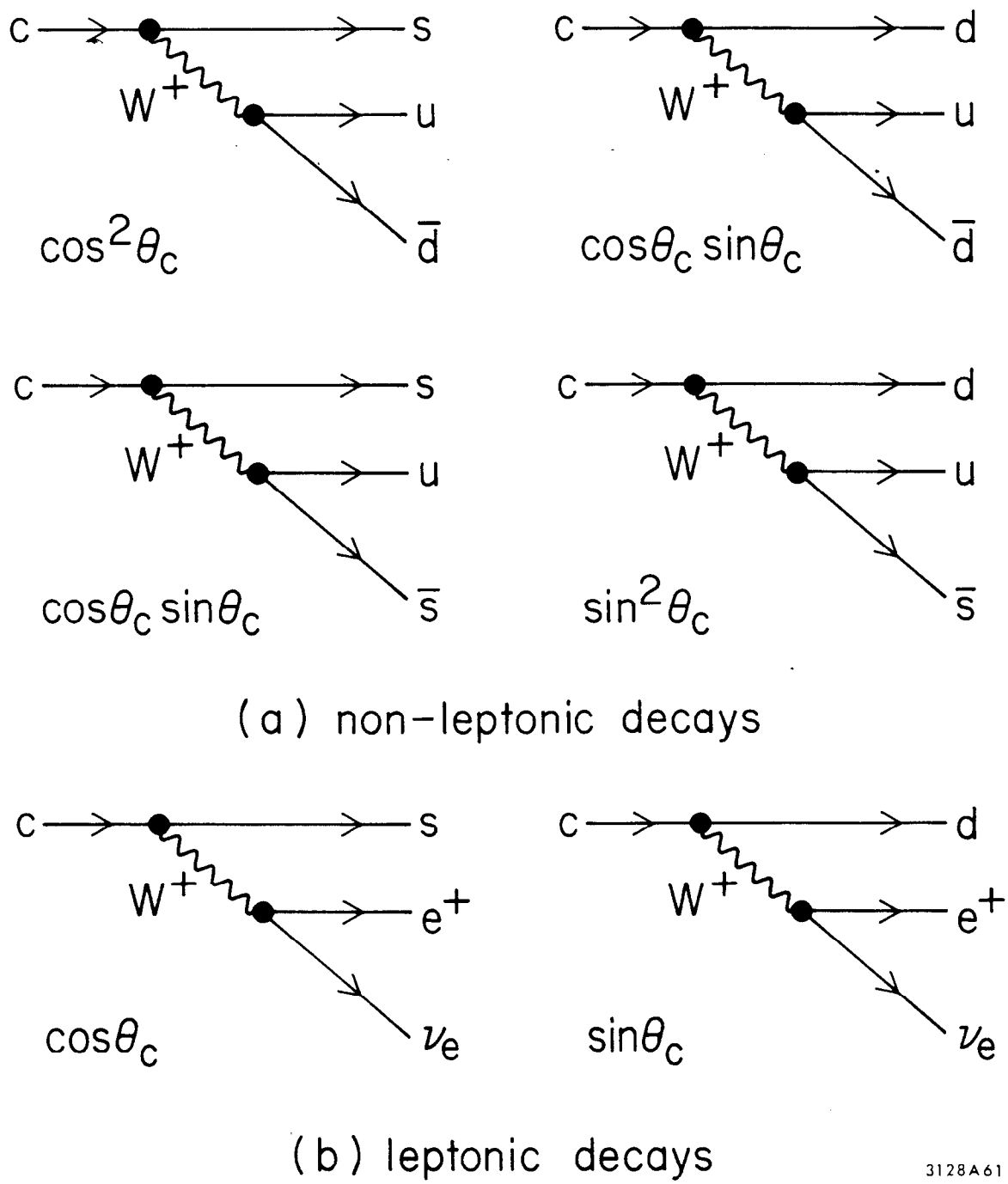
c
s
W+
u
d̄
cos²θc
c
d
W+
u
d̄
cosθc sinθc
c
s
W+
u
s̄
cosθc sinθc
c
d
W+
u
s̄
sin²θc
(a) non-leptonic decays
c
s
W+
e+
νe
cosθc
c
d
W+
e+
νe
sinθc
(b) leptonic decays
3128A61

FIG. 5.2

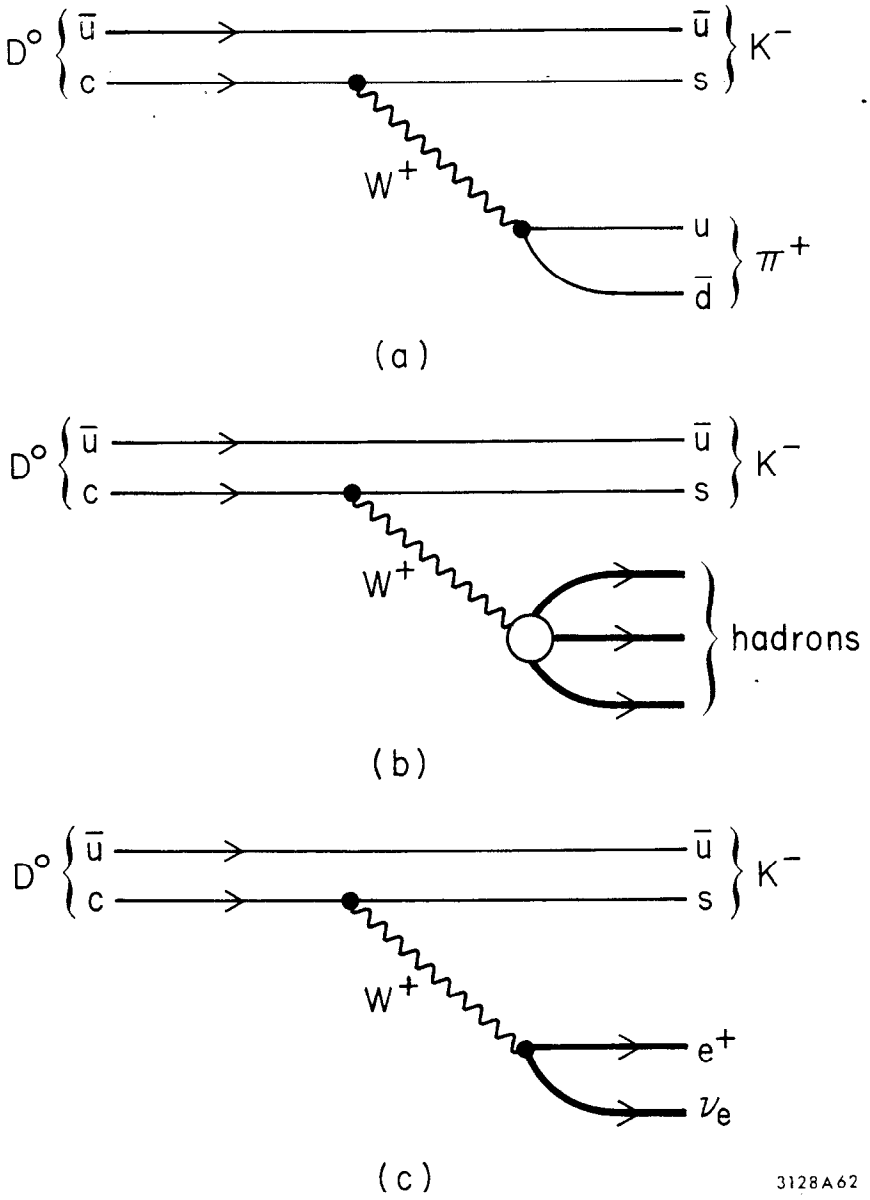

FIG. 5.3

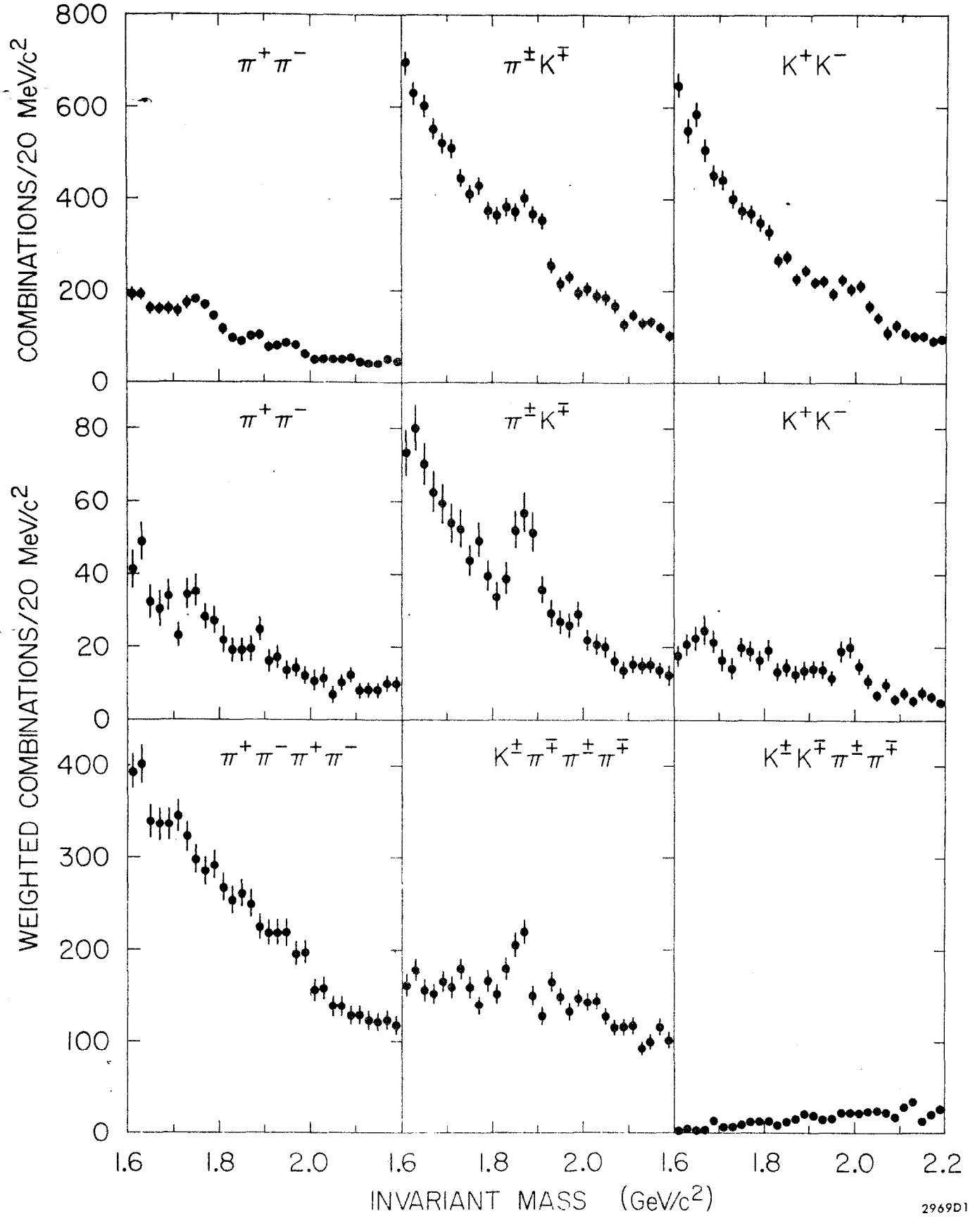
COMBINATIONS/20 MeV/c²
WEIGHTED COMBINATIONS/20 MeV/c²
π⁺π⁻
π±K∓
K⁺K⁻
π⁺π⁻π⁺π⁻
K±π∓π±π∓
K±K∓π±π∓
INVARIANT MASS (GeV/c²)
2969D1

FIG. 5.4

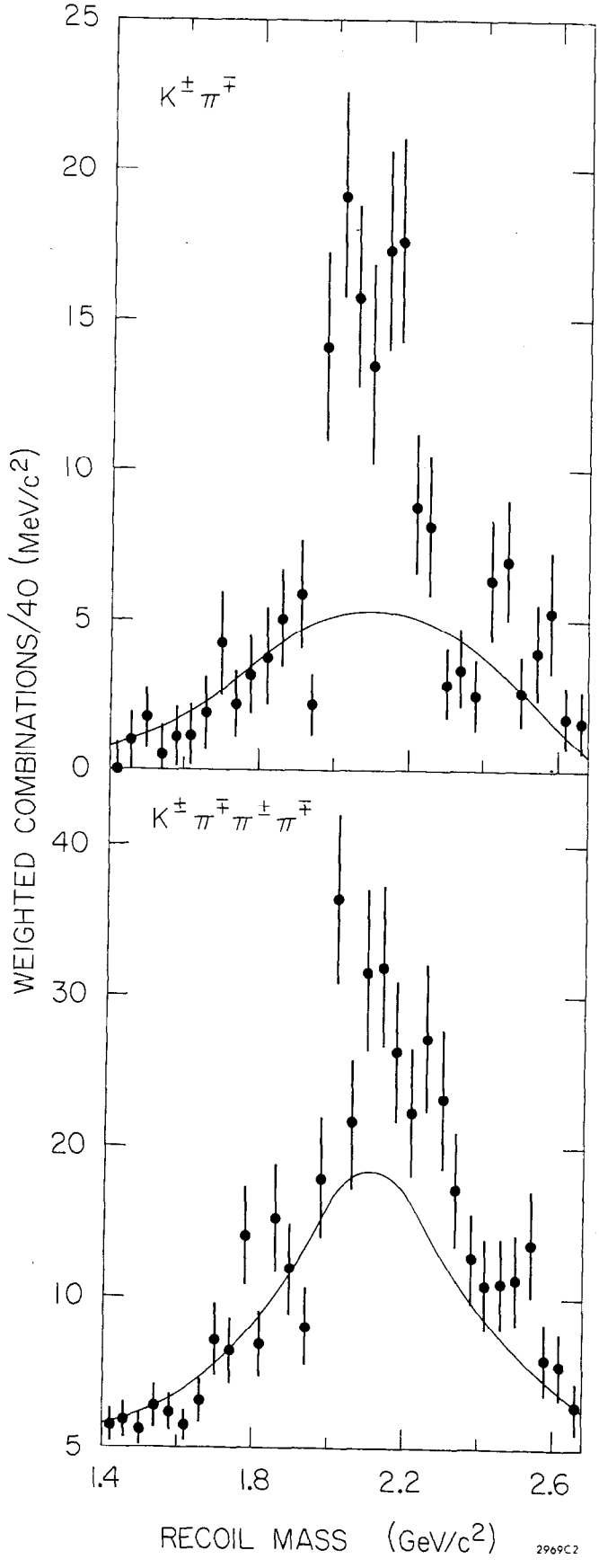
25
20
15
10
5
0
$K^{\pm}\pi^{\mp}$
40
30
20
10
5
$K^{\pm}\pi^{\mp}\pi^{\pm}\pi^{\mp}$
WEIGHTED COMBINATIONS/40 (MeV/c^2)
1.4
1.8
2.2
2.6
RECOIL MASS (GeV/c^2)
2969C2

FIG. 5.5

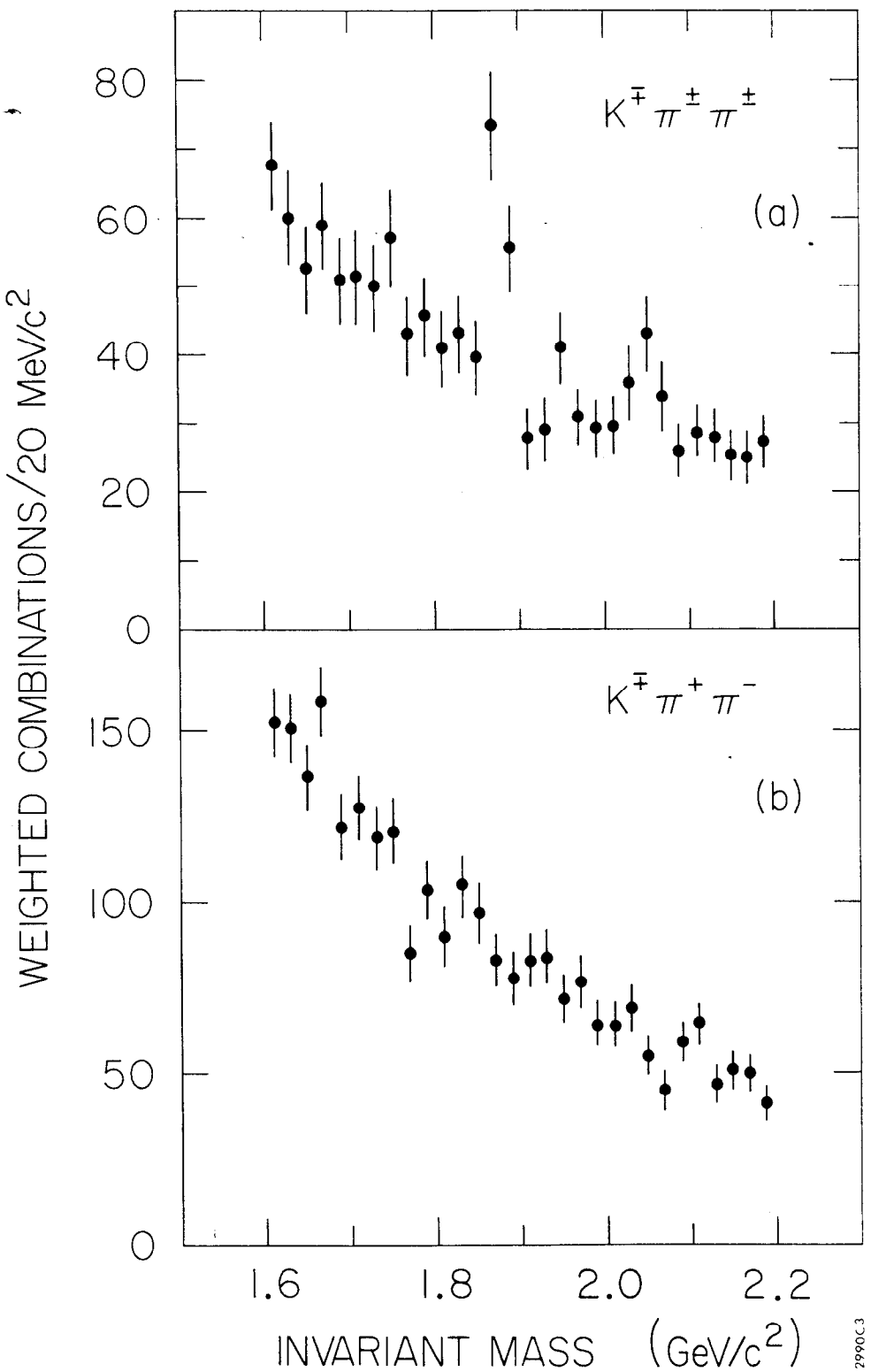
80
60
40
20
0
150
100
50
0
$K^{\mp}\pi^{\pm}\pi^{\pm}$
(a)
$K^{\mp}\pi^{+}\pi^{-}$
(b)
WEIGHTED COMBINATIONS/20 MeV/c^2
1.6
1.8
2.0
2.2
INVARIANT MASS (GeV/c^2)
2990C3

FIG. 5.6

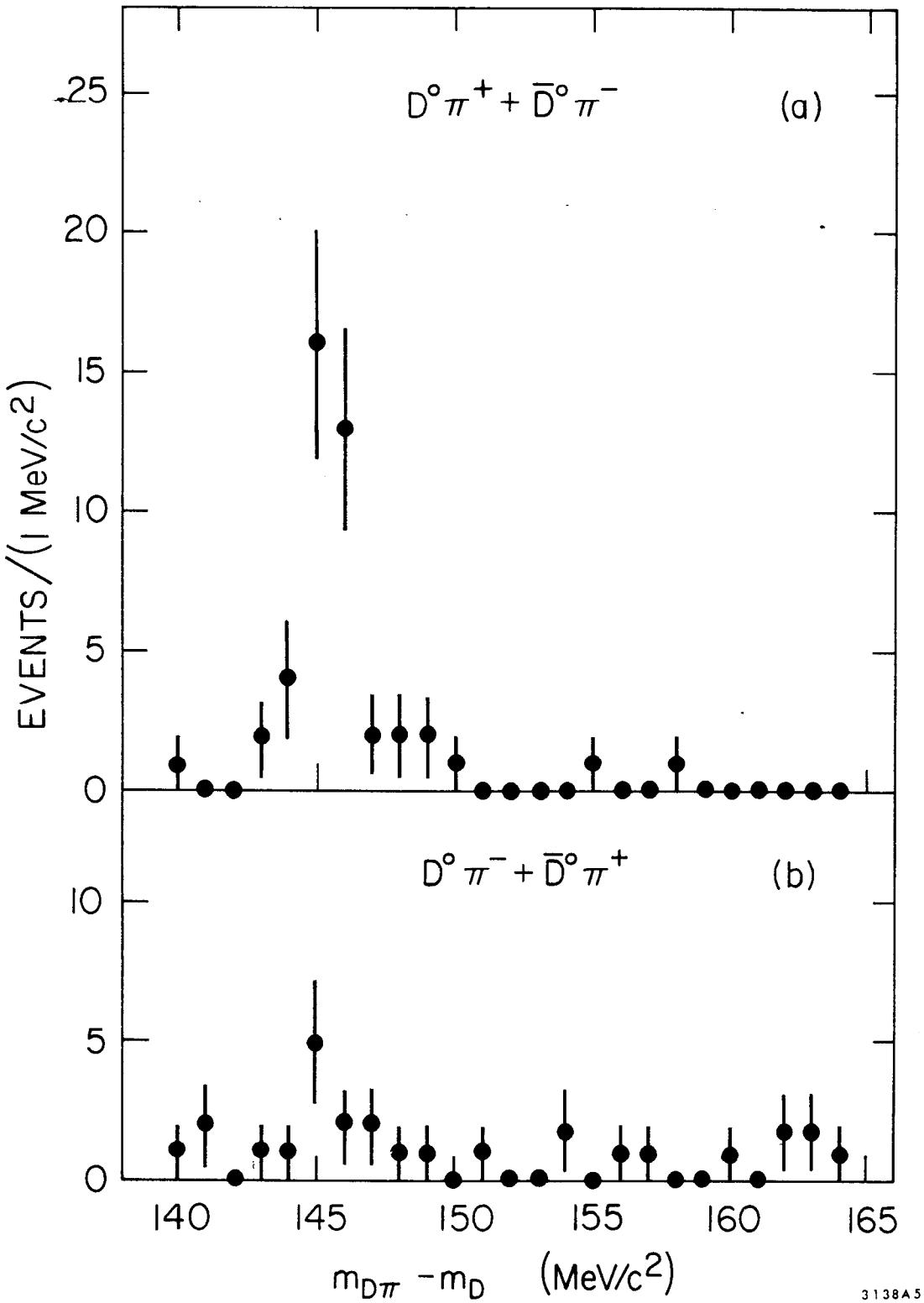
$D^\circ\pi^+ + \bar{D}^\circ\pi^-$
(a)
$D^\circ\pi^- + \bar{D}^\circ\pi^+$
(b)
EVENTS/(1 MeV/c^2)
25
20
15
10
5
0
10
5
0
140
145
150
155
160
165
$m_{D\pi} - m_D$ (MeV/c^2)
3138A5

FIG. 5.7

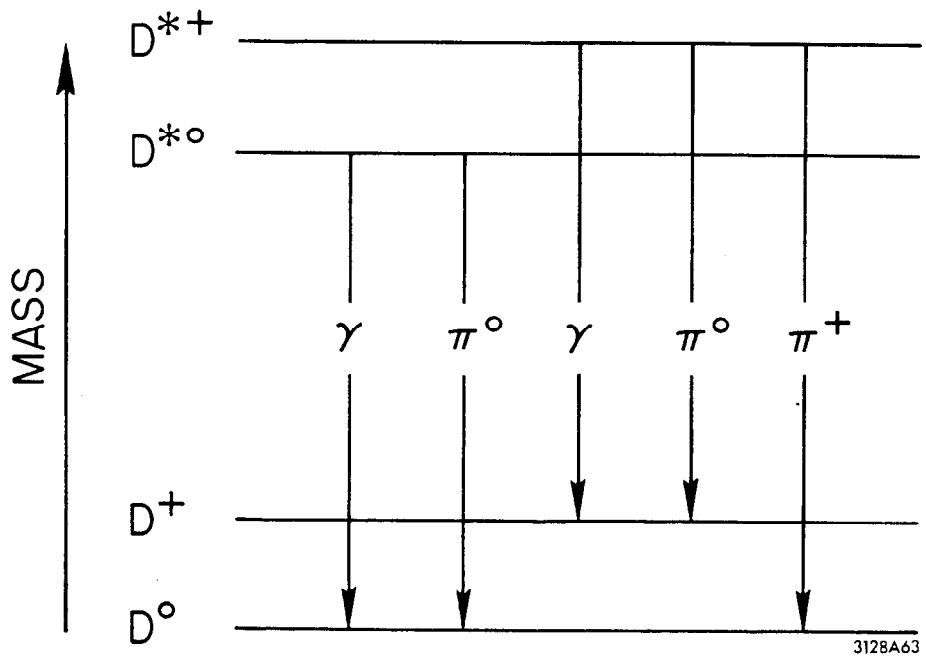

FIG. 5.8

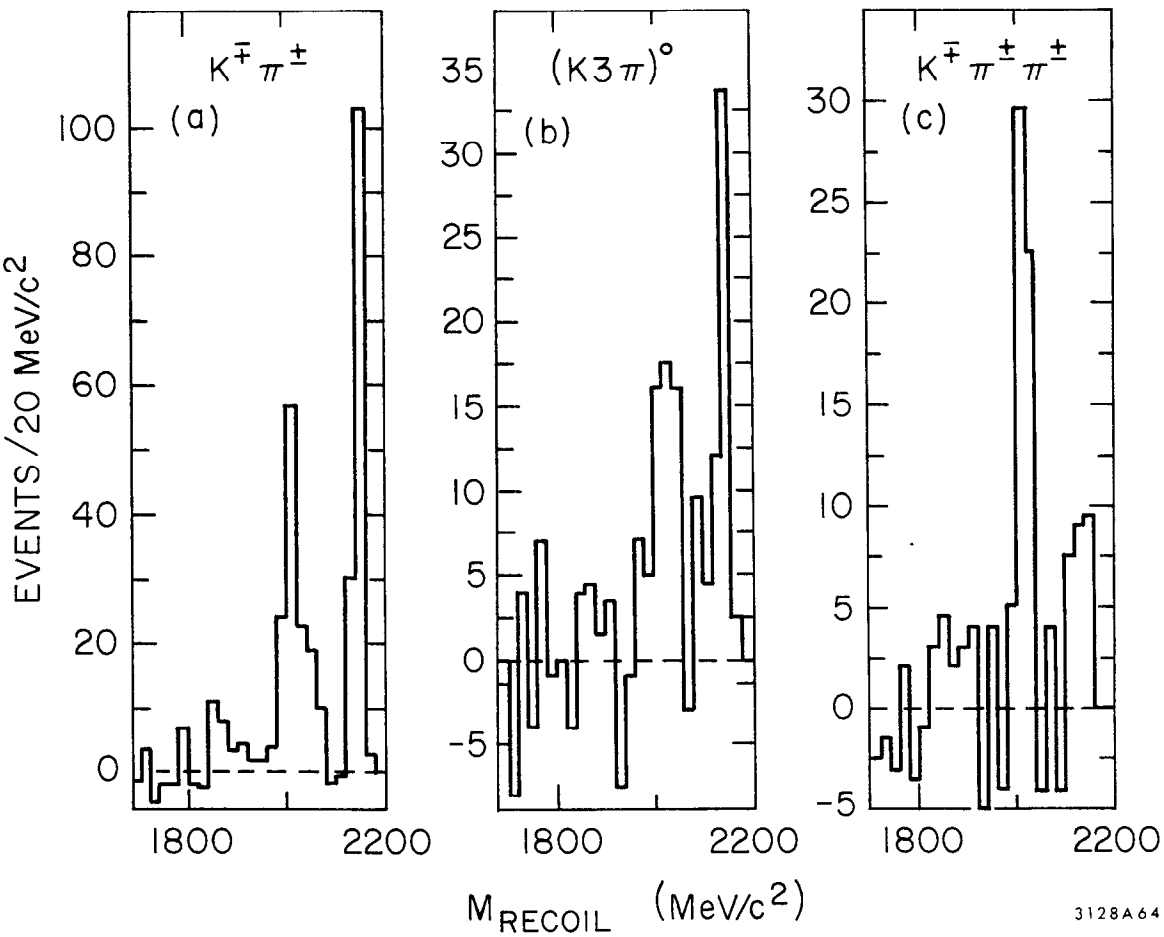
$K^{\mp}\pi^{\pm}$
(a)
$(K3\pi)^{\circ}$
(b)
$K^{\mp}\pi^{\pm}\pi^{\pm}$
(c)
EVENTS/20 MeV/c^2
M_{RECOIL} (MeV/c^2)
1800
2200
3128A64

FIG. 5.9

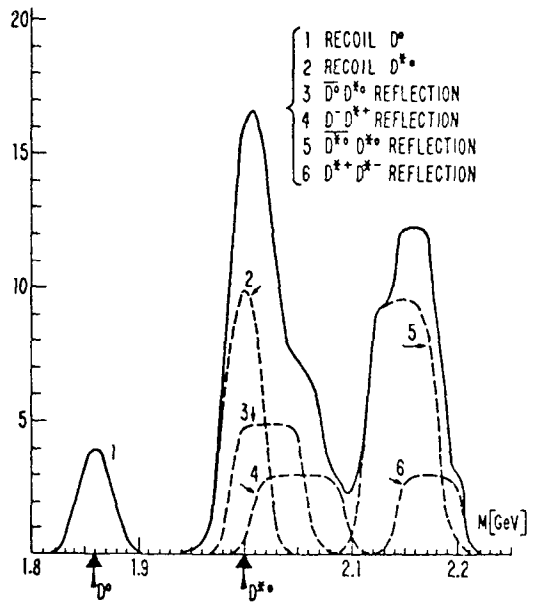
20
15
10
5
1 RECOIL D°
2 RECOIL D*°
3 $\overline{D^0}D^{*0}$ REFLECTION
4 D^-D^{*+} REFLECTION
5 $\overline{D^{*0}}D^{*0}$ REFLECTION
6 $D^{*+}D^{*-}$ REFLECTION
1
2
3
4
5
6
M[GeV]
1.8
1.9
2.1
2.2
D^0
D^{*0}

FIG. 5.10

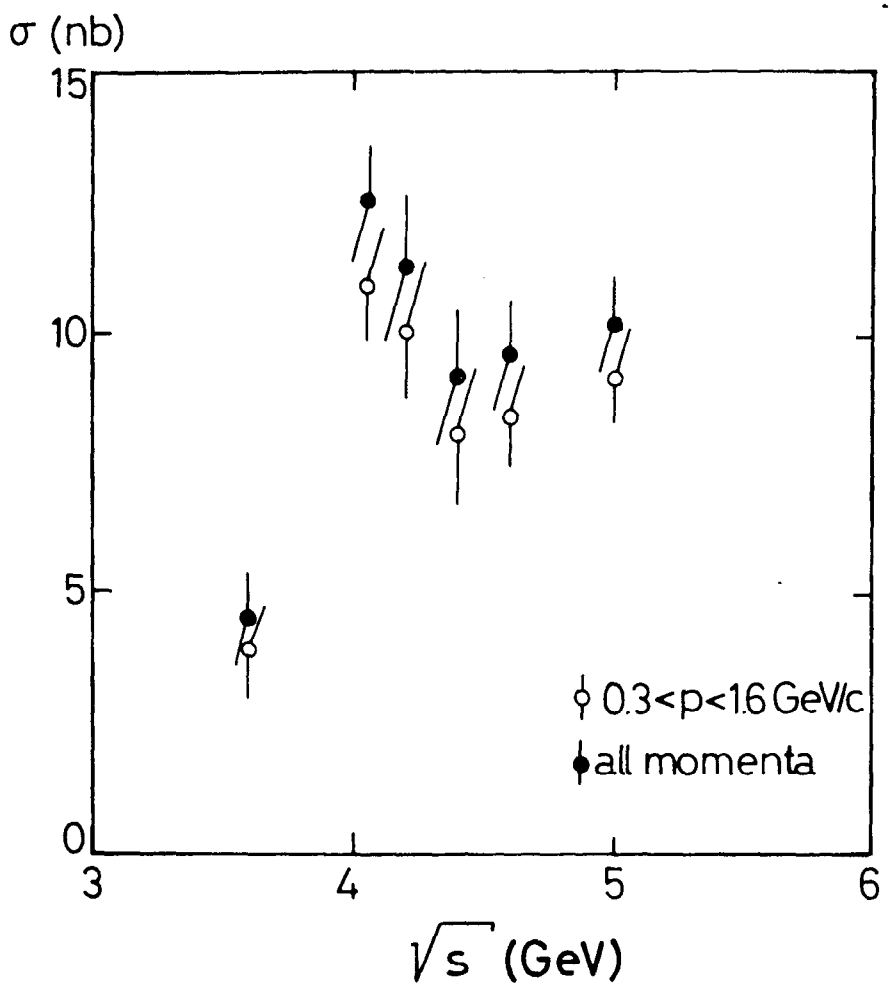

FIG. 5.11

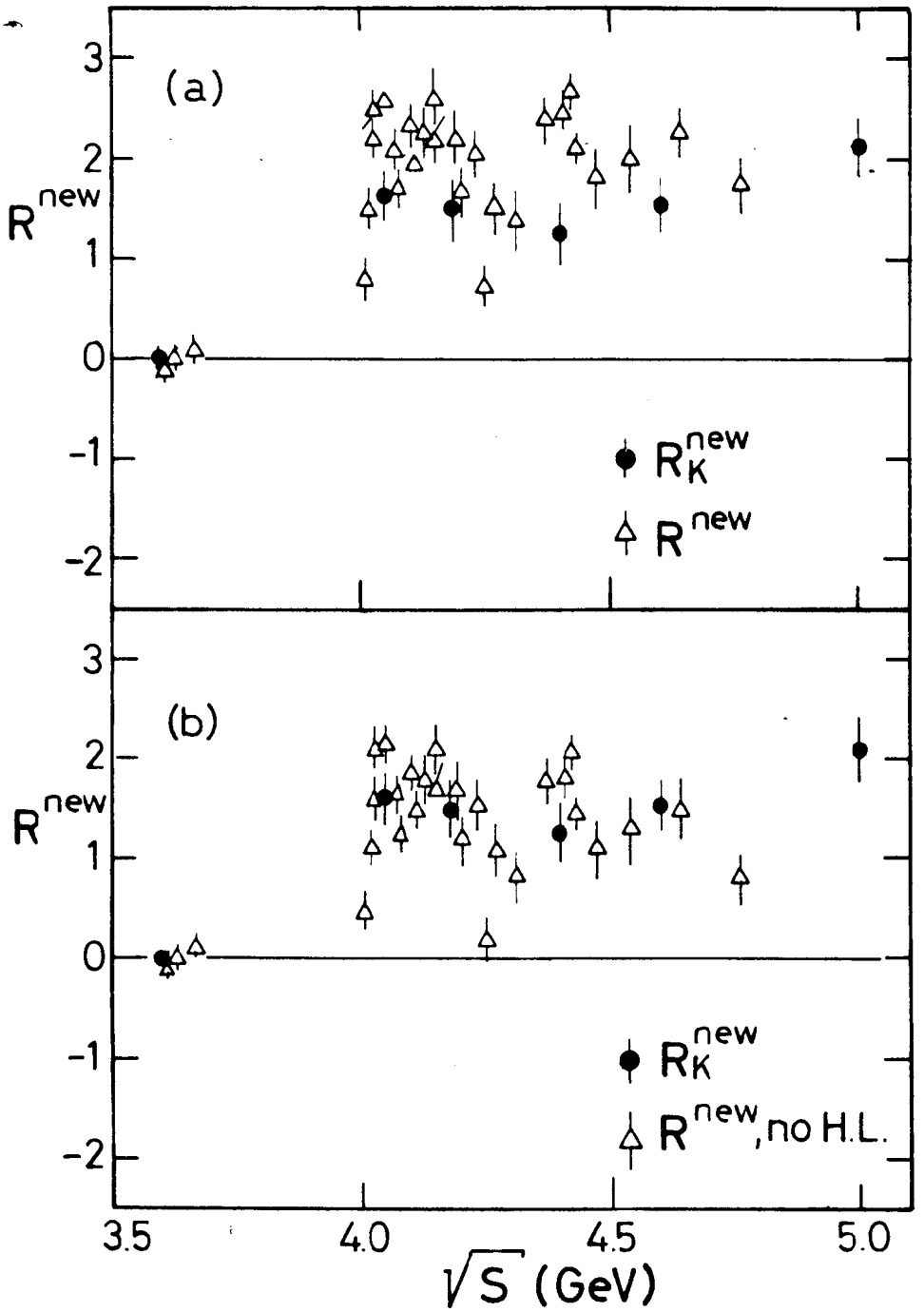

FIG. 5.12

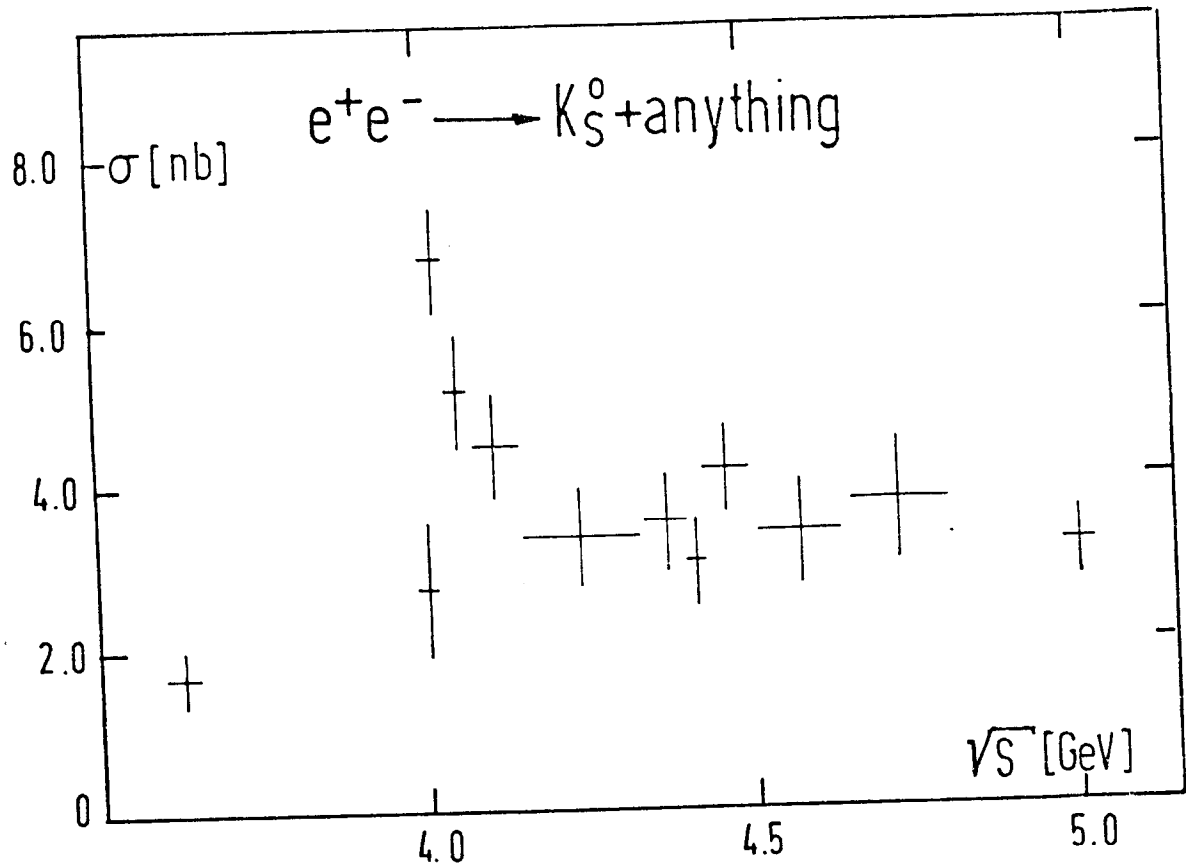
$e^+e^- \longrightarrow K_S^0$+anything
σ [nb]
8.0
6.0
4.0
2.0
0
$\sqrt{S}$ [GeV]
4.0
4.5
5.0

Fig. 5.13

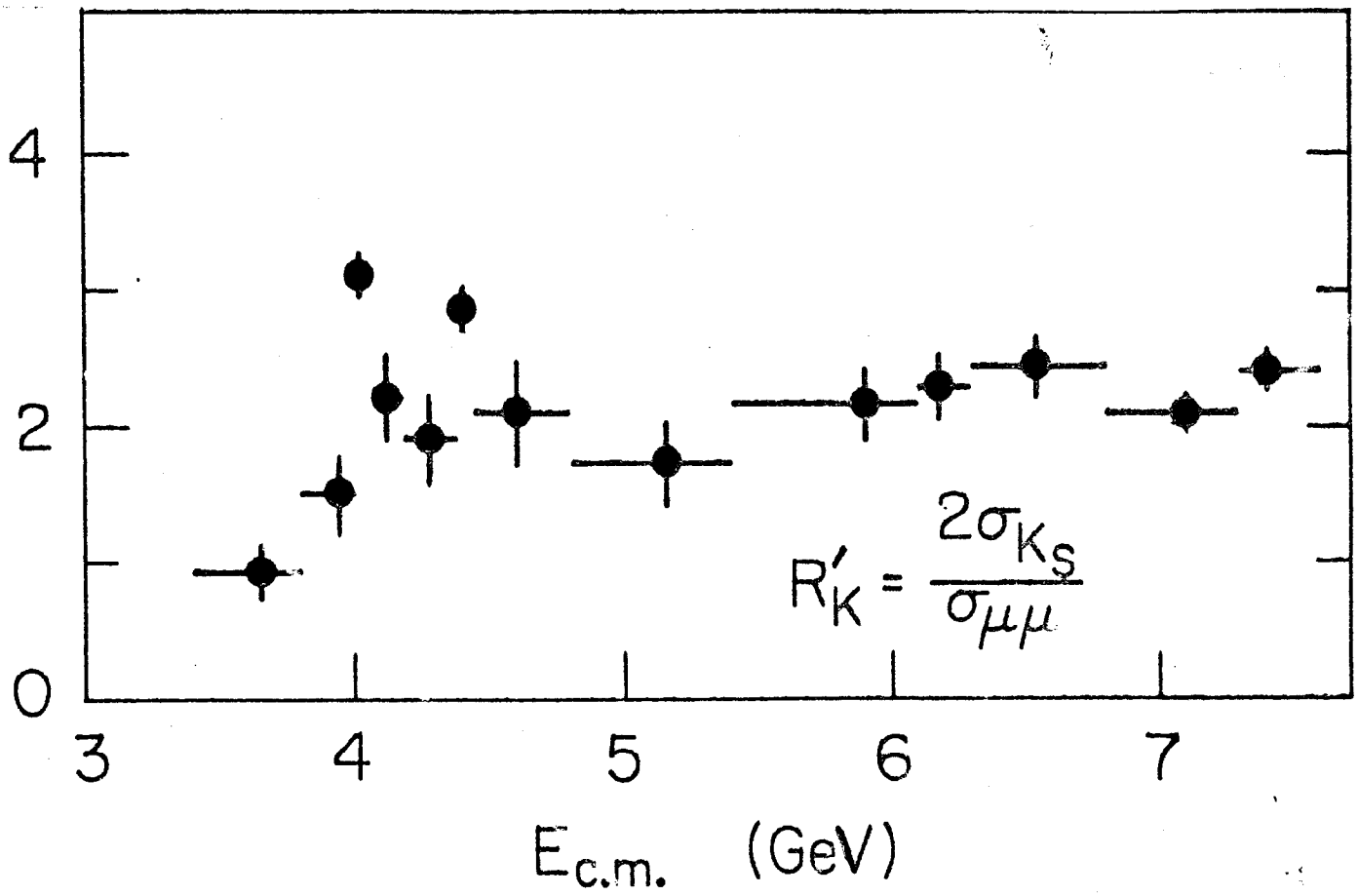

FIG. 5.14

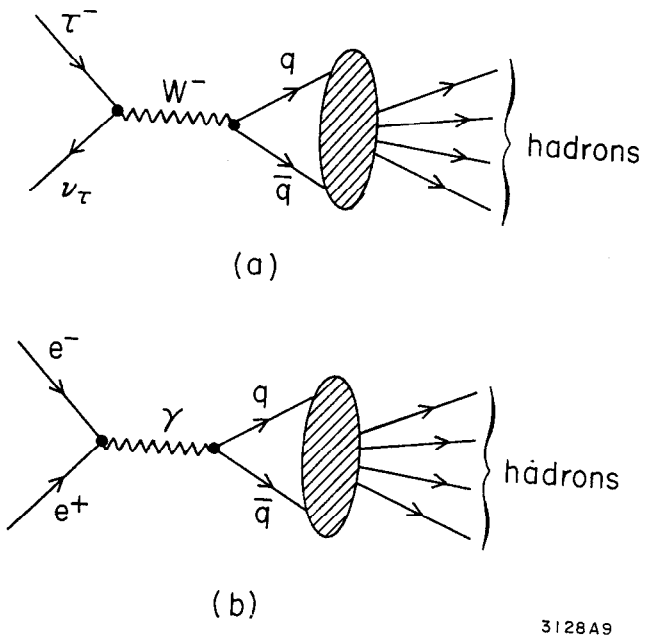

FIG. 6.1

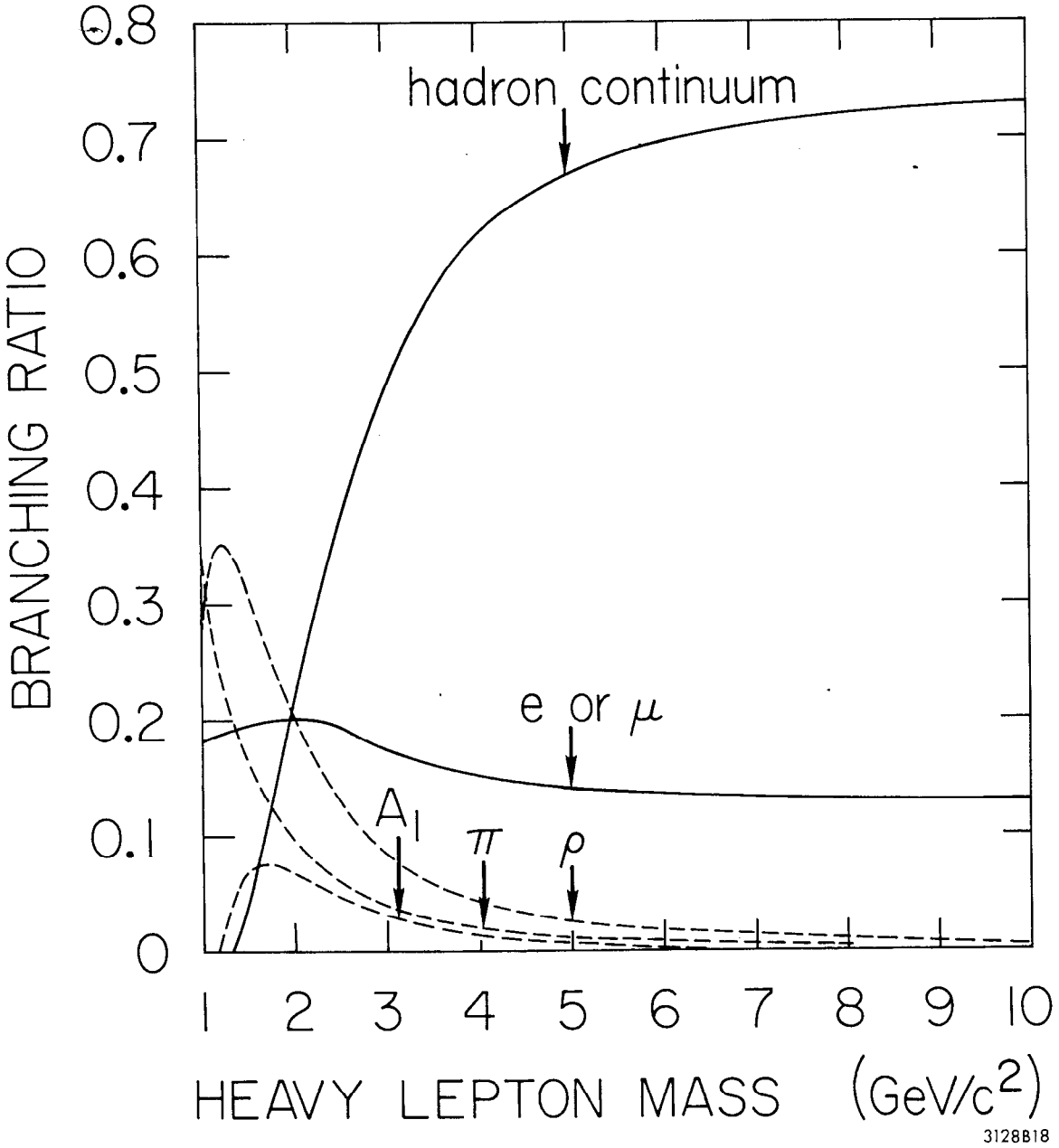
0.8
0.7
0.6
0.5
0.4
0.3
0.2
0.1
0
BRANCHING RATIO
hadron continuum
e or μ
A1
π
ρ
1 2 3 4 5 6 7 8 9 10
HEAVY LEPTON MASS (GeV/c2)
3128B18

FIG. 6.2a

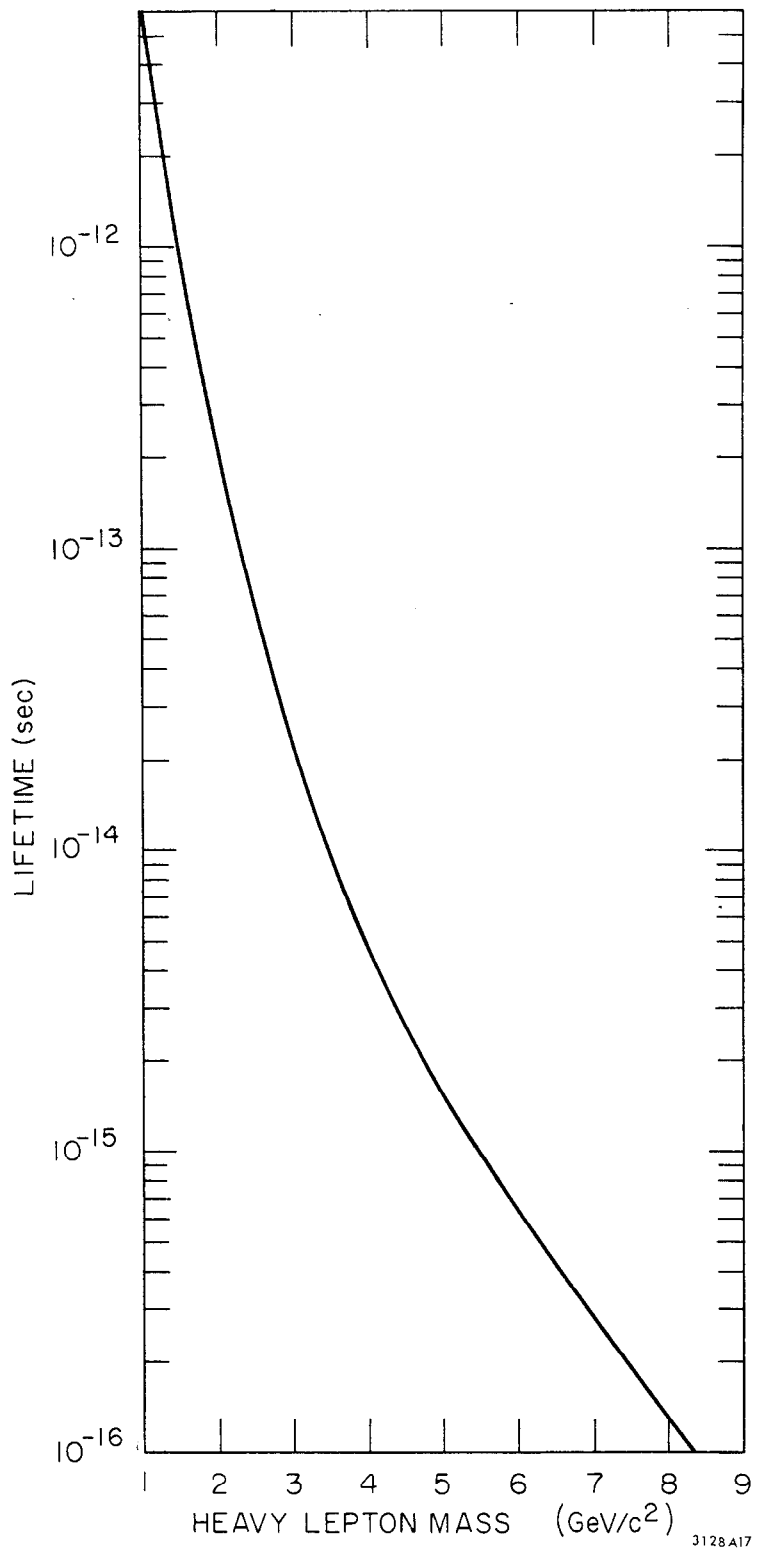
LIFETIME (sec)
10^{-12}
10^{-13}
10^{-14}
10^{-15}
10^{-16}
1 2 3 4 5 6 7 8 9
HEAVY LEPTON MASS (GeV/c^2)
3128A17

FIG. 6.2b

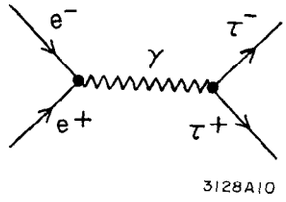

FIG. 6.3

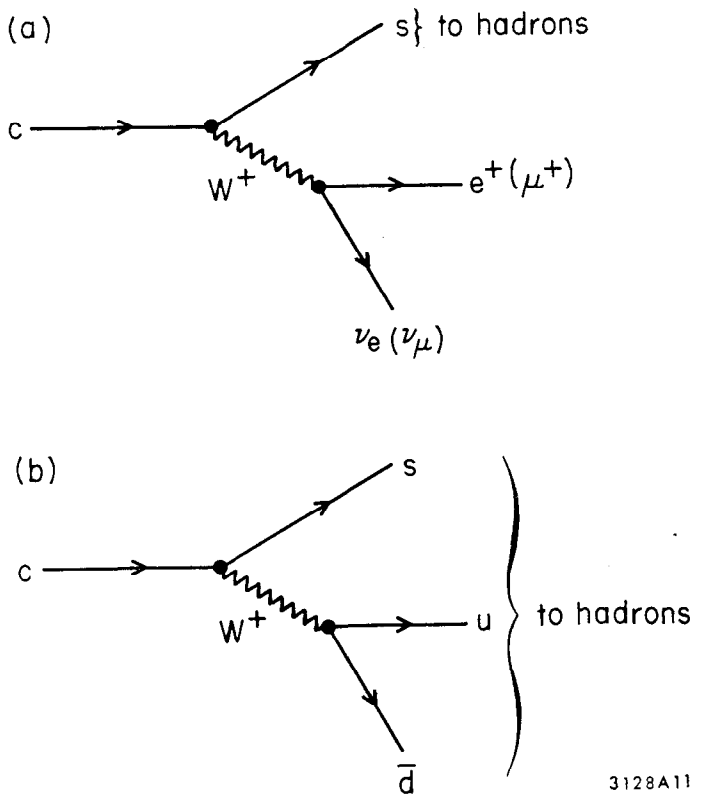

FIG. 6.4

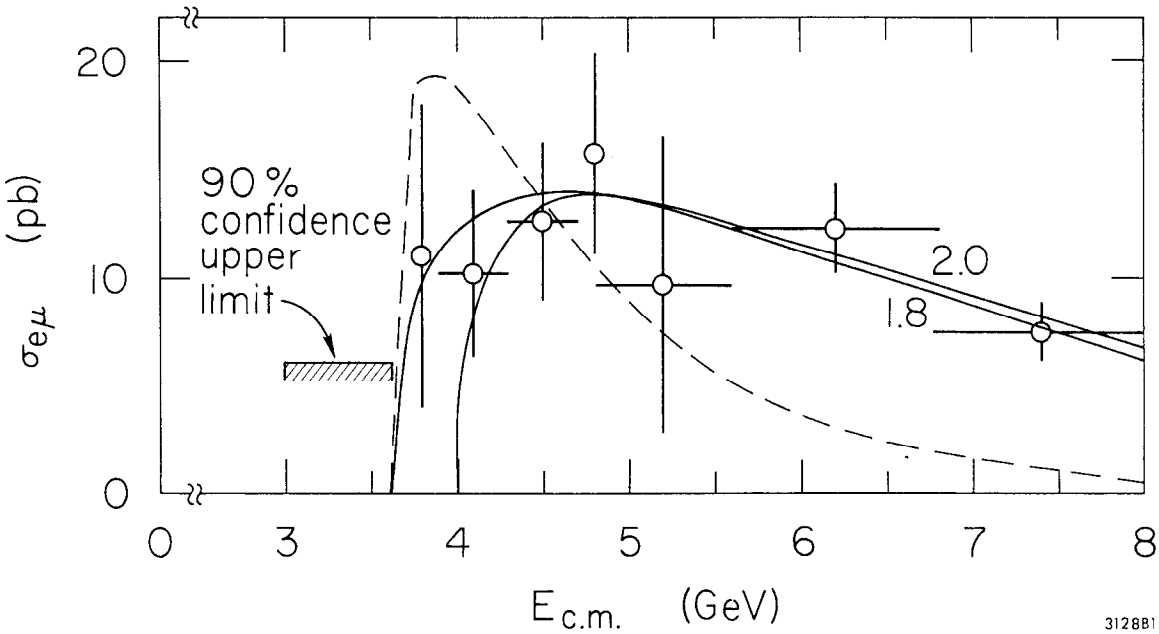
20
10
0
$\sigma_{e\mu}$ (pb)
90 %
confidence
upper
limit
2.0
1.8
0
3
4
5
6
7
8
$E_{c.m.}$ (GeV)
3128B1

FIG. 6.5

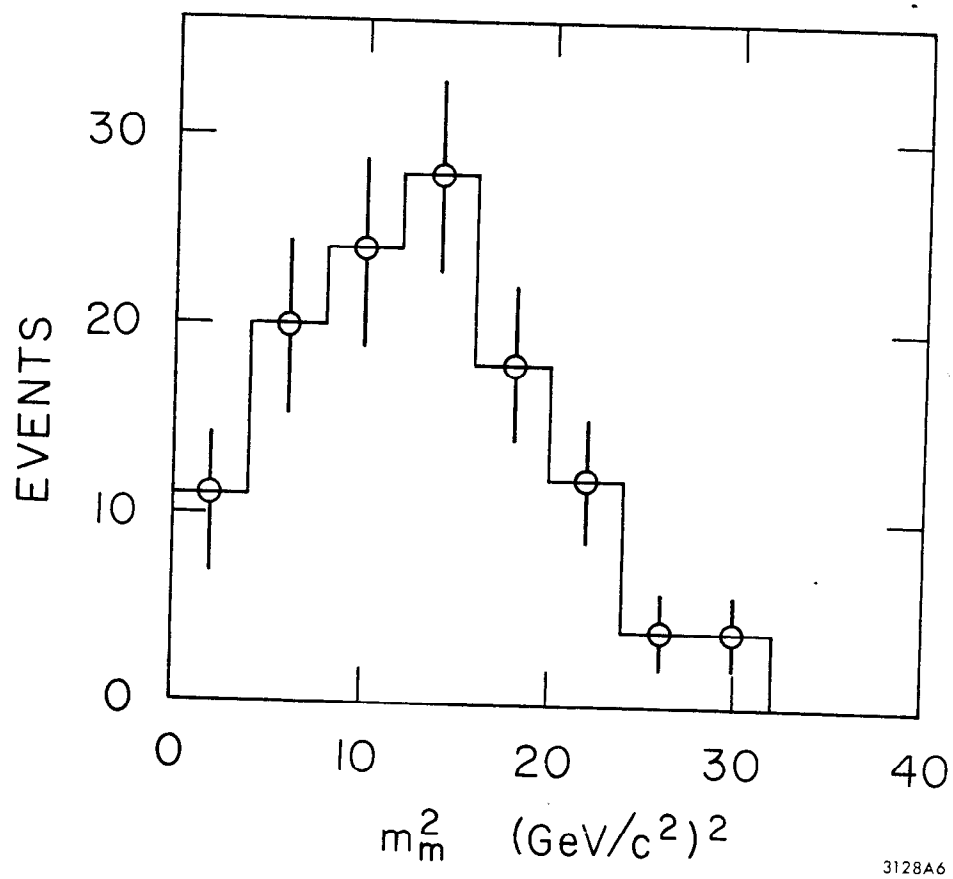

FIG. 6.6

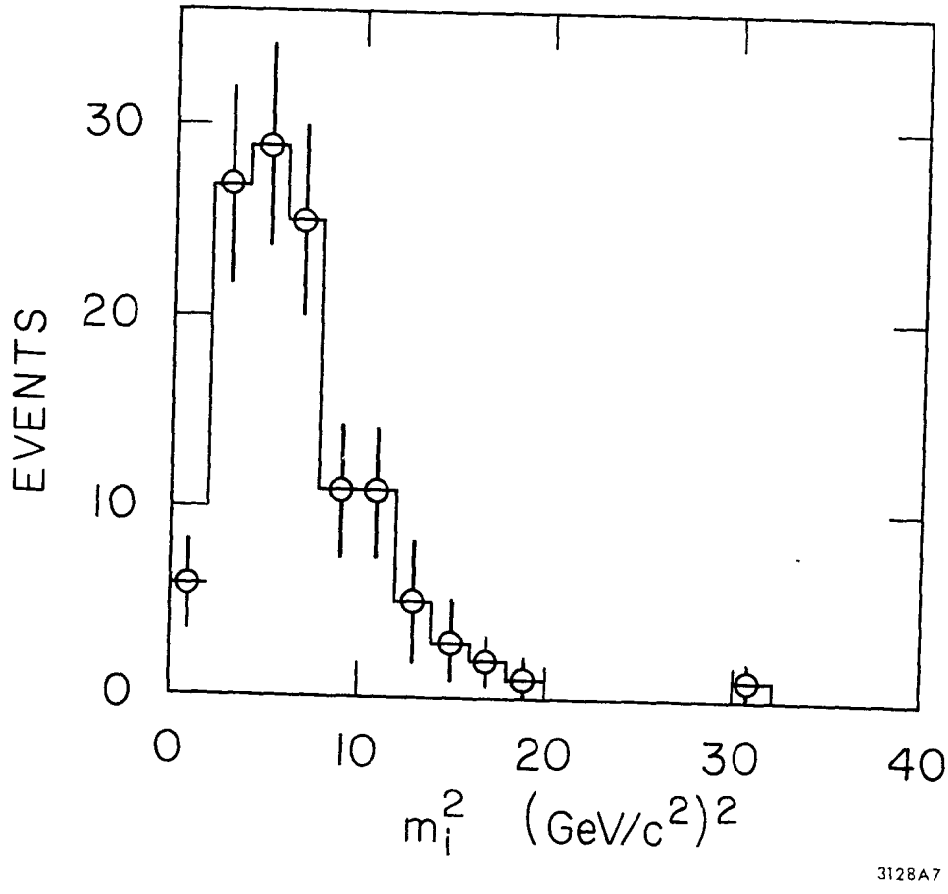

FIG. 6.7

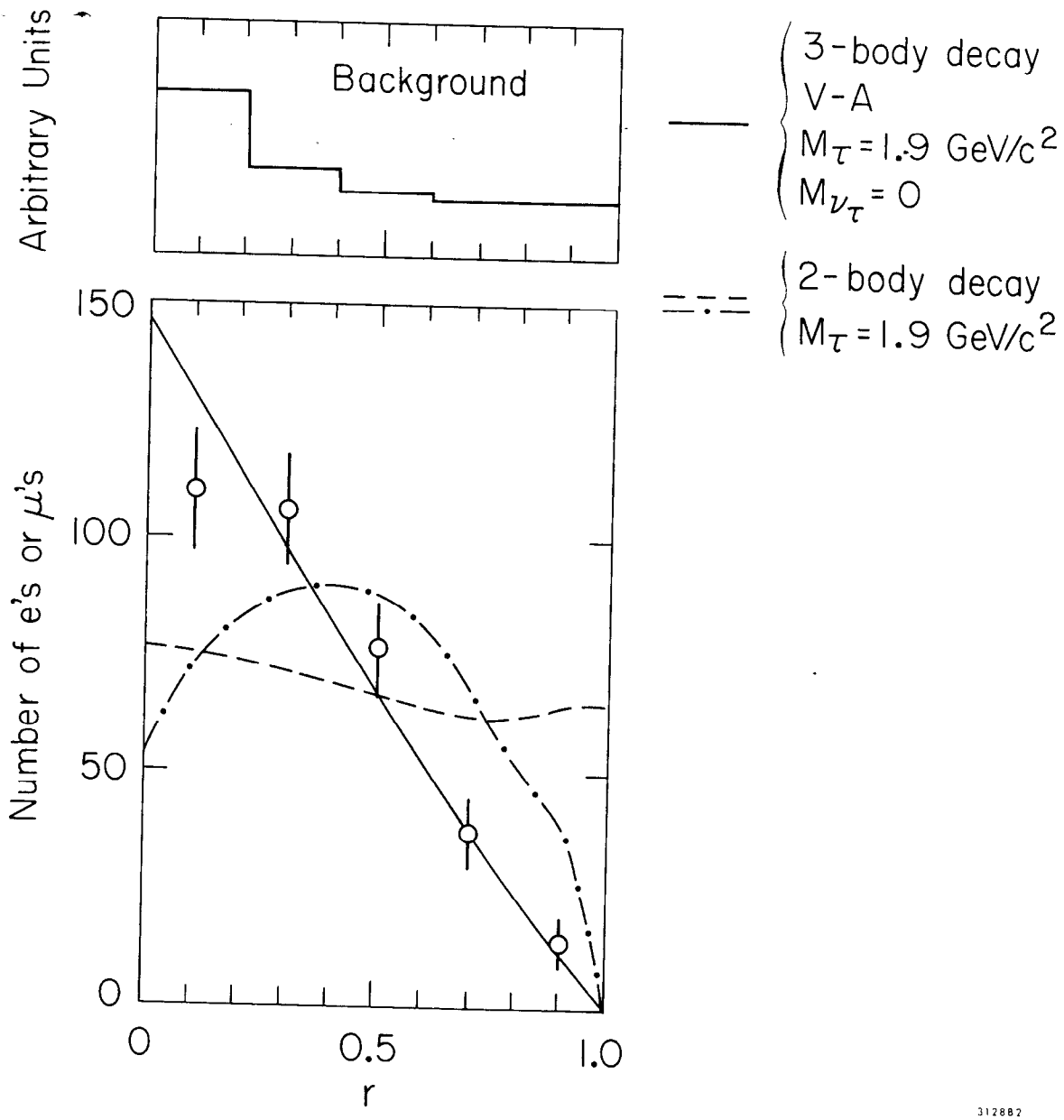
Arbitrary Units
Background
3-body decay
V-A
$M_\tau = 1.9$ GeV/c^2
$M_{\nu_\tau} = 0$
2-body decay
$M_\tau = 1.9$ GeV/c^2
Number of e's or μ's
150
100
50
0
0
0.5
1.0
r
312882

FIG. 6.8 a

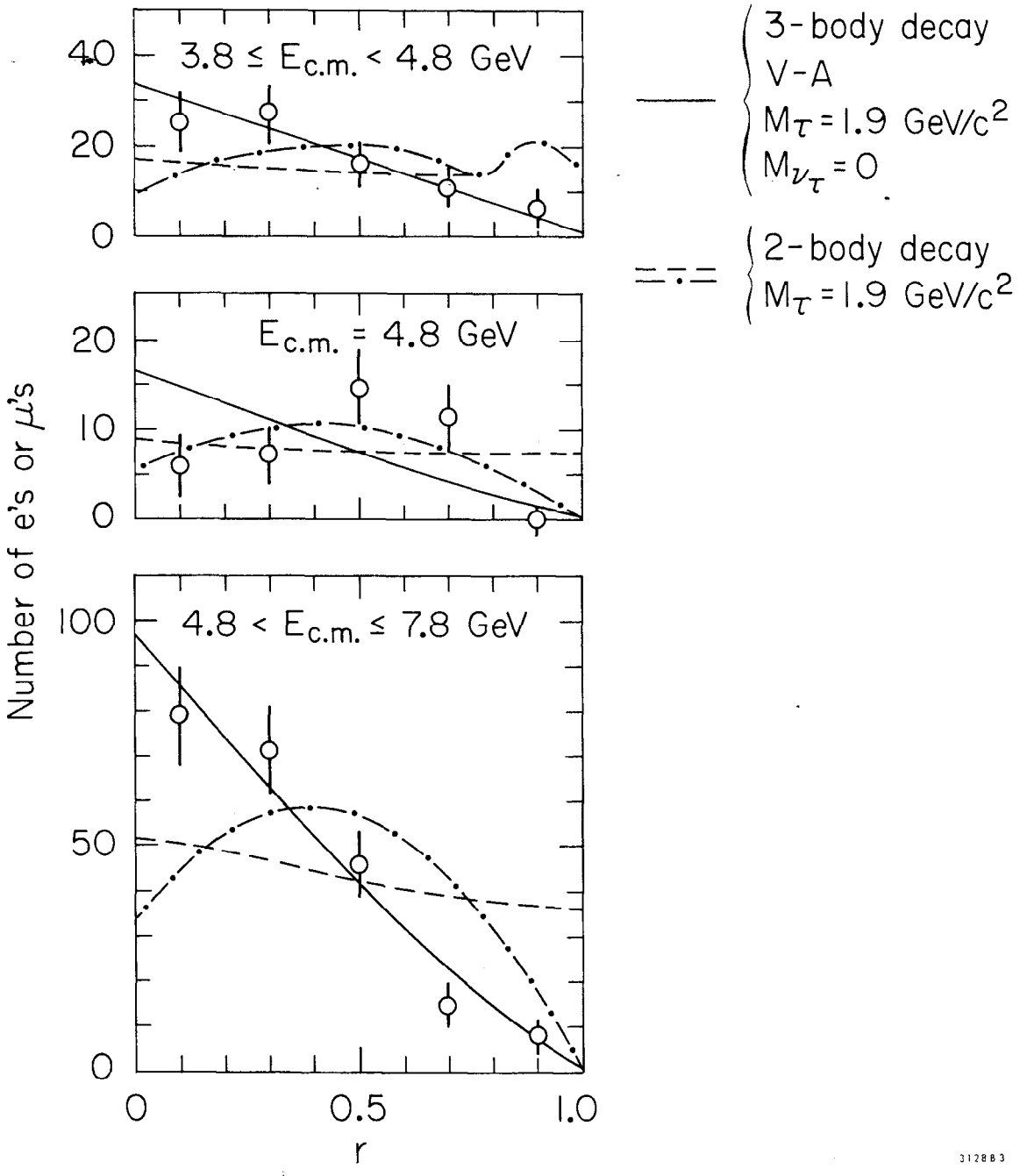
3.8 ≤ Ec.m. < 4.8 GeV
Ec.m. = 4.8 GeV
4.8 < Ec.m. ≤ 7.8 GeV
Number of e's or μ's
r
3-body decay
V-A
Mτ = 1.9 GeV/c2
Mντ = 0
2-body decay
Mτ = 1.9 GeV/c2
312883

FIG. 6.8b

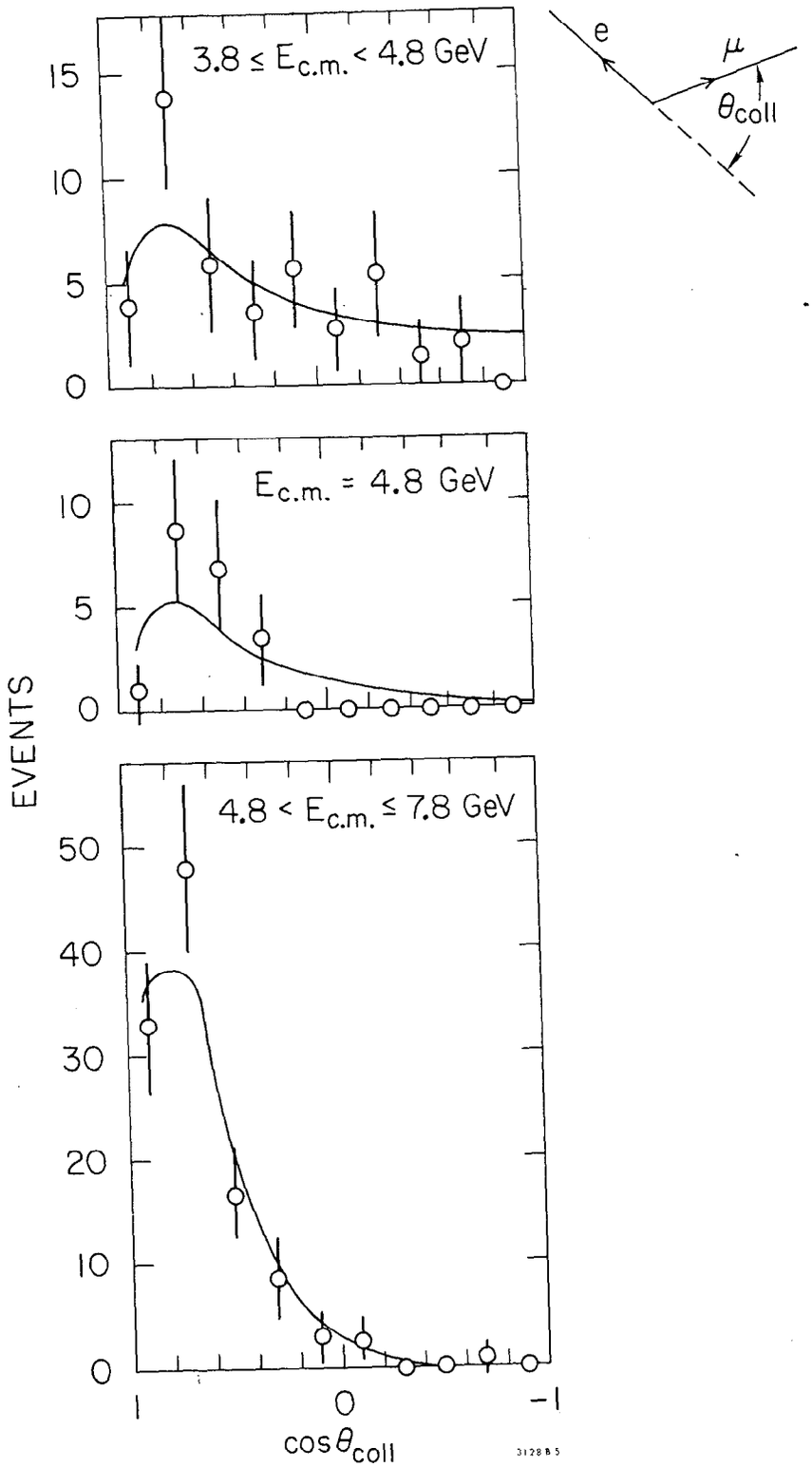
3.8 ≤ E c.m. < 4.8 GeV
E c.m. = 4.8 GeV
4.8 < E c.m. ≤ 7.8 GeV
EVENTS
cos θ coll
e
μ
θ coll
3128B5

FIG. 6.9

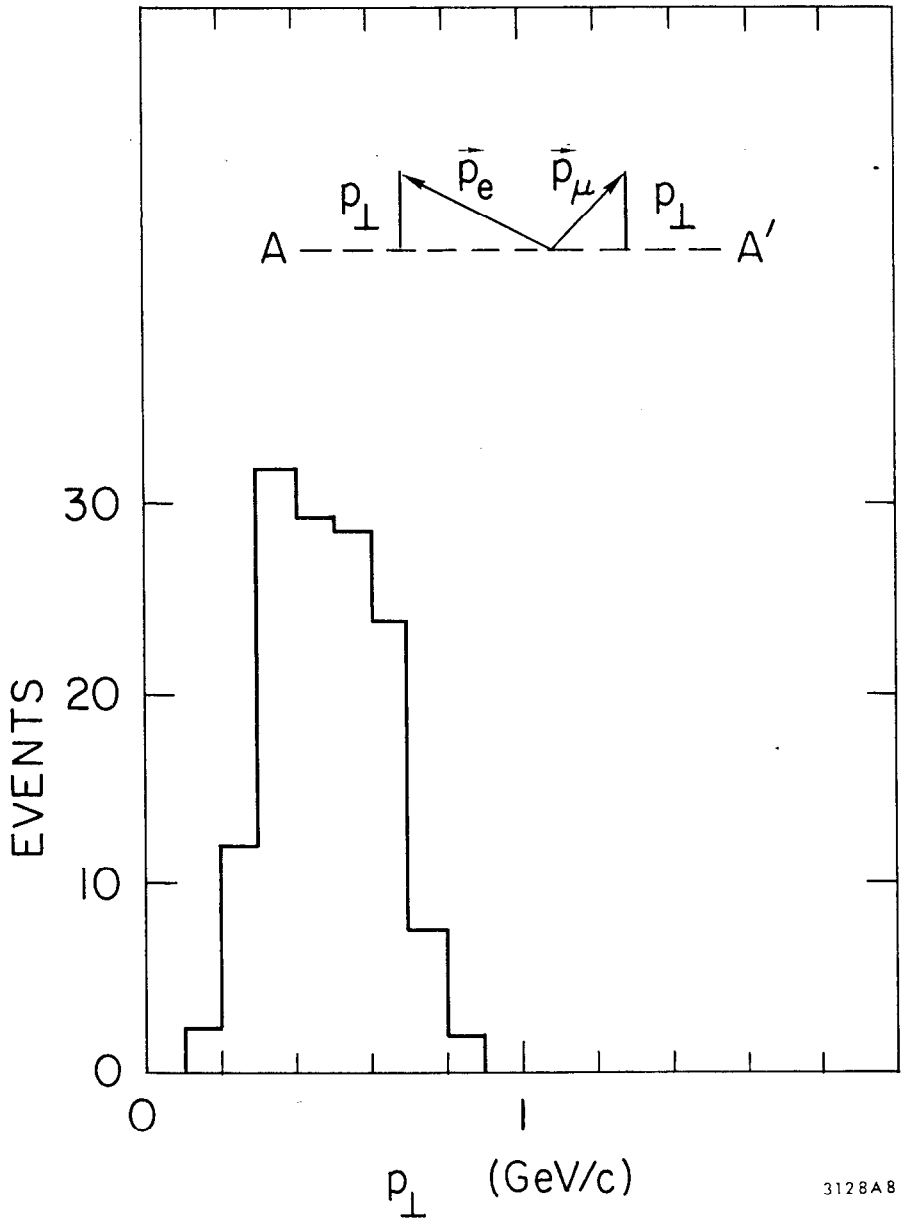
$p_\perp$
$\vec{p}_e$
$\vec{p}_\mu$
$p_\perp$
A
A′
30
20
10
0
EVENTS
0
1
$p_\perp$ (GeV/c)
3128A8

FIG. 6.10

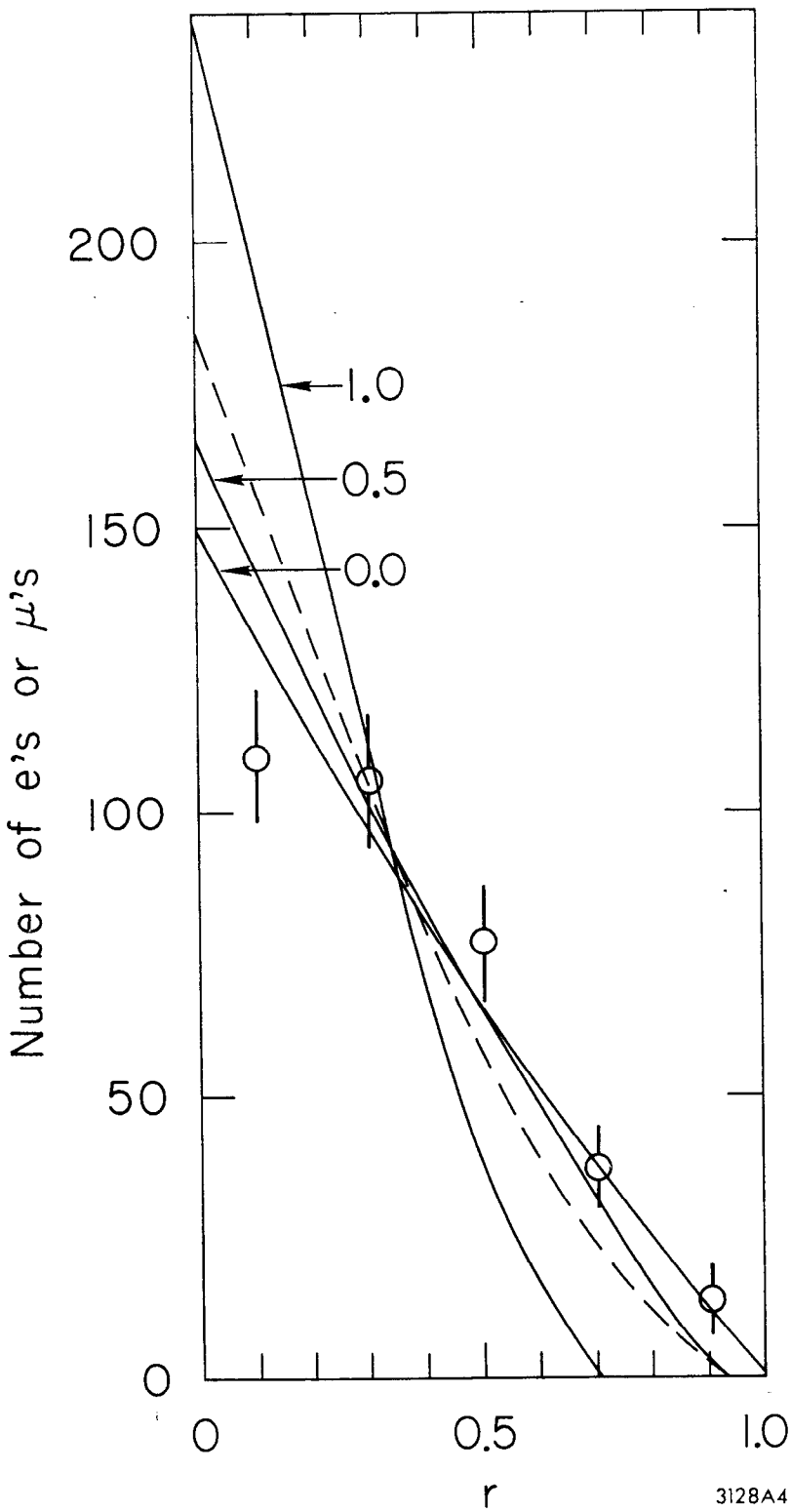

FIG. 6.11

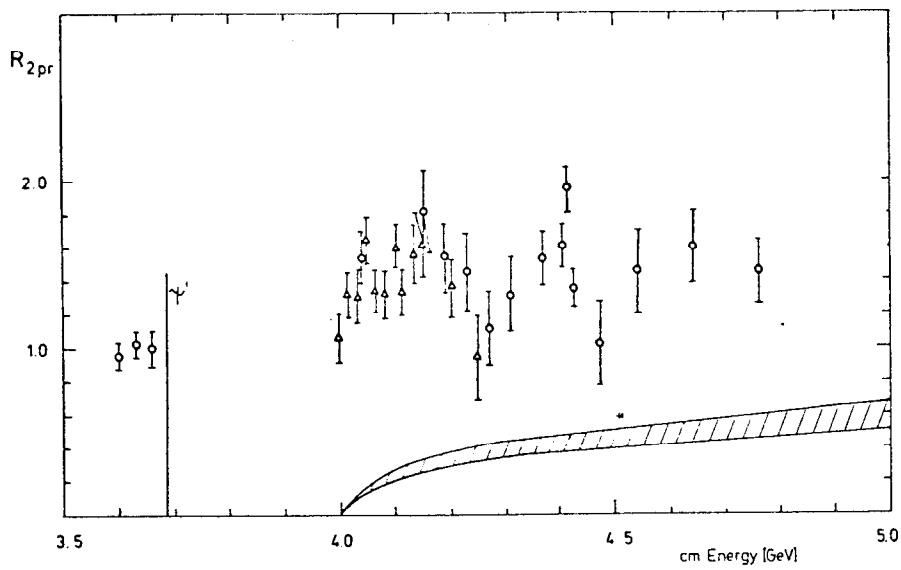

FIG. 6.12

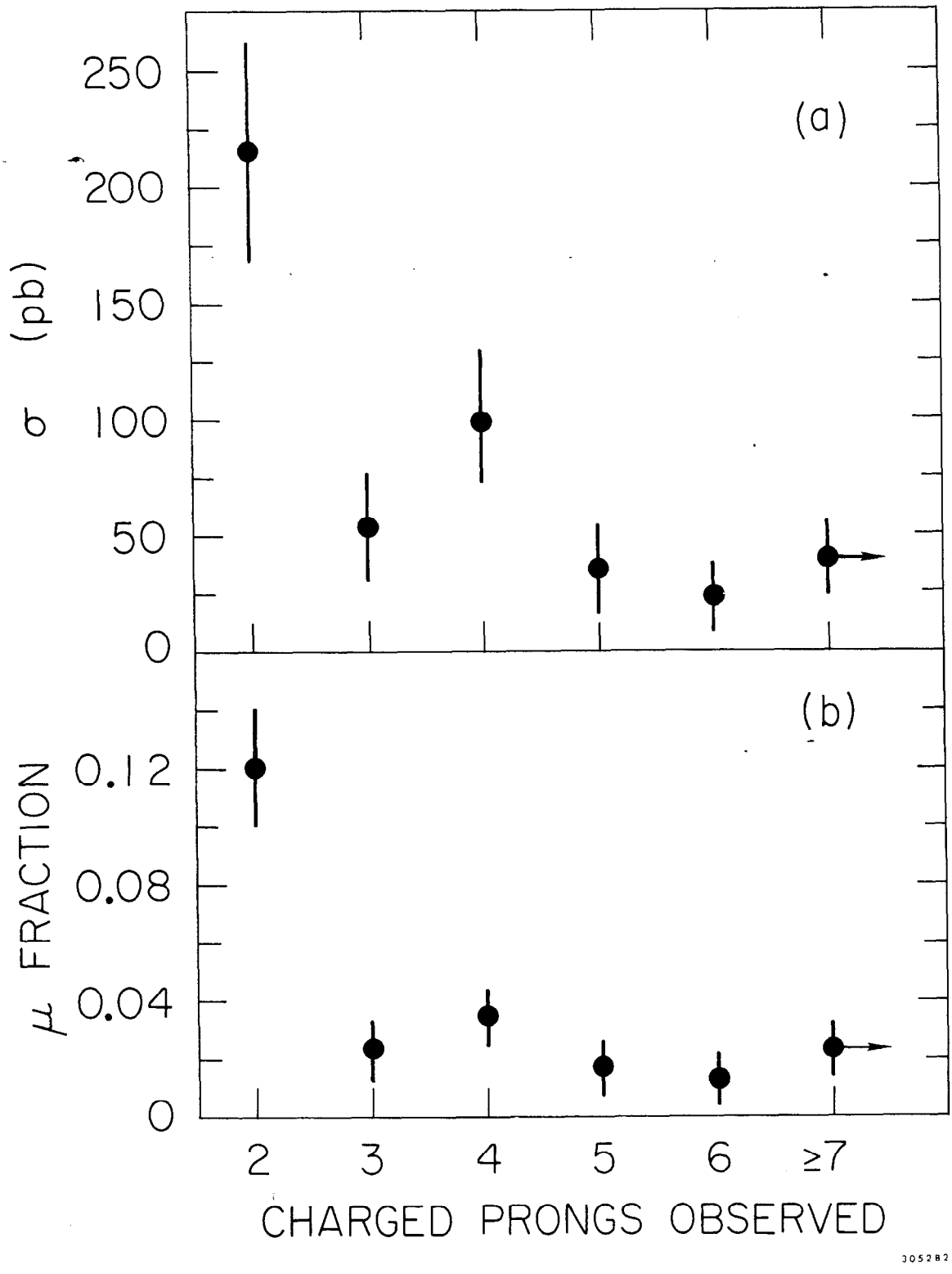
250
200
150
100
50
0
σ (pb)
(a)
(b)
0.12
0.08
0.04
0
μ FRACTION
2
3
4
5
6
≥7
CHARGED PRONGS OBSERVED
305282

FIG. 6.13

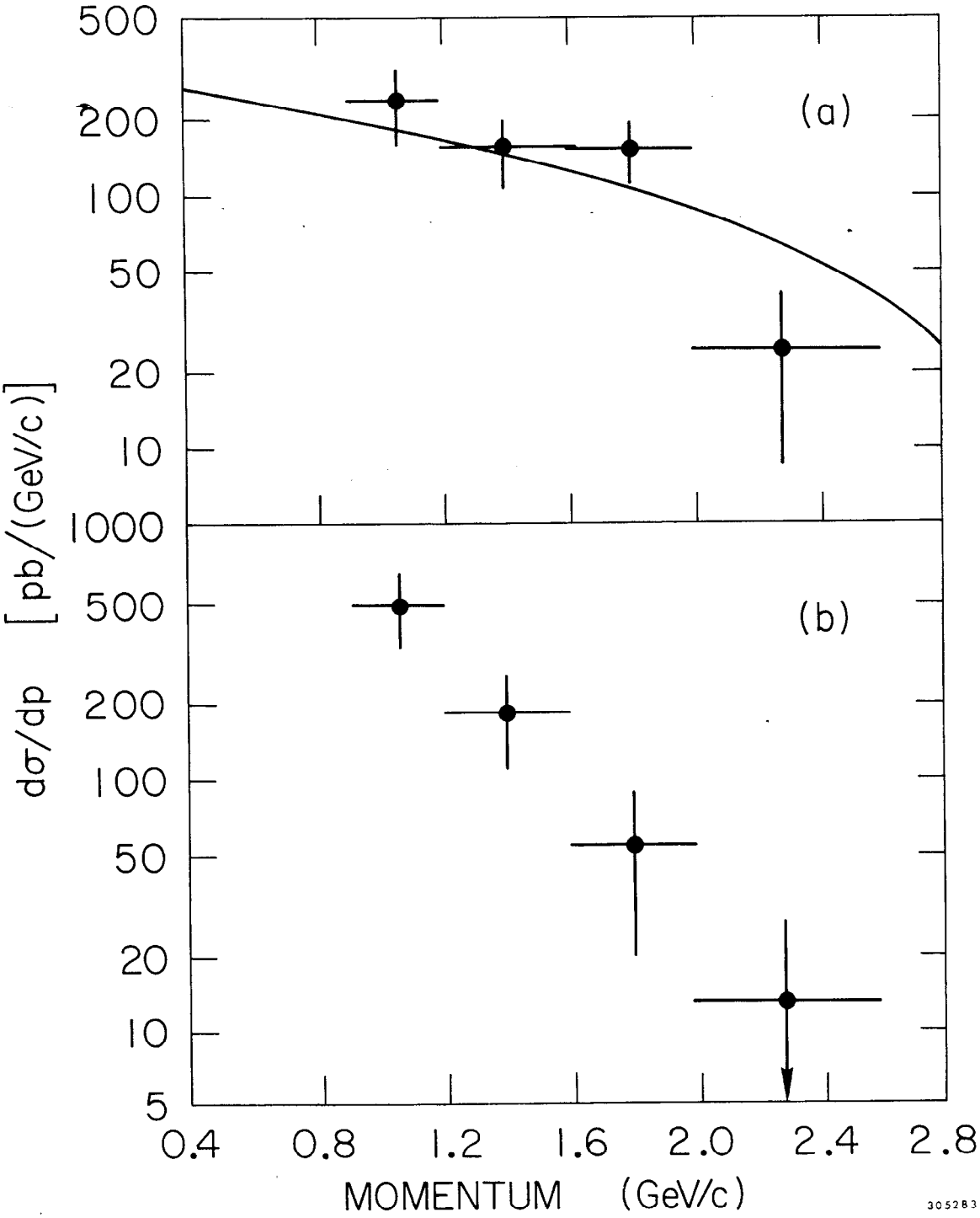
500
200
100
50
20
10
1000
500
200
100
50
20
10
5
(a)
(b)
dσ/dp [pb/(GeV/c)]
0.4
0.8
1.2
1.6
2.0
2.4
2.8
MOMENTUM (GeV/c)
305283

FIG. 6.14

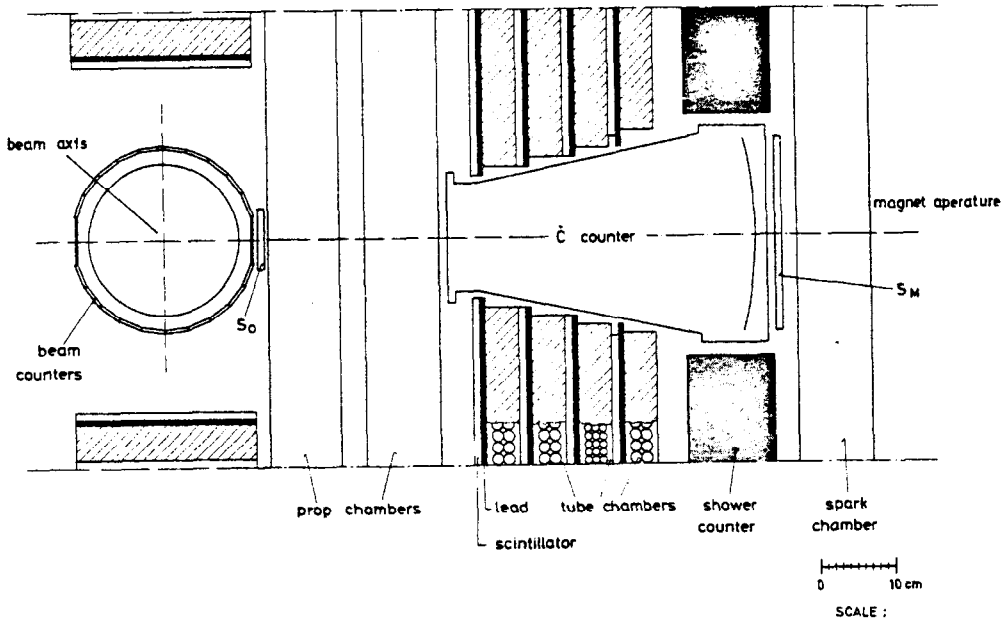
beam axis
beam counters
S_0
Č counter
magnet aperature
S_M
prop chambers
lead
scintillator
tube chambers
shower counter
spark chamber
0
10 cm
SCALE :

FIG. 6.15

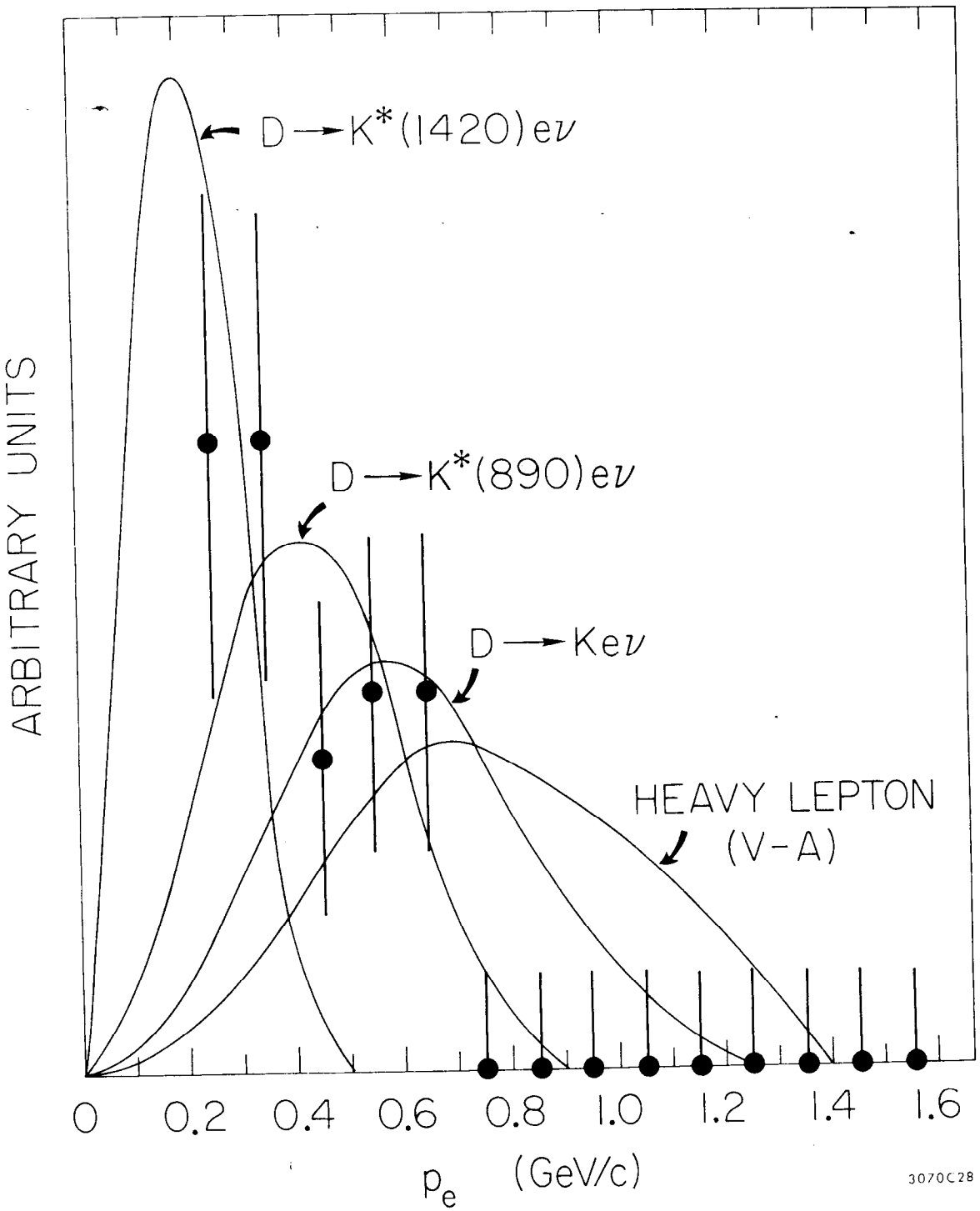
D → K*(1420)eν
D → K*(890)eν
D → Keν
HEAVY LEPTON
(V-A)
ARBITRARY UNITS
0
0.2
0.4
0.6
0.8
1.0
1.2
1.4
1.6
p_e (GeV/c)
3070C28

FIG. 6.16

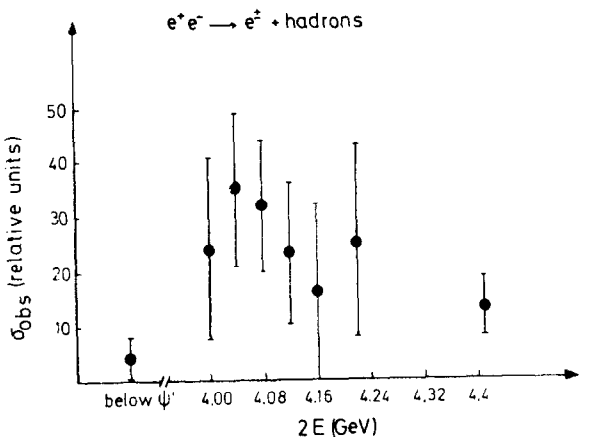
$e^+e^- \longrightarrow e^\pm$ + hadrons
σ_{obs} (relative units)
50
40
30
20
10
below ψ'
4.00
4.08
4.16
4.24
4.32
4.4
2 E (GeV)

FIG. 6.17

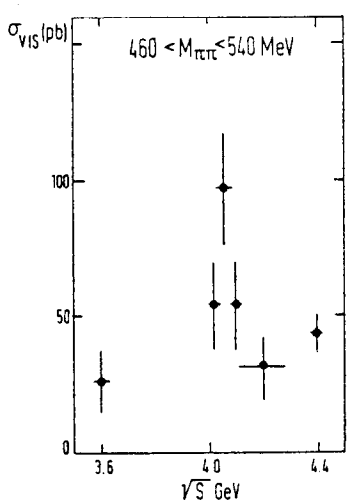

FIG. 6.18

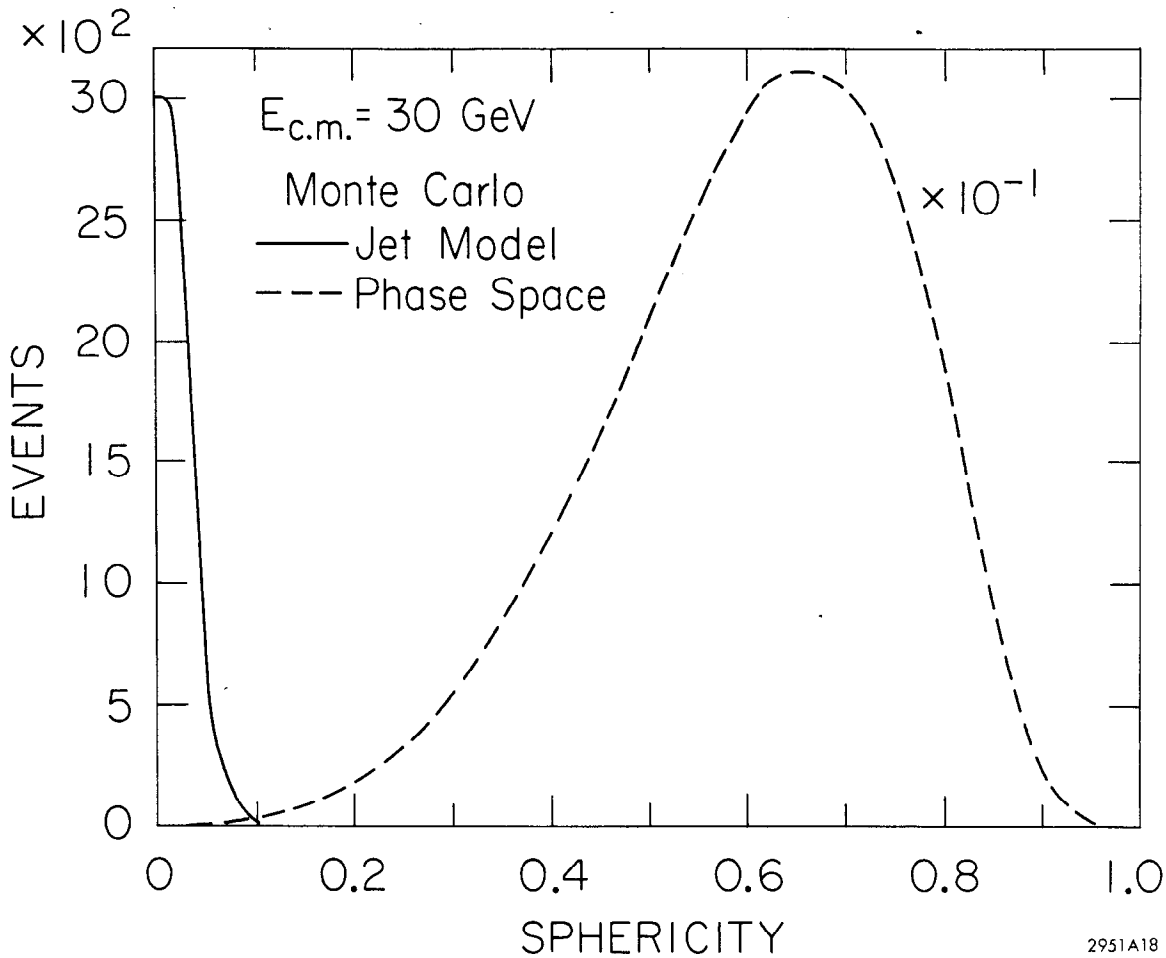
×10²
30
25
20
15
10
5
0
EVENTS
E c.m. = 30 GeV
Monte Carlo
Jet Model
Phase Space
×10⁻¹
0
0.2
0.4
0.6
0.8
1.0
SPHERICITY
2951A18

FIG. 7.1

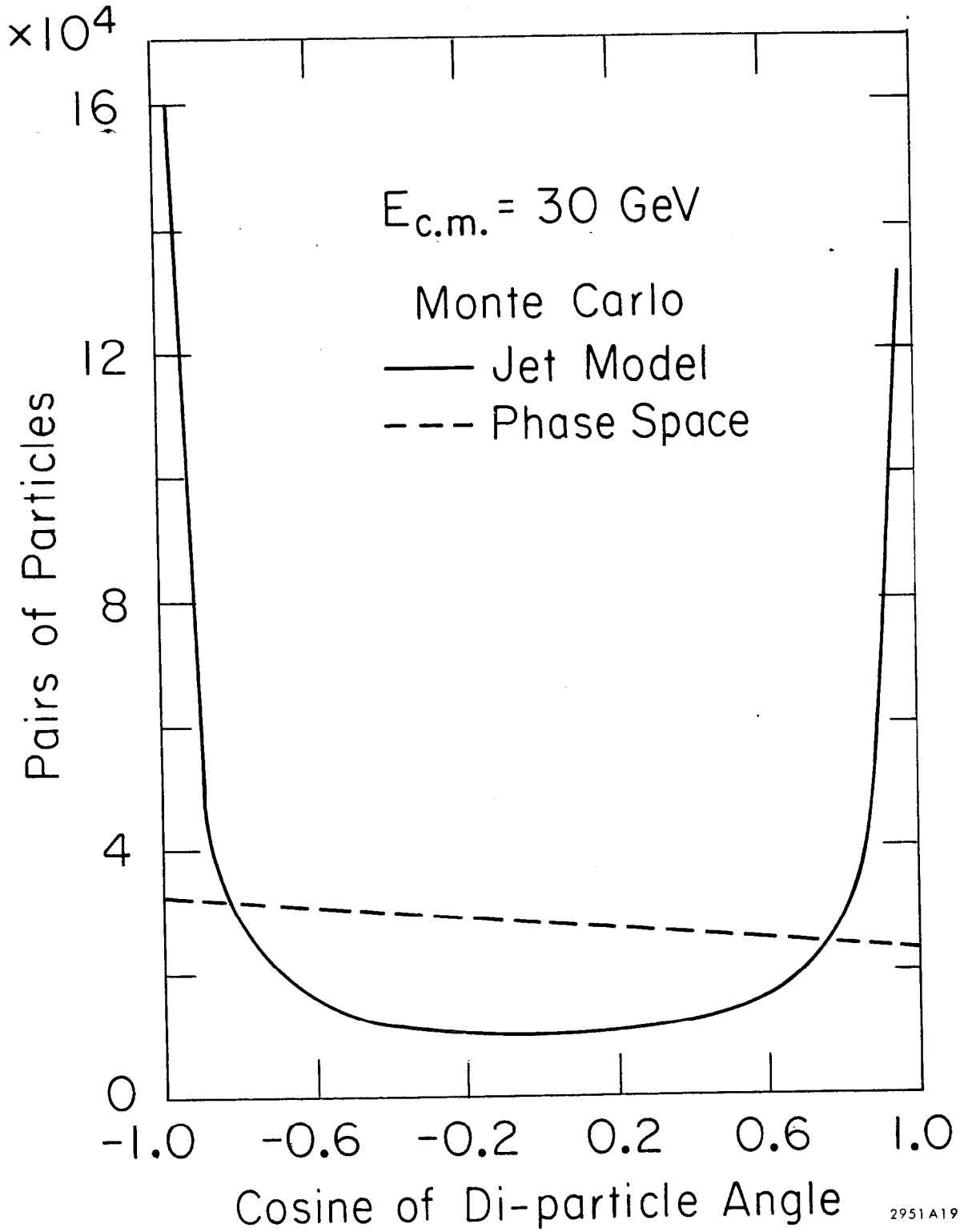
×10^4
16
12
8
4
0
Pairs of Particles
E c.m. = 30 GeV
Monte Carlo
Jet Model
Phase Space
-1.0
-0.6
-0.2
0.2
0.6
1.0
Cosine of Di-particle Angle
2951A19

FIG. 7.2

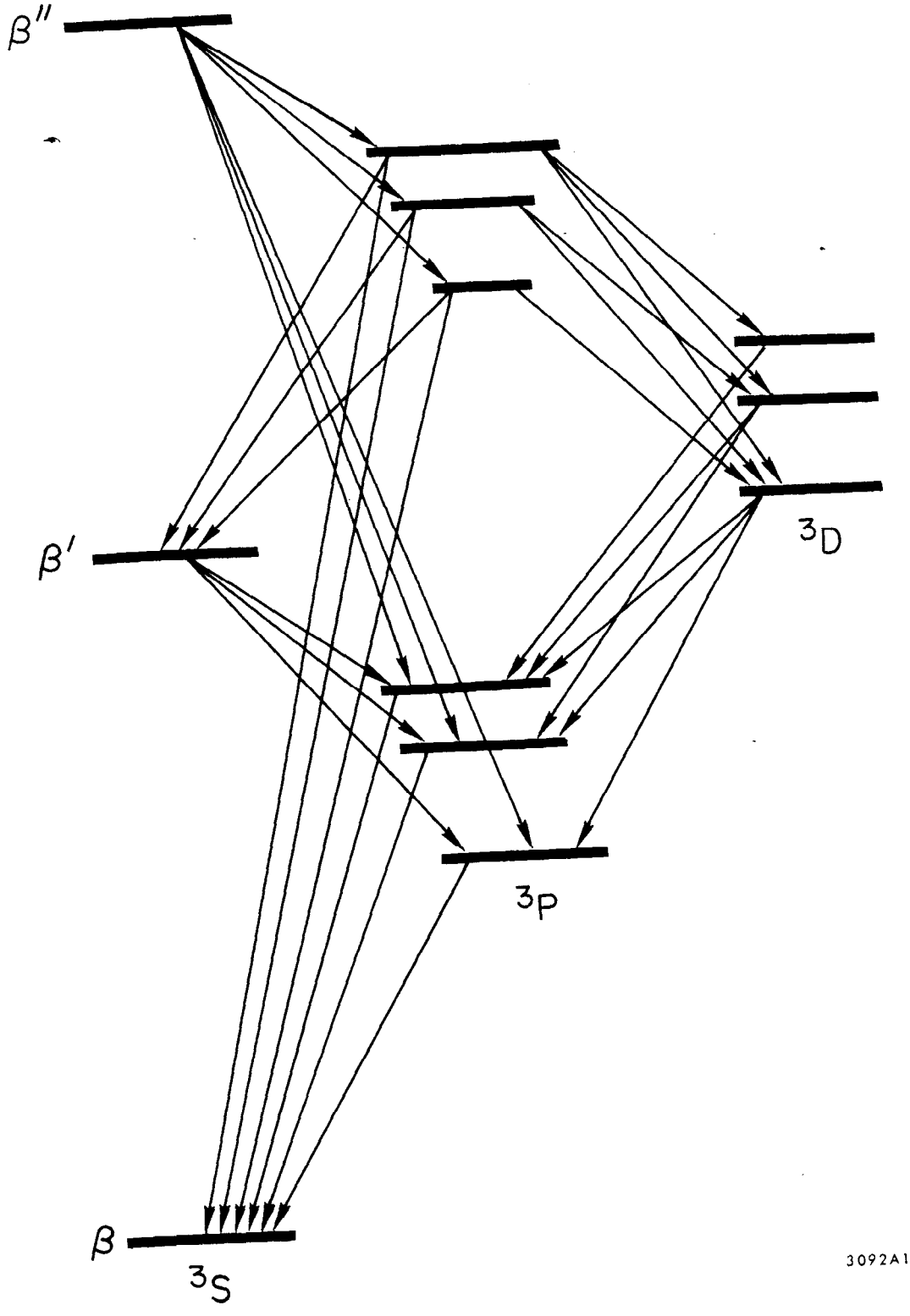

FIG. 7.3

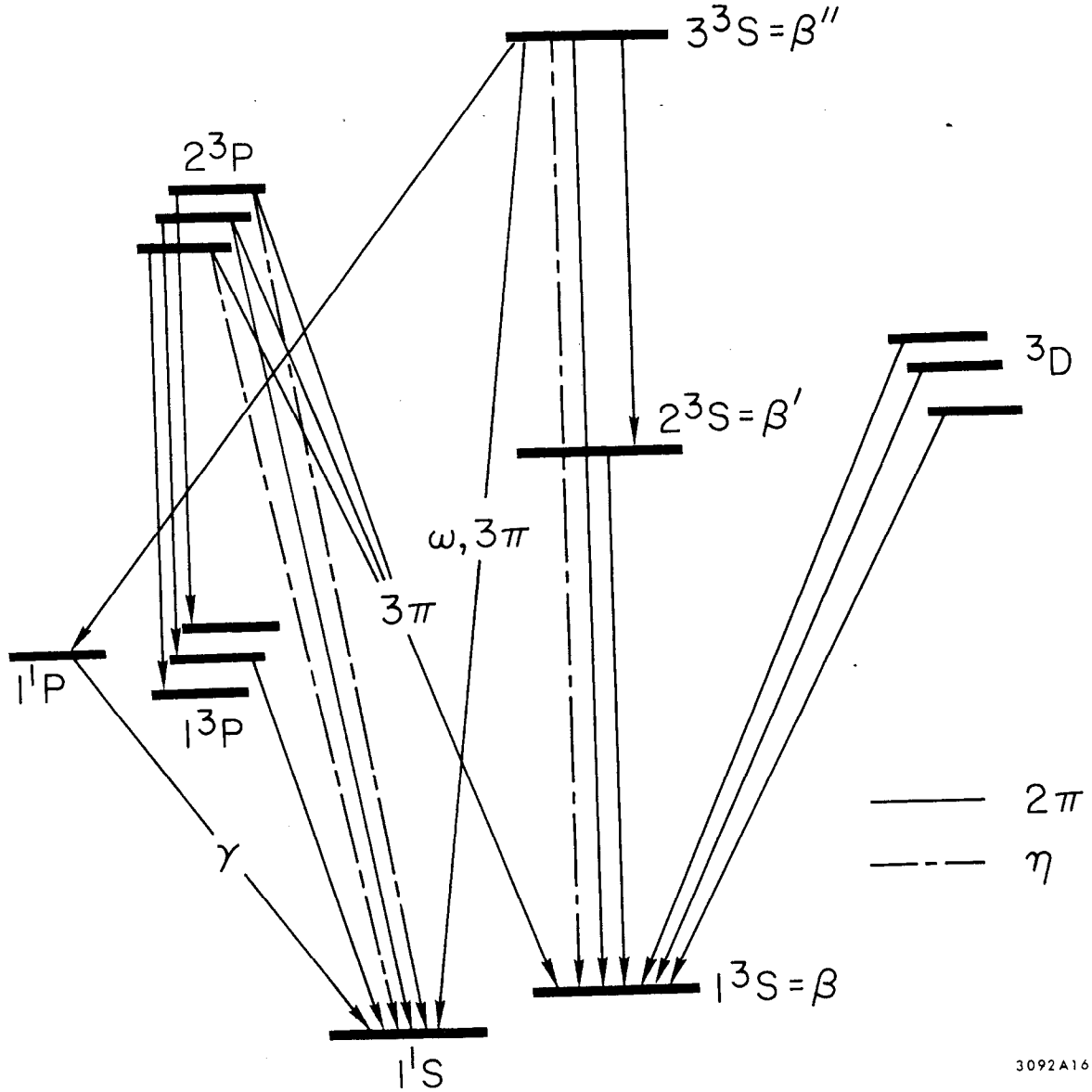
$3^3S = \beta''$
2^3P
^3D
$2^3S = \beta'$
$\omega, 3\pi$
3π
1^1P
1^3P
2π
η
γ
$1^3S = \beta$
1^1S
3092A16

FIG. 7.4